**THESIS OF DOCTORAL (Ph.D.) DISSERTATION**

# Comparative solution and structural studies on anticancer copper complexes of thiosemicarbazones and 2-substituted sterane-based compounds

**Tatsiana Petrasheuskaya**

**SUPERVISOR:**

**Dr. Éva Anna Enyedy**

Associate professor, D.Sc. of Hungarian Academy of Sciences


**UNIVERSITY OF SZEGED**

**Faculty of Natural Sciences and Informatics**

**Department of Molecular and Analytical Chemistry**

**Doctoral School of Chemistry**

**Szeged**

**2023.**

# TABLE OF CONTENTS

## LIST OF ABBREVIATIONS

| | |
|---|---|
| 2AE | 2-aminoestradiol |
| 2AP | 2-aminophenol |
| 5-HP | 5-hydroxyl-2-formylpyridine thiosemicarbazone |
| AA | ascorbic acid |
| AcFTSC | 2-acetylpyridine TSC |
| ATO | arsenic trioxide, $As_2O_3$ |
| benzimidazole-TSC | (*E*)-2-((1*H*-benzo[d]imidazol-2-yl)methylene)hydrazine-1-carbothioamide |
| BOLD-100 | sodium *trans*-[tetrachlorobis(1*H*-indazole)ruthenate(III)] |
| COTI-2 | (*E*)-*N*'-(6,7-dihydroquinolin-8(5*H*)-ylidene)-4-(pyridin-2-yl)piperazine-1-carbothiohydrazide |
| CT | charge-transfer |
| CV | cyclic voltammetry |
| $D_{7.4}$ | partition coefficient at pH = 7.4 |
| DFT | density functional theory |
| DMSO | dimethyl sulfoxide |
| DNA | deoxyribonucleic acid |
| Dp44mT | di-2-pyridylketone-4,4-dimethyl-3-thiosemicarbazone |
| DPPH | 2,2-diphenyl-1-picrylhydrazyl |
| DSS | sodium 3-(trimethylsilyl)propane-1-sulfonate |
| EDTA | ethylenediaminetetraacetic acid |
| EMEM | Eagle's minimum essential medium |
| EPR | electron paramagnetic resonance |
| ESI-MS | electrospray ionisation mass spectrometry |
| estradiol-SC | 2-[(3,17$\beta$-dihydroxy-estra-1,3,5(10)-triene-2-yl)methylene]hydrazine-1-carboxamide |
| estradiol-TSC | 2-((3,17$\beta$-dihydroxy-estra-1,3,5(10)-triene-2-yl)methylene)hydrazine-1-carbothioamide |
| estrone-SC | 2-((3-hydroxy-estra-1,3,5(10)-triene-2-yl)methylene)hydrazine-1-carboxamide |
| estrone-TSC | 2-((3-hydroxy-estra-1,3,5(10)-triene-2-yl)methylene)hydrazine-1-carbothioamide |
| $Et_3N$ | triethylamine |
| $Et_2O$ | diethyl ether |
| EtOH | ethanol |
| FTSC | 2-formylpyridine thiosemicarbazone |
| GSH | glutathione |
| HBS | human blood serum |
| HEPES | 4-(2-hydroxyethyl)-1-piperazineethanesulfonic acid |
| *I* | ionic strength |
| $IC_{50}$ | half-maximal inhibitory concentration |
| Imidazole-TSC | 2-((1*H*-imidazol-4-yl)methylene)hydrazine-1-carbothioamide |
| *K'* | conditional constant |
| $K_a$ | proton dissociation constant (p$K_a$: decimal negative logarithm of $K_a$) |
| $k_{obs}$ | observed rate constants |
| L-Pro-FTSC | (*S*,*E*)-1-((6-((2-carbamothioylhydrazono)methyl)pyridin-2-yl)methyl)pyrrolidine-2-carboxylic acid |
| L-Pro-STSC | (*R*,*E*)-1-(3-((2-carbamothioylhydrazono)methyl)-2-hydroxy-5-methylbenzyl)pyrrolidine-2-carboxylic acid |
| MeOH | methanol |

| | |
|---|---|
| $Me_2$-estradiol-TSC | 2-((3,17$\beta$-dihydroxy-estra-1,3,5(10)-triene-2-yl)methylene)-*N*,*N*-dimethylhydrazine-1-carbothioamide |
| Me-estradiol-TSC | 2-((3,17$\beta$-dihydroxy-estra-1,3,5(10)-triene-2-yl)methylene)-*N*-methylhydrazine-1-carbothioamide |
| $Me_2$-estrone-TSC | 2-((3-hydroxy-estra-1,3,5(10)-triene-2-yl)methylene)-*N*,*N*-dimethylhydrazine-1-carbothioamide |
| Me-estrone-TSC | 2-((3-hydroxy-estra-1,3,5(10)-triene-2-yl)methylene)-*N*-methylhydrazine-1-carbothioamide |
| $Me_2$-imidazole-TSC | 2-((1*H*-imidazol-4-yl)methylene)-*N*,*N*-dimethylhydrazine-1-carbothioamide |
| Me-imidazole-TSC | 2-((1*H*-imidazol-4-yl)methylene)-*N*-methylhydrazine-1-carbothioamide |
| $Me_2$-thn-TSC | 2-((1-hydroxy-5,6,7,8-tetrahidronaphthalene-2-yl)methylene)-*N*,*N*-dimethylhydrazine-1-carbothioamide |
| Me-thn-TSC | 2-((1-hydroxy-5,6,7,8-tetrahidronaphthalene-2-yl)methylene)-*N*-methylhydrazine-1-carbothioamide |
| Morf-PTSC | (*E*)-*N*,*N*-dimethyl-2-((6-(morpholinomethyl)pyridin-2-yl)methylene)hydrazinecarbothioamide |
| mPip-PTSC | (*E*)-*N*,*N*-dimethyl-2-((6-((4-methylpiperazin-1-yl)methyl)pyridin-2-yl)methylene)hydrazinecarbothioamide |
| $NaH_2PO_4$ | sodium dihydrogen phosphate |
| $Na_2HPO_4$ | disodium hydrogen phosphate |
| $n$Bu$_4$NPF$_6$ | tetrabutylammonium hexafluorophosphate |
| NHE | normal hydrogen electrode |
| NMR | nuclear magnetic resonance |
| PAMPA | parallel artificial membrane permeability assay |
| PBS | phosphate-buffered saline |
| pCu | the decimal negative logarithm of the equilibrium concentration of the copper ion (Cu(II)) not bound to the ligand |
| $P_{eff}$ | effective permeability |
| PTSC | 2-pyridinecarboxaldehyde thiosemicarbazone |
| RNR | ribonucleotide reductase |
| ROS | reactive oxygen species |
| RPMI 1640 | Roswell Park Memorial Institute 1640 medium |
| SC | semicarbazone |
| SSC | salicylaldehyde semicarbazone |
| STSC | salicylaldehyde thiosemicarbazone |
| SXRD | single-crystal X-ray diffraction |
| TEAC | trolox equivalent antioxidant capacity |
| thn-SC | 2-((1-hydroxy-5,6,7,8-tetrahydronaphtalene-2-yl)methylene)hydrazine-1-carboxamide |
| thn-TSC | 2-((1-hydroxy-5,6,7,8-tetrahydronaphthalen-2-yl)methylene)hydrazine-1-carbothioamide |
| triapine | 3-aminopyridine-2-carboxaldehyde thiosemicarbazone |
| trolox | 6-hydroxy-2,5,7,8-tetramethylchroman-2-carboxylic acid |
| TSC | thiosemicarbazone |
| UV-vis | ultraviolet–visible |
| VA1 | 2-formylpyridine-4-(4-hydroxy-3,5-dimethylphenyl)-thiosemicarbazone |
| VA2 | 2-acetylpyridine-4-(4-hydroxy-3,5-dimethylphenyl)-thiosemicarbazone |
| VA3 | 3-amino-2-formylpyridine-4-(4-hydroxy-3,5-dimethylphenyl) thiosemicarbazone |
| VA4 | (*E*)-*N*-(4-hydroxy-3,5-dimethylphenyl)-2-((4-(morpholinomethyl) pyridin-2-yl)methylene)hydrazinecarbothioamide |

| | |
|---|---|
| VA5 | (*E*)-*N*-(4-hydroxy-3,5-dimethylphenyl)-2-((5-(morpholinomethyl) pyridin-2-yl)methylene)hydrazinecarbothioamide |
| VA6 | (*E*)-*N*-(4-hydroxy-3,5-dimethylphenyl)-2-((3-(morpholinomethyl) pyridin-2-yl)methylene)hydrazinecarbothioamide |
| VA7 | (*E*)-*N*-(4-hydroxy-3,5-dimethylphenyl)-2-((6-(morpholinomethyl) pyridin-2-yl)methylene)hydrazinecarbothioamide |
| VA8 | (*E*)-1-(3-((2-carbamothioylhydrazono)methyl)-4-hydroxyphenyl)-*N*,*N*,*N* trimethylmethanaminium |
| VA9 | (*E*)-1-(4-hydroxy-3-((2-(methylcarbamothioyl)hydrazono)methyl) phenyl)-*N*,*N*,*N*-trimethylmethanaminium |
| VA10 | (*E*)-1-(3-((2-(ethylcarbamothioyl)hydrazono)methyl)-4-hydroxyphenyl)-*N*,*N*,*N*-trimethylmethanaminium |
| VA11 | (*E*)-1-(4-hydroxy-3-((2-(phenylcarbamothioyl)hydrazono)methyl) phenyl)-*N*,*N*,*N*-trimethylmethanaminium |

# 1. INTRODUCTION

Metal ions play significant roles in biological and biomedical processes, since without them the course of many important vital processes in the human body – like the optimal functioning of enzymes, osmotic balance in cells, photosynthesis and other processes – would not be possible [1-5]. The versatile biological roles of metal ions in the living organisms have stimulated the development of metal-based therapeutics. Metal-containing compounds have been used for the treatment of different diseases since ancient times, namely the Egyptians had the knowledge about the therapeutic potential of gold salts, the Chinese used the metalloid arsenic containing drugs such as arsenic trioxide (ATO), what was later applied for the treatment of *rheumatoid diseases*, *syphilis*, *psoriasis* and as antiseptic agents in the beginning of the 20$^{th}$ century. Moreover, ATO was suggested to be used against *leukemia* in the 18$^{th}$ and 19$^{th}$ centuries. Nevertheless, metal-containing compounds were in the spotlight as potential chemotherapeutic agents against tumors only after the serendipitous discovery of the anticancer properties of the platinum(II) complex, cisplatin, in 1960s [1]. Since that time a pronounced surge in research interest has been directed towards platinum complexes as potential anticancer drugs due to the success of cisplatin [6]. Currently, cisplatin and related compounds (carboplatin and oxaliplatin) are the most frequently used chemotherapeutics against different types of cancer [1]. Besides that, four more platinum-containing compounds have obtained regulatory approval locally: lobaplatin (China), heptaplatin (Korea), nedaplatin (Japan) and miriplatin (Japan) [1]. However, platinum compounds, as well as most of the organic chemotherapeutic drugs, have two major disadvantages, namely the appearance of serious side effects (*e.g.* nephrotoxicity, weakened immune system, vomiting) during the treatment and later on, and they often induce resistance in tumors, which decreases the efficacy of other chemotherapeutics as well [1,7-9]. Employing non-essential metal ions for cancer treatment also bears environmental implications, since the selected platinum agents end in natural water leading to the elevated concentration of water-soluble platinum [10,11]. This poses a high risk for all forms of life, switching to complexes of essential metal ions as means to overcome this threat [12,13].

The abovementioned problems initiated the investigation of other non-platinum metal-based anticancer compounds with different mechanisms of action. In spite of the fact that none of the non-platinum metal-containing drugs has been approved till now for cancer chemotherapy, a significant progress has been achieved in this field [14-19]. Several metal-containing compounds, such as motexafin lutetium, palladium bacteriopheophorbide and purlytin, showed promising anticancer activity in photodynamic therapy; however, finally they were not approved worldwide

due to their toxicity, photosensitivity or insufficient efficacy [20]. On the contrary, there are some potential metal-based compounds, which are currently in clinical trials, such as complexes of ruthenium(II/III), gallium(III), iron(II) and gold(I) [21-23]. Moreover, it should be noted that one of these compounds (sodium *trans*-[tetrachlorobis(1*H*-indazole)ruthenate(III)], BOLD-100) got orphan drug designation status from the U.S. Food and Drug Administration for the treatment of gastric and pancreatic cancer [24].

Taking these issues into consideration, another strategy was implemented. In the literature, there are some examples of anticancer compounds like 8-hydroxyquinolines, $PA_N$ inhibitors, adamantane sulfonamides, dithiocarbamates, salicylate metal-binding isosteres, hydroxypyridinethiones and hydroxamic acids [25-27], which can form stable metal complexes *in situ* with essential metal ions. These organic compounds can be involved in the inhibition of vital metalloenzymes, which participate in the proper functioning of the cell (*e.g.* cell division); or the formed metal complexes may catalyze processes, which can induce the production of reactive oxygen species (ROS) and disrupt the redox homeostasis [28].

In this thesis, studies on thiosemicarbazones, semicarbazones and 2-aminophenols are reported, as these compounds also show affinity to essential metal ions (Cu(II) and Fe(II/III)) and may exert their anticancer effect in a similar way. To find out the most probable mechanism of action of the title compounds, detailed solution equilibrium studies are needed.

# 2. Literature overview

## *2.1 Thiosemicarbazones*

Thiosemicarbazones (TSCs) are a class of compounds similar by structure to semicarbazones (SCs), in which the oxygen atom is substituted by a sulfur atom. They can be obtained by a condensation reaction between a thiosemicarbazide and an aldehyde or a ketone [29].

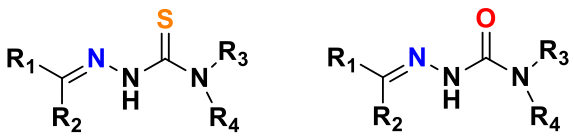


**thiosemicarbazone** **semicarbazone**

**Chart 1.** General structural formula of thiosemicarbazones and semicarbazones.

In general, the thiosemicarbazone scaffold contains (N,S) donor atoms (Chart 1) and can act as mono- or bidentate chelating agents. Moreover, their coordination capacity can be expanded, if aldehydes or ketones with additional functional groups are used for their preparation incorporating coordinating donor atoms in positions suitable for chelation [29]. It is also noteworthy to mention that TSCs can occur in the tautomeric thione and thiol forms (Scheme 1). They can coordinate to metal ions in neutral or anionic forms, where the latter can be obtained by the deprotonation of NH of the thiosemicarbazide moiety (or the SH group in the case of the thiol form, Scheme 1) [30]. The most commonly studied type of TSCs are the tridentate α-*N*-heterocyclic TSCs, which contain an extra coordinating moiety (typically a pyridine ring) and can coordinate via ($N_{pyridyl}$,N,S) binding set. Another type of TSCs are the salicylaldehyde derivatives, where a phenolate group can also participate in the coordination to metal ions besides the usual (N,S) donor atoms.

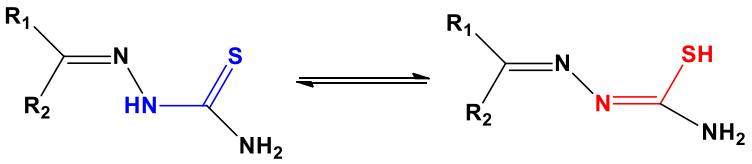


**thione** **thiol**

**Scheme 1.** Structural formula of thiosemicarbazones in thione and thiol tautomeric forms.

Although thiosemicarbazones were first mentioned in the end of the 19$^{th}$ century, interest on these compounds has appeared much later due to their diverse range of biological activity [31]. Namely, antitubercular, antibacterial, antimalarial, antileprosy, antiparasitic, antiviral, antiproliferative and antitumor activities were found [32]. The first compound, which was clinically approved from the group of TSCs, was thioacetazone (Chart 2) for the treatment of

*tuberculosis* [33]. Later on, another TSC derivative, methisazone (Chart 2) was developed and used against smallpox [33]. The anticancer activity of TSCs was mentioned for the first time in 1956, where 2-formylpyridine thiosemicarbazone (FTSC (2-formylpyridine thiosemicarbazone), Chart 2) showed remarkable activity against *leukemia* in mice [33]. Based on that, further comprehensive structure-activity relationship studies revealed the most promising compound, namely 5-hydroxyl-2-formylpyridine thiosemicarbazone (5-HP, Chart 2), which was tested in phase I clinical trials. This compound showed significant anticancer activity against *leukemia*, however further evaluation was stopped due to the occurrence of severe side effects like gastrointestinal toxicity and the fast inactivation by glucoronidation [34].

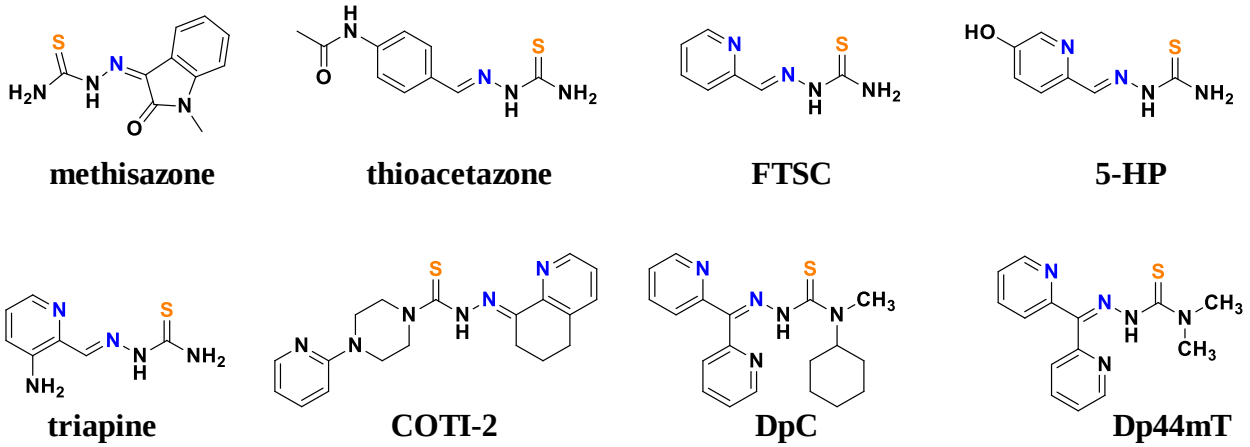


**Chart 2.** Structural formula of some important thiosemicarbazones with abbreaviation of their names, highlighting the possible coordinating donor atoms.

Currently, there are three α-*N*-heterocyclic TSC derivatives, which are in clinical trials. Namely, 3-aminopyridine-2-carboxaldehyde thiosemicarbazone (triapine, Chart 2), which has already been involved in ~30 different phase I–III clinical trials for the treatment of hematologic and gynecologic malignancies [35]. Triapine showed promising results in mono- and combined therapies (*e.g.* with cisplatin, gemcitabine, doxorubicin) in the treatment of *myeloid leukemia* but it was much less effective against solid tumors due to its short biological half-life [36-39]. However, triapine has also many side effects, such as vomiting and methemoglobinemia [36]. Based on these findings, the development of new TSC derivatives is required to overcome these problems. In 2015, the α-*N*-heterocyclic TSC derivative COTI-2 ((*E*)-*N*'-(6,7-dihydroquinolin-8(5*H*)-ylidene)-4-(pyridin-2-yl)piperazine-1-carbothiohydrazide) (Chart 2) entered to phase I clinical trials against advanced or recurrent gynecologic malignancies [33]. This compound showed strong anticancer activity in the nanomolar concentration range. The last currently tested thiosemicarbazone is DpC (Chart 2), which also entered to clinical phase I investigations in 2016

[33]. It should be noted that each of these compounds has distinct mode of action, making the elucidation of their underlying anticancer activity an area of high interest [33].

*2.2 Mode of action of (thio)semicarbazones*

The anticancer activity of thiosemicarbazones usually corresponds to their metal chelating ability [33,40]. Based on the proposed mechanism of action, activity of triapine is connected to the inhibition of the ribonucleotide reductase (RNR) enzyme [41]. This enzyme catalyzes the reduction of ribonucleotides to deoxyribonucleotides, which are the building blocks required for the replication and repair of DNA in all living cells [41]. There are three classes of RNRs, namely the members of the first class contain a diiron-oxygen cluster, while in the second and third classes vitamin B12 or an iron-sulfur cluster coupled to *S*-adenosylmethionine is present as cofactor, respectively [42]. Human ribonucleotide reductase belongs to the first class and has two subunits: R1 (RRM1) and R2 (RRM2) (Fig. 1) [43]. The first subunit (R1) binds allosteric effectors and substrates, whereas the second subunit (R2) is much smaller than subunit (R1) and contains the diiron centre. This centre takes part in the tyrosyl radical stabilization, what is essential for the enzymatic activity [44]. It should be noted that RNR plays a crucial role in anticancer therapy, since a strong dependence was found between its activity and the development of cancer [45]. Based on this finding, many chemotherapeutic agents were developed including triapine, which are used to sequester the iron from the diiron centre of the enzyme and to quench the tyrosyl radical leading to the inhibition of the enzyme [46]. It was proposed that triapine can form a very stable redox active iron(II)-triapine complex *in situ*, which generates ROS inhibiting RNR by quenching the active-site tyrosyl radical [41].

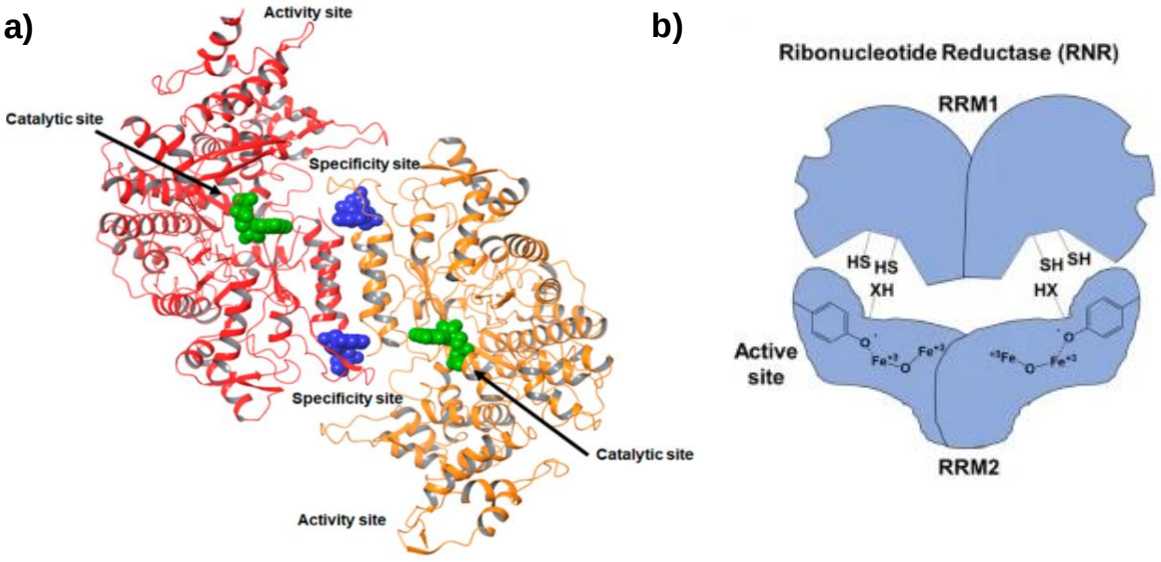


**Figure 1.** a) Structure of ribonucleotide reductase; b) the schematic active center of ribonucleotide reductase [47].

Another mechanism of action was suggested for COTI-2, which can restore the function of the mutant p53 and inhibit the PI3K/AKT/mTOR pathway [48]. The multifunctional protein p53 mostly operates as a tumor suppressor, regulating many important cellular responses like apoptosis and cell growth arrest [48]. It was found that zinc chelation by COTI-2 allows for mutant p53 a conformation change similar to the wild type that restores sequence-specific p53 transcription and promote apoptosis [48].

Moreover, another mechanisms of action have been suggested for other anticancer thiosemicarbazones. For instance, Dp44mT (di-2-pyridylketone-4,4-dimethyl-3-thiosemicarbazone, Chart 2) forms metal complex with the intracellular copper ions, which seems to be crucial in the mechanism [49-51]. In the case of certain TSCs, the Cu(II) complexes show higher cytotoxic activity than the free ligands [52-54]. The anticancer activity of these compounds is related to their redox properties, particularly to their redox reaction with physiological reductants such as glutathione (GSH) and ascorbic acid (AA) [49]. GSH is one of the most abundant non-protein thiol (0.5−15 mM) in mammalian cells [55], and it is responsible for the defense against oxidative stress, control of the thiol oxidation state of proteins and detoxification. Moreover, it can behave as an antioxidant by directly scavenging ROS and then repairing received damage via enzymatic processes [56]. That is why GSH is an important compound for living organisms, and also the disturbances in the homeostasis of GSH have been involved in tumor initiation, progression and treatment response for fighting cancer [55,56]. It should be noted that cancer cells have higher GSH concentrations than healthy cells, which can be an indicator of tumor progression and increased drug resistance [51]. GSH can be found in its reduced and oxidized forms (GSH/GSSG), namely under physiological conditions GSH exists mostly in the reduced form with a ratio of GSH:GSSG = 1000:1 in nucleus and cytosol; the higher amount of the oxidized form can lead to apoptosis or necrosis [57]. Based on these findings, depletion of GSH can be utilized as a valuable strategy in anticancer treatment especially in combined therapy [58]. For example, it was reported that GSH can reduce Cu(II) complexes of α-*N*-pyridyl TSCs and the formed Cu(I) species can interact with oxygen generating intracellular ROS [49,59,60]. In more details, this process was reported by Faller *et al*. for Dp44mT (Scheme 2), where the reaction between its Cu(II) complex and GSH at high excess (50 equivalents) was studied spectrophotomerically under strictly anaerobic conditions and similar reactions were reported for other related TSCs [51,61,62]. First of all, a ternary [Cu(II)-Dp44mT-GS] complex (Scheme 2, where $GS^-$ is the deprotonated form of GSH) was formed immediately after mixing the reagents. Afterwards, unbound Dp44mT appeared because of the dissociation of the generated Cu(I) complex in the presence of the high excess of GSH, as Cu(I) forms a stable complex with GSH. It should be noted that $O_2$ bubbled through the sample can reoxidize Cu(I) to Cu(II) regenerating the initial Cu(II) complex.

Moreover, the suggested mechanism was confirmed by electron paramagnetic resonance (EPR) spectroscopy as well [63].

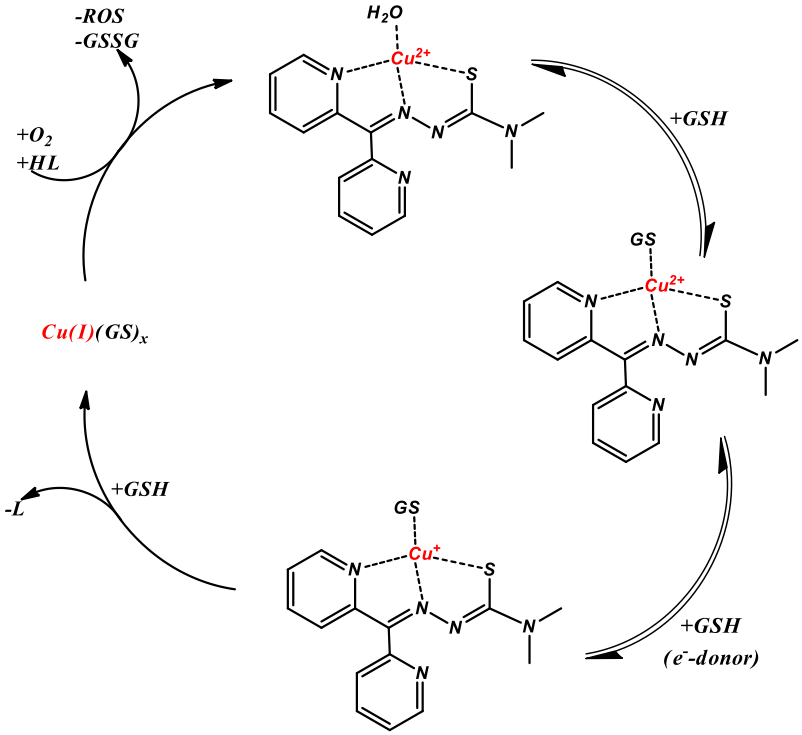


**Scheme 2.** Suggested redox cycle for the interaction of Cu(II) complex of Dp44mT with GSH [49,51].

Another important reducing agent in the living tissue is ascorbic acid with a concentration in the nucleus and cytosol between 1 and 5 mM, and in the blood serum within a range of 0.050-0.15 mM, depending on several factors such as dietary intake, individual metabolism and health status [64-67]. Ascorbic acid stimulates hydroxylation reactions (cytochrome P450 activity, cholesterol metabolism, collagen synthesis, *etc*.) and it also participates in the catalysis of other enzymatic reactions like amidation, which is crucial for the hormonal activity of cholecystokinin, vasopressin, oxytocin and α-melanotropin [68,69]. Moreover, AA is also a possible endogenous reducing agent for Cu(II) and can enhance ROS production [70,71]. However, AA is a weaker reducing agent than GSH, thus no reaction could be observed between AA and the most of the Cu-TSC complexes [61,63]. Otherwise, it was reported that several Cu(II)-semicarbazone complexes can cleave DNA in the presence of AA, which is most probably also related to the formation of ROS as it was described above [72]. The reason for this behavior can be connected with the redox activity of Cu(II) complexes of TSCs and SCs. Namely, the formal redox potential of Cu(II)-TSC complexes is usually much higher than that of Cu(II)-SCs, therefore it can explain the stronger reactivity toward GSH in comparison to AA [63].

Based on these findings, it can be concluded that the characterization of the stability and redox properties of the Cu(II) complexes of (T)SCs is necessary to understand better their

mechanism of action. These types of studies can provide comprehensive information about chemical form (*e.g.* protonation processes, lipophilicity, stability, solution structure), in which the tested compounds are present predominantly under physiological conditions. These data also can help us to get information about the possible transformations, however, there are still some unanswered questions in the field, especially for the newly developed compounds. Our research group is dedicated to investigate this field over a decade, and the upcoming chapter serves as a summary of the most significant findings the group has made so far.

*2.3 Recent results in solution chemical studies of (thio)semicarbazones*

Behavior in the aqueous solution of the two main classes of (thio)semicarbazones, namely α-*N*-pyridyl and salicylaldehyde (T)SCs was investigated in details until now. In Chart 3 the structural formulae of the already tested (T)SCs are presented. Solution chemical properties such as protonation and isomerization processes, lipophilicity, stability and solution structure were investigated by pH-potentiometry, UV-visible (UV-vis) spectrophotometry, $^{1}$H NMR (nuclear magnetic resonance) spectroscopy and spectrofluorimetry. These parameters can provide information about the actual form of compounds under physiological conditions and help to understand better the mechanism of action of the given compound [73,74].

Based on the literature data, solution equilibrium studies of the (T)SCs were usually performed mostly in 30% (*v/v*) DMSO (dimethyl sulfoxide)/$H_2O$ solvent mixture due to the poor solubility of the complexes in water, while the ones with improved aqueous solubility like L-Pro-STSC ((*R*,*E*)-1-(3-((2-carbamothioylhydrazono)methyl)-2-hydroxy-5-methylbenzyl)pyrrolidine-2-carboxylic acid), L-Pro-FTSC ((*S*,*E*)-1-((6-((2-carbamothioylhydrazono)methyl)pyridin-2-yl)methyl)pyrrolidine-2-carboxylic acid), Morf-PTSC ((*E*)-*N*,*N*-dimethyl-2-((6-(morpholinomethyl)pyridin-2-yl)methylene)hydrazinecarbothioamide) and mPip-PTSC ((*E*)-*N*,*N*-dimethyl-2-((6-((4-methylpiperazin-1-yl)methyl)pyridin-2-yl)methylene)hydrazine-carbothioamide) were tested in aqueous solution [61,63,75-82]. The proton dissociation constants ($K_a$) and *n*-octanol/water distribution coefficients (*D*) are collected for comparison in Table 1, determined by UV-vis spectrophotometric methods in the different media. The fully protonated α-*N*-pyridyl-TSCs have two dissociable protons, namely the pyridinium nitrogen ($N^1H^+$) and the CH=N-***N*$^3$*H***-hydrazonic nitrogen from the thiosemicarbazide moiety. During the deprotonation of the latter group the negative charge is mainly localized on the sulfur atom thanks to the thione-thiol tautomerism (Chart 3).

**Basic α-*N*-pyridyl (T)SCs**

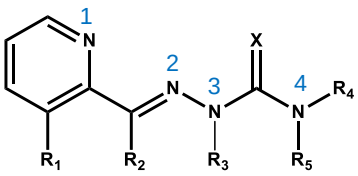

| | $R_1$ | $R_2$ | $R_3$ | $R_4$ | $R_5$ | X |
|---|---|---|---|---|---|---|
| **FTSC** | H | H | H | H | H | S |
| **PTSC** | H | H | H | $CH_3$ | $CH_3$ | S |
| **triapine** | $NH_2$ | H | H | H | H | S |
| **O-triapine** | $NH_2$ | H | H | H | H | O |
| **Se-triapine** | $NH_2$ | H | H | H | H | Se |
| **Me-triapine** | $NH_2$ | H | $CH_3$ | H | H | S |
| **AcFTSC** | H | $CH_3$ | H | H | H | S |
| **AcPTSC** | $NH_2$ | H | H | $CH_3$ | $CH_3$ | S |
| **FATSC** | H | $NH_2$ | H | H | H | S |
| **$H_2$NNHMe** | $NH_2$ | $CH_3$ | H | $CH_3$ | H | S |
| **$H_2$NNM$e_2$** | $NH_2$ | $CH_3$ | H | $CH_3$ | $CH_3$ | S |
| **MeHNNM$e_2$** | NH-$CH_3$ | $CH_3$ | H | $CH_3$ | $CH_3$ | S |
| **$Me_2$NN$H_2$** | $N(CH_3)_2$ | $CH_3$ | H | H | H | S |
| **$Me_2$NNHMe** | $N(CH_3)_2$ | $CH_3$ | H | $CH_3$ | H | S |
| **$Me_2$NNM$e_2$** | $N(CH_3)_2$ | $CH_3$ | H | $CH_3$ | $CH_3$ | S |

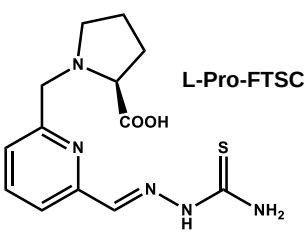

**L-Pro-FTSC**

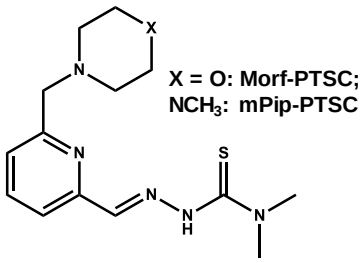

**X = O: Morf-PTSC;**
**$NCH_3$: mPip-PTSC**

**COTI-2 derivatives**

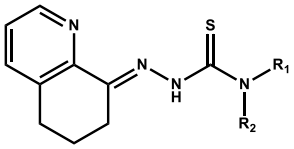

**$R_1$ = $R_2$ = H : COTI-$NH_2$;**
**$R_1$ = $R_2$ = $CH_3$ : COTI-$NMe_2$;**
**$R_1$ = $CH_3$; $R_2$ = cyclohexyl : COTI-MeCy**

**Imidazole-TSC derivatives**

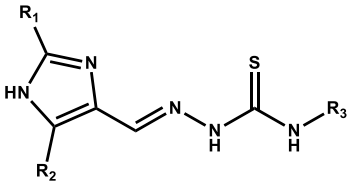

**$R_1$ = $CH_3$; $R_2$ = H; $R_3$ = H: $HL^1$;**
**$R_1$ = $CH_3$; $R_2$ = H; $R_3$ = $CH_3$ : $HL^2$;**
**$R_1$ = $CH_3$; $R_2$ = H; $R_3$ = $C_6H_5$ : $HL^3$;**
**$R_1$ = H; $R_2$ = $CH_3$; $R_3$ = H : $HL^4$;**
**$R_1$ = H; $R_2$ = $CH_3$; $R_3$ = $CH_3$ : $HL^5$;**
**$R_1$ = H; $R_2$ = $CH_3$; $R_3$ = $C_6H_5$ : $HL^6$**

**STSC and its derivatives**

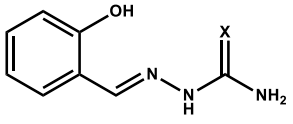

**X = S: STSC; O: SSC**

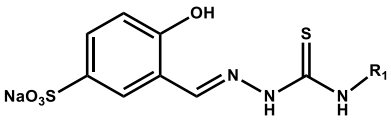

**$R_1$ = H : $NaH_2L^H$;**
**$R_1$ = $CH_3$ : $NaH_2L^{Me}$;**
**$R_1$ = $C_2H_5$ : $NaH_2L^{Et}$;**
**$R_1$ = $C_6H_5$ : $NaH_2L^{Ph}$;**

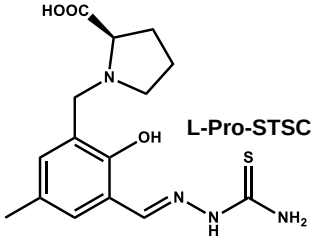

**L-Pro-STSC**

**Chart 3.** The structural formula and abbreviation of recently examined (thio)semicarbazones. (See structures also in Chart 2.)

It is worth to mention that the presence of methyl and amino groups clearly affects the p$K_a$ values of the ligands, and the position of the substituents also can vary these values. Namely, the *N*-terminal electron-donating methyl groups ($R_4$ or $R_5$ in Chart 3) increase p$K_{a1}$, while the value of the dissociation constant of the second proton decreases by *ca.* half an order of magnitude (*e.g.* FTSC *vs.* PTSC (2-pyridinecarboxaldehyde thiosemicarbazone), Table 1). Similar effect was found for p$K_{a2}$ in the case of COTI-2 and their derivatives. COTI-2 (Chart 2) has three dissociable groups: pyridinium-$NH^+$, dihydroquinolinium-$NH^+$ and hydrazonic-NH, while its derivatives (COTI-$NH_2$, COTI-$NMe_2$, and COTI-NMeCy, Chart 3) have the latter two groups only (dihydroquinolinium-$NH^+$ and hydrazonic-NH). The functionalization of *N*-terminal $NH_2$ group by dimethyl and cyclohexyl groups or conjugation with piperazine also decreases the dissociation constant of the hydrazonic-NH group [75]. Furthermore, the presence of a methyl group in the $R_2$ and/or $R_3$ positions increases both p$K_a$ values (*e.g.* FTSC *vs.* AcFTSC (2-acetylpyridine TSC), DpC and Dp44mT; triapine *vs.* Me-triapine, Table 1). Besides that, the amino group ($R_1$) in triapine significantly increases the basicity of the pyridinium nitrogen compared to FTSC but decreases the p$K_a$ of the hydrazonic nitrogen (Table 1). Similar effect was found for the same amino group substituted by one or two methyl groups (MeHNNMe$_2$, Me$_2$NNH$_2$, Me$_2$NNHMe and Me$_2$NNMe$_2$). Notably, the exchange of the sulfur atom (triapine) for oxygen (O-triapine) and selenium (Se-triapine) causes a change in the p$K_a$ in the opposite direction in values according to the changing electronegativity: in the case of Se-triapine they are lower, whereas for O-triapine they are higher than those of triapine. Huge difference was also found when pyridyl moiety was exchanged for imidazole, where p$K_{a2}$ was higher by *ca.* half an order of magnitude (*e.g.* FTSC *vs.* imidazole-TSC-HL[1], Table 1).

Moreover, exchange of the pyridyl scaffold to phenol moiety also affects the (de)protonation processes. Namely salicylaldehyde thiosemicarbazone (STSC) has two dissociable groups (phenolic hydroxyl and hydrazonic nitrogen), where the fully protonated form ($H_2L$) is neutral. The first deprotonation step takes place on the phenolic hydroxyl group, while p$K_{a2}$ is the same as for α-*N*-pyridyl (T)SCs. The negative charge of the $HL^-$ form, which appears after deprotonation of the phenolic hydroxyl group, is responsible for the increase of the second proton dissociation constant by more than one order of magnitude compared to FTSC. Similarly, the exchange of the sulfur atom to oxygen (STSC to salicylaldehyde semicarbazone (SSC)) increases the p$K_a$ of the hydrazonic nitrogen, where p$K_{a2}$ of SSC belongs to the dissociation of the phenolic hydroxyl group and p$K_{a1}$ belongs to the carbamoyl group (Table 1). It should be noted that the attachment of a sulfonate group to the phenol moiety considerably lower the p$K_a$ value of phenolic-OH group in comparison to STSC ($NaH_2L^{H\text{-}Ph}$ *vs.* STSC; Table 1), what could be explained by the large electron withdrawing effect of the sulfonate substituent [76].

It is noteworthy that the medium has also an effect on the p$K_a$ values. For example, the p$K_{a1}$ value for α-*N*-pyridyl-TSCs decreases, while the p$K_{a2}$ increases in the presence of DMSO, which can be explained by the Born electrostatic solvent model [83]. Based on that, the p$K_a$ of cationic acids (such as pyridinium nitrogen) decreases, while that of neutral acids increases as the relative permittivity of the solvent decreases. In this particular case, DMSO can solvate the neutral forms better than charged ones, which makes deprotonation more favorable in the first case and less favorable in the second one. In the case of STSC, p$K_{a1}$ increases in the DMSO/$H_2O$ mixture due to the charge neutralization by protonation of phenolic OH group, which belongs to the anionic bases.

TSCs possess another important feature that is the intrinsic fluorescence due to the conjugated electron system and rigid structure, which makes possible the determination of proton dissociation constants in water (*e.g.* for STSC, L-Pro-STSC, FTSC, PTSC) [78,79,82]. Moreover, this characteristic property can be used for monitoring the uptake and intracellular accumulation of TSCs in living human cancer cells by fluorescence microscopy [84].

**Table 1.** p$K_a$ values of some selected (T)SCs determined by UV-vis spectrophotometric titrations in $H_2O$ and/or 30% (*v*/*v*) DMSO/$H_2O$ ($I$ = 0.1 M (KCl)); log$D_{7.4}$ (*n*-octanol/$H_2O$) (partition coefficient at pH = 7.4), at 25 °C. Data taken from references [61,63,75-82], n.d. = not determined.

| | medium | p$K_{a1}$ | p$K_{a2}$ | log$D_{7.4}$ |
|---|---|---|---|---|
| **FTSC** | DMSO/$H_2O$ | 3.13 | 11.13 | +0.73 |
| | $H_2O$ | 3.48 | 10.72 | |
| **PTSC** | DMSO/$H_2O$ | 3.38 | 10.54 | +1.15 |
| | $H_2O$ | 3.61 | 10.22 | |
| **triapine** | DMSO/$H_2O$ | 3.92 | 10.78 | +0.85 |
| | $H_2O$ | 4.25 | 10.58 | |
| **O-triapine** | DMSO/$H_2O$ | 4.24 | >12.5 | +0.22 |
| **Se-triapine** | DMSO/$H_2O$ | 3.87 | 9.48 | +0.85 |
| **Me-triapine** | DMSO/$H_2O$ | 4.30 | >12.5 | +1.17 |
| **AcFTSC** | DMSO/$H_2O$ | 3.64 | 11.52 | +1.02 |
| **AcPTSC** | DMSO/$H_2O$ | 4.31 | 10.29 | +1.30 |
| | $H_2O$ | 4.64 | 10.09 | |
| **$H_2$NNHMe** | $H_2O$ | 4.40 | 11.03 | n.d. |
| **$H_2$NNMe$_2$** | $H_2O$ | 4.64 | 10.09 | n.d. |
| **MeHNNMe$_2$** | $H_2O$ | 4.87 | 9.87 | n.d. |
| **Me$_2$NNH$_2$** | $H_2O$ | 4.43 | 10.87 | n.d. |
| **Me$_2$NNHMe** | $H_2O$ | 4.53 | 10.98 | n.d. |
| **Me$_2$NNMe$_2$** | $H_2O$ | 4.93 | 10.69 | n.d. |
| **Dp44Mt** | $H_2O$ | 3.44 | 10.44 | n.d. |
| **DpC** | DMSO/$H_2O$ | 3.03 | 11.38 | n.d. |
| **Imidazole-TSC-HL$^1$** | $H_2O$ | 5.64[a] | 11.53 | n.d. |
| **Imidazole-TSC-HL$^4$** | $H_2O$ | 5.34[a] | 11.56 | n.d. |
| **COTI-2** | DMSO/$H_2O$ | 3.23 | 10.97 | n.d. |
| **COTI-NH$_2$** | DMSO/$H_2O$ | n.d. | 12.22 | +1.64 |
| **COTI-NMe$_2$** | DMSO/$H_2O$ | n.d. | 12.09 | n.d. |
| **COTI-NMeCy** | DMSO/$H_2O$ | n.d. | 12.40 | n.d. |
| **STSC** | DMSO/$H_2O$ | 8.89[b] | 12.59 | +1.74 |
| | $H_2O$ | 8.53[b] | >11.5 | |
| **SSC** | DMSO/$H_2O$ | ~1.9[c] | 9.32 | +1.04 |
| **L-Pro-STSC** | DMSO/$H_2O$ | 7.79[b] | 11.66 | n.d. |
| **NaH$_2$L$^{H}$** | $H_2O$ | 7.73[b] | n.d. | n.d. |
| **NaH$_2$L$^{Me}$** | $H_2O$ | 7.82[b] | n.d. | n.d. |
| **NaH$_2$L$^{Et}$** | $H_2O$ | 7.79[b] | n.d. | n.d. |
| **NaH$_2$L$^{Ph}$** | $H_2O$ | 7.73[b] | n.d. | n.d. |

[a] p$K_{a1}$ corresponds to deprotonation process of imidazole $NH^+$ group

[b] p$K_{a1}$ corresponds to deprotonation process of phenolic-OH group

[c] p$K_{a1}$ corresponds to deprotonation process of carbamoyl group

Another crucial property of TSCs was found during the solution studies; it is the Z/E isomerism (Chart 4) formed along the C=N double bond of TSCs, which can be investigated mainly by $^1$H NMR spectroscopy and DFT (density functional theory) calculations [79]. Usually, isomer E is the dominant species in the solution, although the distribution of isomers is extremely influenced by the pH and the solvent [85-87]. For instance, the presence of isomers for FTSC, PTSC, AcFTSC and AcPTSC ligands was examined by $^1$H NMR spectroscopy in DMSO-$d_6$, $D_2O$ and 30% (*v/v*) DMSO-$d_6$/$H_2O$ solvent mixture (at pH = 6, where the HL forms are dominant). It was found that only E form occur (*e.g.* in the case of FTSC) in polar solvents.

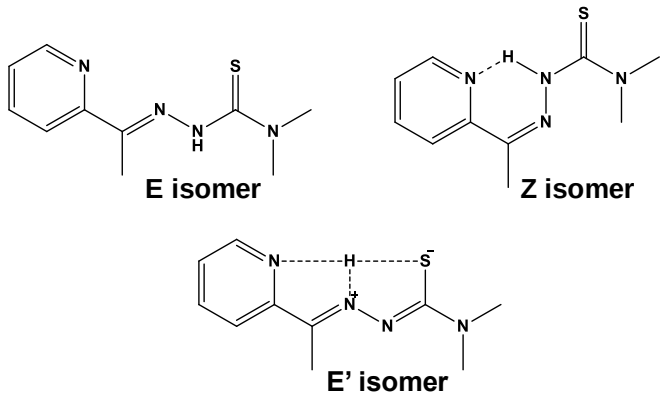


**Chart 4.** Proposed structure of the E, Z and E' isomers of the AcPTSC ligand (HL). The structures were taken from ref. [79].

In the *N*-terminal dimethyl substituted derivatives, the presence of the Z isomer is also significant, *e.g.* the ratio of the Z isomer around ~40% for PTSC in 30% (*v/v*) DMSO-$d_6$/$H_2O$ mixture at pH = 6. In the case of the AcPTSC ligand, besides Z and E isomers, a third species appears (E', Chart 4), which is a thioamide-type intramolecular bridged form with an extensively delocalized π electron system. PTSC derivatives such as morpholine and methylpiperazine conjugates (Chart 4) contain extra groups capable for deprotonation (Morf-PTSC: morpholinium-$NH^+$, mPip-PTSC: two piperazinium-$NH^+$) in addition to the pyridinium and hydrazonic nitrogens. For them the ratio of E and Z isomers were determined as well as the microconstants associated with their deprotonation. In those cases, where the p$K_a$ values of the same process greatly differ for the two isomers, a hydrogen bond system is supposed. Namely, the p$K_a$ microconstant of the given deprotonation process markedly increases due to the stabilization of the proton by more intramolecular hydrogen bonds (*e.g.* Morf-PTSC: p$K_{a3}$ (hydrazonic nitrogen) = 10.14 (E); >11.5 (Z)) [88].

Moreover, lipophilicity of (T)SCs was also investigated and their log$D_{7.4}$ are listed in Table 1. These ligands are present in their neutral HL form at physiological pH except STSC, which is partially negatively charged (in $H_2O$: 93% $H_2L$, 7% $L^-$). On one side, if a compound has

no charge, it can pass through cell membranes more easily than charged species, on the other side, it is accompanied with low aqueous solubility. It is important to take into account the current protonation state and the charge of the compounds during the comparison of log$D_{7.4}$ determined at physiological pH, which can be easily specified with the help of the determined p$K_a$ values. Taking into consideration the published data of some of them, it can be concluded that they depend on the substituents. Comparing FTSC with its derivatives, increased lipophilicity can be seen; the amino group at the $R_1$ position only slightly, while the *N*-terminal dimethyl substitution greatly increased it (Table 1). Moreover, methylation of the amino group of the pyridine ring also increases lipophilicity. It is worth to mention that changing the chalcogen atom also has an effect: O-triapine has decreased lipophilicity compared to that of triapine and Se-triapine, which were similar. The presence of the phenolic OH group instead of the pyridine nitrogen scaffold increases $D_{7.4}$ value by one order of magnitude (see Table 1, FTSC *vs.* STSC), and exchange of sulfur to oxygen reduces it (see in Table 1 STSC *vs.* SSC). It was an attempt to modify the hydrophilic-lipophilic property by pharmacophore substituents containing dissociable protons like *L*-Pro, morpholine, methylpiperazine, which were attached to the FTSC, PTSC and STSC ligand scaffolds. Indeed, it was possible to obtain much more hydrophilic compounds in water (log$D_{7.4}$ values: Morf-PTSC = +0.61, mPip-PTSC = –0.03, L-Pro-FTSC < –1.7, L-Pro-STSC = –0.60), which also resulted in remarkable aqueous solubility [82,88,89].

*2.4 The latest results of solution chemical studies of Cu(II)-(T)SC complexes*

Copper(II) complexes of TSCs often show anticancer activity, which can be even stronger than that of their corresponding free ligands [32,59,60,90-93]. At the same time, different mechanisms of action were suggested for Cu(II)-(T)SCs, in which the redox properties of Cu(II) ions play a crucial role [49,50,59,93]. A high number of Cu(II)-(T)SC complexes were developed, even so their behavior in aqueous solution has not always been thoroughly explored. Nevertheless, numerous data were reported by our research group over the past few years [33,40,61-63,75,77-82,88,89,94-98].

The Cu(II)-TSC complexes have different coordination modes and compositions depending on the type of the metal binding moiety, the actual pH and the metal-to-ligand ratio in the samples, however, the common feature of them is that they showed high stability in aqueous medium under biologically relevant conditions (pH = 7.4). Several methods were applied such as pH-potentiometry, EPR spectroscopy and UV-visible spectrophotometry for the investigation of the solution speciation of Cu(II)-(T)SC complexes in solution. These studies were performed usually in aqueous solution or in 30% (*v/v*) DMSO/$H_2O$ solvent mixture depending on the aqueous solubility of the compounds. For example, the α-*N*-pyridyl FTSC with (N,N,S) and the

salicylaldehyde STSC with (O,N,S) donor sets, respectively, mainly form mono-ligand complexes with Cu(II) ions; and different types of Cu(II) complexes were found by varying the pH [78,79]. In the case of the complexation of STSC, three different species of Cu(II) complexes was found, namely the protonated complex $[CuLH]^+$ in the acidic pH range, in which the ligand is coordinated via ($O^-$,N,S) donor atoms and the hydrazonic nitrogen is still protonated (Scheme 3).

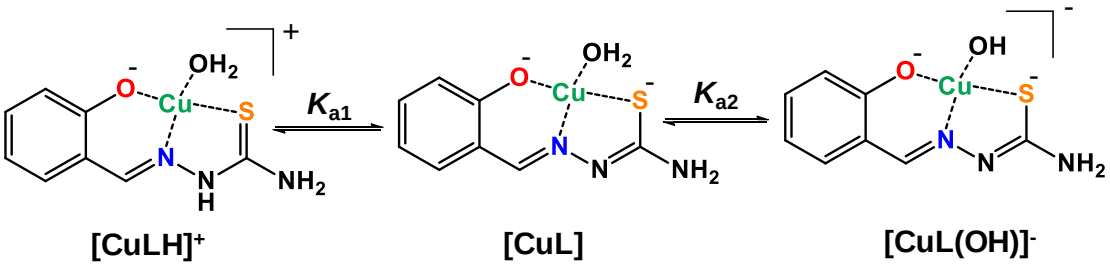


**Scheme 3.** Suggested structures for the Cu(II) complexes formed with STSC ligand [78].

Following the deprotonation of the hydrazonic nitrogen, the neutral [CuL] complex is formed with increasing pH, in which the ligand coordinates via ($O^-$,N,$S^-$) donor set and a mixed hydroxido $[CuL(OH)]^-$ complex appears in the basic pH range (Scheme 3) [78]. Similar behavior was observed for the L-Pro-STSC and sodium 5-sulfonate-STSC ($NaH_2L$) derivatives [76,82]. In the case of α-*N*-pyridyl-TSC derivatives (*e.g.* FTSC, triapine) mono complexes with similar compositions were also found, the only difference is the coordination of the neutral pyridine-N instead of the negatively charged phenolato-$O^-$, thus the $[CuL]^+$ complex has a positive charge. It is worth to mention that the excess of α-*N*-pyridyl-TSCs can lead to the formation of bis-ligand complexes and a dinuclear complex $[Cu_2L_3]^+$ [77].

Introduction of proline, morpholine and methylpiperazine moieties to the α-*N*-pyridyl and salicylaldehyde scaffolds provides extra donor atoms, which can participate in the coordination to Cu(II) ions [88,94-98]. It was confirmed by single-crystal X-ray diffraction (SXRD) analysis that the ligands L-Pro-FTSC, Morf-PTSC and mPip-PTSC are penta- or tetradentately coordinated to Cu(II) ions, and form only mono-ligand complexes (Fig. 2) [88,95].

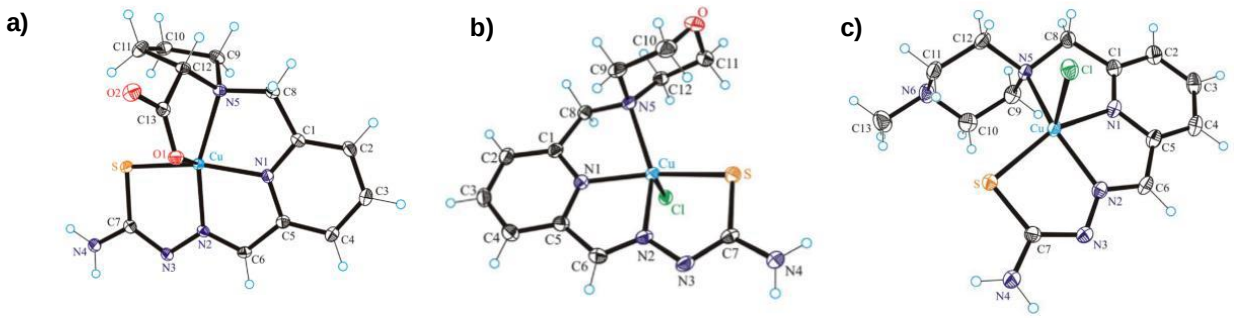


**Figure 2.** (a) L-Pro-FTSC, (b) Morf-PTSC and (c) mPip-PTSC ligands [CuL(Cl)] complexes; structures determined by X-ray crystallography and taken from ref. [88,95].

The stability of the reported Cu(II)-(T)SC complexes in solution usually expressed by the comparison of pCu(II) values, which is the negative decadic logarithm of the equilibrium concentration of the unbound Cu(II) ions under a chosen condition. It provides a solid basis for comparison of the stability of the complexes as the higher pCu value indicates stronger metal binding ability. In Fig. 3 some selected pCu values are presented for Cu(II)-(T)SC complexes at physiological pH. Based on these data, several trends can be observed, namely: the presence of the $NH_2$ group on the pyridine ring of triapine does not increase stability compared to FTSC; the stability of Cu(II)-(T)SC complexes decreases significantly with the S → O exchange (*e.g.* triapine *vs.* O-triapine, STSC *vs.* SSC); the *N*-terminal disubstitution by methyl groups increases the stability of Cu(II) complexes (*e.g.* triapine *vs.* AcPTSC); the replacement of the pyridine nitrogen with a phenolic OH group also increases the Cu(II)-binding capacity (*e.g.* FTSC *vs.* STSC); *N*-terminal substitution by methyl group of the amino group of the pyridine ring also increases the stability of Cu(II) complexes (*e.g.* triapine *vs.* $Me_2NNH_2$; AcPTSC *vs.* $Me_2NNMe_2$); the stability of the complexes in solution increases in the case of TSCs with extra donor atoms participating in the coordination [61,63,78,81]. It should be noted that the presence of DMSO can decrease the complex stability due to the possible competitive coordination of DMSO to the Cu(II) ions [99].

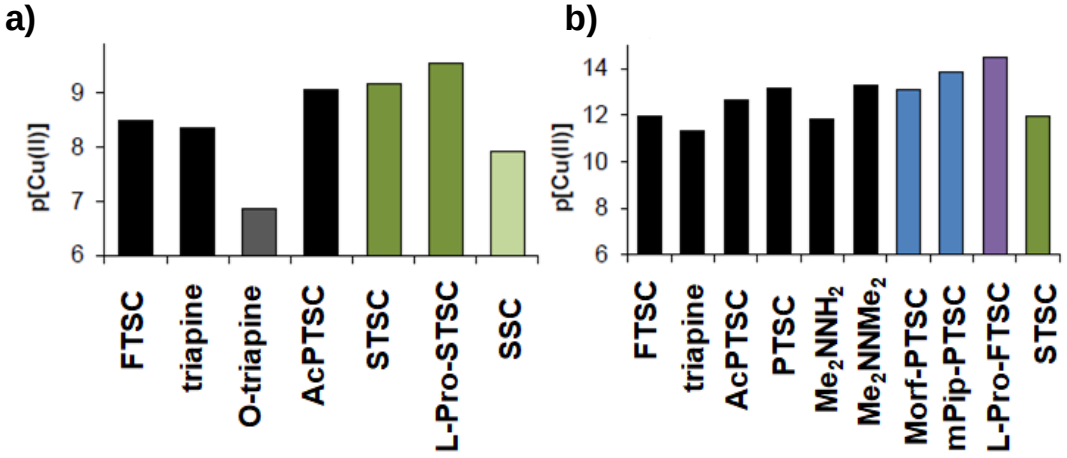


**Figure 3.** pCu values of some selected Cu(II)-(T)SC complexes a) determined in 30% (*v*/*v*) DMSO/$H_2O$ and b) in $H_2O$. {$c_L$=$c_{Cu}$ = 1 μM; pH = 7.4}. Figures were made based on the refs. [61,63,88,95,96].

Numerous *in vitro* cytotoxicity data measured for (T)SCs and their Cu(II) complexes on human cancer cell lines have been already published. Whereas in the case of triapine and its analogoues, primarily the anticancer activity was suggested to be related to the inhibition of RNR enzymes and the affinity towards iron ions (as mentioned above), other mechanisms of action was also assumed especially for the Cu(II) complexes of certain TSCs, which are formed intracellularly (*e.g.* Dp44mT, $Me_2NNMe_2$, see chapter 2.2) [60,92,100]. Furthermore, ligands such as, STSC, Morf-PTSC, mPip-PTSC and L-Pro-FTSC were practically non-toxic but their anticancer activity

significantly increased in the presence of Cu(II) [78,88,95]. All these four ligands form highly stable complexes with Cu(II) ions at physiological pH as well as α-*N*-pyridyl TSCs. However, an opposite trend was found for triapine, PTSC and $Me_2NNMe_2$, where the complexation with Cu(II) ions decreased the anticancer activity. It should be noted that the Cu(II) complexes of the latter two ligands exhibited the slowest reduction by GSH, which is most probably linked to their mechanism of action [61].

The presence of methyl substituent in different positions has also strong influence on the biological activity of TSCs. For example, the *N*-terminal dimethyl substitution of α-*N*-pyridyl-TSCs significantly increased cytotoxicity, while the same substitution of the amino group of the pyridine ring led to the opposite effect [61]. It is noteworthy that the conjugation of proline, methylpiperazine and morpholine to α-*N*-pyridyl and salicylaldehyde rings diminished the cytotoxicity, most probably due to the strongly increased aqueous solubility [88,94-98], highlighting the importance of the optimization of the hydrophilic-lipophilic character of the ligands for the proper activity.

*2.5 Aminophenols*

Aminophenols and their derivatives are important and well-known compounds due to their pharmaceutical, photographic and chemical dye industrial applications [101,102]. They possess a broad spectrum of biological activity, namely antiviral, antioxidant, antimalarial, antibacterial and even anticancer effects [103-108]. Also, several aminophenol derivatives are widely used as common drugs such as acetaminophen (paracetamol) and aminosalicylate compounds: para-aminosalicylic acid, balsalazide, olsalazine, sulfasalazine and mesalazine [101,109] Acetaminophen is one of the most frequently used drugs in the world, which shows analgesic and antipyretic effect [110,111]. Aminosalicylate compounds are commonly used for the treatment of inflammatory bowel disease, such as *ulcerative colitis* and Crohn's disease, and besides that sulfasalazine is also used against *rheumatoid arthritis*, para-aminosalicylic acid is used for the treatment of *tuberculosis* [112-114].

Aminophenols can behave as weak acids or weak bases, although their basic character predominates mostly. These compounds are also assigned as one of the most common class with redox active properties. These properties are originated from their two functional groups ($NH_2$ and OH), which could be oxidized and show similar behavior like anilines, phenols or hydroquinones. It should be noted that the relative position of the amino and hydroxyl group in the aromatic ring has a crucial role for the redox properties of these compounds [115].

The unsubstituted aminophenols have three isomeric forms, which depend on the positions of the amino and hydroxyl groups around the benzene ring, namely 2-aminophenol, 3-

aminophenol and 4-aminophenol (Chart 5). 3-Aminophenol is air-stable but 4-aminophenol and 2-aminophenol are oxidized easily under aerobic conditions [101]. It was found that 2-aminophenol and 4-aminophenol can act as a pro-oxidant in the presence of transition metals, however 3-aminophenol did not show this activity, what most probably could explain the pharmacological and toxicological properties of drugs with aminophenol scaffold [101].

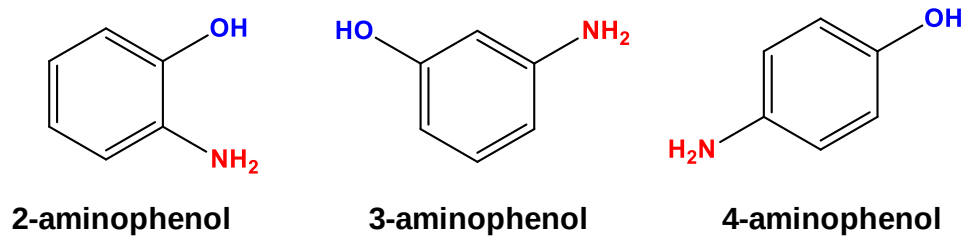


**2-aminophenol** **3-aminophenol** **4-aminophenol**

**Chart 5.** The three isomers of aminophenols.

Thanks to the amino and hydroxyl groups they can form coordinative bonds with metal ions, and 2-aminophenols usually bind to metal ions via (N,O) donor set and can form stable complexes. Metal complexation can enhance the biological activity of drugs, as it may result in higher lipophilicity leading to greater intracellular accumulation in addition to altered size, charge and redox properties. Various Zn(II), Cu(II), Ni(II), Co(II), VO(II)/(IV) and Mn(II) complexes bearing aminophenol derivatives were reported to possess antibacterial, antifungal and antimicrobial activities [116-121].

Despite the fact that until now many compounds with aminophenol derivatives and their metal complexes were synthesized displaying some biological activity, a comprehensive investigation on their behavior in solution was lacking. In the literature a few data were found about proton dissociation constants for some aminophenol derivatives and stability constants of their metal complexes [122-125], which are still quite incomplete, presumably due to the limited solubility of the compounds in water and their complicated redox nature.

## 3. Aims and objectives of the thesis

Unlike organic drug molecules, metal complexes usually behave as prodrugs, since their physiologically active form is different from the solid one due to the possible various transformation processes in biological systems. The pH of the extracellular and intracellular biological fluids (*e.g.* gastric and gastrointestinal fluid, blood, interstitial fluid and cytoplasm in cells) might change significantly, and various endogenous molecules are present as well, which can differ from the original form of compounds. Especially in the case of metal complexes, transformation processes show a wider diversity compared to the corresponding organic molecules. For example, in solution (de)protonation, ligand exchange, mixed ligand complex formation, redox reactions or irreversible decomposition can occur. These processes can change the original composition of the metal complex and have a strong impact on the physico-chemical properties as well. Moreover, in order to understand better the mechanism of action of biologically active compounds and establish their structure-activity relationships, it is important to know their behavior in aqueous solutions. Thus, detailed solution equilibrium studies can help in the structure optimization, specific targeting of bioactive compounds and successful development of future drugs.

In my doctoral thesis I have studied the behavior of anticancer (thio)semicarbazones, 2-substituted sterane-based compounds and their Cu(II) complexes in solution, where the main goals were the following:

i) Synthesis and characterization of Cu(II) complexes with (thio)semicarbazones and 2-aminophenols bearing (N,N,S), (O,N,S), (O,N,O) and (N,O) donor atoms. ii) Preparation of single crystals suitable for determining the structure of complexes by X-ray crystallography. iii) Detailed solution equilibrium studies with the combined use of different methods for ligands and their Cu(II) complexes. Namely, determination of proton dissociation constants of the ligands, the formation constants of the metal complexes, lipophilicity, membrane permeability, the stoichiometry of the formed species and the most plausible forms of the ligands and Cu(II) complexes at biologically relevant conditions. iv) Investigation of the redox properties of some selected Cu(II)-(T)SC complexes and interaction with physiological reductants such as GSH and AA in order to understand better their mechanism of action. v) Characterisation of antioxidant activity with 2,2-diphenyl-1-picrylhydrazyl (DPPH) assay.

Based on the obtained data, I tried to find correlations between the determined thermodynamic/kinetic parameters, physico-chemical properties, redox activity, crystallographic data and the biological effectiveness.

# 4. Materials and Methods

*4.1 Chemicals*

4-(2-Hydroxyethyl)-1-piperazineethanesulfonic acid (HEPES), GSH, AA, 6-hydroxy-2,5,7,8-tetramethylchroman-2-carboxylic acid (trolox), DPPH, $CuCl_2$, ethylenediaminetetraacetic acid (EDTA), tetrabutylammonium hexafluorophosphate ($n$Bu$_4$NPF$_6$), STSC, SSC, triapine, estradiol, 2-aminophenol, Eagle's Minimum Essential Medium cell culture (EMEM), Roswell Park Memorial Institute (RPMI) 1640 medium cell culture and human blood serum (HBS) were purchased from Sigma-Aldrich (Merck KGaA, Darmstadt, Germany). Methanol (MeOH), ethanol (EtOH), diethyl ether ($Et_2O$), *n*-octanol, DMSO, KCl, KOH, KH-phthalate, HCl, $NaH_2PO_4$ (sodium dihydrogen phosphate) and $Na_2HPO_4$ (disodium hydrogen phosphate) were obtained from Reanal Laborvegyszer Kft (Budapest). All these compounds were used without further purification.

*Sterane-based compounds and their models*: estrone-TSC (2-((3-hydroxy-estra-1,3,5(10)-triene-2-yl)methylene)hydrazine-1-carbothioamide), estrone-SC (2-((3-hydroxy-estra-1,3,5(10)-triene-2-yl)methylene)-hydrazine-1-carboxamide), Me-estrone-TSC (2-((3-hydroxy-estra-1,3,5(10)-triene-2-yl)methylene)-*N*-methylhydrazine-1-carbothioamide), Me$_2$-estrone-TSC (2-((3-hydroxy-estra-1,3,5(10)-triene-2-yl)methylene)-*N*,*N*-dimethylhydrazine-1-carbothioamide), thn-TSC (2-((1-hydroxy-5,6,7,8-tetrahydronaphthalene-2-yl)methylene)hydrazine-1-carbothioamide), thn-SC (2-((1-hydroxy-5,6,7,8-tetrahydronaphtalene-2-yl)methylene)hydrazine-1-carboxamide), Me-thn-TSC (2-((1-hydroxy-5,6,7,8-tetrahidronaphthalene-2-yl)methylene)-*N*-methylhydrazine-1-carbothioamide), Me$_2$-thn-TSC (2-((1-hydroxy-5,6,7,8-tetrahidronaphthalene-2-yl)methylene)-*N*,*N*-dimethylhydrazine-1-carbothioamide), estradiol-TSC (2-((3,17$\beta$-dihydroxy-estra-1,3,5(10)-triene-2-yl)methylene)hydrazine-1-carbothioamide), estradiol-SC (2-((3,17$\beta$-dihydroxy-estra-1,3,5(10)-triene-2-yl)methylene)hydrazine-1-carboxamide), Me-estradiol-TSC (2-((3,17$\beta$-dihydroxy-estra-1,3,5(10)-triene-2-yl)methylene)-*N*-methylhydrazine-1-carbothioamide), Me$_2$-estradiol-TSC (2-((3,17$\beta$-dihydroxy-estra-1,3,5(10)-triene-2-yl)methylene)-*N*,*N*-dimethylhydrazine-1-carbothioamide), 2-aminoestradiol (2-aminoestra-1,3,5(10)-triene-3,17$\beta$-diol), imidazole-TSC (2-((1*H*-imidazol-4-yl)methylene)hydrazine-1-carbothioamide), Me-imidazole-TSC (2-((1*H*-imidazol-4-yl)methylene)-*N*-methylhydrazine-1-carbothioamide), Me$_2$-imidazole-TSC (2-((1*H*-imidazol-4-yl)methylene)-*N*,*N*-dimethylhydrazine-1-carbothioamide) and benzimidazole-TSC (2-((1*H*-benzimidazol-2-yl)methylene)hydrazine-1-carbothioamide) were synthesized and characterized in the research group of Dr. Éva Frank (University of Szeged, Department of Molecular and Analytical Chemistry).

*Triapine analogues*: 2-formylpyridine 4-(4-hydroxy-3,5-dimethylphenyl)-thiosemicarbazone (VA1), 2-acetylpyridine 4-(4-hydroxy-3,5-dimethylphenyl)-thiosemicarbazone (VA2), 3-amino-2-formylpyridine 4-(4-hydroxy-3,5-dimethylphenyl)thiosemicarbazone (VA3); 5-methylenetrimethylammonium-thiosemicarbazonates: (*E*)-1-(3-((2-carbamothioylhydrazono)methyl)-4-hydroxyphenyl)-*N*,*N*,*N* trimethylmethanaminium (VA4), (*E*)-1-(4-hydroxy-3-((2-(methylcarbamothioyl)hydrazono)methyl)phenyl)-*N*,*N*,*N*-trimethylmethanaminium (VA5), (*E*)-1-(3-((2-(ethylcarbamothioyl)hydrazono)methyl)-4-hydroxyphenyl)-*N*,*N*,*N*-trimethylmethanaminium (VA6), (*E*)-1-(4-hydroxy-3-((2-(phenylcarbamothioyl)hydrazono)methyl)phenyl)-*N*,*N*,*N*-trimethylmethanaminium (VA7); morpholine conjugates with 2,6-dimethylphenol substituent: (*E*)-*N*-(4-hydroxy-3,5-dimethylphenyl)-2-((4-(morpholinomethyl)pyridin-2-yl)methylene)hydrazinecarbothioamide (VA8), (*E*)-*N*-(4-hydroxy-3,5-dimethylphenyl)-2-((5-(morpholinomethyl)pyridin-2-yl)methylene)hydrazinecarbothioamide (VA9), (*E*)-*N*-(4-hydroxy-3,5-dimethylphenyl)-2-((3-(morpholinomethyl)pyridin-2-yl)methylene)hydrazinecarbothioamide (VA10), (*E*)-*N*-(4-hydroxy-3,5-dimethylphenyl)-2-((6-(morpholinomethyl)pyridin-2-yl)methylene)hydrazinecarbothioamide (VA11) and their Cu(II) complexes were synthesized at the Institute of Inorganic Chemistry of the University of Vienna in the research group of Prof. Vladimir B. Arion.

The stock solutions of the tested compounds were prepared on a weight-in-volume basis dissolved in DMSO or $H_2O$. Their concentration was determined by pH-potentiometric titrations or based on the elemental analysis data of these compounds. $CuCl_2$ stock solution was made by the dissolution of anhydrous $CuCl_2$ in water and its exact concentration was determined by complexometry using EDTA. The stock solution of DPPH was stored in a place protected from light to avoid photolytic decomposition of the compound. The stock solutions of DPPH, GSH and AA were prepared freshly every day, before the measurements on a weight-in-volume basis in volumetric flask, where DPPH was dissolved in absolute EtOH, GSH and AA were dissolved in $H_2O$.

### *4.2 Preparation and characterization of Cu(II) complexes*

#### *4.2.1 Preparation of Cu(II) complexes of imidazole/benzimidazole-TSCs containing (N,N,S) donor atoms*

Imidazole/benzimidazole thiosemicarbazone Cu(II) complexes were obtained in a good yield (up to 84%) after the reaction between the corresponding TSC (1 equiv.) and $CuCl_2 \times 2\ H_2O$ (1 equiv.) in the presence of triethylamine ($Et_3N$) (1 equiv.). Afterwards, the solution was allowed to stand

in an open beaker at room temperature. The green crystalline product was filtered off, washed with $Et_2O$ (5-10 mL) and dried in air. Compounds were characterized by electrospray ionization mass spectrometry (ESI-MS) and UV-vis spectroscopy.

Cu(II)-imidazole-TSC: yield: 69%; ESI-MS (MeOH, positive): m/z 230.9635, 230.9639 calcd. for $[C_5H_6CuN_5S]^+$; m/z 498.8938, 498.8950 calcd. for $[C_{10}H_{12}Cu_2N_{10}S_2]Cl^-$; $\lambda_{max}$ in MeOH: 284, 338 nm.

Cu(II)-Me-imidazole-TSC: yield: 74%; ESI-MS (MeOH, positive): m/z 244.9786, 244.9796 calcd. for $[C_6H_8CuN_5S]^+$; m/z 526.9239, 526.9263 calcd. for $[C_{12}H_{16}Cu_2N_{10}S_2]Cl^-$; $\lambda_{max}$ in MeOH: 294, 334 nm.

Cu(II)-$Me_2$-imidazole-TSC: yield: 81%; ESI-MS (MeOH, positive): m/z 258.9948 , 258.9952 calcd. for $[C_7H_{10}CuN_5S]^+$; m/z 554.9562, 554.9576 calcd. for $[C_{14}H_{20}Cu_2N_{10}S_2]Cl^-$; $\lambda_{max}$ in MeOH: 298, 342 nm.

Cu(II)-benzimidazole-TSC: yield: 84%; ESI-MS (MeOH, positive): m/z 280.9794, 280.9796 calcd. for $[C_9H_8CuN_5S]^+$; m/z 598.9256, 598.9263 calcd. for $[C_{18}H_{16}Cu_2N_{10}S_2]Cl^-$; $\lambda_{max}$ in MeOH: 316, 407 nm.

*4.2.2 Synthesis of Cu(II) complexes of the thn-(T)SCs and estrone/estradiol (T)SCs containing (O,N,S) and (O,N,O) donor atoms*

These Cu(II) complexes were prepared by reaction between thn-(T)SCs or estrone/estradiol-(T)SCs (1 equiv.) with $CuCl_2$; the ligands were dissolved in MeOH (10 mL) and then the aqueous solution of $CuCl_2 \times 2\ H_2O$ (1 equiv.) was added. The pH was adjusted to pH ~ 7.4 by the addition of HEPES (10 mM, 5 mL). Green precipitate was formed. The precipitate was decanted, washed four times with water (5 mL each) and dried overnight at 50 °C. The Cu(II) complexes were characterized by ESI-MS, UV-vis spectrophotometry and elemental analysis.

Complex [Cu(thn-$TSCH_{-2}$)]: yield: 45%; ESI-MS (MeOH, positive): m/z 311.0156, 311.0154 calcd. for $[C_{12}H_{14}CuN_3OS]^+$; $\lambda_{max}$ in MeOH: 305, 396 nm.

Complex [Cu(Me-thn-$TSCH_{-2}$)]: yield: 49%; ESI–MS (MeOH, positive): m/z 325.0313, 325.0310 calcd. for $[C_{13}H_{16}CuN_3OS]^+$; $\lambda_{max}$ in MeOH: 318, 328, 397 nm.

Complex [Cu($Me_2$-thn-$TSCH_{-2}$)]: yield: 52%; ESI–MS (MeOH, positive): m/z 339.0452, 339.0467 calcd. for $[C_{14}H_{18}CuN_3OS]^+$; $\lambda_{max}$ in MeOH: 322, 333, 402 nm.

Complex [Cu(estrone–$TSCH_{-2}$)]: yield: 61%; ESI-MS (MeOH positive): m/z 433.0883, 433.0891 calcd. for $[C_{20}H_{24}CuN_3O_2S]^+$; $\lambda_{max}$ in MeOH: 318, 328, 392 nm.

Complex [Cu(Me-estrone-$TSCH_{-2}$)]: yield: 66%; ESI–MS (MeOH, positive): m/z 447.1028, 447.1042 calcd. for $[C_{21}H_{26}CuN_3O_2S]^+$; $\lambda_{max}$ in MeOH: 318, 329, 396 nm.

Complex [Cu($Me_2$-estrone-TSCH$_{-2}$)]: yield: 72%; ESI–MS (MeOH, positive): m/z 461.1196, 461.1198 calcd. for $[C_{22}H_{28}CuN_3O_2S]^+$; $\lambda_{max}$ in MeOH: 322, 335, 402 nm.

Complex [Cu(estradiol-SCH$_{-1}$)]: yield: 62%; Anal. calcd. for $C_{20}H_{25}CuN_3O_3 \times 1.75H_2O$: C, 53.32; H, 6.38; N, 9.33. Found: C, 53.32; H, 6.06; N, 9.14. ESI-MS (MeOH, positive): m/z 419.1261, 419.1270 calcd. for $[C_{20}H_{25}N_3O_3Cu]^+$; $\lambda_{max}$ in MeOH: 265, 303 and 383 nm.

Complex [Cu(estradiol-TSCH$_{-1}$)]: yield: 68%; Anal. calcd. for $C_{20}H_{25}CuN_3O_2S \times 1.3H_2O \times 0.4CH_3OH$: C, 51.99; H, 6.25; N, 8.92; S, 6.8. Found: C, 52.24; H, 6.4; N, 8.45; S, 6.4. ESI-MS (MeOH, positive): m/z 435.1038, 435.1042 calcd. for $[C_{20}H_{26}CuN_3O_2S]^+$; $\lambda_{max}$ in MeOH: 318 and 390 nm.

Complex [Cu(Me-estradiol-TSCH$_{-1}$)]: yield: 73%; Anal. calcd for $C_{21}H_{27}CuN_3O_2S \times 1.3H_2O$: C, 53.38; H, 6.31; N, 8.89; S, 6.79. Found: C, 53.60; H, 6.3; N, 8.56; S, 6.51. ESI-MS (MeOH, positive): m/z 449.1193, 449.1198 calcd. for $[C_{21}H_{28}CuN_3O_2S]^+$; $\lambda_{max}$ in MeOH: 322 and 400 nm.

Complex [Cu($Me_2$-estradiol-TSCH$_{-1}$)]: yield: 85%; Anal. calcd for $C_{22}H_{29}CuN_3O_2S \times 1.5\ H_2O$: C, 53.91; H, 6.58; N, 8.57; S, 6.54. Found: C, 53.55; H, 6.44; N, 8.69; S, 6.81. ESI-MS (MeOH, positive): m/z 463.1345, 463.1355 calcd. for $[C_{22}H_{30}CuN_3O_2S]^+$; $\lambda_{max}$ in MeOH: 320 and 401 nm.

*4.3 Methods used for the investigation of solution equilibrium processes*

*4.3.1 pH-potentiometry*

pH-potentiometry is one of the main methods for determining overall protonation constants of the ligands ($\beta(H_rL)$) and the overall stability constants of the metal complexes $\beta(M_pL_qH_r)$ by equilibrium titrations. In addition, determining the exact concentration of stock solutions of the ligands can also give information about the purity of the synthesized compounds by using this method. The competition between $H^+$ and the metal ion for the binding sites of the ligand allows us to perform pH-potentiometric studies:

$$qHL + M^{m+} \rightleftharpoons ML_q^{(m-q)+} + qH^+ \quad (1)$$

Therefore, the stability of the metal complex can be determined via the changes in the concentration of the $H^+$. The charges of the species are omitted for simplicity in the following equations. Equilibrium equations for the formation of the metal complex can be described in the following way:

$$pM + qL + rH \rightleftharpoons M_pL_qH_r \quad (2)$$

where, M denotes the metal ion, L the completely deprotonated ligand and H the proton.

The overall stability constants of the species can be defined as follows on the basis of the equations above:

$$\beta = \frac{[MpLqHr]}{[M]^p[L]^q[H]^r} \quad (3)$$

However, in order to obtain good-quality data from pH-potentiometric titrations, a trustable calibration of the electrode is required. For that purpose, a set of titrations with strong acid (HCl) and strong base (KOH) should be done, where titration data were evaluated using the Gran method [126] and the measurement system was calibrated using the Irving method [127].

The pH-potentiometric measurements for determination of the protonation constants and the overall stability constants of the metal complexes were carried out at 25.0 ± 0.1°C in water and/or in DMSO/$H_2O$ solvent mixtures (30:70 and/or 60:40 *v/v*) at an ionic strength (*I*) of 0.10 M (KCl) to keep the activity coefficients constant. The titrations were performed with carbonate-free KOH solution of a known concentration (0.10 M). The exact concentration of the KOH solution was determined by pH-potentiometric titrations using a standard solution of potassium hydrogen phthalate, and the HCl solution was standardized with the KOH titrant. An Orion 710A pH meter equipped with a Metrohm combined electrode (type 6.0234.100) and a Metrohm 665 Dosimat burette were used for the pH-potentiometric measurements. The electrode system was calibrated to the pH = –log[$H^+$] scale in water and in the DMSO/$H_2O$ solvent mixtures by the same method as it was mentioned above. The average water-ionization constants are 13.75 ± 0.01 in water, 14.53 ± 0.05 in 30% (*v/v*) DMSO/$H_2O$ and 16.22 ±0.05 in 60% (*v/v*) DMSO/$H_2O$ at 25°C, which corresponds well to the literature data [128-130]. The reproducibility of the titration points included in the calculations was within 0.005 pH units. The pH-potentiometric titrations were performed in the pH range 2.0–11.5 in water, 2.0–12.5 and 2.0–14.5 in 30% (*v/v*) and 60% (*v/v*) DMSO/$H_2O$ mixtures, respectively. The initial volume of the samples was 10.0 mL. The ligand concentration was in the range 1–2 mM, and metal-to-ligand ratios of 1:1–1:3 were used, where the initial concentration of the ligand was constant. Samples were deoxygenated by bubbling purified argon through them for approximately 10 min prior to the measurements. Argon was also passed over the solutions during the titrations. The proton dissociation constants of the ligands, the stoichiometry and overall stability constants of the complexes were determined with the computer program Hyperquad2013 [131]. The program gives the refined stability products by solving the mass balance equations (equations 4-6) written for the M, L and H components, where n denotes the number of associates formed in the system:

$$c_L = [L] + \sum_{i=1}^{n} q_i \beta_{qrp} [L]_i^q [H]_i^r [M]_i^p \quad (4)$$

$$c_H = [H] + \sum_{i=1}^{n} r_i \beta_{qrp} [L]_i^q [H]_i^r [M]_i^p \quad (5)$$

$$c_M = [M] + \sum_{i=1}^{n} p_i \beta_{qrp} [L]_i^q [H]_i^r [M]_i^p \quad (6)$$

*4.3.2 UV-vis spectrophotometry*

Ultraviolet-visible spectrophotometry is a fast analytical technique that measures the absorbance (or transmittance) of light. UV wavelength (200–380 nm) and visible light (380-800 nm) were used. Compounds absorb photons at specific wavelengths, whose energy is equivalent with the electronic transition energy differences. When UV-vis radiation interacts with chromophores, the electrons in the ground state will be excited, which we refer to as electron-excitation. In the case of metal complexes, absorption can be caused by the d-d transitions of the metal ions, the charge transfer band (CT band) between the metal ion and the ligand, or electron transitions within the ligand molecule (ligand band).

UV-vis spectrophotometry was used for determination of protonation (or proton dissociation) constants of the ligands, the overall stability constants of the Cu(II) complexes, and for the characterization of the prepared ligands and their Cu(II) complexes. For that purpose, an Agilent Cary 8454 diode array spectrophotometer was used to record the UV-vis spectra at an interval of 200–800 nm. The path length was 0.5-2 cm. Spectrophotometric titrations were performed at 25.0 ± 0.1ºC using a 0.1 M KOH titrant solution with or without 30% (*v/v*) DMSO content. Ionic strength of 0.10 M (KCl) was used in all UV-vis titrations and they were performed in the pH range 1.0–11.5 in water, 1.0–12.5 in 30% and 1.0–14.5 in 60% (*v/v*) DMSO/$H_2O$ mixture. The ligand concentration was varied between 20 μM and 120 μM concentration in the absence or in the presence of 1 or 0.5 equiv. Cu(II) ions. Proton dissociation constants ($K_a$) of the tested ligands, the overall stability constants ($\beta$) of the Cu(II) complexes and the UV-vis spectra of the individual species were calculated by the computer program PSEQUAD [132]. During titrations, pH was measured with the tools described in the pH-potentiometry section (chapter 4.3.1). Calculations were based on equations 1-6, with the addition of the molar absorbances of the light-absorbing species approximated by the program.

The redox reaction of the Cu(II) complexes with GSH and AA was studied at 25.0 ± 0.1 °C, at pH 7.40 (10 mM HEPES with 0.1 M KCl) on an Agilent Cary 8454 diode array spectrophotometer using a special, tightly closed tandem cuvette (Hellma Tandem Cell, 238-QS). The complex and the reducing agent were separated until the reaction was triggered. Both isolated pockets of the tandem cuvette were completely deoxygenated by bubbling argon for 10 min before mixing the reactants. Spectra were recorded before and then immediately after the mixing, and changes were followed till no further absorbance change was observed.

During the calculations, the absorbance (A)−time (t) curves were fitted and analyzed at the $\lambda_{max}$ of the complex. $(A_0 - A_{final}) \times e^{(-a \times t)} + A_{final}$ equation was used, where $A_0$, $A_{final}$ and $a$ parameters were refined and accepted at the minimal value of the weighted sum of squared residuals (difference between the measured and calculated absorbance values) at the given

wavelength. Then observed rate constants ($k_{obs}$) of the redox reaction were obtained from the data points of the simulated absorbance–time curves as the slope of the $\ln(A/A_0)$ versus $t$ plots.

The DPPH free radical scavenging capacity was studied at 25.0 ± 0.1 °C on an Agilent Cary 3500 spectrophotometer with tightly closed tandem cuvette. The reactants were separated until the reaction was triggered. UV-vis spectra were recorded before and then immediately after the mixing, and changes were followed till no further absorbance change was observed. From the stock solution of DPPH (100 μM) 0.5 mL was added to one pocket of the cuvette and 0.5 mL of the tested compound in different concentrations in EtOH was added to the other pocket. The final concentration of the studied compounds was in the range 5–50 μM, where the DPPH concentration was always 50 μM. A standard compound (trolox) was used as a positive control. The percentage of the scavenging activity, $IC_{50}$ values (the concentration of compound at which it reduced 50% of DPPH (half-maximal inhibitory concentration)) and trolox equivalent antioxidant capacity (TEAC, $IC_{50}$(trolox)/$IC_{50}$(compound)) were calculated [133].

$D_{7.4}$ values of ligands and the complexes were determined by the traditional shake-flask method in *n*-octanol/buffered aqueous solution at pH 7.40 (20 mM phosphate buffered saline (PBS)) at 25.0 ± 0.2 °C [134].

Parallel artificial membrane permeability assay (PAMPA) was applied for the ligands and complexes with a Corning Gentest pre-coated PAMPA Plate System [135]. In summary, the 96-well filter plate was used as the permeation acceptor and the 96-well bottom plate was used as the permeation donor. For simplicity, PBS (containing 4% (*v/v*) DMSO) was used both as donor and acceptor buffer throughout this study. The initial donor solutions were prepared by diluting DMSO stock solutions (500 μM) in PBS (25-fold dilution). The donor plate was filled with 300 μL of the donor solutions (containing the tested compounds). Each well of the filter plate contained 200 μL buffer as acceptor phase. The resulting 'sandwich' was protected with parafilm to prevent evaporation and incubated at room temperature at 25 °C for 5 h. Then, solutions from the donor and acceptor wells were transferred to Eppendorf microcentrifuge tubes and their UV-vis spectra were recorded to determine the concentration of the components. Effective permeability ($P_{eff}$) values were calculated according to the equation reported by Yu *et al*. [136].

*4.3.3 Fluorescence spectroscopy*

Fluorescence spectroscopy is a type of electromagnetic spectroscopy, which analyzes the fluorescence from a sample. In this spectroscopy, light passes through the sample and interacts with the fluorophore; during the relaxation of the excited state the molecule emits photons with lower energy (and longer wavelength) than the excitation wavelength, which are detected in 90° from the light source. Fluorescence is the molecular absorption of light energy at one wavelength

and its nearly instantaneous reemission at another longer wavelength. Fluorescent compounds have two characteristic spectra: an excitation spectrum (the wavelength and amount of light absorbed) and an emission spectrum (the wavelength and amount of light emitted). These spectra are often referred to as a compound's fluorescence signature or fingerprint. No two compounds have the same fluorescence signature. This is the principle that makes fluorometry a highly specific analytical technique. This has contributed to the use of this spectroscopy successfully in the detection of many organic compounds, numerous active substances in drugs, in the field of biochemical and medical analysis of organic compounds [137].

Herein fluorescence spectroscopy was used for recording three-dimensional spectra for the ligands and in some cases the deprotonation processes of the ligands were followed. The emission fluorescence spectra were recorded for ligands on a Hitachi-4500 spectrofluorometer using a 1 cm quartz cell. The fluorometric titrations were performed on samples containing the ligands at 1 μM concentration in the pH range from 5.0 to 11.5 titrated by KOH solution in pure aqueous solution. The titration system was the same as used for pH-potentiometry and UV-vis titrations (4.3.1 and 4.3.2). Spectra were corrected by the inner filter effect [137]. Proton dissociation constants ($K_a$) of the ligands were calculated by the computer program PSEQUAD [132] as it was discussed in chapter 4.3.2.

The fluorescence three-dimensional spectra for the ligands were recorded on the same spectrofluorometer using a 1 cm quartz cell. Samples contained 10 μM ligand in water at pH 7.40 (adjusted by PBS buffer) at 25.0 ± 0.1 °C.

*4.3.4 Nuclear magnetic resonance spectroscopy*

NMR spectroscopy is a method, which registers transitions between magnetic energy levels of atomic nuclei, caused by radio frequency radiation. Herein, $^1$H NMR spectroscopy was used for the investigation of the (de)protonation processes of the ligands.

NMR is the resonant absorption of electromagnetic waves by atomic nuclei, which occurs when the orientation of the vectors of their own moments of momentum (spins) changes. The only NMR-active nuclei are those whose spin quantum number ($I$) > 0 (in case of $^1$H $I$ = 1/2). The simple explanation of this method is that all nuclei are electrically charged and have multiple spins. Based on this, the external magnetic field creates the possibility of an energy transfer. When the proton is placed into an external magnetic field, the proton's magnetic dipole moment will orient itself along that magnetic field. However, since the proton can spin in one of two ways in any external magnetic field, it has two magnetic dipole moment orientations and so will align with the external magnetic field in one of two ways. One of these orientations will be along the same direction as the magnetic field and this is known as the spin-up (+1/2). This will be the lower in

energy and more stable spin state. The other orientation will be along the same axis as the magnetic field but in the opposite direction and this is known as the spin-down state (-1/2). This will be the higher in energy and less stable quantum spin state. If we now direct electromagnetic waves with just the right frequency at the spin-up state, the spin-up proton will absorb energy and transition to the spin-down state. Depending on the local electronic environment, the different protons in the molecule resonate at different frequencies. This frequency shift is converted into a dimensionless quantity independent of the magnetic field, known as the chemical shift (δ). The position and number of chemical shifts are characteristics of the structure of the molecule.

Herein, $^{1}$H NMR was used for performing pH-dependent NMR titrations in order to determine proton dissociation constants ($K_a$) of the ligands. $^{1}$H NMR spectroscopic studies were carried out on a Bruker Avance III HD instrument. All spectra were recorded with the WATERGATE water suppression pulse scheme using sodium trimethylsilylpropanesulfonate (DSS) internal standard. Samples usually contained 1 mM concentration of the ligand in a 10% (*v*/*v*) $D_2O/H_2O$, 30% or 60% (*v*/*v*) DMSO-$d_6$/$H_2O$ mixture and were titrated at 25.0 °C, at $I$ = 0.10 M (KCl). During the titrations the changing of chemical shifts of the different group of the molecules were observed, which were sensitive for deprotonation processes. Since deprotonation processes are fast on the NMR time scale, deprotonated and protonated forms cannot be detected separately. This is the result of the fast exchange between two forms, where only one signal is observed reflecting the population-weighted averages of chemical shifts, intensity and linewidth. Afterwards, chemical shifts of the protons were collected in all measured pH values, which were sensitive for deprotonation process and from these data the p$K_a$ proton dissociation constant of ligands were calculated with the PSEQUAD program [132]. The pH was measured with the tools described in the case of pH-potentiometry (chapter 4.3.1).

*4.3.5 Electron paramagnetic resonance spectroscopy*

This type of spectroscopy is used to study systems containing unpaired electrons (paramagnetic compounds). The basic concepts of EPR are analogous to those of NMR (see chapter 4.3.4), however, the difference is that the spin of the electrons are excited instead of the atomic nuclei. Herein, EPR spectroscopy was used to study the structures of paramagnetic Cu(II) complexes, since this technique is extremely sensitive to the chemical environment of the unpaired electron. EPR spectra were recorded at room temperature (isotropic spectra) and at 77 K (anisotropic spectra) in DMSO solution in order to confirm the coordination modes of isolated Cu(II) complexes. Evaluation of the obtained EPR spectra by simulation software [138] provides the isotropic and anisotropic parameters. Namely, isotropic parameters reveal the types of the coordinating donor atoms around the Cu(II) and *g*-factor relates the energy of an unpaired electron,

whereas anisotropic parameters provide information about the geometry and symmetry (the number, identity and distance of the coordinating donor atoms) of the complexes.

For that purpose, a BRUKER EleXsys E500 spectrometer (microwave frequency 9.54 GHz, microwave power 13 mW, modulation amplitude 5 G, modulation frequency 100 kHz) was used. Powder of the Cu(II) complexes was dissolved in pure DMSO to obtain ~3 mM concentration in the solutions. The room temperature EPR spectra were recorded in capillaries applying 12 scans. For the frozen solution spectra 0.10 mL samples were diluted with 0.10 mL water and transferred into EPR tubes and the spectra were recorded in Dewar containing liquid nitrogen (77 K). Also, in order to obtain information about the major species at physiological pH EPR spectra of the frozen solutions of $CuCl_2$ in EMEM, RPMI 1640 cell culture media and in HBS were recorded at a concentration of 2 mM and in HEPES (0.6 mM, pH 7.4). The Cu(II) complexes were dissolved in HEPES, EMEM, RPMI 1640 media and in serum in 1.7 mM concentration and measured in frozen solution (77 K). The room temperature spectra were corrected by substracting the background spectrum of pure DMSO. The spectra were simulated by the "EPR" program [138] using the parameters $g_o$, $A_o$ copper hyperfine ($I_{Cu}$ = 3/2) coupling and four linewidth parameters. The anisotropic EPR spectra were analyzed with the same program. Rhombic g-tensor ($g_x$, $g_y$, $g_z$) and copper hyperfine tensor ($A^{Cu}{}_x$, $A^{Cu}{}_y$, $A^{Cu}{}_z$) have been used. The nitrogen superhyperfine structure was taken into account with a rhombic hyperfine tensor ($a^N{}_x$, $a^N{}_y$, $a^N{}_z$), where the *xyz* directions referred to the g-tensor orientations. Orientation-dependent linewidth parameters ($\alpha$, $\beta$, and $\gamma$) were used to fit the linewidths through the equation $\sigma_{MI} = \alpha + \beta M_I + \gamma M_I^2$, where $M_I$ denotes the magnetic quantum number of Cu(II) ion. Since $CuCl_2$ was used for the measurements, all spectra were calculated by the summation of spectra $^{63}$Cu and $^{65}$Cu weighted by their natural abundances. The hyperfine and superhyperfine coupling constants and the relaxation parameters were obtained in field units (1 G = $10^{-4}$ T).

All these measurements and data evaluation were perfomed with the help of Dr. Nóra V. May (Research Centre for Natural Sciences, Budapest).

*4.3.6 Cyclic voltammetric and spectroelectrochemical studies*

Cyclic voltammetry (CV) is a simple and direct method for measuring the formal potential of a half-reaction when both oxidized and reduced forms are stable during the time required to obtain the voltammogram (current-potential curve). A CV system includes an electrolysis cell, a potentiostat, a current-to-voltage converter and a data acquisition system. The electrolysis cell requires three electrodes: reference electrode, working electrode and counter electrode. The potential of the working electrode is varied linearly with time, while the reference electrode maintains a constant potential. The counter electrode conducts electricity from the signal source

to the working electrode. In addition, the electrolytic solution is required to provide ions to the electrodes during oxidation and reduction. A potentiostat is an electronic device, which used as a power source to produce the needed potential, which can be maintained and accurately determined, while allowing small currents to be drawn into the system without changing the voltage. The current-to-voltage converter measures the resulting current, and the data acquisition system produces the resulting voltammogram.

Herein, CV was used in combination with UV-vis spectrophotometry, which can provide comprehensive information about the chemical processes driven by the electron transfer for investigation the redox properties of Cu(II) complexes. The method of UV-vis spectrophotometry was described in the chapter 4.3.2.

Cyclic voltammograms of Cu(II) complexes were recorded at 25.0 ± 0.1 °C. *n*$Bu_4NPF_6$ was used as supporting electrolyte and measurements were performed at different pH values (2, 3, 5, 7.4 and 12). The complexes were obtained *in situ* by mixing the ligand (dissolved in DMSO) with aqueous solution of $CuCl_2$ in 1:1 ratio. The final concentration of the complexes in the stock solution was 1 mM. Measurements were performed on a conventional three-electrode system under argon atmosphere using an Autolab PGSTAT 204 potentiostat/galvanostat monitored with Metrohm's Nova software [139]. Samples were purged for 10 min with argon before recording the cyclic voltammograms. Platinum electrode was used as the working and auxiliary electrode and Ag/AgCl/3 M KCl as the reference electrode. The electrochemical system was calibrated with an aqueous solution of $K_3[Fe(CN)_6]$ ($E_{1/2}$ = +0.458 V vs. NHE (normal hydrogen electrode)) [140]. Redox potentials were obtained at different scan rates between 10-100 mV/s in the range of −1.3 to +1.0 V.

*In situ* UV-vis spectroelectrochemical measurements were performed on a spectrometer (Avantes, Model AvaLight-DHc light source) equipped with an AvaSpec-UL2048XL-EVO in the spectroelectrochemical cell kit (AKSTCKIT3) with the Pt-microstructured honeycomb working electrode, purchased from Pine Research Instrumentation (Lyon, France). The cell was positioned in the CUV-UV cuvette holder connected to the diode-array UV-vis spectrometer by optical fibers. The spectra were processed using the AvaSoft 8.1.1 software package.

Measurements and data evaluation for Cu(II) complexes of imidazole-derived thiosemicarbazones were done with the help of Prof. Peter Rapta (Slovak University of Technology, Institute of Physical Chemistry and Chemical Physics, Bratislava, Slovakia).

*4.4 Other experiments*

Several single crystals of the Cu(II) complexes were synthesized by me, which were used for the **single-crystal X-ray diffraction** analyzed and solved by Dr. Nóra V. May (Research Centre for

Natural Sciences, Budapest, Hungary). **Elemental analysis** was performed for Cu(II)-estradiol-(T)SCs and Cu(II)-Me-thn-TSC complexes by Mr. Johannes Theiner (Institute of Inorganic Chemistry, University of Vienna, Vienna, Austria). **ESI-MS** measurements were performed by Dr. Zoltán Kele (Department of Medicinal Chemistry, University of Szeged) and by the Mass Spectrometry Centre (University of Vienna, Austria). Our collaborating partners performed **antibacterial activity and *in vitro* cytotoxicity assay** measurements. Different cell lines and bacterial strains were used. Determination of anticancer activity on Colo205 doxorubicin-sensitive colon adenocarcinoma, Colo320 doxorubicin-resistant colon adenocarcinoma, MCF-7 breast cancer, HeLa cervical cancer, SH-SY5Y neuroblastoma and non-cancerous MRC-5 embryonal lung fibroblast cells were done by Dr. Gabriella Spengler (Department of Medical Microbiology, Albert Szent-Györgyi Health Center and Albert Szent-Györgyi Medical School, University of Szeged). Moreover, she tested antibacterial activity on Gram-positive (*Staphylococcus aureus* and *Enterococcus faecalis*) and Gram-negative (*Escherichia coli* and *Klebsiella pneumoniae*) bacterial strains. MCF-7 breast cancer, MCF-7KCR multidrug-resistant breast cancer, DU145 prostate cancer, A549 lung carcinoma cells were used by Dr. Mónika Kiricsi (Department of Biochemistry and Molecular Biology, University of Szeged). 3D spheroids were also used for investigation of anticancer activity such as A549 lung carcinoma, CH1/PA ovarian carcinoma, SW480 colonic adenocarcinoma, HCT-116 colorectal carcinoma cells by Dr. Debora Wernitznig (Institute of Inorganic Chemistry, University of Vienna, Vienna, Austria). MES-SA (human uterine sarcoma) and in its multidrug-resistant counterpart (MES-SA/Dx5) cells by Dr. Gergely Szakács (Medical University of Vienna).

# 5. Results and discussion

## *5.1 Formaldehyde TSCs with 2,6-dimethylphenol substituent and their Cu(II) complexes*

### *5.1.1 Triapine analogues with 2,6-dimethylphenol substituent*

In the introduction, triapine was already mentioned as a well-known representative of the α-*N* heterocyclic TSCs class, which is currently under clinical studies. Nevertheless, its efficacy and physico-chemical properties can be improved for a better pharmacokinetic profile and to overcome adverse effects via structural modifications (chapter 2.2). Novel derivatives with a redox active phenolic moiety at the terminal nitrogen atom were developed by our collaboration partner (V.B. Arion, University of Vienna). The solution chemical properties of three triapine analogues (Chart 6) were studied as well as the stability and redox properties of their Cu(II) complexes.

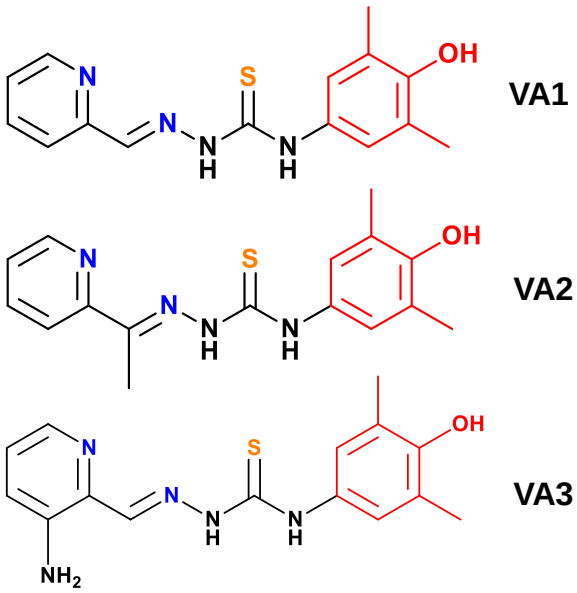


**Chart 6**. Chemical structures of the studied ligands with 2,6-dimethylphenol substituent: VA1, VA2 and VA3.

#### *5.1.1.1 Investigation of the proton dissociation processes and lipophilicity of VA1-3*

First of all, solution stability of the VA1-3 ligands was studied in the presence of 30% (*v/v*) DMSO/$H_2O$ at various pH values under argon due to the redox activity of the aminophenolic moiety [115]. For that purpose, UV-vis spectra were recorded during 3 h at pH 1.5, 7.4 and 12. It is worth to mention that at pH 1.5 the relatively slow decomposition (around 6%) was observed for the ligand VA2 (Fig. 4), which is most probably due to the cleavage of the C=N imine bond, whereas for VA1 and VA3 no significant spectral changes were observed. This hydrolytic decomposition was already reported for AcFTSC [79]. On the contrary, all studied ligands were stable at pH 7.4. However, significant spectral changes were detected at pH 12 for all ligands,

which is a consequence most probably of the oxidation 4-aminophenyl moiety to *p*-benzoquinone imine.

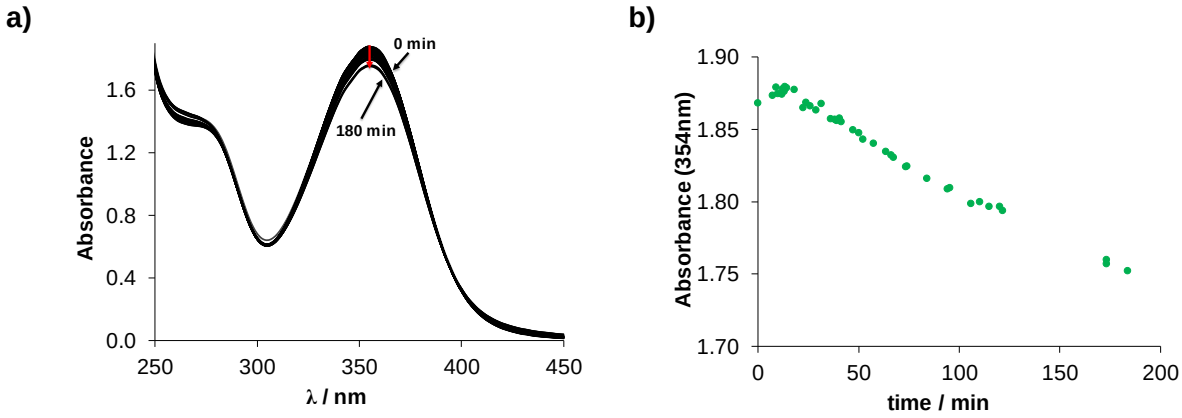


**Figure 4.** a) UV-vis absorption spectra recorded for VA2 at pH 1.5 over 3 h. b) Absorbance values at 354 nm plotted against the time. {$c_L$ = 100 μM; 30% (*v*/*v*) DMSO/$H_2O$; $I$ = 0.1 M (KCl); $T$ = 25 °C; $\ell$ = 1 cm}. These figures were adapted from publication [P4].

Investigation of the (de)protonation processes of bioactive compounds is an important task, since they have the major effect on the actual protonation form and charge of the dominant species at a given pH. The proton dissociation constant ($K_a$) is one of the main parameters, which has an impact on aqueous solubility and lipophilicity. Herein, proton dissociation processes of VA1-3 were studied by UV-vis spectrophotometry in 30% (*v*/*v*) DMSO/$H_2O$ solvent mixture at fairly low concentrations (50 μM) due to the limited aqueous solubility of the ligands. The protonated forms of these α-*N*-pyridyl TSCs have three dissociable groups, namely pyridinium-$NH^+$, the hydrazonic-NH and the phenolic-OH; however, only two p$K_a$ values could be determined in the studied pH-range (1.0 – 12.5). Representative UV-vis spectra for VA2 are shown in Fig. 5. Significant spectral changes can be observed, and two individual steps were distinguished by deconvoluting the spectra. Due to the structural similarity to triapine, the first deprotonation process can be attributed to pyridinium-$NH^+$, where the shift of the absorption band was observed to the higher wavelengths with $\lambda_{max}$ = 316 nm in the acidic pH range (Fig. 5.a). The second step was seen at pH > 7, where the $\lambda_{max}$ moved from 316 nm to 390 nm (Fig. 5.b) belonging most probably to the deprotonation of hydrazonic-NH. Moreover, irreversible alteration of the spectra was seen at pH > 11 in the range 370-570 nm, which can be explained by the oxidation of the ligand by the atmospheric oxygen to 4-aminophenoxyl radical and/or to 4-benzoquinone imine, which hindered the accurate determination of the p$K_a$ of the phenolic-OH group.

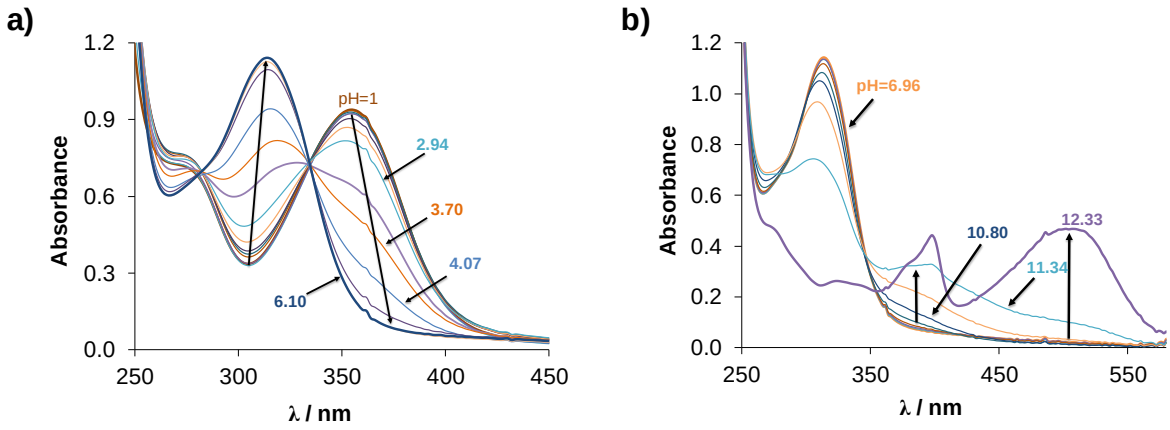


**Figure 5.** UV-vis absorption spectra recorded for VA2 in the pH range a) 1.00 – 6.10 and b) 6.96 – 12.33. {$c_L$ = 50 μM; 30% (*v*/*v*) DMSO/$H_2O$; $I$ = 0.1 M (KCl); $T$ = 25 °C; $\ell$ = 1 cm}

Similar processes were observed for the VA1 and VA3 ligands. Accordingly, two p$K_a$ values were determined based on the measured UV-vis spectra for the ligands VA1 and VA2 (Table 2). Only one p$K_a$ value was determined for VA3 ligand, namely for pyridinium-$NH^+$, due to the fact that the deprotonation process of hydrazonic-NH partly overlapped in the pH range of the oxidation of the 4-aminophenyl moiety. Taking into account the differences between the p$K_a$ values of the ligands, the following trend was found for pyridinium-$NH^+$: VA3 > VA2 >VA1. This can be explained by the electron-donating effect of methyl group in the VA2 ligand and amino group at the pyridine ring in the VA3 ligand, respectively. A similar trend was observed for FTSC and AcFTSC analogues [79,141]. The obtained individual molar UV-vis spectra of the VA2 species in the different protonation states are shown together with concentration distribution curves computed on the basis of the obtained p$K_a$ values in Fig. 6. At physiological pH the charge-neutrality of the studied ligands can be seen.

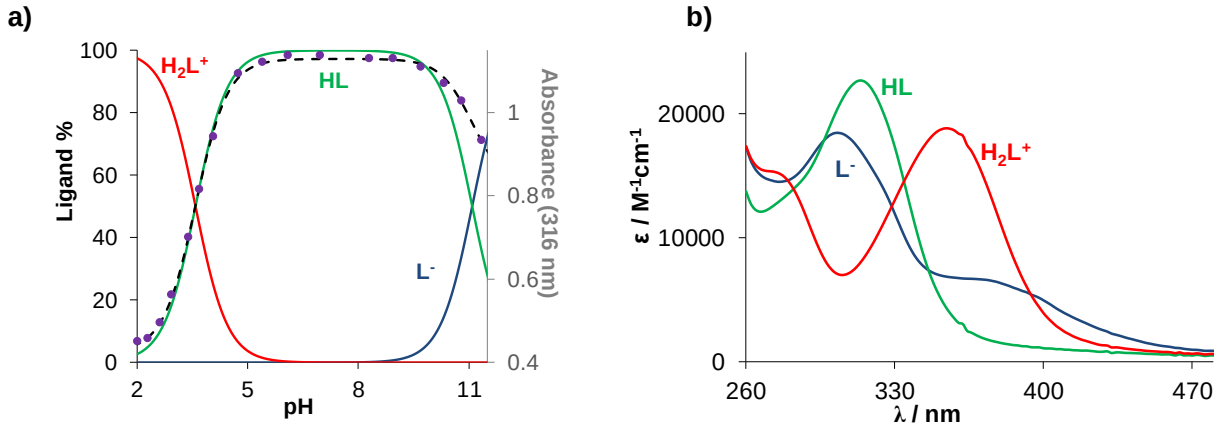


**Figure 6**. a) Concentration distribution curves of VA2 plotted together with the absorbance changes at 316 nm (●) with the fitted curve (dashed line). b) Molar absorbance spectra of VA2 ligand species in the different protonation states. {$c_L$ = 50 μM; 30% (*v*/*v*) DMSO/$H_2O$; $I$ = 0.1 M (KCl); $T$ = 25 °C; $\ell$ = 1 cm}

In addition, the lipophilicity of the studied compounds was investigated as well, which provides information about the ability of compounds to penetrate through biological membranes. First of all, log$D_{7.4}$ values were determined using the traditional shake-flask method in *n*-octanol/HEPES buffered aqueous solution at pH 7.40 (Table 2). Based on the obtained data, it can be concluded that these compounds showed high lipophilic character. The highest lipophilicity was found in case of VA2, which might be the result of the presence of the methyl substituent. These ligands were found more lipophilic than their structural models (log$D_{7.4}$(FTSC) = +0.73; log$D_{7.4}$(AcFTSC) = +1.02; log$D_{7.4}$(triapine) = +0.85) [79] due to presence of the lipophilic 2,6-dimethyl-4-aminophenyl moiety.

**Table 2.** p$K_a$ values determined by UV-vis titrations in 30% (*v/v*) DMSO/$H_2O$ and log$D_{7.4}$ (*n*-octanol/water) values of the ligands VA1, VA2 and VA3 and their Cu(II) complexes. Conditional stability constants (log$K'_{5.9}$) of the complexes determined by UV-vis EDTA displacement studies in 30% (*v/v*) DMSO/$H_2O$ and observed rate constants ($k_{obs}$) obtained for the redox reaction of the complexes with GSH (pH = 7.4 (50 mM HEPES); $c_{Cu} = c_L$ = 25 μM; $c_{GSH}$ = 1.25 mM). (n.d. = not determined) {$T$ = 25 °C; $I$ = 0.1 M (KCl)} This table was adapted from publication [P4].

| | **method** | **VA1** | **VA2** | **VA3** |
|---|---|---|---|---|
| **p$K_a$** ($N_{pyridinium}H^+$) | UV-vis | 3.01±0.01 | 3.59±0.02 | 3.95±0.04 |
| **p$K_a$** ($N_{hydrazonic}H$) | UV-vis | 10.55±0.01 | 11.08±0.02 | n.d. |
| **log$D_{7.4}$** (ligand) | partitioning | +1.30±0.03 | +2.1±0.1 | +1.67±0.01 |
| **log$K'_{5.9}$** (complex) | EDTA displacement | 9.67±0.01 | n.d. | 9.78±0.01 |
| **log$D_{7.4}$** (complex) | partitioning | –0.40±0.06 | n.d. | –0.42±0.03 |
| **$k_{obs}$ ($min^{-1}$)** (complex) | UV-vis (with GSH) | 0.033±0.004 | n.d. | 0.035±0.004 |

*5.1.1.2 Stability of Cu(II) complexes of VA1-3 in solution and their redox properties*

The stability and solution speciation of the Cu(II) complexes of the triapine analogues were studied by UV-vis spectrophotometry. Previously published data for 2-formylpyridine TSC and triapine showed the formation of Cu(II) complexes with considerably high stability, in which the ligands are coordinated through ($N_{pyridine}$,N,$S^-$) donor set, which predominates in a wide pH range [77,79]. In acidic pH range, these complexes are protonated bearing ($N_{pyridine}$,N,S) donors, and in the basic pH range mixed hydroxido species with ($N_{pyridine}$,N,$S^-$)(OH) coordination mode were reported. For studying the complex formation processes of VA1-3 with Cu(II) ions, UV-vis spectrophotometric titrations were conducted in 30% (*v/v*) DMSO/$H_2O$ solvent mixture. Representative UV-vis spectra recorded for the Cu(II)-VA1 system are presented in Fig. 7, which show that significant complex formation undergoes already at low pH values (pH ~ 1) as the obtained spectra are considerably different from that of the ligand. In the pH range between 1 and 3 only one process was observed, which was assigned to the deprotonation of the hydrazonic nitrogen in the bound ligand (Chart 7: $[CuLH]^{2+} \rightarrow [CuL]^+$) with an estimated upper limit for the p$K_a$ value of complex

$[CuLH]^{2+}$ < 1.5. Afterwards, in a wide pH range (2.7 – 7.6) no spectral changes were found indicating the presence of only one type of complex with the tridentate coordination mode ($N_{pyridine}$,N,$S^-$), where the hydrazonic nitrogen is fully deprotonated and corresponds to the suggested structure $[CuL]^+$ as it is shown in Chart 7. This suggested structure was proved by X-ray crystallography, where the ligand coordinates to Cu(II) in a square-planar coordination geometry and the coordination sphere is completed by a chlorido ligand. (The crystallization was done by the group of V.B. Arion, University of Vienna.)

By increasing the pH, two overlapping processes are displayed at pH > 8. Based on these spectral changes two proton dissociation constants (p$K_a$ = 9.80±0.01 and p$K_a$ = 11.02±0.01) were computed. These processes can be attributed to the deprotonation of aqua ligand resulting in a mixed hydroxido complex parallel to the deprotonation of the phenolic OH of the bound ligand.

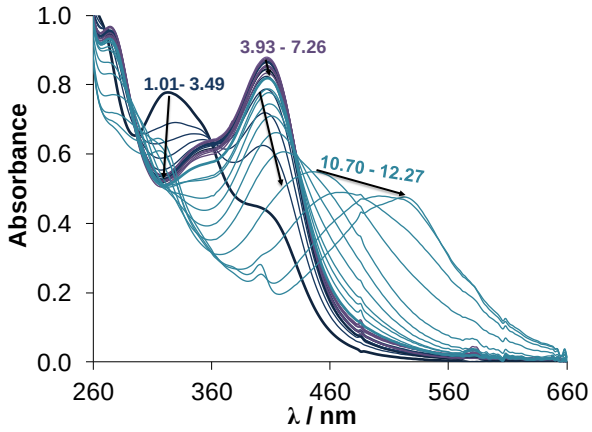


**Figure 7.** UV-vis absorption spectra recorded for Cu(II)-VA1 (1:1) system in the pH range 1.01 – 12.27. {$c_L = c_{Cu}$= 50 μM; 30% (*v*/*v*) DMSO/$H_2O$; $I$ = 0.1 M (KCl); $T$ = 25 °C; $\ell$ = 1 cm}

For the Cu(II)-VA3 system similar spectral changes were observed. Nevertheless, precipitation was observed at pH > 8, which hindered the determination of the proton dissociation constants of the complexes. It should be noted that during the titration of the Cu(II)-VA2 system, precipitation was observed already in the acidic pH range, which hindered data evaluation.

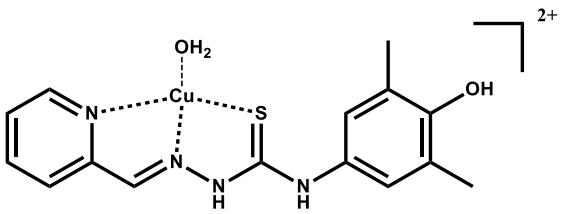


**[CuHL]$^{2+}$**

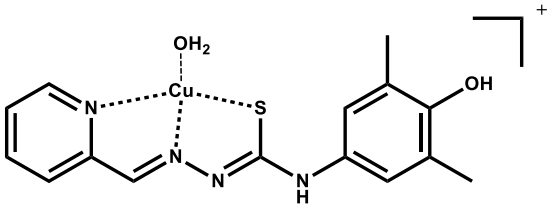


**[CuL]$^{+}$**

**Chart 7.** Suggested structures for the Cu(II) complexes formed with VA1 ligand (Notably, the chloride ions are originally coordinated in solid phase and most likely replaced by water molecules in aqueous solution due to the very weak Cu–Cl coordinative bond.). Chart was taken from publication [P4].

For the sake of comparison, EDTA displacement experiments were performed to characterize the stability of the Cu(II) complexes of VA1 and VA3 in solution using UV-vis spectrophotometry. This study was done at pH 5.9, where all complexes have the dominant $[CuL]^+$ species. Since the displacement of the VA1 and VA3 ligands by EDTA is relatively slow based on the time dependence measurements, a two-hour-equilibration time was applied. The spectral change in Fig. 8.a shows that the absorbance of the S→Cu CT band at $\lambda_{max}$ = 444 nm decreases due to the fact that EDTA replaces the VA3 ligand, while the absorption band of the free ligand increases at $\lambda_{max}$ = 372 nm. Taking into account these spectral changes, the conditional stability constant for the Cu(II)-VA3 complex was computed (Figs. 8.a,b, Table 2). Similarly, the conditional stability constant for the Cu(II)-VA1 complex was obtained (Table 2). These constants are rather similar to each other and just slightly higher than that of the complex of triapine ($\log K'_{5.9}$ = 9.47 calculated based on previously published data [61]). It can be concluded that the 2,6-dimethylphenol moiety does not have significant influence on the thermodynamic stability of these α-*N*-pyridyl TSC complexes. Obtained data revealed the formation of highly stable complexes based on the $\log K'_{5.9}$ values. The conditional stability constant for the Cu(II)-VA2 complex was not determined due to the formation of precipitation, which was observed during the EDTA displacement experiment.

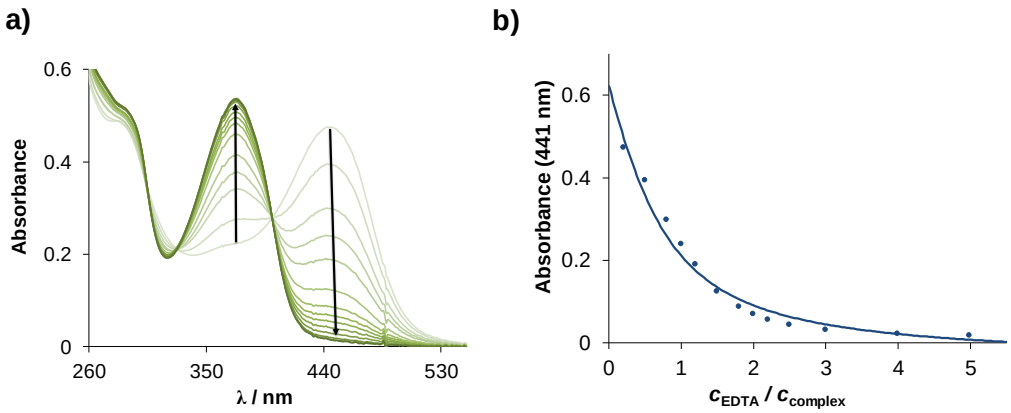


**Figure 8.** a) UV-vis absorption spectra recorded for Cu(II)-VA3 (1:1) system in the presence of increasing concentration of EDTA. b) Measured (●) and fitted (blue line) at 441 nm plotted against the EDTA-to-complex ratio. {$c_L$ = $c_{Cu}$ = 25 μM; $c_{EDTA}$ = 0-150 μM; pH = 5.90; 30% (*v/v*) DMSO/$H_2O$; $I$ = 0.1 M (KCl); $T$ = 25 °C; $\ell$ = 1 cm}

The redox properties of Cu(II) complexes of TSCs are usually linked to their pharmacological activities, as it was mentioned in the chapters 2.2 and 2.4. Based on these findings, the direct redox reaction between the Cu(II) complexes and GSH and AA was followed in order to investigate their reactivity. This reaction was followed under strictly anaerobic condition with the high excess of the reducing agent (50 equiv.) by UV-vis spectrometry in 30% (*v/v*) DMSO/$H_2O$ solvent mixture at pH 7.4 using a tandem cuvette. In Fig. 9.a representative spectral changes are shown for Cu(II)-VA3 system in the presence of high excess of GSH. These recorded spectra reveal that after mixing the reactants a fast and significant change is observed (see spectra at 0 and 0.2 min). This change might be explained by the formation of a ternary complex via the coordination of GSH, what was reported earlier for several TSC complexes [49,61]. Afterwards, an absorbance decrease can be seen at the $\lambda_{max}$, which belongs to the $S_{TSC}$→Cu CT band of the complex and formation of a new band with new $\lambda_{max}$, which corresponds to the free ligand. Bubbling of the oxygen into the system could regenerate the Cu(II) complexes (Fig. 9.b). Similar behavior with GSH was found for the Cu(II)-VA1 system. Based on the obtained data, observed rate constants ($k_{obs}$) were calculated using the measured absorbance−time curves (Table 2), which show similar reduction rates of the two measured Cu(II) complexes. Investigation of the direct redox reaction of the Cu(II)-VA2 complex with GSH was hindered due to precipitation, which appeared immediately after mixing of the reactants. It should be noted that AA was not able to reduce these complexes under the used conditions.

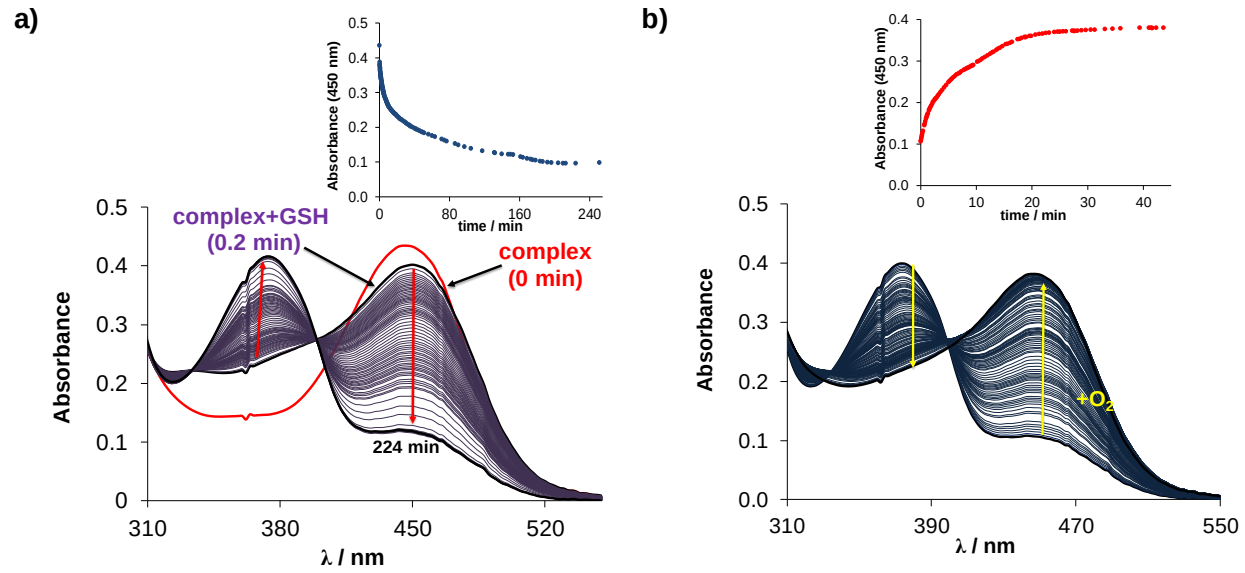


**Figure 9.** Time dependent changes of the UV-vis spectra of a) Cu(II)-VA3 (1:1) system in the presence of 50 equiv. GSH at pH 7.4 under anaerobic conditions; the inserted figure shows the absorbance values at 460 nm plotted against the time. {$c_L$=$c_{Cu}$ = 25 μM; $c_{GSH}$ = 1.25 mM; pH = 7.40; 30% (*v*/*v*) DMSO/$H_2O$; *I* = 0.1 M (KCl); *T* = 25 °C; $\ell$ = 1 cm}; b) Effect of bubbling of $O_2$ through the sample following the reaction of the complex with GSH; the inserted figure shows the absorbance values at 460 nm plotted against time.

*5.1.1.3 Anticancer activity of VA1-3 and their Cu(II) complexes*

The anticancer activity of the tested compounds was investigated in the doxorubicin-sensitive Colo205, the multidrug-resistant Colo320 human colonic adenocarcinoma cell lines and normal human embryonal lung fibroblast cells (MRC-5) by our partner (G. Spengler, University of Szeged). Obtained data (Table S1) revealed that the Cu(II) complexes were much more active on the cancer cells ($IC_{50}$ = 0.159 – 27.6 μM) than the ligands alone ($IC_{50}$ = 6.32 – 100 μM). Moreover, the Cu(II)-VA3 complex showed no toxicity on non-cancerous cells ($IC_{50}$ > 100 μM), although, the other two were cytotoxic also on these cells.

*5.1.2 Formaldehyde TSCs-morpholine conjugates with 2,6-dimethylphenol substituent (VA4-7) and their Cu(II) complexes*

In the previous chapter, triapine analogues were discussed and their Cu(II) complexes with redox active aminophenol moiety at the terminal nitrogen atom of the TSC scaffold. The ligands and their Cu(II) complexes displayed significant antiproliferative effect in cancer cells, although, they have limited aqueous solubility. It was already reported for some TSC derivatives that the aqueous solubility can be increased by the attachment of polar organic molecules, such as morpholine, homoproline, L(D)-proline amino-esters conjugated to the aromatic moiety of TSCs [88,94-98,142]. Based on these results, a morpholine moiety, which confers excellent aqueous solubility as well can improve pharmacological effect, was introduced at the pyridine ring to improve the

solubility of formaldehyde based TSCs with 2,6-dimethylphenol substituent. Herein, the influence of the morpholine moiety at the pyridine ring was studied in four different positions (positions 3-6, Chart 8) of the novel TSCs with redox aminophenol moiety on their solution behavior. Namely, we investigated how proton dissociation processes, stability in solution, lipophilicity, stoichiometry and redox properties of the ligands and Cu(II) complexes are affected by introduction of the morpholine moiety.

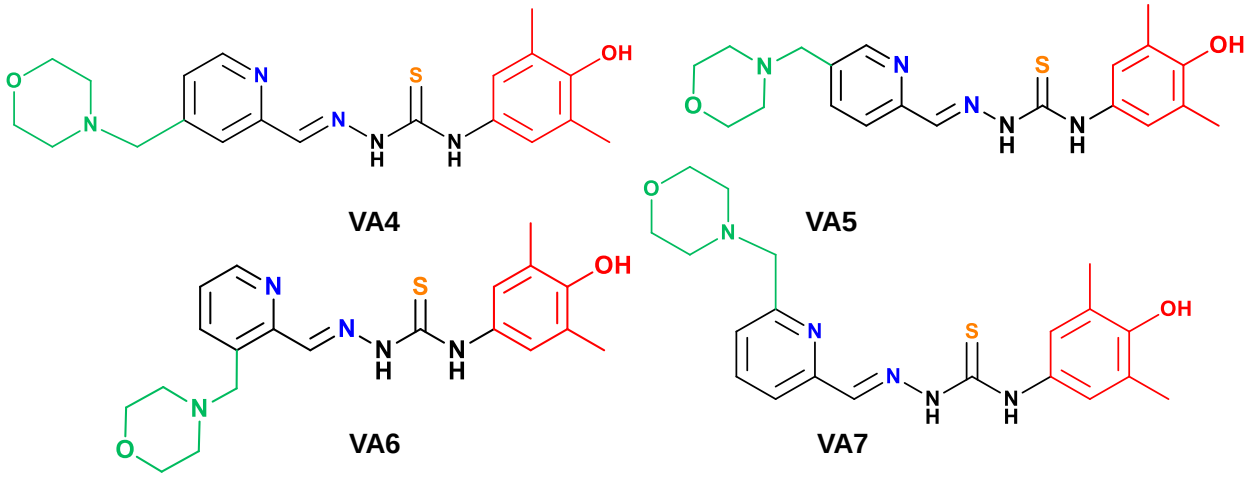


**Chart 8**. Chemical structure of the studied ligands VA4-7.

*5.1.2.1 Proton dissociation processes and lipophilicity of the ligands VA4-7*

The fully protonated forms of the ligands VA4-VA7 contain four proton dissociable groups, namely the pyridinium-$NH^+$ and hydrazonic-NH, which are from the TSC scaffold and in addition to the phenolic-OH and morpholinium-$NH^+$ of the substituents. pH-potentiometric titrations were used for the determination of the proton dissociation constants in 30% (*v/v*) DMSO/$H_2O$ solvent mixture. Based on the obtained data, only one p$K_{a2}$ value could be determined accurately from the recorded titration curves in the range of 5.2 – 5.6 (Table 3), and two other deprotonation processes were also observed at pH < 2.5 and pH > 10. According to it, the deprotonation steps were further studied using $^1$H NMR spectroscopy for pH-dependent titration of VA4 in 30% (*v/v*) DMSO-$d_6$/$H_2O$ in the pH range from 0.7 to 10.1 (Fig. 10.a). Collected data reveals broad signals, which appeared in the spectra between pH 2.0 and 7.9, and may indicate isomer formation. Moreover, significant changes of the chemical shifts of the different protons could be seen with increasing pH. In particular, the peaks of the methyl substituents and C*H* protons of the dimethylphenol ring showed changes only at pH > 9.5 demonstrating the deprotonation of the phenolic-OH in this pH range. However, these peaks are sensitive as well to the deprotonation process of the hydrazonic-NH group. New peaks also appeared at pH > 10, most probably due to oxidation processes involving the potentially redox active 2,6-dimethyl-4-aminophenyl unit of the ligand. Since the methylene-morpholine protons were sensitive to the deprotonation process in the

pH range 4 – 6 (Figs. 10.a,c), a p$K_{a2}$ = 5.2±0.1 was calculated based on these changes. This p$K_{a2}$ value most likely attributed to the deprotonation of the morpholinium-$NH^+$ group. It should be noted that the peaks in the low-field region of the spectra (Figs. 10.a,b) (CH aromatic protons of the pyridine ring and CH=N) were high-field shifted upon the first and second deprotonation steps but they remained unchanged between pH ~7 and ~10.

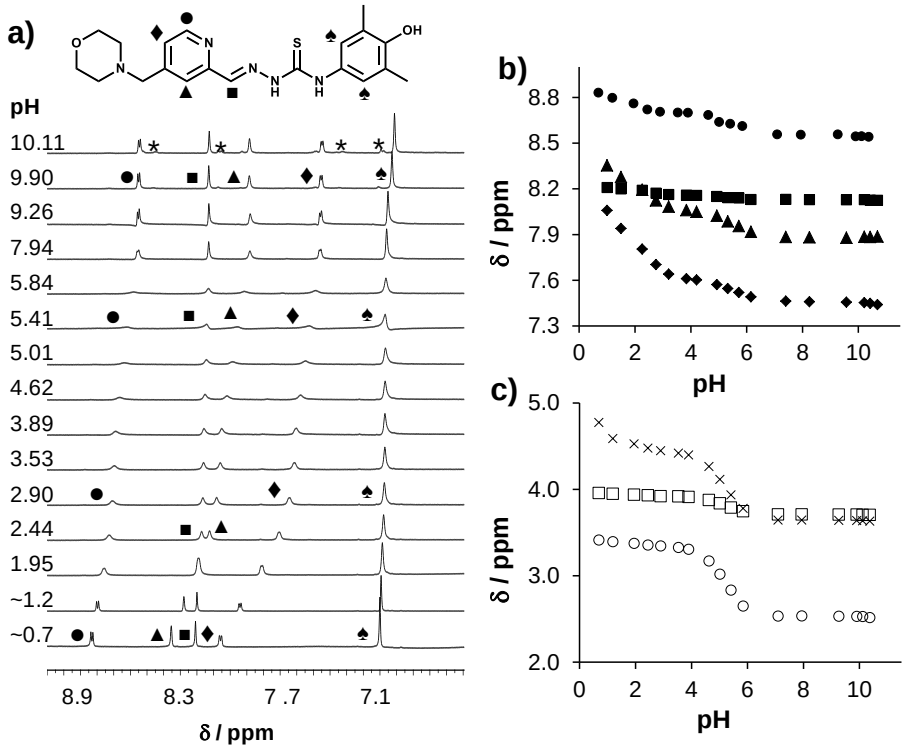


**Figure 10.** a) $^1$H NMR spectra for VA4 ligand in the low-field range at various pH values with symbols used for proton resonance assignment, * denotes the new peaks appearing upon oxidation; b) pH-dependence of the chemical shifts of peaks belonging to the pyridine-ring protons (●,▲,♦) and the C*H*=N (■) moiety and c) to the methylene-morpholine protons: N-C$H_2$-$C_{morpholine}$ (×), C$H_2$-$CH_2$-N (□), $CH_2$-C$H_2$-N (○). {$c_L$ = 1 mM; $I$ = 0.1 M (KCl); $T$ = 25 °C; 30% (*v/v*) DMSO-$d_6$/$H_2O$}

Taking into account these findings, it can be concluded that the first deprotonation step can be attributed to the pyridinium-$NH^+$ group, while the deprotonation of the hydrazonic-NH was not observed up to pH 10. Above pH >10 the overlapping deprotonation processes of the hydrazonic-NH and the phenolic-OH might take place, although in this pH range the oxygen-sensitivity of the ligand is strongly increased. The suggested deprotonation steps at pH < 10 are shown in Scheme 4.

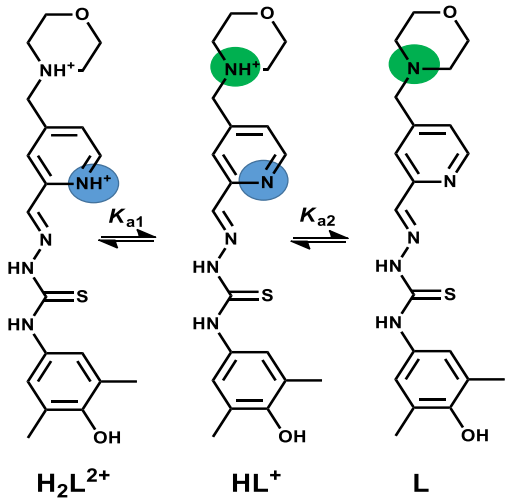


**Scheme 4.** Deprotonation steps of VA4 at pH <10.

Besides pH-potentiometry and $^1$H NMR spectroscopy, UV-vis spectrophotometry was also used for investigation of proton dissociation processes. UV-vis spectra were recorded at various pH values and representative spectra for VA4 are shown in Fig. 11. Determination of the lowest p$K_{a1}$ was done by preparing samples, in which KCl was partially or completely replaced by HCl (while keeping the ionic strength constant) and actual pH values, varying in the range of *ca.* 1.0 – 2.0, were calculated from the HCl content of the solution. In the pH range 1.0 – 3.4 (Fig. 11.a) characteristic spectral changes were observed, which are accompanied by the appearance of an isosbestic point at 350 nm. It is worth to mention that the other ligands (VA5-7) showed similar behavior. Based on the obtained data, p$K_{a1}$ value for the deprotonation process of the pyridinium-NH$^+$ was determined for each ligand using the spectra recorded at pH < 3.4 (Table 3). Unfortunately, p$K_{a1}$ value for the deprotonation process of the pyridinium-NH$^+$ for the ligand VA7 could not be obtained, since deprotonation takes place even at a more acidic pH range than what was used. These p$K_{a1}$ values were lower by *ca.* one and half units than those of triapine analogues with 2,6-dimethylphenol substituent (chapter 5.1.1.1) due to the electron withdrawing effect of methyl-morpholine group. However, deprotonation process of the morpholinium-NH$^+$ caused only minor changes in the UV-vis spectra, what was expected for this non-chromophoric unit.

**Table 3.** Proton dissociation constants (p$K_a$) of the studied ligands by the different methods. {30% (*v/v*) DMSO/$H_2O$; $I$ = 0.1 M (KCl); $T$ = 25 °C}

| | **method** | **VA4** | **VA5** | **VA6** | **VA7** |
|---|---|---|---|---|---|
| **p$K_{a1}$** | pH-potentiometry | < 2 | < 2 | < 2 | < 2 |
| **p$K_{a2}$** | pH-potentiometry | 5.16 ± 0.04[a] | 5.57 ± 0.05 | 5.62 ± 0.06 | 5.64 ± 0.03 |
| **p$K_{a3}$** | pH-potentiometry | ~ 10.5 | ~10.5 | > 10.5 | ~10.6 |
| **p$K_{a1}$** | UV-vis | 1.49 ± 0.01 | 1.16 ± 0.01 | 1.53 ± 0.01 | < 0.8 |

[a] p$K_{a2}$ ($HL^+$) = 5.2 ± 0.1 determined by $^1$H NMR titrations. {$c_L$ = 1 mM; $I$ = 0.1 M (KCl); $T$ = 25 °C; 30% (*v/v*) DMSO-$d_6$/$H_2O$}

Furthermore, in the pH range between 2 and 8 the development of an overlapping and less intense band is seen in the range between 370 and 450 nm most probably due to the concomitant existence of Z and E isomers (similarly to related TSCs in ref. [79]). In the basic pH range, the deprotonation of the 2,6-dimethylphenolic group is observed accompanied by the development of a strong band with $\lambda_{max}$ = 394 nm simultaneously with the decrease of the absorption at 324 nm (Fig. 11.b). At pH > 10.9 irreversible alteration of the spectra was seen, most probably due to the oxidation of the 4-aminophenolate unit to 4-aminophenoxyl radical ($1e^-$ oxidation) and/or to 4-benzoquinone imine ($2e^-$ oxidation with release of two protons in total) by the oxygen traces. These processes hindered the accurate determination of p$K_{a3}$ values in the basic pH range. Based on these findings it can be concluded that all studied ligands are present in their neutral form at physiological pH due to the fact that morpholinium-$NH^+$ moiety becomes deprotonated, and this feature contributes to their fairly lipophilic character of the ligand.

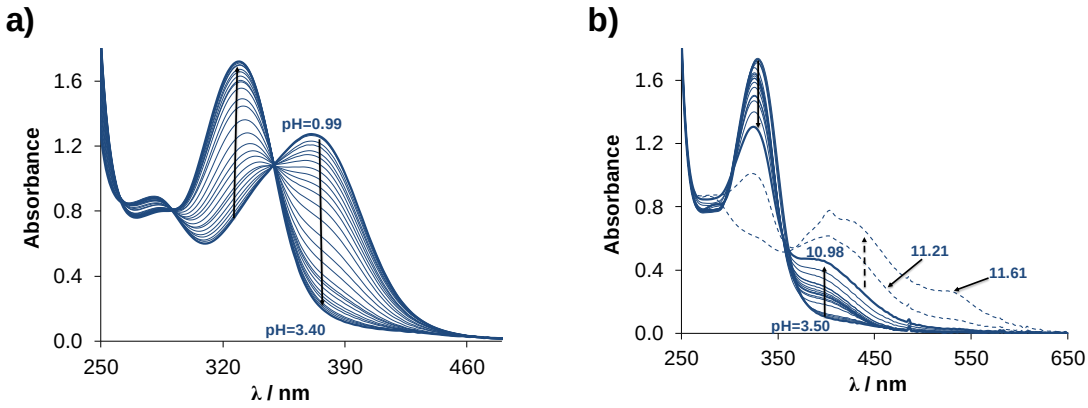


**Figure 11.** UV-vis absorption spectra recorded for VA4 at various pH values a) in the pH range 0.99 – 3.40 and b) 3.50 – 11.61. {$c_L$ = 73.7 μM; 30% (*v/v*) DMSO/$H_2O$; $I$ = 0.1 M (KCl); $T$ = 25 °C; $\ell$ = 1 cm}

Nevertheless, investigation of the lipophilic character by the traditional *n*-octanol/water partitioning failed, only a lower limit ($\log D_{7.4} > +2$) could be estimated since practically the whole amount of the compounds remained in the octanol phase.

*5.1.2.2 Stability of Cu(II) complexes of VA4-7 in solution and their reduction by GSH and AA*

The solution behavior of the Cu(II) complexes of VA4-7 was studied primarily by UV-vis spectrophotometric titrations in 30% (*v/v*) DMSO/$H_2O$. Representative UV-vis spectra are shown for the Cu(II)-VA6 system in Fig. 12.

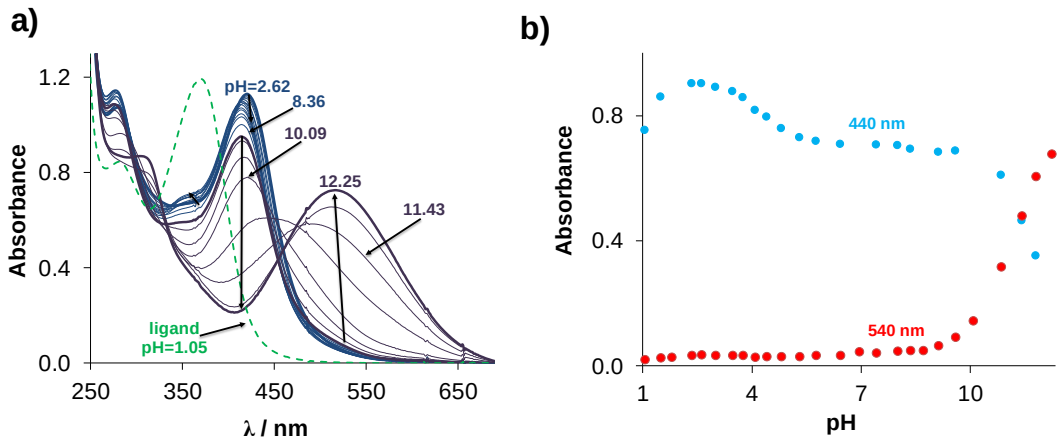


**Figure 12.** a) UV-vis absorption spectra recorded for Cu(II)-VA6 (1:1) system at various pH values together with the spectrum of the ligand at pH 1.05 (dashed green line); b) absorbance changes at 440 (●) and 540 nm (●) as a function of pH. {$c_L$ = $c_{Cu(II)}$ = 67 μM; 30% (*v*/*v*) DMSO/$H_2O$; *I* = 0.1 M (KCl); *T* = 25 °C; $\ell$ = 1 cm}

Comparing the spectra of the ligand in the absence and in the presence of one equivalent of Cu(II) at pH ~1 significant differences can be seen. It indicates the large extent of complex formation already at that low pH. Based on this finding, the direct determination of the stability constant of the complex is not possible; and the same behavior was observed for all complexes. It can be assumed that complex formation, pronounced with the increase of the pH, is supposed to be complete at pH ~3. The ligand binds to the Cu(II) ion via ($N_{pyridine}$,N,$S^-$) donor set in the complex, and this coordination mode could be proved by SXRD studies (the crystallization was done by the group of V.B. Arion, University of Vienna). Somewhat smaller spectral changes were observed in the pH range 3 – 6, where the $\lambda_{max}$ was shifted from 419 to 413 nm and the isosbestic points at 297 and 334 nm also appeared. This can indicate an equilibrium between two species. One p$K_a$ value for each Cu(II) complex was calculated from data collected in the pH range 4.2 and 4.7 (Table 4).

It is worth to mention that no spectral changes were observed in the case of VA7 (morpholine moiety at *ortho* position) and p$K_a$ could not be determined. It can be explained by the involvement of morpholine moiety in the coordination to Cu(II) revealed by the structure determined by X-ray diffraction analysis. Based on these findings, p$K_a$ values of the Cu(II) complexes of VA4, VA5 and VA6 are attributed to the deprotonation of the non-coordinating morpholinium $NH^+$ group in the $[CuL]^{2+}$ complex leading to the formation of $[CuLH_{-1}]^+$, in which the pyridinium-, the morpholinium and the hydrazonic nitrogens become deprotonated, while the phenolic-OH remains protonated.

**Table 4.** Conditional stability constants (log$K'_{5.9}$) determined by EDTA displacement UV-vis studies (in water or in 30% (*v/v*) DMSO/$H_2O$) and p$K_a$ values of the Cu(II) complexes (studied in 30% (*v/v*) DMSO/$H_2O$; $T$ = 25 °C), pCu (= –log[Cu(II)]) values calculated at pH 5.9 ($c_L$ = $c_{Cu(II)}$ = 1 μM) in addition of the observed rate constants ($k_{obs}$) obtained for the redox reaction of the complexes with GSH. {pH = 7.4 (50 mM HEPES); $c_L$ = $c_{Cu}$ = 25 μM; $c_{GSH}$ = 1.25 mM; in water}. {$I$ = 0.1 M (KCl); $T$ = 25 °C} (n.d. = not determined)

| | method | VA4 | VA5 | VA6 | VA7 |
|---|---|---|---|---|---|
| **log$K'_{5.9}$** [a] ($H_2O$) | UV-vis | 13.35 ± 0.02 | 13.39 ± 0.01 | 13.82 ± 0.04 | 13.73 ± 0.02 |
| **log$K'_{5.9}$** [b] (DMSO/$H_2O$) | UV-vis | 10.07 ± 0.01 | 9.99 ± 0.01 | 10.33 ± 0.01 | 10.09 ± 0.04 |
| **p$K_a$ [CuL]$^{2+}$** | UV-vis | 4.48 ± 0.01 | 4.75 ± 0.01 | 4.23 ± 0.01 | n.d. |
| **p$K_a$ [CuL]$^{2+}$** | pH-potentiometry | 4.60 ± 0.02 | 4.95 ± 0.04 | n.d. | n.d. |
| **pCu$_{5.9}$** | calculated | 8.06 | 8.02 | 8.20 | 8.07 |
| **$k_{obs}$ (min$^{-1}$)** | UV-vis | 0.079 ± 0.019 | 0.058 ± 0.010 | 0.059 ± 0.004 | 0.165 ± 0.011 |

[a] Data for p$K_a$ of EDTA and its Cu(II) complex taken from ref. [143] and log$K'_{5.9}$ = 13.89 was calculated for [Cu(EDTA)]$^{2-}$ in pure water. [b] log$K'_{5.9}$ = 10.19 for the Cu(II)-EDTA complex in the 30% (*v/v*) DMSO/$H_2O$ mixture was determined via triapine displacement reaction [61].

The suggested structures for the [CuL]$^{2+}$ and [CuLH$_{-1}$]$^{+}$ complexes of VA6 are shown in Chart 9. Besides UV-vis titrations, pH-potentiometric titrations were also performed for the Cu(II) complexes of VA4 and VA5 (Table 4), and the p$K_a$ values of [CuL]$^{2+}$ obtained by the two different methods are in good agreement.

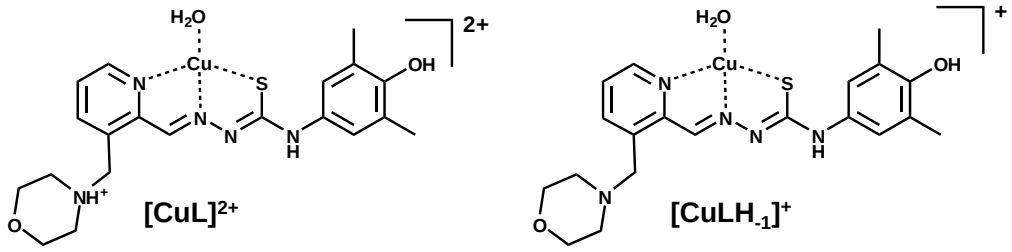


**Chart 9.** Suggested structures for [CuL]$^{2+}$ and [CuLH$_{-1}$]$^{+}$ complexes of VA6.

By further increasing the pH, significant changes of the UV-vis spectra were observed. Notably, at pH > 8.7 (Fig. 12), the $\lambda_{max}$ at 516 nm for VA6 was shifted to the higher wavelengths, most probably due to the deprotonation of the phenolic group, where this process results in the formation of the neutral complex [CuLH$_{-2}$]. Deprotonation of the phenolic group increases the sensitivity of the complex to oxidation (a similar process is demonstrated in chapter 5.1.1.2). For Cu(II) complexes with ligands VA4, VA5 and VA7, the absorbance values decreased in this pH range at λ > 340 nm, when an increase of absorbance was seen at ~310 nm most probably due to precipitation parallel with the oxidation of the phenolate group. Thus, spectral data collected in the basic pH range could not be used for evaluation. In the pH range between 5.5 and 8.7 in the Cu(II) – VA6 sytem (or between 5.5 and ~7 in the case of the other three Cu(II)-ligand systems) the

spectra remained unchanged because of the formation of the predominant $[CuLH_{-1}]^+$ complexes. For the determination of the stability constant of this species, EDTA competition was applied at pH 5.9 ($[CuLH_{-1}]^+$ is dominant) followed by UV-vis spectrophotometry. This displacement reaction was performed in the same way as it was described in chapter 5.1.1.2, where the absorbance of the characteristic $S_{TSC}\rightarrow Cu$ CT band at 400–460 nm decreased upon increasing the concentration of the EDTA (Fig. 13). These experiments were conducted in both aqueous solution and 30% (*v/v*) DMSO/$H_2O$ solvent mixture.

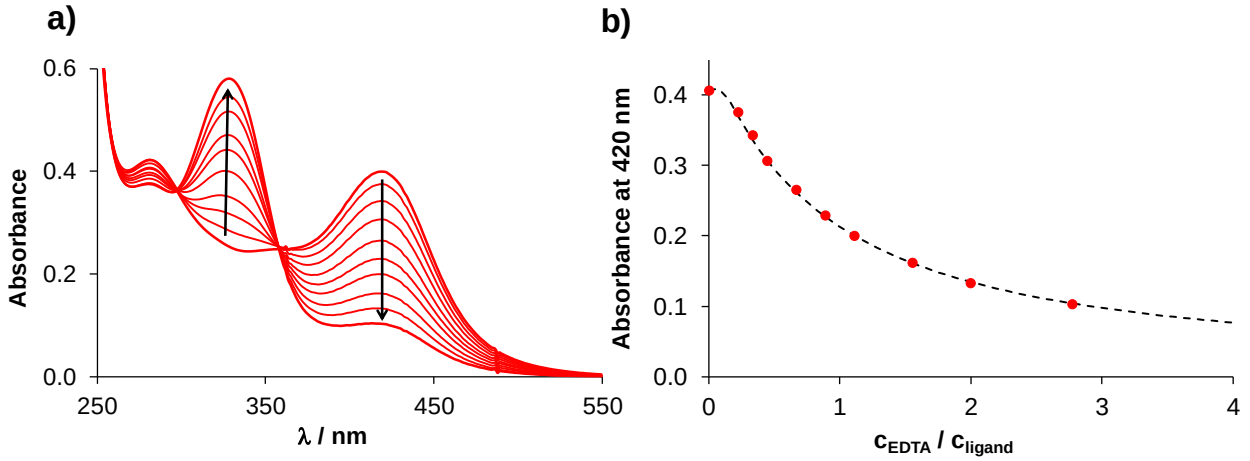


**Figure 13.** a) UV-vis spectra recorded for Cu(II)-VA4 (1:1) system in the presence of increasing concentration of EDTA. b) Measured (●) and fitted (dashed line) absorbance values at 420 nm plotted against the $c_{EDTA}$-to-$c_L$ ratio. {$c_L$ = 25 μM, $c_{Cu}$ = 25 μM, $c_{EDTA}$ = 0-62.5 μM, 30% (*v/v*) DMSO/$H_2O$; pH = 5.90, $I$ = 0.1 M (KCl), $T$ = 25 °C; $\ell$ = 1 cm}

The obtained conditional formation constants ($\log K'_{5.9}$) are collected in Table 4 and show strong similarity. It is worth to mention that the values obtained in the DMSO/$H_2O$ solvent mixture are lower most likely due to the competitive coordination of DMSO to Cu(II). This finding was already reported for the Cu(II) complex of triapine [61]. However, ligands studied here show somewhat higher $\log K'_{5.9}$ values compared to that of the the triapine Cu(II) complex in 30% (*v/v*) DMSO/$H_2O$ ($\log K'_{5.9}$ = 9.47 was calculated by taking the data from ref. [61]). These constants were also higher in comparison to Cu(II) complexes with triapine analogues with 2,6-dimethylphenol substituent, which were discussed above. It can be assumed that the presence of morpholine unit can change slightly the thermodynamic stability of these α-*N*-pyridyl TSC complexes (see Tables 2 and 4). In order to compare the Cu(II) binding ability of the studied TSCs at pH 5.9 (at which the conditional constants were determined), pCu values were also computed using the experimentally determined equilibrium constants (Table 4) and reflect that the ligands have similar Cu(II) binding ability. Moreover, these data show that the additional coordination of the morpholine nitrogen in the Cu(II) complex of VA7 does not result in higher thermodynamic

stability. Similar situation was described for aqueous solutions of the *N*-terminally dimethylated derivative of PTSC [77] and its morpholine-conjugate Morf-PTSC [88].

It was already suggested that the anticancer activity of the Cu(II) complexes of TSCs is often related to their redox reaction with cellular thiols such as GSH [49]. Herein the direct reduction of Cu(II) complexes with GSH was investigated as well under strictly anaerobic condition at pH 7.4 in aqueous solution. At this pH, the complex $[CuLH_{-1}]^+$ predominates based on the speciation studies. Moreover, AA was also tested revaling a very slow reaction. Thus, it can be concluded that these Cu(II) complexes cannot be reduced by this reducing agent efficiently. It should be noted that remarkable spectral changes were detected in the case of GSH as Fig. 14.a shows for the Cu(II) complex of VA7.

Similar behavior was found for the Cu(II) complex of VA7 with GSH as it was shown in chapter 5.1.1.2, where the first recorded spectrum after mixing the reactants showed minor shifts of the absorbance bands most likely due to the formation of a ternary complex with GSH [49,56]. Notable decrease of the absorbance was observed at $\lambda_{max}$ = 406 nm, and the absorbance was increased at the $\lambda_{max}$ of the free ligand (~316 nm). Bubbling oxygen into the solution could regenerate the Cu(II) complex (more specifically its GSH adduct) in all cases (Fig. 14.a for Cu(II) - VA7), which suggests a reversible redox process. Based on the absorbance – time curves (Fig. 14.b), observed rate constants ($k_{obs}$) were calculated (Table 4) as a semi-quantitative description of the reaction kinetics.

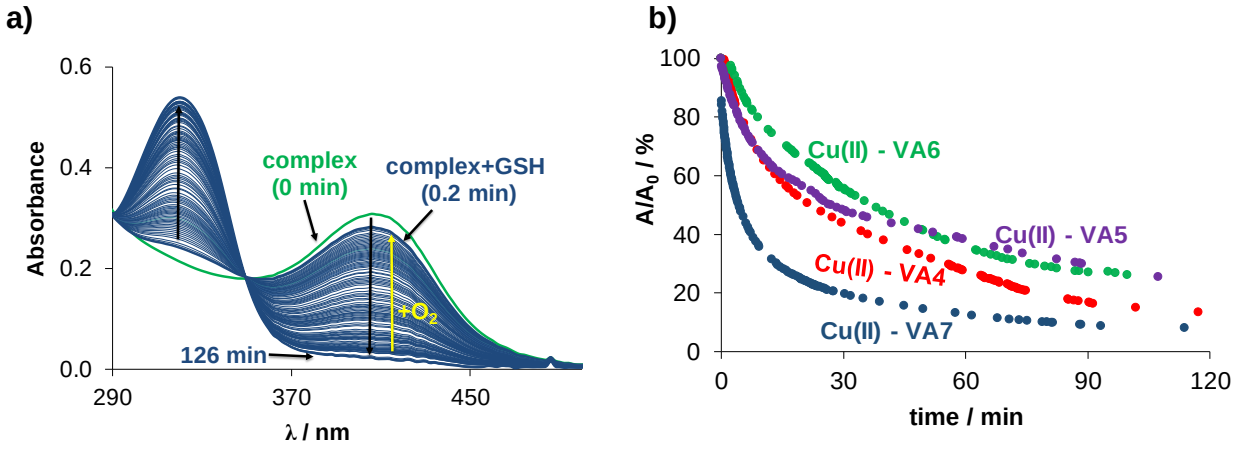


**Figure 14.** a) Time-dependent UV-vis absorption spectra of the Cu(II)-VA7 (1:1) system in the presence of 50 equiv. GSH before (green line) and after mixing their solutions (blue lines) in a tandem cuvette under anaerobic conditions. b) Plot of absorbance changes at 406 nm (blue line) for the Cu(II)-VA7 (1:1) system, at 396 nm (red line) for the Cu(II)-VA4 (1:1) system**,** at 398 nm (violet line) for the Cu(II)-VA5 (1:1) system and at 398 nm (green line) for the Cu(II)-VA6 (1:1) system *vs.* time. {pH = 7.4 (50 mM HEPES); in water; $c_L = c_{Cu}$ = 25 μM; $c_{GSH}$ = 1.25 mM; $I$ = 0.1 M (KCl); $T$ = 25 °C; $\ell$ = 1 cm}

It can be concluded that the studied Cu(II) complexes can be reduced by GSH with a similar reaction rate, although the Cu(II) complex with the ligand VA7 can be reduced somewhat faster compared to the others. It is worth to mention that these Cu(II) complexes can be reduced by GSH much faster than those of triapine analogues VA1-3 under the same conditions.

*5.1.2.3 Anticancer activity of the tested ligands and their Cu(II) complexes*

The cytotoxic activity of ligands VA4-VA7 and their Cu(II) complexes was investigated in MES-SA (human uterine sarcoma) and in its multidrug-resistant counterpart (MES-SA/Dx5). These measurements were performed by G. Szakács (Medical University of Vienna). The cytotoxicity of the ligands falls into the low micromolar concentration range (Fig. 15). The results are remarkable, especially in the case of VA7 with *ca*. 3 times stronger effect than triapine for the free ligand, and its Cu(II) complex exhibited *ca*. 7 times stronger cytotoxic effect in MES-SA cell line compared to the Cu(II)-triapine complex. The Cu(II) complexes are less cytotoxic against the MES-SA cells than the corresponding ligands, the values are comparable only in the case of the VA7 and its Cu(II) complex. The same effect was observed for triapine and its Cu(II) complex [61]. In contrast with the results in MES-SA cells, the complexes are more cytotoxic than the ligands in the MES-SA/Dx5 cells.

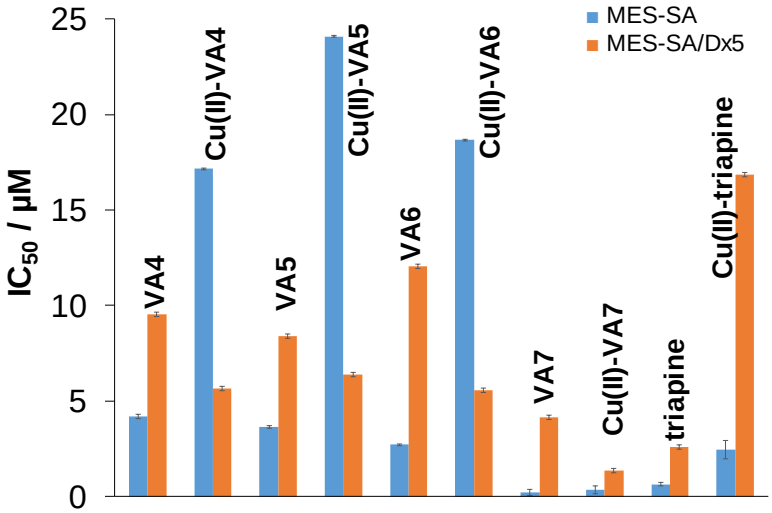


**Figure 15.** *In vitro* cytotoxicity data ($IC_{50}$ expressed in µM) determined for the ligands and their Cu(II) complexes in MES-SA and MES-SA/Dx5 (120 h exposure).

*5.3 Imidazole and benzimidazole-derived thiosemicarbazones and their Cu(II) complexes: impact of N-terminal substitution and hybridization*

To explore the impact of the ligand scaffold exchange on the physico-chemical properties of TSCs, the α-*N*-pyridyl moiety was replaced with imidazole and benzimidazole units. Such modifications

may improve the pharmacokinetic characteristics of TSCs and optimize their solubility and bioavailability [80]. Moreover, substitution of the terminal amino group in the analogous TSCs usually lead to enhanced anticancer activity and formation of high stability Cu(II) complexes (see chapter 2.4). Four imidazole and benzimidazole-based TSCs (Chart 10) were investigated, and their Cu(II) complexes were prepared and characterized.

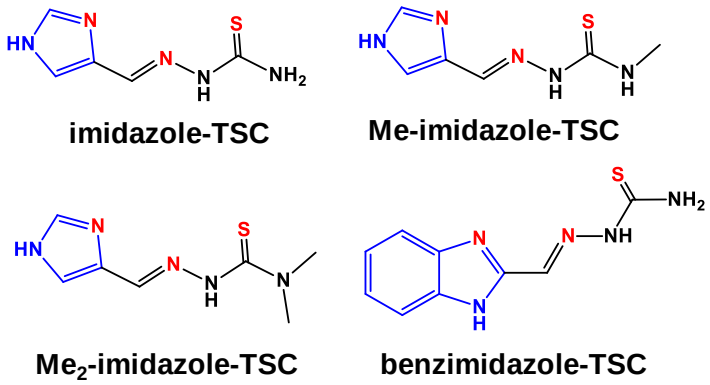


**Chart 10.** Chemical structures of imidazole- and benzimidazole-TSCs in HL form (donor atoms highlighted by red that coordinate to Cu(II) ions in mono complexes). Ligands were provided by the group of É. Frank, University of Szeged.

The previously published results of methyl imidazole-derived TSCs showed anticancer effect on several cancer cells (A549, MDA-MB-453, LS174 and BEAS-2B), which was enhanced by the coordination to Cu(II) and with dichloroacetate as a co-ligand [80]. Based on this finding, anticancer and antibacterial activities of the compounds in Chart 10 and their Cu(II) complexes were investigated by our partner (G. Spengler, University of Szeged). Anticancer activity was tested in two cell lines for all compounds (Colo205 and Colo320). The obtained results showed that ligands alone were not cytotoxic on cancer cells except $Me_2$-imidazole-TSC, which showed high-to-moderate activity ($IC_{50}$: 8.97 – 29.14 μM), especially on Colo205 and Colo320 (Table S2). In the meantime, the presence of the copper salt increased the anticancer activity in all cases, namely, the highest activity was shown by Cu(II) – $Me_2$-imidazole-TSC complex on Colo205 ($IC_{50}$: 2.81 μM) and Cu(II) – benzimidazole-TSC systems on Colo320 cells ($IC_{50}$: 15.70 μM).

Moreover, antibacterial activity was tested as well on the Gram-positive *S. aureus* and the Gram-negative *E. coli* and *K. pneumoniae* strains, and only moderate activity was found on *S. aureus* for complexes of $Me_2$-imidazole-TSC and benzimidazole-TSC (minimal inhibitory concentration (MIC) ~50 μM).

*5.3.1 Proton dissociation processes and lipophilicity of the imidazole and benzimidazole-derived thiosemicarbazones*

The proton dissociation processes of the tested compounds were monitored by pH-potentiometric titrations at 1–2 mM concentrations in 30% (*v/v*) DMSO/$H_2O$. Although, the protonated ligands have three dissociable protons, namely two on the imidazolium- and one on the hydrazonic nitrogens, only two p$K_a$ values (p$K_{a1}$ and p$K_{a2}$, Table 5) could be determined. p$K_{a1}$ is attributed to the deprotonation process of one of the imidazolium nitrogens ($N^3$), which is involved in the coordination to Cu(II) ions (see Chart 10), while p$K_{a2}$ belongs to the hydrazonic nitrogen.

**Table 5.** Protonation (log $\beta$ HL) and proton dissociation constants (p$K_a$)[a] of the studied ligands determined by pH-potentiometric titrations in 30% (*v/v*) DMSO/$H_2O$ {$I$ = 0.1 M (KCl)} and their *n*-octanol/water distribution coefficients (log$D_{7.4}$ values) at $T$ = 25 °C. [a]

| | **imidazole-TSC** | **Me-imidazole-TSC** | **$Me_2$-imidazole-TSC** | **benzimidazole-TSC** |
|---|---|---|---|---|
| **log $\beta$ HL** | 11.26 ± 0.02 | 11.48 ± 0.04 | 10.85 ± 0.01 | 10.38 ± 0.02 |
| **log $\beta$ $H_2L^+$** | 15.62 ± 0.02 | 15.97 ± 0.05 | 15.30 ± 0.01 | 13.51 ± 0.05 |
| **p$K_{a1}$** | 4.36 | 4.49 | 4.45 | 3.13 |
| **p$K_{a2}$** | 11.26 | 11.48 | 10.85 | 10.38 |
| **log$D_{7.4}$** | +0.03 ± 0.03 | +0.64 ± 0.02 | +0.25 ± 0.02 | > +2 |

[a] Triapine (for comparison): p$K_{a1}$(pyridinium-$NH^+$) = 3.92; p$K_{a2}$(hydrazonic-NH) = 10.78; log$D_{7.4}$ = +0.85 [77]

The benzimidazole analogue possesses lower p$K_a$ values than the imidazole derivatives, which can be explained by the electron-withdrawing effect of the fused benzene ring. The *N*-terminal monomethylation does not have a strong influence on the proton dissociation constants of the compounds, whereas dimethylation results in undoubtedly lower p$K_{a2}$ value of the hydrazonic nitrogen. It should be noted that triapine has somewhat lower p$K_a$ values in comparison to imidazole-TSC (Table 5).

As it was mentioned in chapter 2.3, the TSCs are recognized for their ability to exist as both E and Z isomers around the C=N double bond, which were also detected for imidazole-TSCs by $^1$H NMR spectroscopic titrations [79,80]. The $^1$H NMR spectra of imidazole-TSC recorded in the pH range 1.3 – 12.7 in 30% (*v/v*) DMSO-$d_6$/$H_2O$ solvent mixture are shown in Fig. 16.

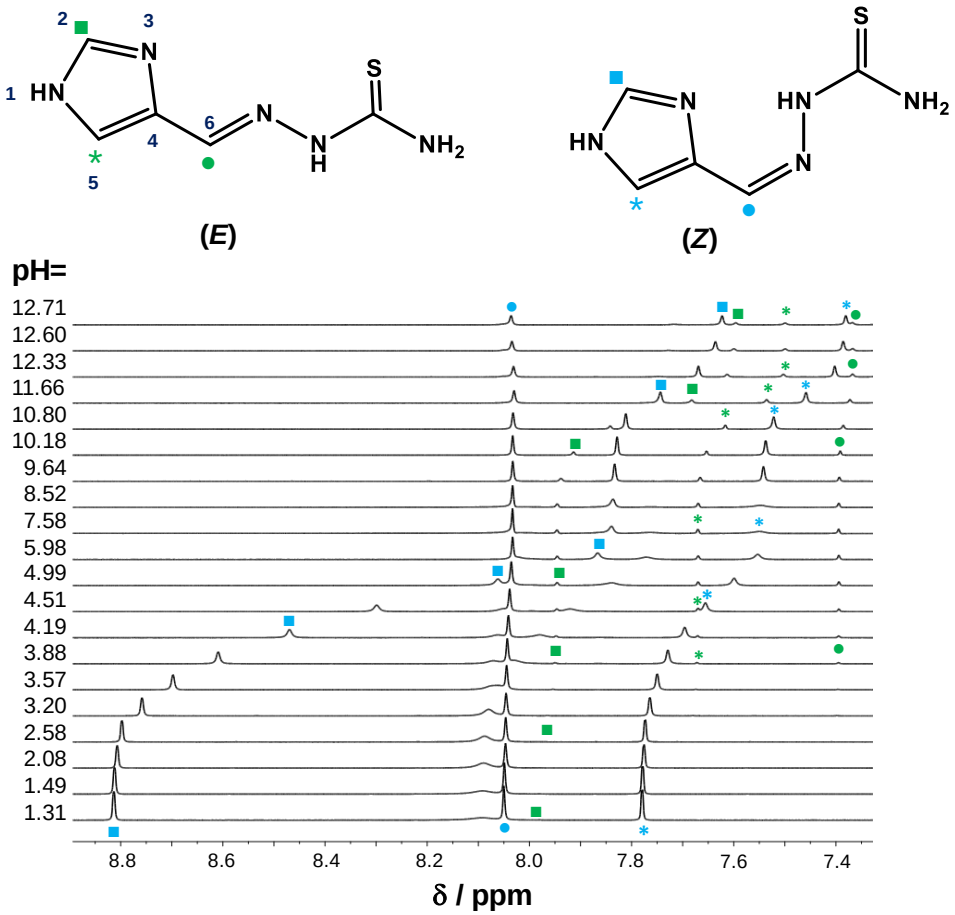


**Figure 16.** $^{1}$H NMR spectra of imidazole-TSC at various pH values with symbols used for proton resonances assignment in case of the major Z isomer (blue symbols) and minor E isomer (green symbols), where ligand is shown in its HL form. {$c_L$ = 3 mM; $I$ = 0.1 M (KCl); $T$ = 25 °C; 30% ($v$/$v$) DMSO-$d_6$/$H_2O$}

Three sets of signals (see Fig. 16) were registered in the whole studied pH range, where CH2 and CH5 protons (indicated as ■ and * in Fig. 16, respectively) were very sensitive for both deprotonation steps. The p$K_{a1}$ calculated for the minor isomer is *ca.* half logarithm unit lower than that of the major isomer (minor: 3.94 *vs.* major: 4.47) probably due to the formation of intramolecular hydrogen bond(s) that makes the deprotonation of the imidazole NH group more feasible. The p$K_{a2}$ of the minor isomer is 11.18, whereas it was not possible to calculate a constant for the major isomer (>11.5). The high p$K_{a2}$ value for the major isomer is most probably connected with a strong intramolecular hydrogen bonding. The identification of the isomers was mostly based on the determined p$K_a$ values. Considering the possible hydrogen bonds in the different protonated species (Scheme 5), the Z isomer is able to form more stable hydrogen bonds in the whole pH range, and it is the more favorable species. It is assumed to be the major ligand form in the whole pH range: its molar fraction is ~ 99% at pH 1.31, which decreases to ~ 78% at pH > 12.

Although both isomers may have hydrogen bond in the protonated $H_2L^+$ form as it is shown in Scheme 5, the bond in E isomer forms a more strained ring thus it is weaker than the one in the

Z isomer. After deprotonation of imidazolium nitrogen (N3), a sterically preferable hydrogen bond will be formed between imidazolium nitrogen and hydrazonic NH group in Z isomer, while in E isomer no hydrogen bond will be present. Based on this, the first deprotonation step has higher impact on chemical shifts in Z isomer, which is clearly visible in NMR spectra (see Fig. 16, blue symbols).

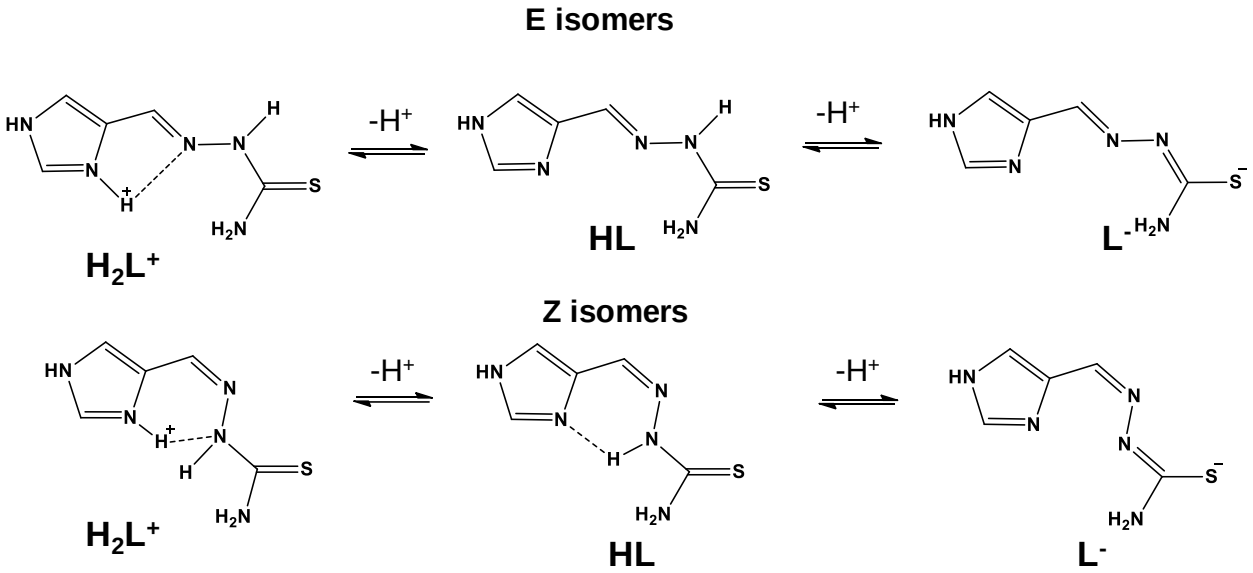


**Scheme 5**. E/Z isomers of imidazole-TSC in their $H_2L^+$, HL and $L^-$ forms, where the suggested hydrogen bonds indicated with dashed lines based on ref. [79].

The lipophilic character of the studied imidazole-TSC derivatives was investigated and expressed as log$D_{7.4}$ values (Table 5). Obtained data reveal that the introduction of the methyl groups and benzene ring annulation increases the lipophilic character as expected, especially in the latter case (benzimidazole-TSC), where only threshold limit could be estimated due to its high value. Imidazole-TSC and its mono- and dimethylated derivatives are less, whereas benzimidazole-TSC is much more lipophilic than triapine at pH 7.4.

*5.3.2 Stability of Cu(II) complexes in solution formed with imidazole and benzimidazole-TSC derivatives*

The complex formation processes of imidazole and benzimidazole-TSC derivatives with Cu(II) ions were investigated by UV-vis spectrophotometry in 30% (*v/v*) DMSO/$H_2O$. The overall stability constants (log $\beta$) and p$K_a$ values of the studied Cu(II) complexes are collected in Table 6. Data obtained from pH-potentiometric titrations for the imidazole-TSC-Cu(II) (1:1, 1:1.5, 1:2 and 1:3) systems reveal that the complex formation is almost complete already at the starting pH value of the titrations (pH = 2).

**Table 6.** Overall stability constants (log $\beta$), p$K_a$ of the Cu(II) complexes of imidazole/benzimidazole-TSC determined by UV-vis titrations in 30% (*v/v*) DMSO/$H_2O$ and calculated pCu values at pH 5.0 using $c_{Cu}$ = 20 μM and $c_L$ = 20 μM together with triapine for comparison; (n.d. = not determined). [a]{*T* = 25 °C; *I* = 0.1 M (KCl)}

| | **imidazole-TSC** | **Me-imidazole-TSC** | **$Me_2$-imidazole-TSC** | **benzimidazole-TSC** |
|---|---|---|---|---|
| **log $\beta$ $[CuLH]^{2+}$** | 19.87±0.01 | 19.48±0.02 | 19.47±0.05 | n.d. |
| **log $\beta$ $[CuL]^{+}$** | 17.25±0.02 | 16.82±0.02 | 16.68±0.05 | 14.04±0.01 |
| **log $\beta$ $[Cu_4L_4H_{-4}]$** | 56.89±0.07 | 56.78±0.08 | n.d. | 41.28±0.04 |
| **log $\beta$ $[CuLH_{-2}]^{-}$** | 2.29±0.04 | n.d. | n.d. | -2.91±0.02 |
| **p$K_a$ $[CuLH]^{2+}$** | 2.62 | 2.66 | 2.79 | n.d. |
| **$pCu_{5.0}$** | 7.9 | 7.5 | 7.8 | 6.8 |

[a] Triapine: $pCu_{5.0}$ = 6.4 under the same conditions.

Based on this finding, UV-vis spectrophotometric titrations were performed starting at pH < 2 for all studied compounds. The spectrum recorded at pH 1.59 represents significant complex formation, as it is completely different from the spectrum of the free ligand (Fig. 17.a). At this pH, $[CuLH]^{2+}$ is formed and its formation is completed to pH ~2.7. Then the subsequent process starts, which corresponds to the formation of $[CuL]^{+}$ species (Fig. 17.a). Remarkable spectral changes were seen in the pH range 5 – 7, which is dedicated to the deprotonation process of the non-coordinated imidazole nitrogen ($NH^1$, see Fig. 16) and the formation of a tetrameric species $[Cu_4L_4H_{-4}]$ (Fig. 17.b). The formation of this tetrameric species was assumed based on the literature data, where similar tetrameric species were found for Cu(II) complexes with imidazole derivatives in solution [144-146]. Moreover, dimeric species were detected for the isolated Cu(II) complex by ESI-MS (MeOH, positive, m/z for Cu(II)-imidazole-TSC: $C_{10}H_{12}N_{10}S_2Cu_2]Cl^-$: theoretical: 498.8950, measured: 498.8938), which was formed most probably due to the decomposition of the tetramer under the conditions of the ESI-MS analysis (Fig. S1). Additional process was observed at pH > 9, which corresponds most probably to the formation of a mixed hydroxido complex $[CuLH_{-2}]^{-}$. This species is formed by the deprotonation of the water molecule that coordinates in the fourth equatorial position, as it is drawn in Fig. 17.b.

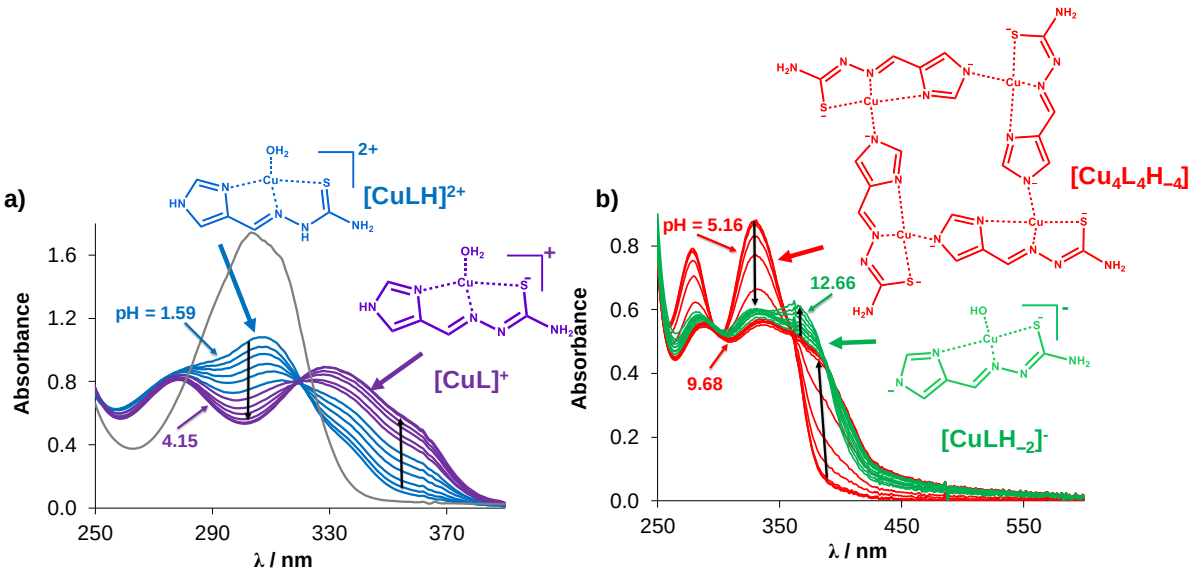


**Figure 17.** UV-vis absorption spectra recorded for the Cu(II)-imidazole-TSC (1:1) in the pH range a) 1.59 – 4.15 together with a ligand's spectrum at pH 1.79 (grey line) and b) between pH 5.16 and 12.66 in 30% (*v*/*v*) DMSO/$H_2O$ together with the suggested structures of species formed. {$c_L = 117$ μM; $c_{Cu} = 114$ μM; $I = 0.1$ M (KCl); $T = 25.0$ °C; $\ell = 0.5$ cm}

Concentration distribution curves were computed for the Cu(II)-imidazole-TSC (1:1) system using the obtained formation constants (Table 6, Fig. 18.a), where $[CuLH]^{2+}$ and $[CuL]^{+}$ species were found predominant in the acidic pH values. $[Cu_4L_4H_{-4}]$ species was found predominant in pH range 5 – 9 (also including the physiological pH), while $[CuLH_{-2}]^{-}$ species was the most abundant at pH > 10. $[CuLH]^{2+}$ contains the protonated ligand, where the proton is present on the non-coordinating hydrazonic nitrogen. In the $[CuL]^{+}$ complex the ligand coordinates most probably via the ($N_{imidazole}$,N,$S^{-}$) tridentate donor set. Moreover, the suggested coordination mode was confirmed by X-ray crystallography for the $Me_2$-imidazole-TSC complexes, which coordinates through ($N_{imidazole}$,N,$S^{-}$) chelating mode, and the fourth position is occupied by a chlorido ligand (Fig. 18.b; coordination of $Cl^{-}$ is assumed only in the solid phase).

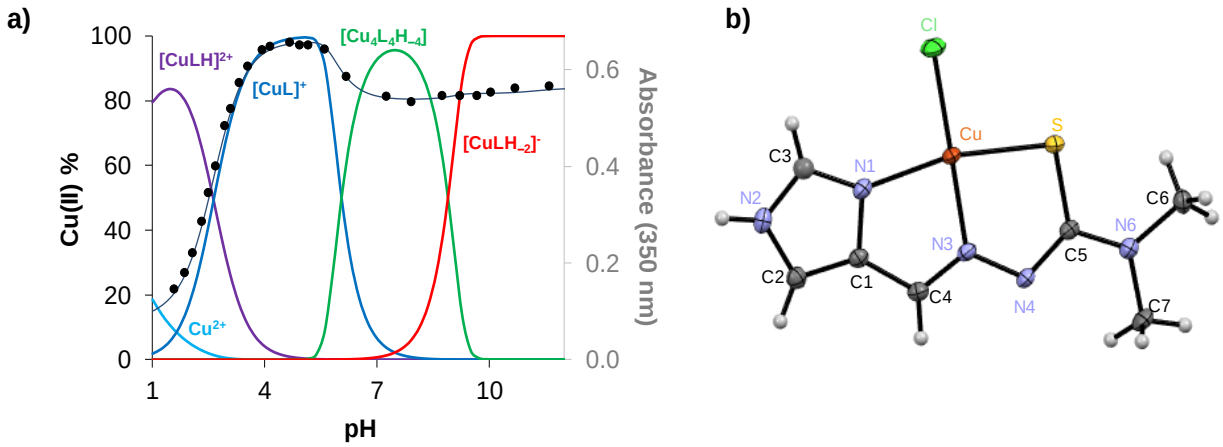


**Figure 18.** a) Concentration distribution curves for the Cu(II)-imidazole-TSC (1:1) system plotted together with the absorbance changes at 350 nm (●) with the fitted curve (dotted line). {$c_{ligand}$ = 117 μM; $c_{Cu(II)}$ = 114 μM; $T$ = 25.0 °C; $I$ = 0.1 M (KCl); $\ell$ = 0.5 cm }; b) Molecular structure and atom labeling of the Cu(II) – $Me_2$-imidazole complex as [CuL]Cl.

It is worth to mention that only $[CuLH]^{2+}$ and $[CuL]^{+}$ species were detected for $Me_2$-imidazole-TSC due to appearance of precipitation at pH > 6.0 that hindered further data evaluation. In order to compare the stability of the investigated Cu(II) complexes in solution, pCu values were calculated at pH 5.0, where no precipitation occurred (Table 6). Obtained data show that there are minor differences between the calculated pCu values for the studied imidazole-TSCs, and the *N*-terminal substitution does not have significant effect on the stability. However, lower value was found for benzimidazole-TSC. In contrast, triapine exhibits a lower pCu value, indicating that the substitution of the pyridine ring with the imidazole moiety significantly increases the Cu(II) binding affinity at pH 5.0.

*5.3.3 Redox properties of the Cu(II) complexes of imidazole-TSC derivatives*

To investigate the redox properties of the Cu(II) complexes, detailed electrochemical and spectroscopic studies were performed using CV and UV-vis spectroelectrochemistry. The cyclic voltammograms of Cu(II) complexes of imidazole-TSCs were recorded in 99% (*v*/*v*) DMSO/*n*-$Bu_4NPF_6$/$H_2O$ in which all tested compounds exhibit good solubility and for the sake of comparison, the Cu(II)-triapine complex was tested as well. Cyclic voltammograms of all tested compounds were collected in Fig. 19 and the complexes showed similar redox behavior. Namely, the electrochemical analysis reveals the presence of a single reduction peak accompanied by a strongly shifted re-oxidation peak.

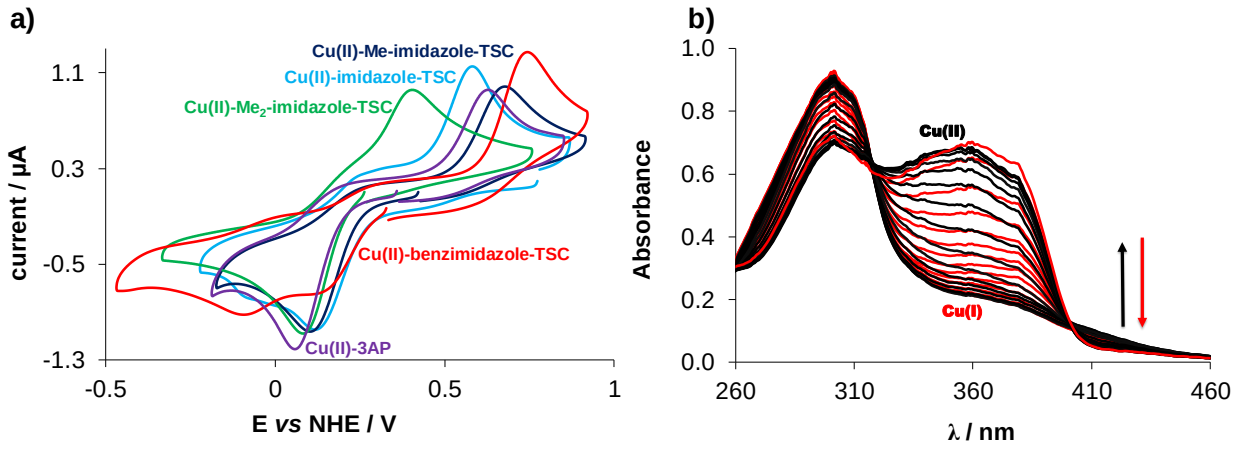


**Figure 19.** a) Cyclic voltammograms of the Cu(II)-(T)SC (1:1) systems in 99% (*v/v*) DMSO/$H_2O$ at 100 mV/s scan rate {$c_L$ = 1 mM, $c_{Cu(II)}$ = 1 mM, $T$ = 25 °C, $I$ = 0.1 M (*n*-$Bu_4NPF_6$)} *E' vs.* NHE; b) UV-vis absorption spectra recorded for the Cu(II)-$Me_2$-imidazole (1:1) system at the various potential values using the spectroelectrochemical cell. {$c_{Cu(II)}$ = $c_L$ = 100 µM; $I$ = 0.1 M (*n*-$Bu_4PF_6$); $T$ = 25.0 °C, scan rate: 20 mV/s; $\ell$ = 0.17 cm}

These complexes showed very similar reduction peaks in the range –0.09 – + 0.1 V *vs.* NHE and a sharp oxidation peak during the reverse scan in the range +0.4 – + 0.74 V *vs.* NHE. The electrochemical process is irreversible. It can be explained by an electrochemical dual-pathway square scheme (Scheme 6), where the electron transfer processes in Cu(II/I) systems were accompanied by strong changes in their coordination geometry [147]. Herein, Cu(II)L and Cu(I)L forms are the thermodynamically stable species with their usual coordination geometry (square-planar and pseudo-tetrahedral, respectively), whereas Cu(II)L' and Cu(I)L' are metastable intermediates in which the coordination geometry nearly resembles that of the thermodynamically stable species of the opposite oxidation state (pseudo-tetrahedral and square-planar, respectively).

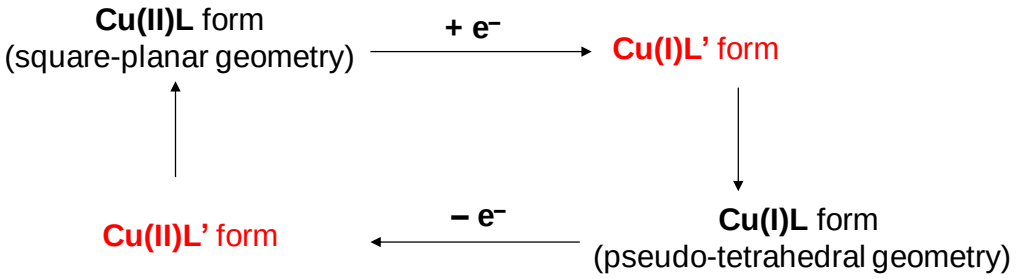


**Scheme 6.** Electrochemical dual-pathway square scheme, where L indicates the tested ligands [147].

In order to better understand these processes, UV-vis spectroelectrochemical measurements were performed and the result is shown for Cu(II)-$Me_2$-imidazole-TSC complex in Fig. 19.b. In the UV-vis spectra two absorption bands are present with the wavelength maxima 300 and 360 nm, whereas the first is assigned as the ligand absorption band and the second is

considered as the S → Cu charge transfer band. During the reduction, simultaneous decrease of the initial UV-vis absoption band at 360 nm and increase at 300 nm through an isosbestic point at 316 nm was observed (Fig. 19.b). The reoxidation process leads to the complete restoration of the initial bands (in Fig. 19.b). This observation confirms the stability of the Cu(I) complex of $Me_2$-imidazole-TSC generated cathodically, and demonstrates the chemical reversibility of this redox process. Slightly different behavior was found for all other compounds tested here, where a nearly full recovery of the initial optical bands was detected.

Our findings are consistent with the results obtained from the direct reduction of the Cu(II)-TSC complexes with GSH. This reaction was followed by UV-vis spectrophotometry under anaerobic conditions at pH 7.4 in an aqueous solution. All Cu(II) complexes were reduced by GSH in a relatively fast reaction (< 1 h), and the final spectrum corresponded to that of the free ligand (Fig. 20.a).

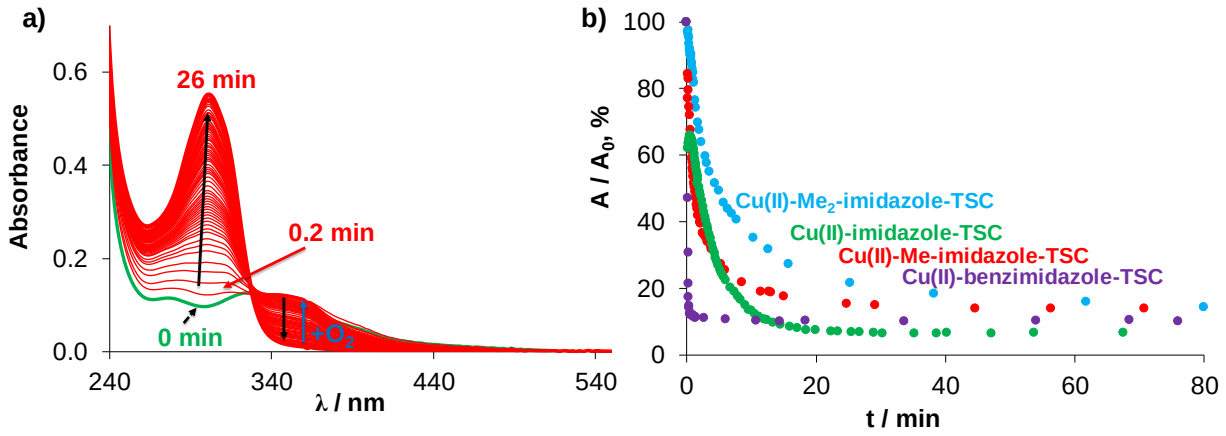


**Figure 20.** a) Time-dependent UV-visible absorption spectra of Cu(II)-imidazole-TSC (1:1) system in the presence of 50 equiv. GSH at pH = 7.4 (50 mM HEPES); {$c_{Cu} = c_L$ = 25 μM; $c_{GSH}$ = 1.25 mM; $I$ = 0.1 M (KCl); $\ell$ = 1 cm; $T$ = 25 °C}. b) Absorbance values at 360 nm (●) for Cu(II)-imidazole, (●) for Cu(II)-Me-imidazole-TSC, (●) for Cu(II)-$Me_2$-imidazole-TSC, at 416 nm (●) for Cu(II)-benzimidazole-TSC complexes with GSH in dependence of time. Absorbance read from the first spectrum recorded after mixing is considered as 100%.

Reaction rates of the tested Cu(II) complexes were found to be somewhat different (Fig. 20.b), *e.g.* the benzimidazole-TSC complex reacted the fastest, reaching equilibrium in less than 2 min. Furthermore, passing oxygen through the solutions of the reduced complexes could regenerate the complex, what was also observed in spectroelectrochemical studies (Fig. 19.b).

## *5.4 Salicylaldehyde thiosemicarbazones (STSCs) with methylenetrimethylammonium moiety and their Cu(II) complexes*

### *5.4.1 STSC analogues with* 5-*methylenetrimethylammonium substituent*

As it was already mentioned in chapter 2, STSCs are a class of thiosemicarbazones, which behave as tridentate ligands with (O,N,S) donor set. The presence of a phenol OH group at a chelation position instead of the pyridyl nitrogen might provide a different and more favourable coordination for harder Lewis-acid metal ions. However, STSC derivatives have usually lower aqueous solubility than α-*N* heterocyclic TSCs [78]. Based on this finding, the increase of their aqueous solubility was aimed by introducing a positively-charged methylenetrimethylammonium group to the aromatic unit. Moreover, the presence of this group in the TSCs gave opportunity to be mediated through the cell membrane by organic cation transporters (OCTs), which provides a more efficient cellular uptake [148]. The *N*-terminal substitution of the $NH_2$ groups in the case of several α-*N*-pyridyl TSCs increased the anticancer activity (*e.g. N*-terminal derivatives of triapine), thus similar modifications were done for STSC analogoues. Herein, four new STSC derivatives (Chart 11) and their Cu(II) complexes were studied (provided by our collaborating partner: V.B. Arion, University of Vienna). Anticancer activity of these compounds was tested by our partner (G. Spengler, University of Szeged) on the doxorubicin-sensitive Colo205, the multidrug-resistant Colo320 human colonic adenocarcinoma cell lines, neuroblastoma SH-SY5Y and normal human embryonal lung fibroblast cells MRC-5 (Table S3). It was found that Cu(II) complexes of the tested compounds VA8-11 showed higher anticancer activity ($IC_{50}$ = 8.93 – 100 μM) compared to the ligands alone ($IC_{50}$ = 31.46 – 100 μM). It was also suggested that interaction with OCTs can be responsible for the anticancer activity and are considered as possible targets for TSCs. In order to elucidate the influence of the methylenetrimethylammonium group and the *N*-terminal substitution of the $NH_2$ group on physico-chemical properties, detailed solution equilibrium studies were performed, where the proton dissociation constants of the ligands were determined, stability and redox properties of their Cu(II) complexes and lipophilicity of ligands and complexes were characterized.

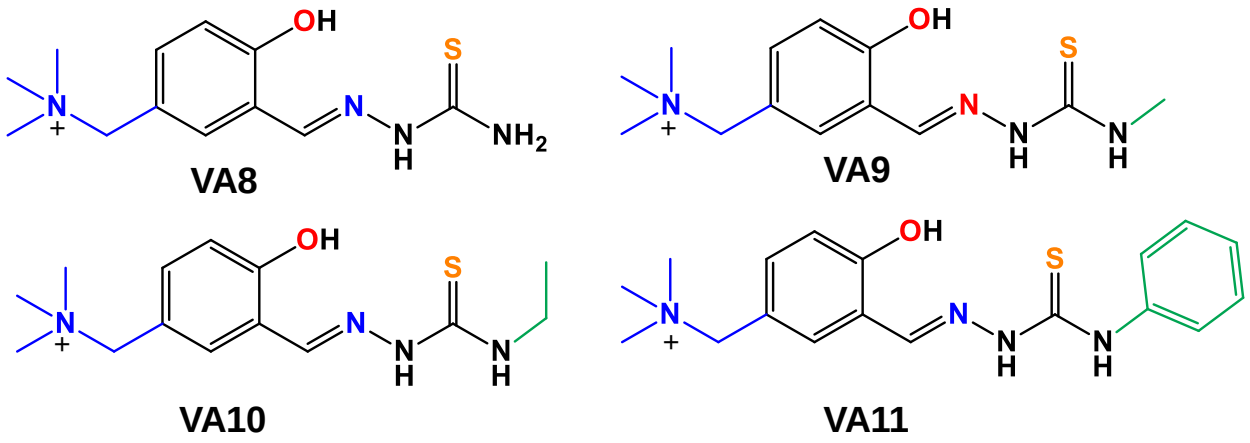


**Chart 11**. Chemical structures of the investigated ligands with methylenetrimethylammonium moiety: VA8, VA9, VA10 and VA11.

*5.4.2 Characterization of the proton dissociation processes and lipophilicity of the ligands VA8-11*

The main aim of this ligand design was to enhance the aqueous solubility of the ligands. Lipophilicity was measured at pH 7.4 and the obtained data were expressed as log$D_{7.4}$ (Table 7). It was found that the insertion of phenyl, ethyl and methyl groups increases the lipophilicity in the following order: VA8 < VA9 < VA10 < VA11. Comparison of these compounds to their structural analogue STSC (log$D_{7.4}$: +1.59) [149] revealed that the tested compounds are indeed much more hydrophilic than the unsubstituted counterpart.

The protonation processes of the ligands VA8-11 were investigated mainly by UV-vis spectrophotometric titrations in the pH range 1.0−11.5 in water. Representative spectra are shown recorded for VA10 in Fig. 21.a. Taking into account the spectral changes, which were detected in the pH range 5−10, only one deprotonation process was observed. The spectra reveal the appearance of the isosbestic points at 227, 279 and 348 nm. Based on this finding, one p$K_a$ value was calculated for each ligand (Table 7). This process is most probably attributed to the deprotonation of the phenolic OH group [78]. It should be noted that these compounds have one more proton dissociable group (hydrazonic-NH), which is expected to deprotonate at higher pH values and p$K_a$ could not be determined under the used conditions.

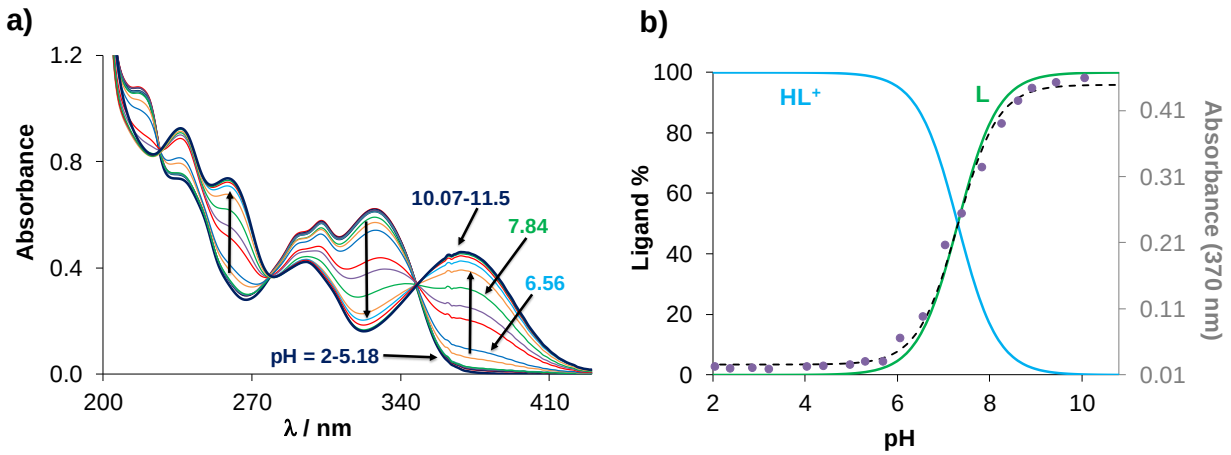


**Figure 21**. a) UV-vis absorption spectra recorded for the ligand VA10 at various pH values; b) concentration distribution curves plotted together with the absorbance changes at 370 nm (●) and the fitted curve (dotted line). {$c_L$ = 46.9 μM; $I$ = 0.1 M (KCl); $T$ = 25 °C; $\ell$ = 1 cm}

It is worth to mention that the p$K_a$ value for the same deprotonation process of STSC is 8.53 determined in aqueous solution [149]. All of the tested derivatives showed lower proton dissociation constants by more than one order of magnitude compared to STSC. This can be explained by the electron-withdrawing effect of the methylenetrimethylammonium group. The unsubstituted ligand VA8 has a similar p$K_a$ value compared to the methyl (VA9) and ethyl (VA10) *N*-terminally substituted derivatives, whereas the ligand VA11 with phenyl group at the *N*-terminal position showed somewhat stronger acidity. Using these data, concentration distribution curves were computed (Fig. 21b for ligand VA10), which show that these compounds are partly deprotonated at the physiological pH.

**Table 7.** Proton dissociation constants (p$K_a$) of the studied ligands; overall stability constants (log$\beta$), p$K_a$ of their Cu(II) complexes, pCu values calculated ($I$ = 0.1 M (KCl); $T$ = 25 °C), log$D_{7.4}$ of the ligands and complexes at pH 7.4 at $c_{Cu(II)} = c_L$ = 10 μM, in addition of the observed rate constants ($k_{obs}$) obtained for the redox reaction of the complexes with GSH (pH = 7.4; $c_{complex}$ = 25 μM; $c_{GSH}$ = 1.25 mM). Table was adapted from publication [P6].

| | **VA8** | **VA9** | **VA10** | **VA11** |
|---|---|---|---|---|
| **p$K_a$ (HL$^+$)** | 7.46 ± 0.01 | 7.54 ± 0.01 | 7.31 ± 0.01 | 7.03 ± 0.01 |
| **% L** at pH 7.4 | 47% | 42% | 55% | 70% |
| **log$D_{7.4}$** (ligand) | −0.84 ± 0.03 | −0.39 ± 0.01 | +0.06±0.04 | +0.68 ± 0.04 |
| **log$\beta$ [CuL]$^{2+}$** | 12.00 ± 0.01 | 11.73 ± 0.02 | 11.66 ± 0.03 | 11.26 ± 0.02 |
| **log$\beta$ [CuLH$_{-1}$]$^+$** | 8.14 ± 0.01 | 7.76 ± 0.02 | 7.67 ± 0.03 | 8.55 ± 0.02 |
| **log$\beta$ [CuLH$_{-2}$]** | −1.66 ± 0.02 | −1.48 ± 0.08 | −1.65 ± 0.09 | −1.31 ± 0.05 |
| **p$K_a$ [CuL]$^{2+}$** | 3.86 | 3.97 | 3.99 | 2.71 |
| **p$K_a$ [CuLH$_{-1}$]$^+$** | 9.80 | 9.24 | 9.32 | 9.86 |
| **pCu** [a] | 12.21 | 11.79 | 11.82 | 12.80 |
| **log$D_{7.4}$** (complex)[b] | −1.00 ± 0.01 | −0.79 ± 0.01 | −0.40 ± 0.01 | −0.17 ± 0.01 |
| **$k_{obs}$ (min$^{-1}$)** | 0.061 ± 0.022 | 0.073 ± 0.002 | 0.058 ± 0.001 | 0.025 ± 0.005 |

[a] pCu = −log[Cu(II)] at pH = 7.4; $c_{Cu(II)}$ = 10 μM; $c_L$ = 10 μM, pCu(STSC) = 11.9;
[b] log$D_{7.4}$ (Cu(II) – STSC) = +0.97 ± 0.01.

Namely, 42-55% of the ligands VA8, VA9 and VA10 are in the neutral L form, whereas for VA11 70% was found in this form. It can be concluded that this neutral form is a zwitterionic structure (phenolate and trimethylammonium moieties), which explains the excellent aqueous solubility.

The proton dissociation process was also studied by $^1$H NMR spectroscopy in the case of VA8. Moreover, formation of E/Z isomers with respect to the C=N double bond could be determined by this method as well. $^1$H NMR spectroscopic titration was performed in the aqueous solution (Fig. 22), and two sets of signals were detected in the pH range from 1.0 till 11.9. It is worth to mention that the extent of peak separation was dependent on the type of protons, and some peaks were strongly overlapping (CH=N; $CH_2$; $CH_3$). Taking into account the integrated peaks, the molar fraction of the major isomer was found around 70% at pH ~1. At pH > 4 the molar fraction was increased and did not change up to ~85%. Isomers were identified based on the chemical shifts of the NH proton of the hydrazonic group, whereas the p$K_a$ values were determined for the isomers (Fig. 22) assumed on the pH-dependence of the chemical shifts (Fig. 23).

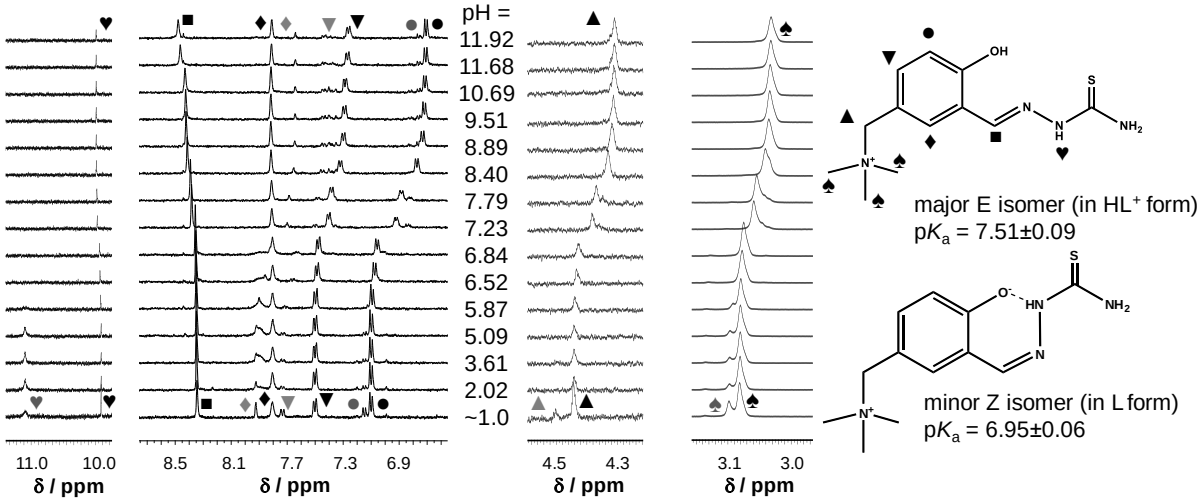


**Figure 22**. $^1$H NMR spectra recorded for ligand VA8 (with different enlargement of the selected regions for the better visibility) at various pH values with symbols used for proton resonances assignment in case of the major E isomer (black symbols) and minor Z isomer (grey symbols) and their p$K_a$ values calculated on the basis of the chemical shift changes. {$c_L$ = 200 μM; $I$ = 0.1 M (KCl); $T$ = 25 °C; 10% (*v*/*v*) $D_2O/H_2O$}. Figure was taken from the publication [P6].

This hydrazonic NH group is quite sensitive for the isomer identification. Taking into account literature data [61,79,150], the major species was defined as the E isomer characterized by a NH peak at 10.02 ppm at pH ~1 shifted up to 10.09 ppm with increasing pH parallel to the deprotonation of the phenolic OH group. The NH peak (at 11.08 ppm) of the minor, Z isomer could be detected only in the acidic pH range, most probably as a consequence of the hydrogen bond formation between this NH moiety and the deprotonated phenolate (L form of the minor

isomer in the Fig. 22). Furthermore, p$K_a$ value which was calculated for the minor isomer was approximately half logarithm unit lower (6.95 *vs.* 7.51) than that of the other isomer. This can be due to the formation of the intramolecular hydrogen bond, which makes the deprotonation of the OH group easier. Interestingly, $^1$H NMR spectra recorded in DMSO-$d_6$ for the same VA8 ligand did not show isomer formation and also isomers were not found in case of STSC in 30% DMSO-$d_6$/$H_2O$ [78].

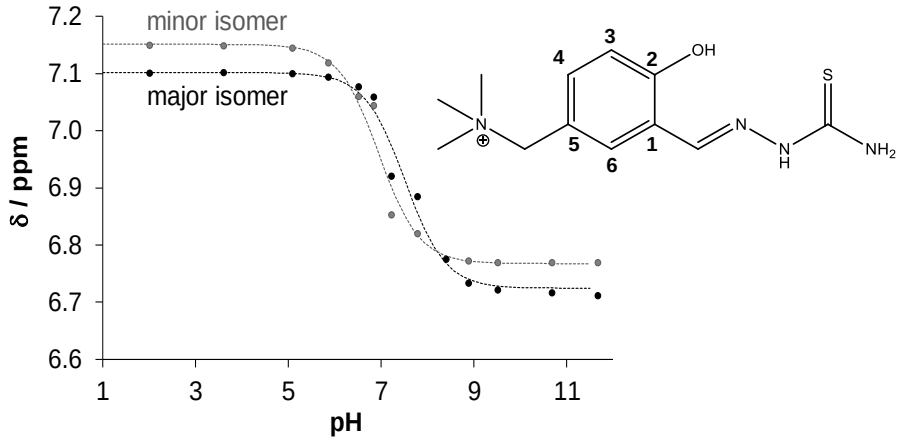


**Figure 23.** Chemical shifts of the CH3 proton of the major (●) and minor (●) isomers of VA8 plotted against the pH values in addition to the fitted curves (dashed lines). {$c_L$ = 200 μM; $I$ = 0.1 M (KCl); $T$ = 25 °C; 10% (*v/v*) $D_2O$/$H_2O$}. Figure was adapted from the publication [P6]

*5.4.3 Stability of Cu(II) complexes in aqueous solution, lipophilicity and their reduction by GSH*

Solution speciation of Cu(II) complexes with VA8-11 compounds was evaluated by spectrophotometric titrations at various metal-to-ligand ratio in water. The main goal was to characterize the stability and stoichiometry of Cu(II) complexes in aqueous solution, specifically at physiological pH and to monitor the influence of the *N*-terminal substitutions and the presence of the methylenetrimethylammonium moiety on the stability of the Cu(II) complexes. The complex formation processes of the structurally analogous compound STSC with Cu(II) ions were already investigated in a previous work by our group [78]. Since the same coordinating donor atoms are present in these ligands than in that work, similar binding modes and solution speciation were expected here. Data obtained from UV-vis spectra, which were recorded at different pH values, showed that the complex formation occurs already at pH ~ 1, similarly to the reference compounds STSC. In the monitored pH range two well-separated processes were observed. Particularly, in the acidic pH range the protonated species (denoted as $[CuL]^{2+}$ in Chart 12) complex is formed, in which the ligand binds to Cu(II) through ($O^-$,N,S) donor atoms and the hydrazonic nitrogen, which does not participate in the coordination, is still protonated. The

complex $[CuLH_{-1}]^+$, in which the ligand is bound via ($O^-$,N,$S^-$) mode, is very likely formed due to the deprotonation of the hydrazonic nitrogen.

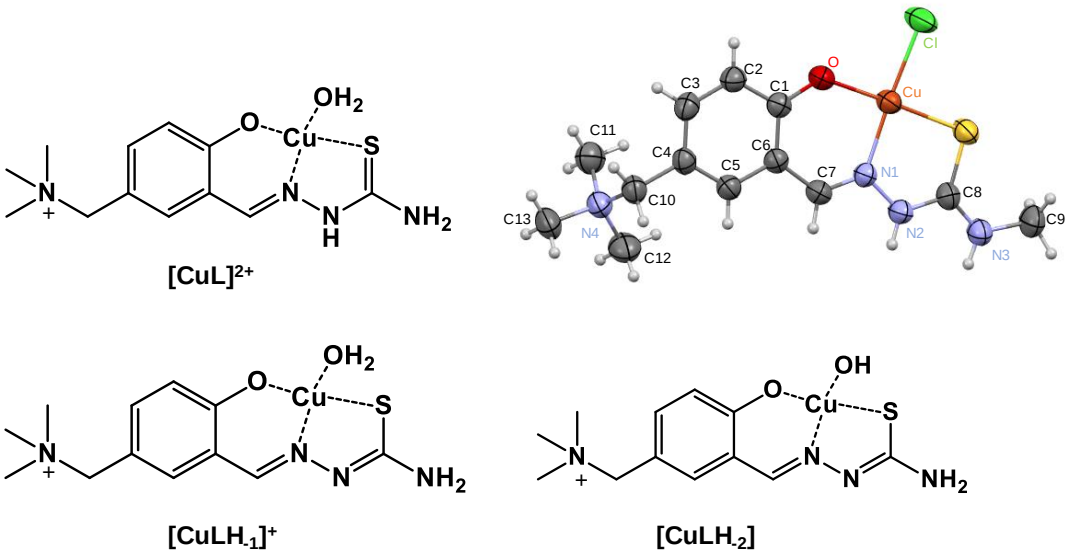


**Chart 12**. Suggested structures for the Cu(II) complexes formed with VA9 ligand and its molecular structure confirmed by SXRD study [P6].

Furthermore, complex $[CuLH_{-2}]$ which is a mixed hydroxido species with ($O^-$,N,$S^-$)($OH^-$) donors set (Chart 12) is formed in the basic pH range for all derivatives. It is worth to mention that the coordination of the chloride ion was found in the single-crystal of the complex confirmed by SXRD (Chart 12) (the crystallization was done by the group of V.B. Arion, University of Vienna.). Overall stability constants (log$\beta$, Table 7) for all Cu(II) complexes, which were mentioned above, were calculated by the analysis of the UV-vis spectra. These equilibrium constants were used for computation of concentration distribution curves and individual molar absorbance spectra; and as an example, the Cu(II)-VA11 system is shown in Figs. 24.a,b.

Based on the concentration distribution curves computed, the species $[CuLH_{-1}]^+$ was found predominant in a wide pH range involving the physiological pH. The stability of this type of Cu(II) complexes was compared through pCu values. These data were calculated at pH 7.4 and presented in Table 7, where the following trend of Cu(II) affinity of the studied ligands and their reference compund was found: VA9 ~ VA10 < STSC < VA8 << VA11. It can be concluded that only the *N*-terminal phenyl substitution could increase the Cu(II) complex stability considerably.

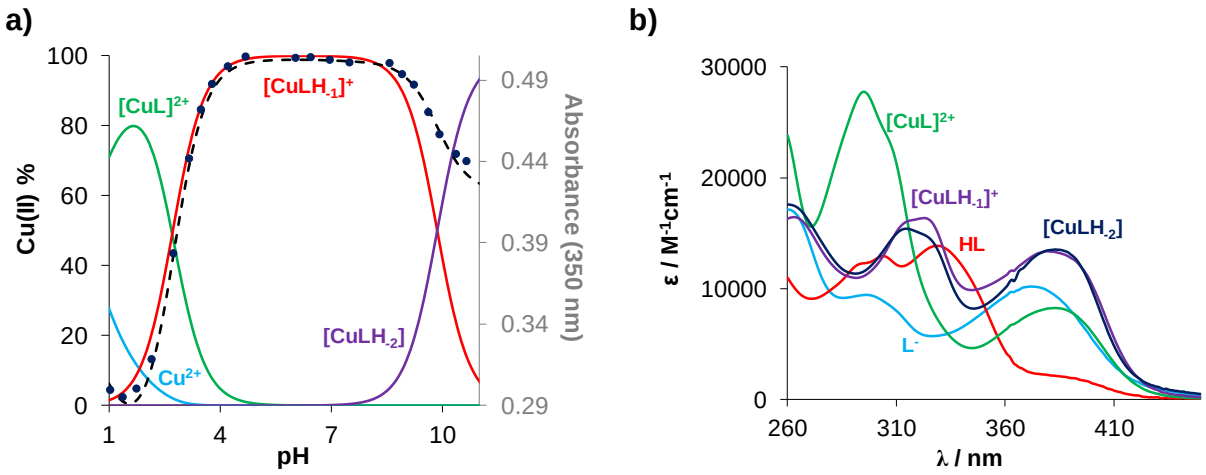


**Figure 24**. a) Concentration distribution curves for the Cu(II)-VA11 system plotted together with the absorbance changes at 350 nm (●) and the fitted curve (dotted line) {$c_{ligand}$ = 50 μM; $c_{Cu}$(II) = 48.4 μM; $T$ = 25.0 °C; $I$ = 0.1 M (KCl); $\ell$ = 1 cm}; b) Individual UV-vis absorption spectra of the different complexes and ligand species calculated for the same system in water.

The lipophilicity (log$D_{7.4}$, Table 7) of the studied Cu(II) complexes was characterized as well and compared to their corresponding ligands showing their more hydrophilic nature due to the positive charge. The same trend in lipophilicity was found for Cu(II) complexes as for ligands. It should be noted that the Cu(II) complex of the structural analog STSC was much more lipophilic compared to the Cu(II) complexes with VA8-VA11 ligands (Table 7), since that complex is charge neutral.

Direct redox reaction between the studied Cu(II) complexes and reducing agents such as GSH was also followed in order to analyze their reactivity. Herein, reaction was followed by UV-vis spectroscopy under anaerobic condition at pH 7.4 with high excess of reducing agent (50 equivalents) as it was applied for the previously described systems. Moreover, interaction of the studied Cu(II) complexes with AA was tested as well, where reaction was quite slow. In a different manner, significant spectral changes were found during the reaction with GSH, which are shown for Cu(II) complex of VA8 in the Fig. 25.a.

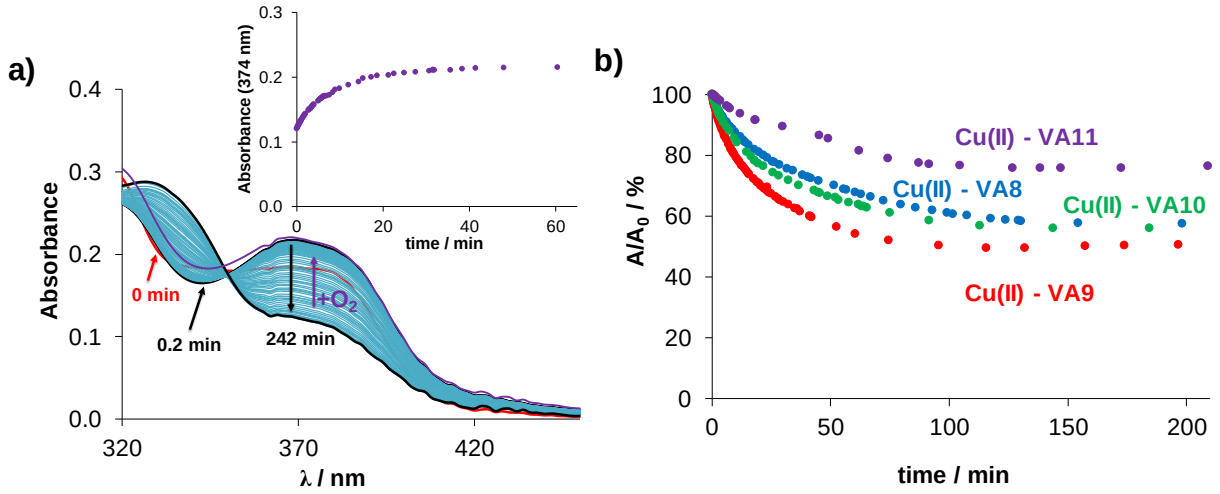


**Figure 25**. Time-dependent UV-visible absorption spectra of Cu(II)-VA8 system in the presence of 50 equivalents of GSH (pH = 7.4 (50 mM HEPES); {$c_{complex}$ = 25 μM; $c_{GSH}$ = 1.25 mM; $I$ = 0.1 M (KCl); $T$ = 25 °C; $\ell$ = 1 cm} and the inserted figure shows effect of bubbling by $O_2$ the absorbance values at 374 nm plotted against the time. b) Absorbance values at 366 nm (●) for Cu(II)-VA8, at 370 nm (●) for Cu(II)-VA9, at 368 nm (●) for Cu(II)-VA10 and at 376 nm (●) for Cu(II)-VA11 complexes with GSH in dependence of time. Absorbance read from the first spectrum recorded after mixing is considered as 100%.

After mixing the reactants, the first recorded spectrum reveals significant and fast change of the absorbance band, which is most probably connected to the formation of a ternary complex with GSH as it was discussed above. Afterwards, the spectral changes represent significant decrease at $\lambda_{max}$ = 366 nm for Cu(II) complex of VA8, whereas new bands appear with the $\lambda_{max}$ of the free ligand (~298 nm). This can be the result of the decomposition of the reduced Cu(I) complex due to the presence of high excess of GSH replacing the TSC ligand. It is worth to mention that bubbling oxygen into the solution can regenerate the Cu(II) complex (Fig. 25.a), which shows the reversibility of the redox process. All the studied Cu(II) complexes showed similar behavior, although the Cu(II)-VA11 complex was somewhat less sensitive to GSH, where less efficient reduction was seen (Fig. 25.b). Observed rate constants ($k_{obs}$) (Table 7) were calculated by analyzing the recorded absorbance – time curves at the $\lambda_{max}$ for comparison of differences in the reaction rates. Obtained $k_{obs}$ values were somewhat different, where the following trend was found: VA9 > VA8 ~VA10 > VA11, which corresponds to the stability order of the complexes.

*5.5 Sterane-based salicylaldehyde (thio)semicarbazones and their Cu(II) complexes: impact of hybridization and N-terminal substitutions*

*5.5.1 S(T)SC analogues with sterane- and 5,6,7,8-tetrahydronaphthalene based moieties*

In the previous chapter, the discussion centered around salicylaldehyde TSC (STSC) derivatives and their Cu(II) complexes exhibiting enhanced aqueous solubility. It was found that the incorporation of a positively-charged methylenetrimethylammonium group into the aromatic unit did not significantly affect the complex stability compared to the STSC-Cu(II) complex. Moreover, STSC-based compounds usually display lower cytotoxic activity in cancer cells in comparison to α-*N*-pyridyl TSCs, while complexation with Cu(II) ions generally increases their anticancer activity, which is most probably linked to their redox properties [52-54,78]. The antiproliferative activity of the STSC-based compounds can be also enhanced by the attachment of electron-donating substituents or by the molecular hybridization with various biologically active molecules. Herein, novel salicylaldehyde (T)SCs with sterane backbone (Chart 13) and their Cu(II) complexes were developed (the ligands were developed by our collaboration partner É. Frank, University of Szeged). The steroidal hybridization can display significant antitumor activity with negligible hormonal effect [151]. Besides that, simpler bicyclic derivatives as structural models were also prepared for the sake of comparison.

In this chapter a detailed comparative study of the prepared sterane (T)SCs with their structural models and Cu(II) complexes is reported. The primary aim was to investigate the effect of hybridization and the substitution of sulfur (TSC) to oxygen (SC) on several aspects, including the proton dissociation processes, stability in solution and redox properties of the corresponding Cu(II) complexes.

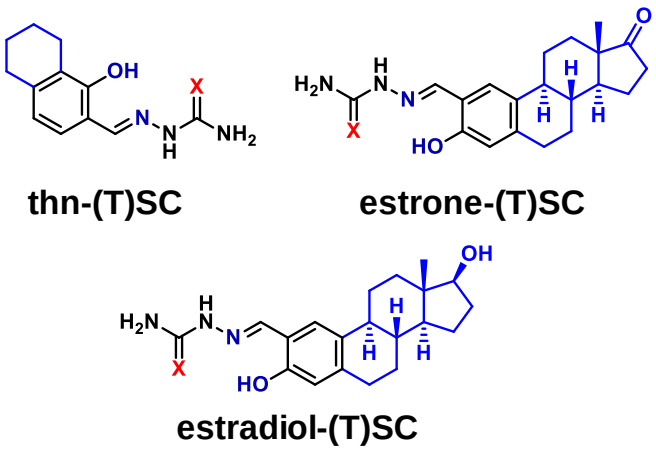


**Chart 13.** Chemical structures of thn-S(T)SCs, estrone-(T)SCs and estradiol-(T)SCs (X = S or O).

*5.5.1.1 Characterization of the solution chemical properties of non-methylated STSC derivatives*

In order to characterize the behavior of these ligands (Chart 13) in solution and compare them to their lead compounds such as STSC and SSC, detailed equilibrium studies were performed by UV-vis spectrophotometry in 30% (*v/v*) DMSO/$H_2O$ at relatively low ligand concentration due to their limited aqueous solubility. The protonated forms of these compounds have two proton-dissociable groups, namely the phenolic OH and the hydrazonic NH group of the thiosemicarbazone moiety, while in the estradiol-(T)SCs one extra OH group is also present, which can deprotonate as well in the highly basic pH range. Representative UV-vis spectra recorded for estradiol-TSC and estradiol-SC in the pH range 2.0-11.7 are presented in Figs. 26.a,b.

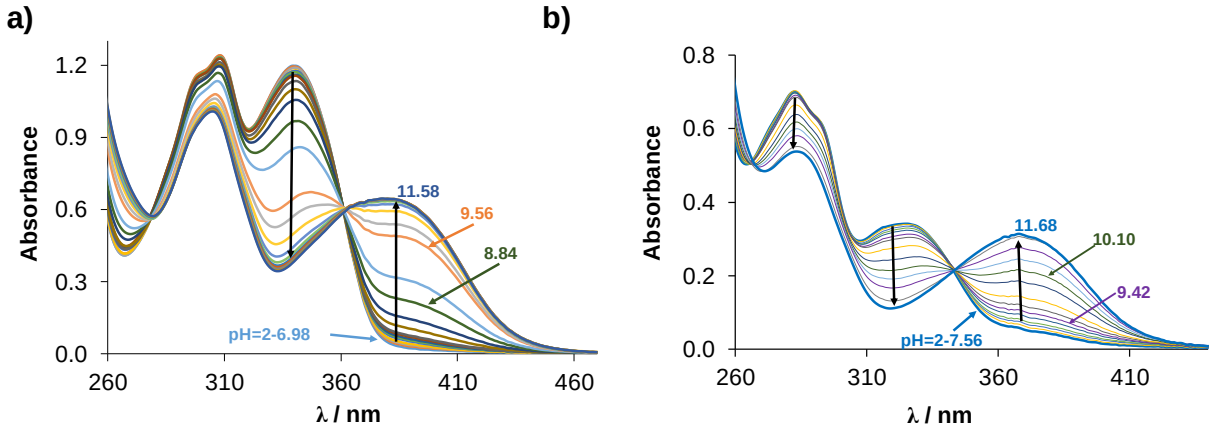


**Figure 26.** UV-vis absorption spectra of a) estradiol–TSC and b) estradiol-SC in the pH range 2.0–11.7 in 30% (*v/v*) DMSO/$H_2O$. {$c_L$ = 20 μM; $T$ = 25.0 °C; $I$ = 0.1 M (KCl); $\ell$ = 1 cm}. These figures were adapted from publication [P1].

The UV-vis spectra recorded at various pH values show only a single deprotonation process, which appears at pH > 7 up to pH ~ 12. The development of a new intense absorption band with a higher wavelength of maximum absorbance was observed (thn-TSC: $\lambda_{max}$ = 360 nm, thn-SC: $\lambda_{max}$ = 366 nm, estrone-TSC: $\lambda_{max}$ = 374 nm; estrone-SC: $\lambda_{max}$ = 362 nm, estradiol-TSC: $\lambda_{max}$ = 381 nm, estradiol-SC: $\lambda_{max}$ = 374 nm), which can be dedicated to the deprotonation of the phenolic-OH group. Based on these finding only one p$K_a$ value was computed for each ligand (Table 7) by the analysis of the UV-vis spectra.

**Table 8.** p$K_a$ values determined by UV-vis and fluorimetric titrations in 30% (*v/v*) DMSO/$H_2O$ and in water, respectively, log$D_{7.4}$ (*n*-octanol/water) and $P_{eff}$ values of compounds studied. {$T$ = 25 °C; $I$ = 0.1 M (KCl)}

| | **p$K_a$ (UV-vis) 30% (*v/v*) DMSO/$H_2O$** | **p$K_a$ (fluorimetry) $H_2O$** | **log$D_{7.4}$ *n*-octanol/$H_2O$, pH 7.4** | **$P_{eff}$ $H_2O$, pH 7.4 ($\times10^{-6}$ cm$\times$s$^{-1}$)** |
|---|---|---|---|---|
| **SSC** | 9.30±0.03 | n.d. | +0.94[a] | n.d. |
| **STSC** | 8.53[a] | 8.74±0.01 | 1.59[a] | 5.7±0.6 |
| **thn-TSC** | 9.40±0.01 | 9.15±0.01 | > +1.7 | 19±6 |
| **thn-SC** | 10.10±0.03 | n.d. | n.d. | n.d. |
| **estrone-TSC** | 9.00±0.01 | 8.94±0.01 | > +2 | n.d. |
| **estrone-SC** | 9.50±0.04 | n.d. | n.d. | n.d. |
| **estradiol-TSC** | 9.23±0.03 | n.d. | n.d. | n.d. |
| **estradiol-SC** | 10.02±0.03 | n.d. | n.d. | n.d. |

[a] Data taken from ref [149].

Based on the obtained proton dissociation constants of the phenolic OH groups, it can be concluded that the studied SCs have higher p$K_a$ values by approximately half logarithmic units in comparison to the corresponding TSCs. Moreover, the conjugation to the estrone/estradiol scaffold increases p$K_a$ values most probably due to the electron-donating effect of the neighboring cyclohexyl moiety in sterane-based (T)SCs and thn-(T)SC. Moreover, the neutral HL form predominates in a wide pH range (2–8) also including the physiological pH.

All studied compounds possess intrinsic fluorescence as the representative 3D spectra recorded for estradiol-TSC and estradiol-SC show in Fig. 27.a,b. Taking into account this finding, fluorimetric titrations were performed for STSC, estrone-TSC and thn-TSC in aqueous solutions, as the emission spectrum was found to be sensitive to the deprotonation of the OH group (Fig. 28).

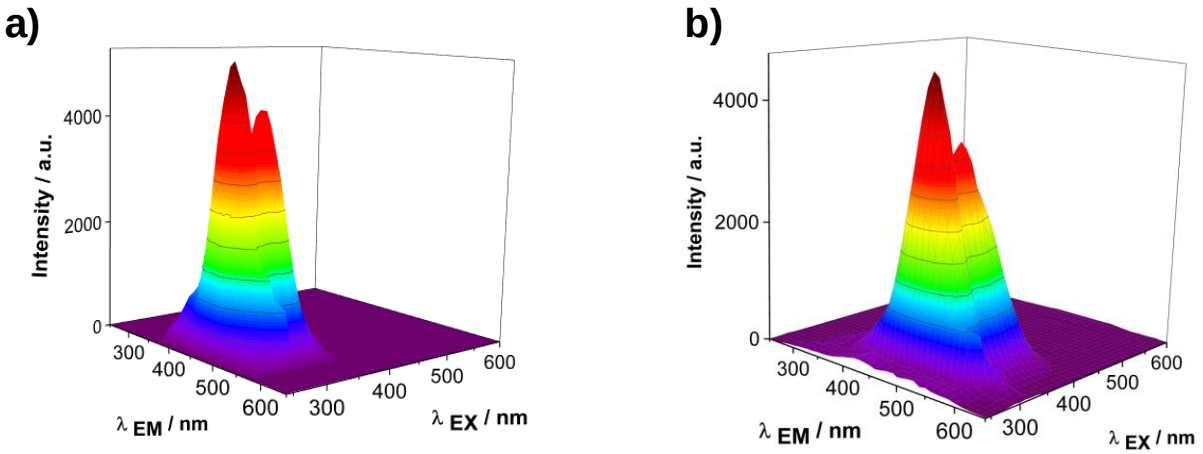


**Figure 27**. Three-dimensional fluorescence spectra of a) estradiol-SC and b) estradiol-TSC in $H_2O$ at pH 7.4. {$c_L$ = 10 μM; $I$ = 0.1 M (KCl); $T$ = 25.0 °C; $\ell$ = 1 cm}. These figures were adapted from publication [P1].

Based on these spectral changes, p$K_a$ values were determined in the aqueous solution for the phenolic hydroxyl group as well (Table 8). It is worth to mention that the p$K_a$ values are higher in the presence of DMSO compared to those obtained in the aqueous solution, what was expected, since the formation of anionic bases ($L^-$) is less favorable in the DMSO/$H_2O$ mixture making the proton dissociation more difficult.

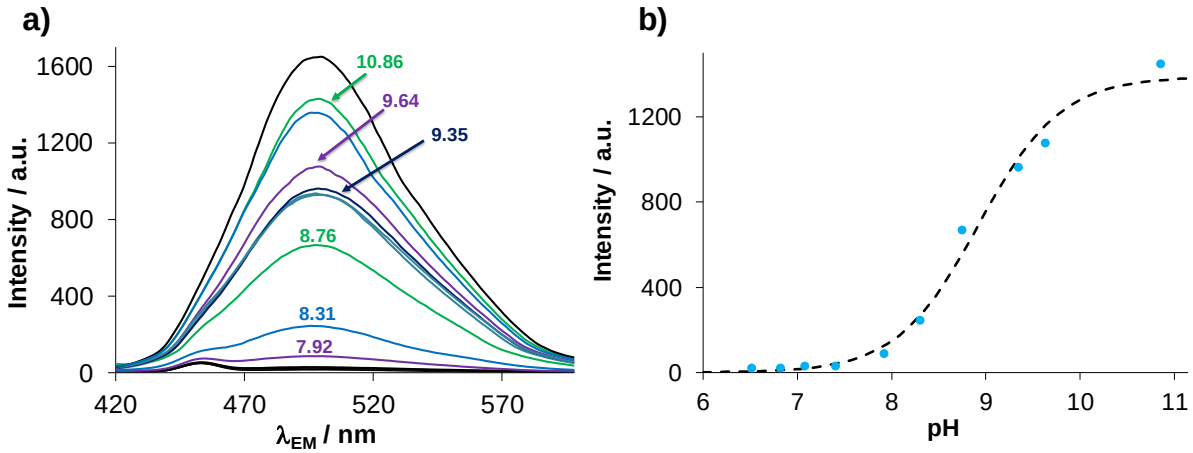


**Figure 28.** Emission spectra recorded at 390 nm excitation wavelength for estrone-TSC in the pH range 6–12 in aqueous solution. {$c_L$ = 1 μM; $T$ = 25.0 °C; $I$ = 0.1 M (KCl); $\ell$ = 1 cm}; b) change of measured (●) and calculated (dotted line) intensity at 505 nm emission wavelength. These figures were adapted from publication [P7].

The lipophilic character and membrane permeability were also investigated in order to monitor the ability of these compounds to pass through biological membranes passively, which is an important step to reach their intracellular targets. The determination of the lipophilic character using the traditional *n*-octanol/water partitioning method failed, as only a lower limit could be estimated (log$D_{7.4}$ > +1.7), since mostly the whole amount of the compounds retained in the *n*-octanol phase. Afterwards, the *in vitro* cell-free PAMPA was used, where the $P_{eff}$ coefficients (Table 8) for thn-TSC and STSC at pH 7.4 were determined based on UV-vis spectra recorded for the donor and acceptor phases. Formation of precipitate in the case of estrone-TSC under the experimental setup hindered the determination of its $P_{eff}$ value. (The value obtained for thn-TSC is merely an estimated value due to the high level of retention.) Data obtained for thn-TSC and STSC reveal that these compounds exhibit high membrane permeability ($P_{eff} \geq 1.5 \times 10^{-6}$ cm s$^{-1}$).

*5.5.1.2 Solution equilibrium of Cu(II) complexes with estradiol-(T)SCs, estrone–(T)SCs and thn-(T)SCs*

The complex formation processes of the analogous STSC and SSC were already investigated previously [78,81], and based on the structural similarity of the metal binding moieties of these compounds similar coordination modes and solution speciation were expected. Interaction of

S(T)SC derivatives with Cu(II) ions was studied by UV-vis spectrophotometric titrations in a 30% (*v/v*) DMSO/$H_2O$ solvent mixture due to the limited aqueous solubility. Based on the variation of the pH values, the characteristic spectral changes revealed the formation of three different species $[CuL]^+$, $[CuLH_{-1}]$ and $[CuLH_{-2}]^-$ (Scheme 7).

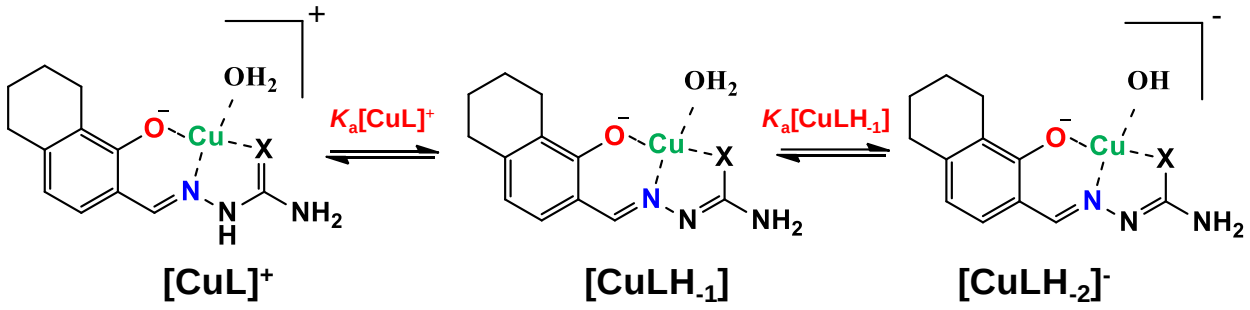


**Scheme 7.** Suggested structures for the Cu(II) complexes formed with thn-(T)SC ligands (X = S or O).

Namely, in the acidic pH range a protonated species $[CuL]^+$ is formed with ($O^-$,N,S) donor set, where the non-coordinating hydrazonic nitrogen is still protonated. The complex $[CuLH_{-1}]$, in which the ligand is coordinated in the ($O^-$,N,$S^-$) mode due to the deprotonation of the hydrazonic nitrogen, is found in the pH range 6–9. A mixed hydroxido species $[CuLH_{-2}]^-$ with ($O^-$,N,$S^-$)($OH^-$) coordination mode is present in the basic pH range. It should be noted that in the case of estradiol-SC and estradiol-TSC some precipitate was observed at pH > ~8 even at fairly low ligand concentrations (20 μM) hindering the determination of the formation constants for $[CuLH_{-2}]^-$ species, which appears in the basic pH range. In order to prove the suggested coordination modes, Cu(II) complexes were isolated from a MeOH/$H_2O$ mixture at pH ~ 7.4. After washing and drying, the green products were characterized by UV-vis, EPR spectroscopy, elemental analysis and ESI-MS. EPR spectroscopy (N.V. May, Research Centre for Natural Sciences Research Centre for Natural Sciences, Budapest) supported the same coordination mode in the isolated $[CuLH_{-1}]$ complexes, which was suggested for the solution structure of the studied SC and TSC complexes above (Scheme 7). Simulation of the EPR spectra (Figs. S2-6) resulted in the isotropic and anisotropic EPR parameters (*g* and *A* values in Tables S4-6), which were compared to each other and to the isotropic values of the complexes of STSC and SSC [78,81]. The Cu(II) complexes of estrone-TSC and thn-TSC have similar Hamiltonian EPR parameters with well-resolved hyperfine coupling of one nitrogen donor atom, where similar binding mode is suggested based on these parameters.

The coordination mode was also confirmed by X-ray crystallographic analysis for the solid complex [CuL]Cl formed with thn-TSC, [CuL]Cl × $H_2O$ for thn-SC and $[Cu(HL)Cl_2]$ × $H_2O$ × 2 $CH_3OH$ for estradiol-SC (Fig. 29). In the crystal [CuL]Cl formed with thn-TSC, the ligand coordinates to the Cu(II) ion through the deprotonated $O^-$ and its N1 and S atoms and the fourth

position is occupied by a chloride ion in a square planar arrangement. Similarly, in the case of semicarbazone analogue, Cu(II) ions are coordinated by the monoanionic form of the ligand via ($O^-$,N,O) donor set and in the fourth position a chlorido co-ligand and the coordination is supplemented with an axial water molecule (Figs. 29.a,b). It is worth to mention that in the case of crystal structure for the Cu(II) complex of estradiol-SC different species was found. Namely, the complex forms a square pyramidal system where estradiol-SC coordinates to the Cu(II) ion via the (O,N,O) donor set, and two coordinated chloride ions neutralize the charge of the central ion (Fig. 29.c). Crystal data and structure refinement data are collected for these crystals in Table S7-8.

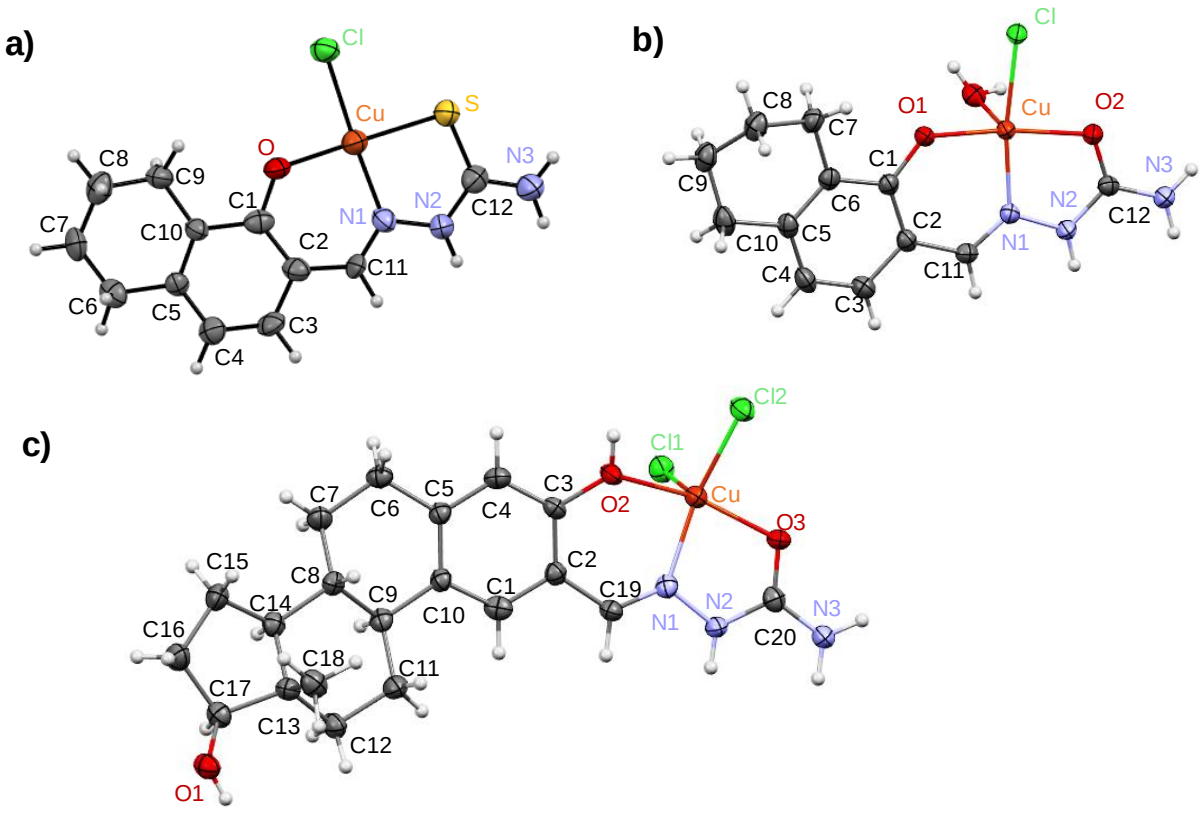


**Figure 29**. Molecular structures and atom labeling of the Cu(II) complexes of a) thn-TSC as [CuL]Cl, b) thn-SC as [CuL]Cl × $H_2O$ and c) estradiol-SC as [Cu(HL)$Cl_2$], where HL is full protonated form. These figures were adapted from publications [P1,P5,P7].

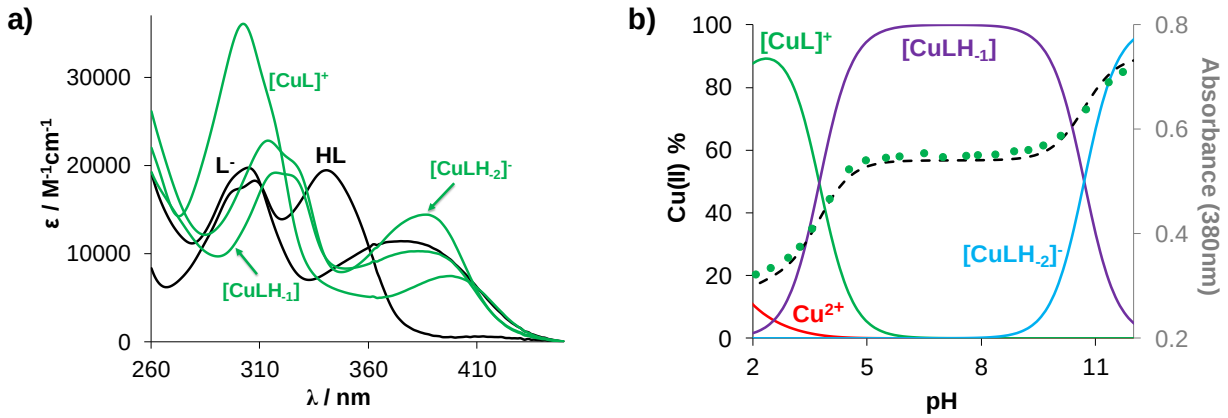


**Figure 30.** a) Individual UV-vis absorption spectra of the different complexes (green lines) and ligand species (black lines) calculated for the same system in 30% *(v/v)* DMSO/$H_2O$ solvent mixture. b) Concentration distribution curves for the Cu(II)-estrone-TSC (1:1) system plotted together with the absorbance changes at 380 nm (●) with the fitted curve (dotted line). {$c_{ligand}$ = 52.8 μM; $c_{Cu}$ = 52.6 μM; $T$ = 25.0 °C; $I$ = 0.1 M (KCl); $\ell$ = 1 cm}

Overall stability constants were calculated on the basis of the recorded spectra for $[CuL]^+$, $[CuLH_{-1}]$ and $[CuLH_{-2}]^-$ species (Table 9) together with their individual molar spectra (Fig. 30.a). Concentration distribution curves were also computed using these obtained stability constants (for the Cu(II)-estrone-TSC system, Fig. 30 b).

**Table 9.** Overall stability constants (log$\beta$), p$K_a$ of the Cu(II) complexes of estrone-TSC, thn-TSC and STSC[a]/SSC for comparison determined by UV-vis titrations in 30% (*v/v*) DMSO/$H_2O$. Log$D_{7.4}$ and $P_{eff}$ values determined for the complexes. {$T$ = 25 °C; $I$ = 0.1 M (KCl)}

| | log$\beta$ $[CuL]^+$ | log$\beta$ $[CuLH_{-1}]$ | log$\beta$ $[CuLH_{-2}]^-$ | log$D_{7.4}$ | $P_{eff}$ ($\times10^{-6}$ cm s$^{-1}$) |
|---|---|---|---|---|---|
| **SSC** | 10.58[b] | 4.30[b] | n.d | +1.04[b] | n.d |
| **thn-SC** | 11.71 ± 0.01 | 5.29 ± 0.02 | -5.01 ±0.02 | n.d | n.d |
| **thn-TSC** | 13.58 ± 0.01 | 9.35 ± 0.01 | -1.15 ± 0.02 | +1.23 ± 0.2 | 5.6 ± 0.2 |
| **estrone-SC** | 11.26 ± 0.01 | 4.82 ± 0.02 | -5.51 ± 0.04 | n.d | n.d |
| **estrone-TSC** | 13.18 ± 0.01 | 9.44 ± 0.01 | -1.26 ± 0.04 | n.d | n.d |
| **estradiol-SC** | 11.63 ± 0.03 | 5.16 ± 0.03 | n.d | n.d | n.d |
| **estradiol-TSC** | 13.79 ± 0.03 | 9.84 ± 0.03 | n.d | n.d | n.d |

[a]STSC: log$\beta$ $[CuLH]^+$ = 23.03; log$\beta$ [CuL] = 19.02; log$\beta$ $[CuLH_{-1}]^-$ = 8.75 [78], where; $[CuLH]^+$ corresponds to $[CuL]^+$, [CuL] to $[CuLH_{-1}]$ and $[CuLH_{-1}]^-$ to $[CuLH_{-2}]^-$ in the case of STSC and thn/estrone/estradiol-(T)SCs derivatives; STSC: log$D_{7.4}$ = +0.97 ± 0.01; $P_{eff}$ = 1.5 ± 0.4. [b] Data taken from ref [81].

In order to compare the conditional stability of the complexes, pCu values were calculated at pH 5 at 50 μM concentrations of both the ligand and the metal ion, using the overall stability constants (Fig. 31). First of all, stronger binding ability was found for all studied TSC compounds compared to their model STSC and slightly stronger for the studied SC derivatives compared to SSC. Furthermore, obtained data reveal that the studied TSC ligands have much stronger affinity

to Cu(II) ions than the corresponding SCs. Moreover, similar stability was found for the estradiol-(T)SC complexes compared to the corresponding estrone-(T)SC derivatives, while somewhat lower stability was for thn-(T)SCs.

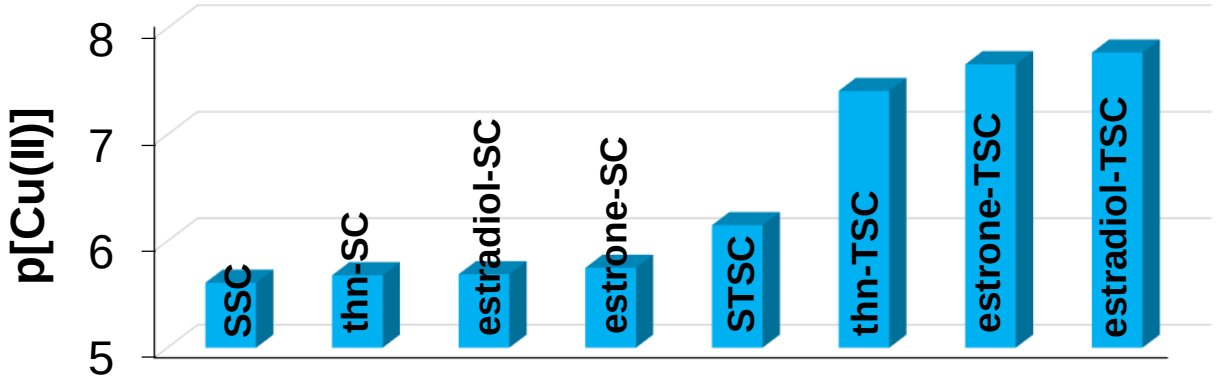


**Figure 31.** pCu values calculated for the Cu(II)-ligand (1:1) systems at pH 5 in 30% (*v*/*v*) DMSO/$H_2O$. {$c_L$ = $c_{Cu(II)}$ = 20 μM; $T$ = 25 °C; $I$ = 0.10 M (KCl)}

*5.5.2 Impact of stepwise $NH_2$-methylation of STSC analogues with sterane-and 5,6,7,8-tetrahydronaphthalene based moieties*

The stepwise $NH_2$-methylation was already studied in the case of some α-*N*-pyridyl thiosemicarbazones and results showed the improvement of anticancer activity (*e.g.* dimethylated triapine, DpC, Dp44mT) [61]. Based on this finding, terminal *N*-mono- and dimethylated derivatives of estrone-TSC, estradiol-TSC, thn-TSC (Chart 14) and their Cu(II) complexes were developed in order to obtain compounds with better anticancer properties. Moreover, impact of these substitutions was analyzed in order to show their influence on the proton dissociation processes, the stability and redox properties of the complexes formed with Cu(II) ions.

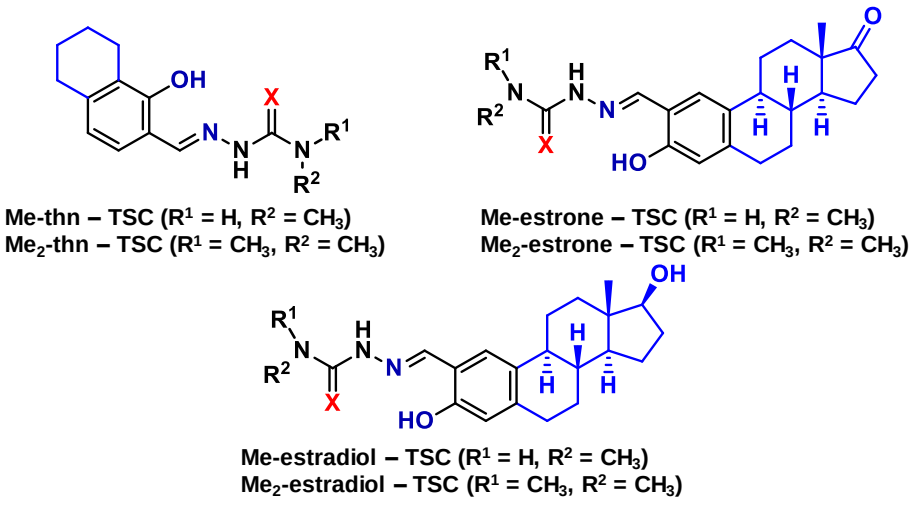


**Chart 14** Chemical structures of the investigated compounds (X = S or O).

*5.5.2.1 Solution chemical behavior of the sterane and 5,6,7,8-tetrahydronaphthalene based STSC derivatives with N-terminal substitutions*

In order to evaluate the actual protonation state of the *N*-terminal mono- and dimethylated estrone-TSC, estradiol-TSC and thn-TSC derivatives at various pH values, the p$K_a$ values were determined spectrophotometrically in the same way as in the case of the non-substituted analogues. The obtained p$K_a$ values assigned to the OH group are found in Table 10.

It can be concluded that the *N*-terminal substitution by methyl group(s) and also estrone/estradiol-hybridization have only a minor influence on the ligand acidity (9.02 – 9.34). Namely, *N*-terminally substituted estrone-TSCs have lower p$K_a$ values compared to thn- and estradiol-TSC derivatives. The introduction of a second methyl group on *N*-terminal nitrogen decreased the p$K_a$ values. Similar finding was reported for a series of α-*N*-pyridyl TSCs [61].

**Table 10.** p$K_a$ values and overall stability constants (log$\beta$) determined by UV-vis titrations. {30% (*v/v*) DMSO/$H_2O$; $T$ = 25.0 °C; $I$ = 0.1 M (KCl)}

| | **p$K_a$** | **log$\beta$ [CuL]$^+$** | **log$\beta$ [CuLH$_{-1}$]** | **log$\beta$ [CuLH$_{-2}$]$^-$** |
|---|---|---|---|---|
| **Me-thn-TSC** | 9.34 ± 0.04 | 13.73 ± 0.02 | 9.56 ± 0.02 | -0.69 ± 0.04 |
| **Me-estrone-TSC** | 9.21 ± 0.03 | 13.70 ± 0.08 | 9.71 ± 0.08 | n.d. |
| **Me-estradiol-TSC** | 9.28 ± 0.03 | 13.68 ± 0.03 | 9.59 ± 0.03 | n.d. |
| **Me$_2$-thn-TSC** | 9.12 ±0.03 | 13.75 ± 0.03 | 9.56 ± 0.03 | -0.68 ± 0.02 |
| **Me$_2$-estrone-TSC** | 9.02 ± 0.03 | 13.36 ± 0.08 | 9.44 ± 0.07 | n.d. |
| **Me$_2$-estradiol-TSC** | 9.20 ± 0.03 | 13.96 ± 0.03 | 10.11 ± 0.03 | n.d. |

Notably, the *N*-monomethyl and *N*,*N*-dimethyl derivatives of estrone-TSC, estradiol-TSC and thn-TSC also possess intrinsic fluorescence, which can be useful for the monitoring of the cellular uptake or intracellular distribution of the ligands by fluorescence microscopy [84].

*5.5.2.2 Complex formation of N-terminally substituted thn-TSC, estrone-TSC and estradiol-TSC derivatives with Cu(II) ions*

In order to characterize the speciation and stability in solution of the Cu(II) complexes of *N*-terminal substituted derivatives of estradiol-TSCs, estrone-TSCs and thn-TSCs, solution equilibrium studies were performed by UV-vis spectrophotometric titrations in 30% (*v/v*) DMSO/$H_2O$, and EPR spectroscopy was also applied. In the previous chapter, the complex formation processes of the analogous estradiol-TSC, thn-TSC and estrone-TSCs have been already discussed. Based on the obtained results, formation of the same type of complexes was found. Namely, only mono-ligand species such as $[CuL]^+$, $[CuLH_{-1}]$ and $[CuLH_{-2}]^-$ (Scheme 7) were detected in similar pH range as it was found for the non-substituted analogues. The determined overall stability constants are collected in Table 10. It should be mentioned that some precipitation

was observed at pH > 8 at both 1:1 and 1:2 metal-to-ligand ratios in the case of estrone- and estradiol-TSC derivatives, which hindered the determination of the formation constants for species present in the basic pH range. EPR spectra were recorded for isolated Cu(II) complexes of studied ligands in DMSO at 77 K and room temperature (Figs. S7-9), where preparation of them was done with the same approach as it was described in chapter 5.5.1.2. The isotropic and anisotropic EPR parameters (*g* and *A* values) were obtained by simulation of the EPR spectra and were collected in Tables S9-S10. The isotropic values were compared to those of the Cu(II) complexes of estrone-TSC, estradiol-TSC and thn-TSC, and the similar isotropic EPR parameters reveal the same ($O^-$,N,$S^-$) coordination mode in the isolated species.

For comparison of the Cu(II) binding ability of the studied ligands, pCu values were computed on the basis of the stability constants at pH 5 at 20 μM concentrations of both the ligand and the metal ion (Fig. 32).

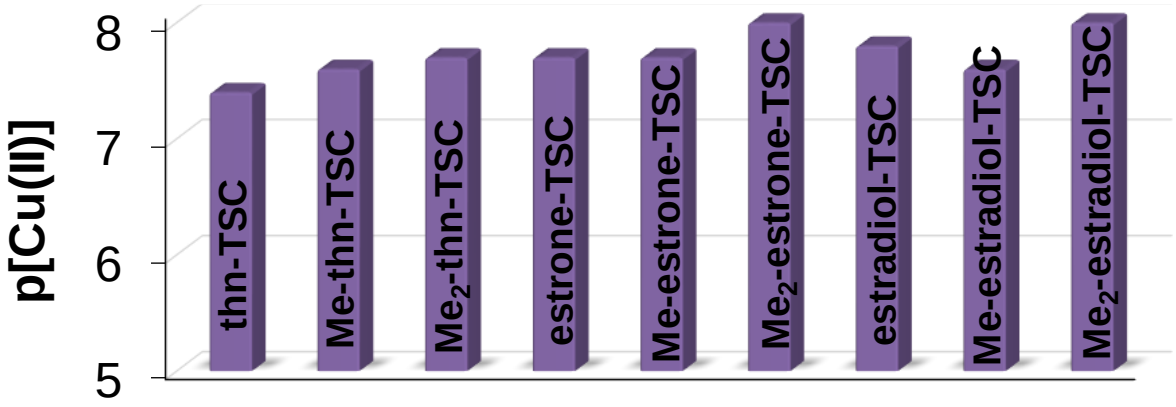


**Figure 32.** pCu values calculated for the Cu(II)-ligand (1:1) systems at pH 5 in 30% (*v/v*) DMSO/$H_2O$. {$c_L = c_{Cu(II)}$ = 20 μM; $T$ = 25 °C; $I$ = 0.10 M (KCl)}

Based on the pCu values, it can be concluded that the Cu(II) binding ability of the sterane-based derivatives is somewhat stronger than that of the thn-based compounds, and the stability of the complexes is increased with the *N*-terminal substitution.

*5.5.3 Redox properties of the Cu(II) complexes of thn-TSCs, estrone-(T)SCs and estradiol-(T)SC derivatives*

For a better understanding of the redox behavior of the complexes, CV and spectroelectrochemical experiments were performed for some selected systems. The voltammograms showed redox activity in both cathodic and anodic regions (Fig. 33.a). The initial reduction step can be attributed to the Cu(II) → Cu(I) process. The strongly shifted reoxidation peak during the reverse scan is in agreement with significant rearrangement of the coordination environment around Cu(I). The TSC complexes showed very similar irreversible reduction peaks: $E_{pc}$ for Cu(II)-estrone-TSC = +0.18 V; Cu(II)-estradiol-TSC = +0.18 V; Cu(II)-Me-estradiol-TSC = +0.19 V; Cu(II)-$Me_2$-

estradiol-TSC = +0.21 V *vs.* Ag/AgCl/3M KCl. However, somewhat different $E_{pc}$ for Cu(II)-estradiol-SC = –0.03 V was obtained, which most probably due to the different coordination mode of estradiol-SC. The oxidation peaks during the reverse scan are also similar: $E_{pa}$ for Cu(II)-estrone-TSC = +0.41 V; Cu(II)-estradiol-TSC = +0.44 V; Cu(II)-Me–estradiol-TSC = +0.39 V; Cu(II)-$Me_2$-estradiol-TSC = +0.46 V *vs.* Ag/AgCl/3M KCl, whereas for Cu(II)-estradiol-SC = +0.24 V. These values indicate the slightly stronger oxidizing power of the TSC complexes in comparison to SC complex. These processes can be explained by an electrochemical dual-pathway square scheme, which was already introduced in the chapter 5.3, Scheme 6.

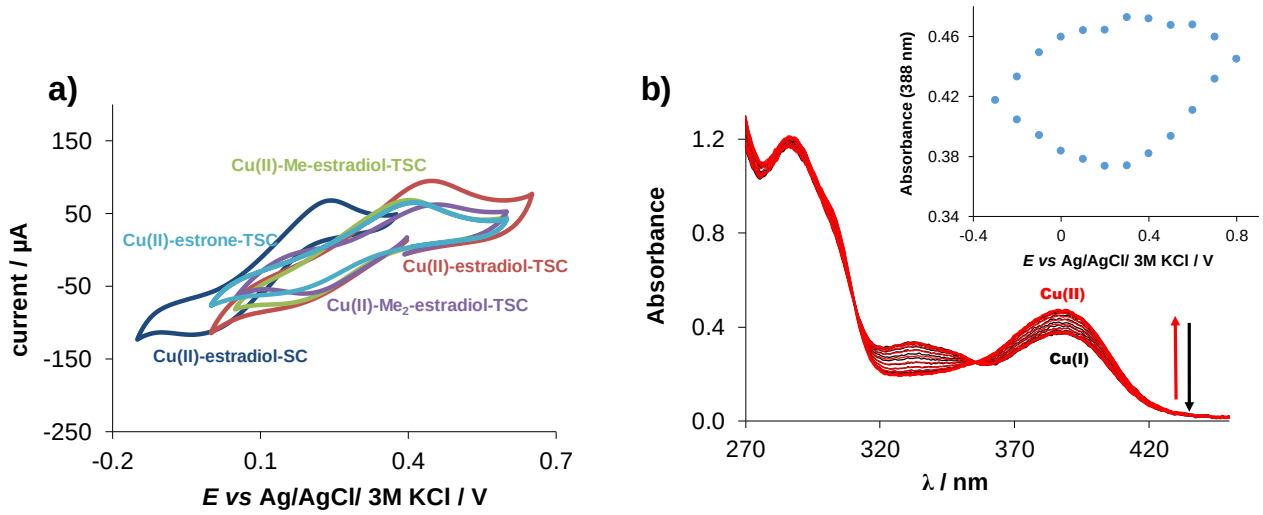


**Figure 33.** a) Cyclic voltammograms of the Cu(II)-(T)SC (1:1) chemical systems in 90% (*v/v*) DMSO/$H_2O$ at 10 mV/s scan rate {$c_{Cu(II)} = c_L$ =1 mM, pH = 7.40 (10 mM HEPES), $T$ = 25 °C, $I$ = 0.1 M ($nBu_4NPF_6$)}: b) UV-vis absorption spectra recorded for the Cu(II)-estradiol-SC system at the various potential values using the spectroelectrochemical cell. Inserted figure shows the absorbance values at 388 nm plotted against the potential. {$c_{Cu(II)}$ = 100 µM; $I$ = 0.1 M ($NBu_4PF_6$); $T$ = 25.0 °C, scan rate: 10 mV/s; $\ell$ = 0.17 cm}; This figure was taken from publication [P1].

Furthermore, in order to elucidate the chemical transformations taking place during the Cu(II)/Cu(I) one-electron transfer process, *in situ* UV-vis spectroelectrochemical measurements were carried out together with CV. The UV-vis spectra measured upon cathodic reduction revealed decreasing absorbance at 388 nm, accompanied by an increase at 330 nm (Fig. 33 b). Upon the reverse scan, the product that was formed upon the reduction of Cu(II) to Cu(I) was re-oxidized to the initial state (Fig. 33 b inserted). This finding definitely indicates that Cu(I) species are most probably stable, dissociation of the metal complex does not occur during the process. Similar behavior was observed for all tested Cu(II) complexes of sterane-based TSCs.

In addition, the direct redox reaction of the Cu(II) complexes with physiological reductants, such as GSH and AA, was monitored in order to check their reactivity and the time-dependence of the redox reaction. The reaction was followed by UV-vis spectrophotometry under strictly

anaerobic conditions in 30% (*v*/*v*) DMSO/$H_2O$ solvent mixture at pH 7.4 with the approach described in details in the previous chapters.

An example is provided for the reaction of the Me-thn-TSC complex with GSH (Fig. 34.a). The spectra, recorded immediately after mixing the reactants, revealed a significant spectral change (see spectra at 0 and 0.2 min). This change most probably due to the formation of a mixed-ligand complex with GSH as it was reported for other TSCs [61,63]. Later on, a notable decrease in the absorbance of the $S_{TSC}$→Cu CT band at $\lambda_{max}$ = 380 nm was observed, while the absorbance was increased at the $\lambda_{max}$ of the free ligand. This behavior can be explained by the liberation of the TSC ligand, where Cu(I) forms complex with GSH, which is present in a high excess in the solution.

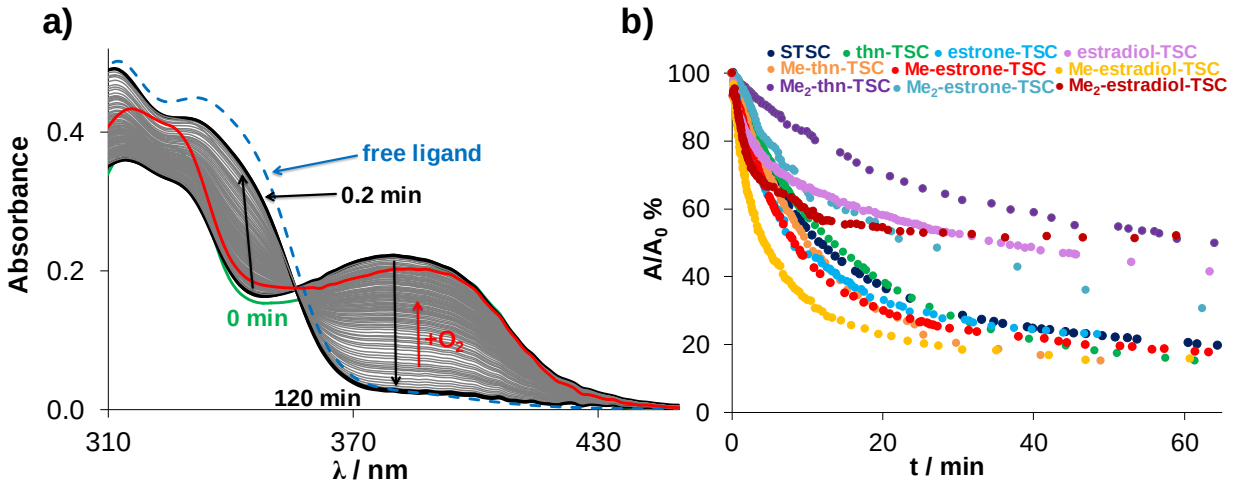


**Figure 34.** Time-dependent UV-visible absorption spectra of Cu(II)-Me-thn-TSC (1:1) system in the presence of 50 equivalents of GSH at pH = 7.4 (50 mM HEPES); {$c_{Cu}$ = $c_L$ = 25 μM; $c_{GSH}$ = 1.25 mM; $I$ = 0.1 M (KCl); $T$ = 25 °C; $\ell$ = 1 cm}; b) Absorbance values at 380 nm (●) for Cu(II)-STSC, (●) for Cu(II)-thn-TSC, (●) for Cu(II)-estrone-TSC, (●) for Cu(II)-estradiol-TSC, (●) for Cu(II)-Me-thn-TSC, (●) for Cu(II)-Me-estrone-TSC, (●) for Cu(II)-Me-estradiol-TSC, (●) for Cu(II)-$Me_2$-thn-TSC, (●) for Cu(II)-$Me_2$-estrone-TSC and (●) for Cu(II)-$Me_2$-estradiol-TSC complexes with GSH in dependence of time. Absorbance read from the first spectrum recorded after mixing is considered as 100%.

Moreover, bubbling oxygen into the solution could regenerate the complex (Fig. 34.a). Similar behavior was found for all other Cu(II) complexes, which were investigated here, except for the Cu(II) complexes with SCs, where fast reduction of Cu(II) complexes was observed. Basically, the first recorded spectrum after mixing the reactants showed the disappearance of the Cu(II) complex and the presence of the free semicarbazone. Furthermore, the reaction was not fully reversible during bubbling $O_2$ into the sample, where in case of TSCs reaction was reversible. In order to compare obtained data, the recorded absorbance-time curves were further analyzed and the observed rate constants ($k_{obs}$) were calculated (Table 11).

**Table 11.** Observed rate constants ($k_{obs}$) obtained for the redox reaction of the studied Cu(II) complexes {$c_{Cu}$ = $c_L$ = 25 μM} with 1.25 mM of GSH at pH 7.4 under anaerobic conditions. {$T$ = 25 °C; $I$ = 0.1 M (KCl); 30% (*v/v*) DMSO/$H_2O$}

| | $k_{obs}$ ($min^{-1}$) | | $k_{obs}$ ($min^{-1}$) |
|---|---|---|---|
| **Cu(II)-STSC** | 0.11 ± 0.02 | **Cu(II)-estrone-TSC** | 0.13 ± 0.02 |
| | | **Cu(II)-Me-estrone-TSC** | 0.05 ± 0.02 |
| **Cu(II)-thn-TSC** | 0.10 ± 0.02 | **Cu(II)-$Me_2$-estrone-TSC** | 0.05 ± 0.02 |
| **Cu(II)-Me-thn-TSC** | 0.05 ± 0.01 | **Cu(II)-estradiol-TSC** | 0.07 ± 0.03 |
| **Cu(II)-$Me_2$-thn-TSC** | 0.04 ± 0.01 | **Cu(II)-Me-estradiol-TSC** | 0.22 ± 0.02 |
| | | **Cu(II)-$Me_2$-estradiol-TSC** | 0.31 ± 0.06 |

The $k_{obs}$ values for the estradiol-TSCs somewhat differ, namely, the following trend was found: estradiol-TSC < Me-estradiol-TSC < $Me_2$-estradiol-TSC, which interestingly follows the stability order of the complexes. Whereas thn- and estrone-based Cu(II) complexes behaved similarly, as the observed rate constants do not differ significantly.

In addition, the reaction with AA was also carried out, revealing a notably slow process for the studied Cu(II)-TSC complexes. It suggests that the studied Cu(II) complexes cannot be reduced efficiently by this reducing agent, which is weaker than GSH. On the other hand, remarkable spectral changes were detected for the Cu(II)-estradiol-SC system, similar to the findings for the Cu(II)-estradiol-TSC complexes during their reaction with GSH.

*5.5.4 Antioxidant activity of thn-(T)SCs, estrone-(T)SCs and estradiol-(T)SCs*

Estradiol and its related compounds were reported to possess antioxidant activity due to the phenolic structure of the A ring [152]. Based on this finding, estradiol-(T)SCs were examined for free radical scavenging activity using the DPPH assay. Moreover, STSC and estradiol were tested as basic models of estradiol-(T)SCs. In order to check the influence of the exchange of 17-ketone to 17-OH on the D-ring of the sterane skeleton estrone-TSC was also screened.

The reaction between the tested compounds and DPPH was studied by UV-vis spectrophotometry at various concentrations in EtOH, where the process was followed till the redox equilibrium was reached. As an example, the UV-vis spectral changes for $Me_2$-estradiol-TSC are presented in Fig. 35.a.

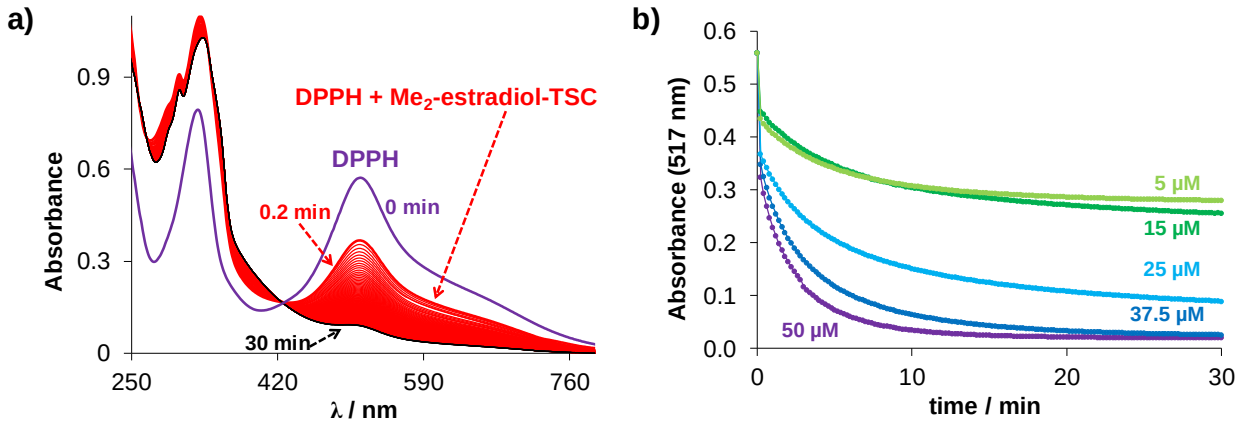


**Figure 35.** a) Time-dependent changes of the UV-vis spectra of the DPPH• ($c$ = 50 μM) in the presence of $Me_2$-estradiol-TSC (50 μM) in EtOH. ($T$ = 25 °C); b) Absorbance changes of DPPH at 517 nm upon reaction with $Me_2$-estradiol-TSC at different concentrations in EtOH plotted against the time. {$c_{DPPH}$ = 50 μM; $c_L$ = 50, 37.5; 25; 15; 5 μM; $T$ = 25°C; $\ell$ = 1 cm}; These figures were taken from publication [P1].

Absorbance changes followed at the $\lambda_{max}$ of DPPH (517 nm) at different DPPH: $Me_2$-estradiol-TSC ratios (from 1:0.1 until 1:1) are compared in Fig. 35.b. The antioxidant capacity was assessed using $IC_{50}$ values, which show the concentration, at which the compound reduces 50% of DPPH in the reaction mixture. These values were compared to that of the reference compound trolox, a well-known antioxidant [153]. The results of the DPPH assay are collected in Table 12, where the lower $IC_{50}$ and the higher TEAC values indicate a stronger antioxidant effect of the compound tested.

**Table 12**. DPPH free radical scavenging activity of estradiol-(T)SC, estrone-TSC, STSC, estradiol and trolox expressed as $IC_{50}$ and TEAC values, and % scavenging effect at 1:1 DPPH-to-compound ratio after 30 min. {$T$ = 25 °C; in EtOH, $c_{DPPH}$ = 50 μM; $c_{compound}$ = 5 – 50 μM}; This table was taken from publication [P1]; (n.d. = not determined).

| | $IC_{50}$ (μM) | % scavenging effect [a] | TEAC |
|---|---|---|---|
| **estradiol-SC** | >50 [b] | 6.5 | n.d. |
| **estradiol-TSC** | 14.6 | 72.0 | 0.8 |
| **Me-estradiol-TSC** | 15.4 | 31.0 | 0.8 |
| **$Me_2$-estradiol-TSC** | 13.6 | 100 | 0.9 |
| **estrone-TSC** | 17.8 | 49.8 | 0.7 |
| **STSC** | 19.0 | 23.4 | 0.6 |
| **estradiol** | >50 [b] | 0.5 | n.d. |
| **estradiol-SC+1 equiv. Cu(II)** | >50 [b] | 8.5 | n.d. |
| **estradiol-TSC+1 equiv. Cu(II)** | 15.7 | 90.8 | 0.8 |
| **Me-estradiol-TSC+1 equiv. Cu(II)** | 20.3 | 33.6 | 0.6 |
| **$Me_2$-estradiol-TSC+1 equiv. Cu(II)** | 16.4 | 40.4 | 0.7 |
| **estrone-TSC+1 equiv. Cu(II)** | 34.8 | 11.1 | 0.3 |
| **STSC+1 equiv. Cu(II)** | >50 [b] | 29.4 | n.d. |
| **trolox** | 12.0 | 100 | 1 |

[a] At DPPH:compound = 1:1 ratio after 30 min.;[b] It did not reach 50% inhibition under the conditions used.

These data reveal that $Me_2$-estradiol-TSC displays the ability to behave as antioxidant agent among other tested (thio)semicarbazones. It is worth to mention that the presence of Cu(II) ions does not improve the antioxidant activity, even decreases it.

*5.5.5 Biological properties of the strerane-based (T)SCs and their Cu(II) complexes*

The antibacterial activity of estrone-(T)SCs, thn-(T)SCs, estradiol-(T)SCs, and STSC and SSC for comparison, was studied on the Gram-positive *Staphylococcus aureus, Enterococcus faecalis* and the Gram-negative *Escherichia coli* and *Klebsiella pneumoniae* strains (performed by G. Spengler, University of Szeged). In addition, influence of the presence of one equivalent of Cu(II) on the antibacterial activity was tested as well. Antibacterial activity is expressed as MIC value, which is the lowest concentration of a compound that inhibits the growth of the bacteria; these values are presented in Table S11. Estradiol-SC and estradiol-TSC showed some activity on the Gram-positive *S. aureus* bacterial strain (50 and 25 μM, respectively). Complexation with Cu(II) did not induce an antibacterial effect in the case of the semicarbazone, while the Cu(II) complexes formed with the thiosemicarbazones displayed a remarkable antibacterial effect. It is worth to mention that the Cu(II) complexes of thn-TSC and STSC had a potent activity on Gram-positive bacteria, especially on *Staphylococcus aureus* strain (MIC: 3.125 μM, 6.25 μM for thn-TSC and STSC, respectively). Besides that, Cu(II) complexes of estradiol-TSC also had a potent activity on Gram-positive bacteria, in particular on the *S. aureus* strain (MIC: 3.125 μM for Cu(II)-estradiol-TSC, 6.25 μM for Cu(II)-Me-estradiol-TSC and 0.78 μM for Cu(II)-$Me_2$-estradiol-TSC complexes).

The anticancer activity of the tested compounds was investigated by three different research groups using various cell lines. Namely, STSC, thn-TSC and estrone-TSC series was tested by G. Spengler, University of Szeged; SSC, thn-SC, estrone-SC and *N*-terminal substituted derivatives of thn-TSC and estrone-TSC by D. Wernitznig, University of Vienna; and estradiol-(T)SCs were investigated by M. Kiricsi, University of Szeged. Therefore, the obtained $IC_{50}$ values determined by the different groups cannot be compared directly.

The anticancer activity of the STSC, estrone-TSC and thn-TSC ligands and their Cu(II) complexes were studied in the doxorubicin-sensitive Colo205, the doxorubicin-resistant Colo320 human colonic adenocarcinoma and the hormone-responsive MCF-7 breast cancer cell lines. It was found that estrone-TSC and thn-TSC ligands are cytotoxic against Colo205 and Colo320 human colon adenocarcinoma cell lines ($IC_{50}$: 10–84 μM), and especially significant activity was seen against MCF-7 breast cancer cells ($IC_{50}$: 3.73–6.42 μM). Moreover, their Cu(II) complexes were found much more cytotoxic ($IC_{50}$: 0.26-1.99 μM).

Cytotoxicity of SSC, estrone-SC, thn-SC and their Cu(II) complexes was tested against A549, SW480 and CH1/PA human cancer cell lines. Estrone-SC and thn-SC were more active in

all tested cell lines ($IC_{50}$: 3.8-149 μM) in comparison to SSC ($IC_{50}$: 89.3 - >200 μM), with the highest anticancer activity against CH1/PA, followed by SW480 and A549. It was found that the addition of one equivalent of Cu(II) ions to the ligands increased the cytotoxicity significantly ($IC_{50}$: 1.53-111 μM). Based on these results, Cu(II) complexes were selected for further investigation, where apoptosis induction was investigated on SW480 cells. The results (Fig. S10) demonstrated that the Cu(II) complex of estrone-SC was the only compound able to induce apoptosis among other Cu(II)-SC complexes. As the Cu(II) complexes of the SC ligands were found to be redox active, their ability to generate ROS was also investigated. The complexes were not able to induce high levels of ROS (Fig. S11), whereas complex of estrone-SC showed the strongest effect on the induction of ROS compared to other tested systems.

Me-estrone-TSC, $Me_2$-estrone-TSC, Me-thn-TSC, $Me_2$-thn-TSC and their complexes were tested on 3D multicellular spheroids of HCT-116, A549 and CH-1 cell lines. The ligands displayed weak cytotoxic activity under the used conditions ($IC_{50}$: 19.6 – >25 μM). Among these Cu(II) complexes, the Cu(II)-Me-thn-TSC complex was found to be the most cytotoxic ($IC_{50}$: 3.90 – 10.16 μM), and was the only compound which was able to induce a pronounced reduction in spheroid size (Fig. 36) compared to untreated cells.

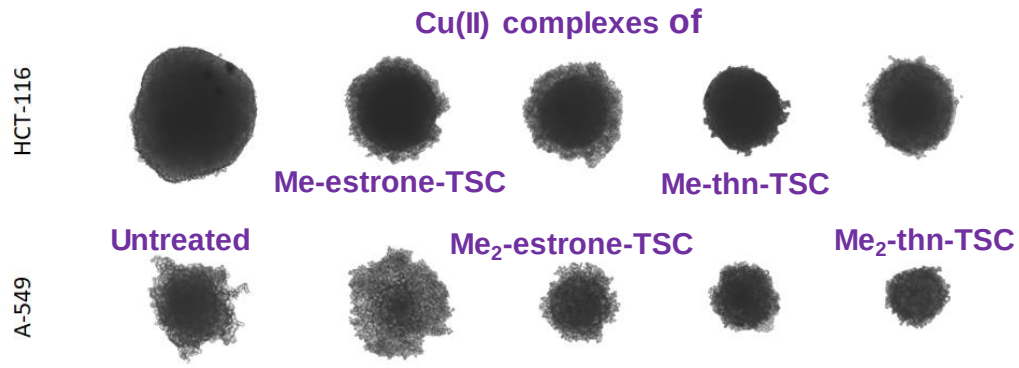


**Figure 36.** Morphological evaluation of A-549 and HCT-116 spheroids treated by tested Cu(II) complexes at the $IC_{50}$ concentration.

The complexes induced measurably more ROS than the untreated control except to the Cu(II)-Me-estrone-TSC complex, and resulted in the induction of apoptosis in all cases. The results also indicated that the Cu(II)-Me-thn-TSC complex possibly induces cell death in a caspase-3- and caspase-7-independent manner.

Estradiol-(T)SCs and their Cu(II) complexes together with estrone-TSC and its Cu(II) complex for comparison were tested on MCF-7, MCF-7 KCR, DU-145 and A549 cells, where Cu(II) complexes were much more cytotoxic than their ligands. Estradiol-SC and its Cu(II) complex did not show cytotoxic effect. A significant difference was observed between the

cytotoxicity of estradiol-TSC and Cu(II)-estradiol-TSC and estrone-TSC and Cu(II)-estrone-TSC complexes on MCF-7 cells (Table S12). Cu(II)-estradiol-TSC showed remarkable activity on MCF-7 ($IC_{50}$ = 8.40 μM), MCF-7 KCR ($IC_{50}$ = 12.95 μM) and on A549 ($IC_{50}$ = 10.03 μM), nevertheless, on DU-145 and A549, Cu(II)-$Me_2$-estradiol-TSC was the most effective complex. Also the Cu(II)-estradiol-TSC complex showed large ROS formation in A549 (Figs. S12-14), MCF-7 and DU-145 cells after treatment.

*5.6 Impact of domain-integrated hybridization of 2-aminophenol with estradiol on cytotoxicity and complexation with Cu(II) ions*

In the previous chapter, novel (thio)semicarbazones conjugated with sterane moiety were discussed, where the beneficial effect of this conjugation strategy on the anticancer activity of TSCs was introduced. Taking into account this finding, another class of compounds was chosen, namely 2-aminophenols, which are the most common members of redox active ligands [101] with a broad spectrum of pharmacological activities (chapter 2.5). In order to study the impact of domain-integrated hybridization, 2-aminoestradiol has been developed by the group of É. Frank, University of Szeged (Chart 15), and used for an in-depth solution chemical investigation. Additionally, 2-aminophenol (2AP, Chart 5, 15) was applied as a structural model for comparison. As a starting point, the *in vitro* anticancer activity was tested on some cancerous and non-cancerous cell lines, namely on doxorubicin-sensitive Colo205, doxorubicin-resistant Colo320, MCF-7, HeLa and MRC-5 cells, and the determined $IC_{50}$ values are shown in Table S13 (these studies were performed by G. Spengler, University of Szeged). Obtained results showed that 2-aminophenol was not active on the tested cell lines ($IC_{50}$ > 100 μM), whereas 2-aminoestradiol displayed moderate cytotoxicity on the human cancer cells ($IC_{50}$: 17.3–100 μM), and showed selectivity to these cancer cells over the non-cancerous MRC-5 cells (selectivity ratios for Colo205 = 5.8 and for Colo320 = 4.1). On the contrary, complexation with Cu(II) ions increased the cytotoxic activity of 2-aminophenol on all tested cancer cells, meanwhile lower $IC_{50}$ values were obtained for 2-aminoestradiol only in the case of MCF-7 cells. Moreover, the addition of Cu(II) to 2-aminoestradiol was able to induce early apoptosis, while no apoptosis was detected in the absence of the metal ion.

In order to understand better the differences between the anticancer activity of the ligands and the influence of the complexation with Cu(II) on their behavior, a detailed solution equilibrium study was performed.

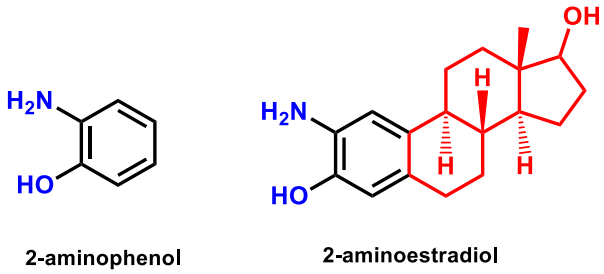


2-aminophenol 2-aminoestradiol

**Chart 15.** Chemical structures of the tested compounds: 2-aminophenol (2AP) and 2-aminoestradiol (2AE) in their neutral forms (HL).

*5.6.1 Investigation of proton dissociation processes, lipophilicity and membrane permeability of 2-aminophenol and 2-aminoestradiol*

As a starting point, the solution stability of the ligands was studied, since aminophenol derivatives have usually high sensitivity to molecular oxygen [154]. For that purpose, UV-vis spectrophotometry was used and compounds were tested in the presence of 30% (*v/v*) DMSO/$H_2O$ at pH 2.0, 7.4 and 12.0 over 3 h. We could conclude that oxidation appeared only at pH 12 for both ligands (Figs. 37.a,b).

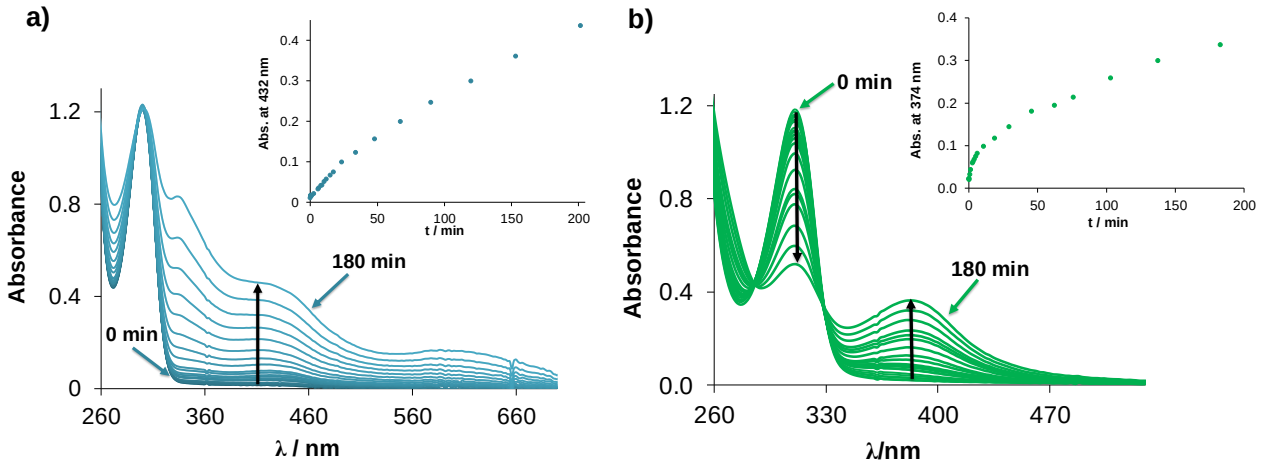


**Figure 37.** UV-vis absorption spectra of a) 2AP and b) 2AE recorded over 3 h at pH 12.0 in 30% (*v/v*) DMSO/$H_2O$ together with inserted time dependence of absorbance values at 432 nm for 2AP and at 374 nm for 2AE ($c_L$ = 100 μM; $I$ = 0.1 M (KCl); $T$ = 25°C; $\ell$ = 1 cm). These figures were adapted from publication [P2].

The significant increase of the absorbance band in the visible wavelength range at pH 12.0 for 2AP (Fig. 37.a) can be explained most probably by the subsequent oxidation, tautomerization and conjugate addition reactions, which led to the generation of 2-amino-3*H*-phenoxazin-3-one through an *o*-quinone imine intermediate [154]. 2AE was also sensitive to $O_2$ at pH 12.0, although, the oxidation reaction was faster for the 2AP than for the 2AE (Figs. 37.a,b), indicating the increased solution stability of the compound in the alkaline pH because of estradiol conjugation, which most probably prevents further polymer conjugation of the compound.

Proton dissociation processes of 2AP and 2AE were investigated by pH-potentiometry, UV-vis spectrophotometric, and $^1$H NMR spectroscopic titrations. Measurements were carried out with different DMSO solvent ratios such as 30% and 60% (*v/v*) DMSO/$H_2O$ mixtures due to the limited aqueous solubility of 2AE, whereas the reference compound 2AP was measured also in water. The protonated forms of these compounds have two functional groups (aromatic $NH_3^+$ and phenolic OH), which can dissociate in the studied pH range. Based on the data obtained from pH-potentiometric titrations, proton dissociation constants were defined and collected in Table 13, where p$K_a$ values determined for 2AP in water and in 30% (*v/v*) DMSO/$H_2O$ mixture are in good agreement with the published data [123].

**Table 13.** Proton dissociation constants (p$K_a$) of the studied compounds determined by the different methods in the different media. {30%, 60% (*v/v*) DMSO/$H_2O$ and in water*; I* = 0.10 M (KCl); *T* = 25 °C}. This table was taken from publication [P2].

| method | | medium | 2-aminophenol | 2-aminoestradiol |
|---|---|---|---|---|
| pH-potentiometry | **p$K_{a1}$** | $H_2O$ | 4.77±0.03[a] | ~4.9[b] |
| | **p$K_{a2}$** | | 9.60±0.05[a] | ~10.2[b] |
| | **p$K_{a1}$** | 30% (*v/v*) | 4.45±0.02 | 4.90±0.01 |
| | **p$K_{a2}$** | | 10.36±0.02 | 10.63±0.02 |
| | **p$K_{a1}$** | 60% (*v/v*) | 4.06±0.02 | 4.77±0.04 |
| | **p$K_{a2}$** | | 11.71±0.02 | 11.99±0.07 |
| UV-vis | **p$K_{a1}$** | 30% (*v/v*) | 4.41[c] | 4.91±0.01 |
| | **p$K_{a2}$** | | 10.36[c] | 10.74±0.01 |
| | **p$K_{a1}$** | 60% (*v/v*) | n.d. | 4.56±0.01 |
| | **p$K_{a2}$** | | n.d. | 11.82±0.01 |
| $^1$H NMR | **p$K_{a1}$** | 60% (*v/v*) | n.d. | 4.61±0.02 |
| | **p$K_{a2}$** | | n.d. | n.d. |
| partitioning | **log$D_{7.4}$** | *n*-octanol/aqueous buffer, pH 7.4 | +0.67±0.03 | >2 |
| PAMPA | $\boldsymbol{P_{eff}}$ (cm/s) | $H_2O$, pH 7.4 | $15.5\pm5\times10^{-6}$ | n.d. |

[a]p$K_{a1}$ = 4.91 and p$K_{a2}$ = 9.78, for 2AP in water, reported in ref [124]. [b]Data obtained by extrapolation and considered as estimated values. [c]p$K_{a1}$ = 4.41 and p$K_{a2}$ = 10.36 for 2AP in 30% (*v/v*) DMSO/$H_2O$ mixture reported in [121].

Herein, the first proton dissociation constant (p$K_{a1}$) belongs to the protonated aromatic-$NH_3^+$ group and another constant (p$K_{a2}$) is attributed to the deprotonation of the phenolic OH. It was found that p$K_a$ values of 2AE were somewhat higher in comparison to 2AP, which can be explained by the electron-donating effect of the condensed cyclohexane moiety. It is worth to mention that the DMSO content also has an effect on the p$K_a$ values, namely, p$K_{a1}$ becomes lower, while p$K_{a2}$ values are higher by increasing DMSO content, as it is explained in section 2.3.

For better visualization of this dependence, the p$K_a$ values determined in water, 30% and 60% (*v/v*) DMSO/$H_2O$ solvent mixtures were plotted against the reciprocal value of the relative permittivity (or dielectric constant, $\varepsilon_r$) of the medium (Fig. 38). It was found that the curves for 2AP and 2AE

have similar slopes due to their structural similarity, and based on this finding, the p$K_a$ values of 2-aminoestradiol in water were obtained by extrapolation from the values determined in the 30% and 60% of DMSO/$H_2O$ mixtures (Table 13). The p$K_a$ values in water indicate that in the dominant species is the neutral HL for both compounds at physiological pH.

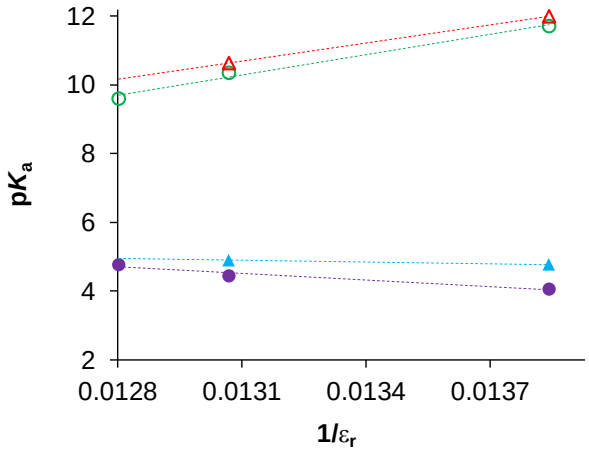


**Figure 38**. Correlation diagram for the p$K_a$ values measured at various DMSO content plotted against the $1/\varepsilon_r$ values of the solvent medium for 2-aminoestradiol (p$K_{a1}$: ▲; p$K_{a2}$: Δ) and 2-aminophenol (p$K_{a1}$: ●; p$K_{a2}$: ○). The $\varepsilon_r$ values are interpolated data taken from ref. [155]. ($T$ = 25.0 ˚C, $I$ = 0.10 M (KCl) in water, 30% and 60% (*v/v*) DMSO/$H_2O$). This figure is adapted from publication [P2].

UV-vis spectrophotometry was also applied for determination of proton dissociation constants, where UV-vis spectra were recorded in 30% and 60% (*v/v*) DMSO/$H_2O$ mixtures (Fig. 39.a) for 2AE. Two well-separated deprotonation processes were seen as it was expected based on the results obtained by the pH-potentiometric titrations.

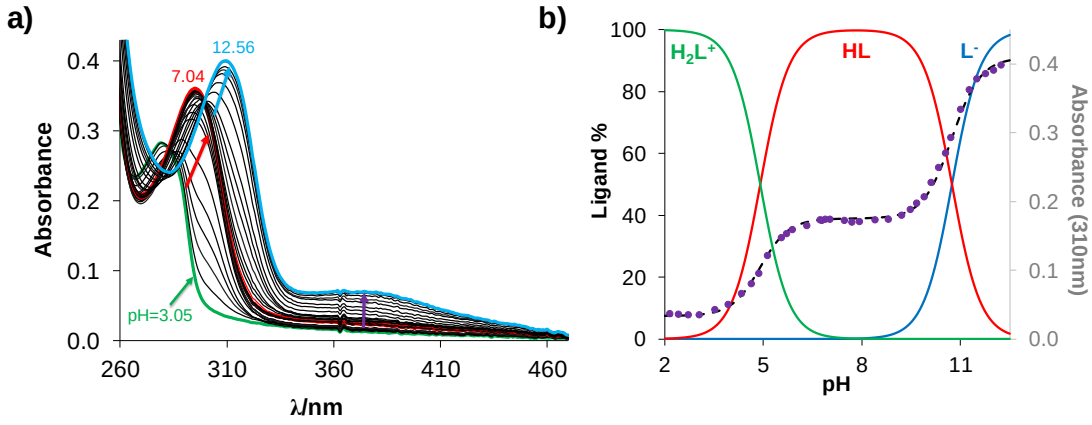


**Figure 39.** a) UV-vis absorption spectra recorded for 2AE in the pH range 3.0 – 12.6. b) Concentration distribution curves plotted together with the absorbance changes at 310 nm (●) with the fitted curve (dashed line) at various pH values. ($c_L$ = 50 μM; 30% (*v/v*) DMSO/$H_2O$; $I$ = 0.10 M (KCl); $T$ = 25.0 °C; $\ell$ = 1 cm). These figures were adapted from publication [P2].

Thus, two p$K_a$ values could be calculated which are in good agreement with data obtained by pH-potentiometry (Table 13). Based on the obtained results, for 2-aminoestradiol concentration distribution curves were computed and shown as an example (Fig. 39.b) plotted together with the absorbance changes at the $\lambda_{max}$ of the fully deprotonated form of ligand.

In addition, the proton dissociation processes of 2AE were followed by $^1$H NMR spectroscopic titrations in 60% (*v/v*) DMSO-$d_6$/$H_2O$, where the chemical shifts (δ) of the aromatic ring protons were found to be very sensitive to the protonation state of the compound (Fig. 40).

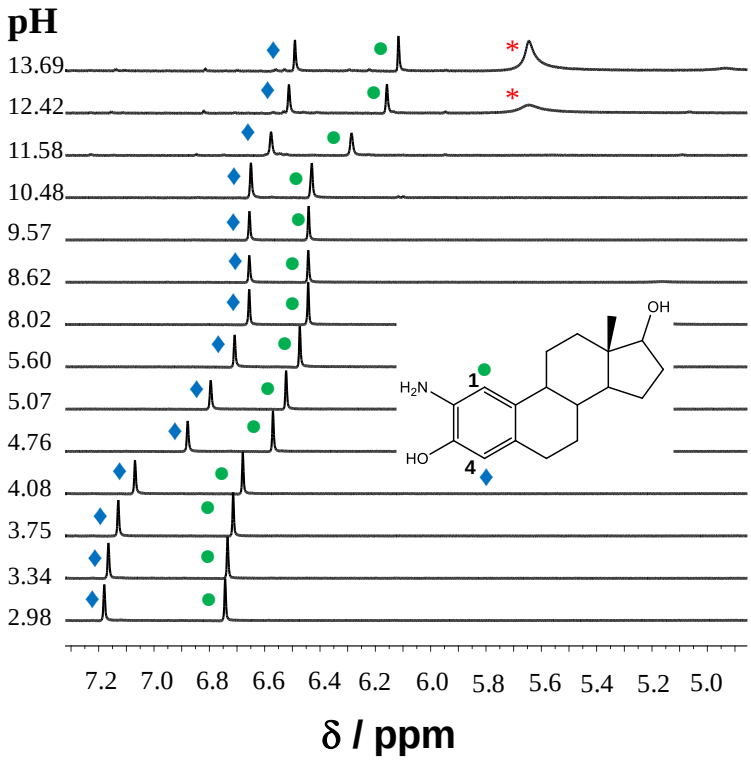


**Figure 40.** $^1$H NMR spectra recorded for 2AE at various pH values with symbols used for proton resonances assignment, * denotes the new peaks appearing upon oxidation; pH-dependence of the chemical shift of peaks belonging to the aromatic ring protons (●,♦). {$c_L$ = 1 mM; $I$ = 0.1 M (KCl); $T$ = 25°C; 60% (*v/v*) DMSO-$d_6$/$H_2O$}. This figure was adapted from publication [P2].

The first deprotonation step occurred between pH 3 and 6, where upfield shift was detected for the aromatic protons. The most sensitive protons for both deprotonation processes were found in positions 1-CH(●) and 4-CH(♦) and based on these spectral changes, p$K_{a1}$ could be calculated (Table 13). Afterwards, notable changes were seen at pH > 11 in parallel with the oxidation process, which hindered the determination of p$K_{a2}$. The new peak found at 5.7 ppm can be linked to the oxidation of the compound to the *o*-benzoquinone derivative.

We attempted to determine the lipophilicity and membrane permeability of 2AP and 2AE (Table 13), however, only a lower limit of log$D_{7.4}$ for 2AE could be estimated due to the fact that almost all amount of the compound remained in the *n*-octanol phase in the partitioning experiment.

Moreover, $P_{eff}$ value for 2AE could not be determined either due to its insufficient aqueous solubility. Based on the obtained data, hybridization of 2-aminophenol with estradiol significantly increases the lipophilicity, which may be associated with the increased anticancer activity of 2AE compared to 2AP.

*5.6.2 Investigation of the complex formation of 2AP and 2AE with Cu(II) ions*

The complex formation equilibrium processes of the 2AP and 2AE with Cu(II) ions were studied by pH-potentiometry in 60% (*v/v*) DMSO/$H_2O$, and strictly anaerobic conditions were applied. Moreover, pH-potentiometric titrations were also performed for 2AP in water and 30% (*v/v*) DMSO/$H_2O$. The obtained overall stability constants of the complexes are collected in Table 14.

Both 2AP and 2AE form Cu(II) complexes with high stability, since the complex formation processes start already at pH ~2 in the 60% (*v/v*) DMSO/$H_2O$ solvent mixture.. Formation of the mono, bis and mixed hydroxido species was found for 2-aminoestradiol ($[CuLH]^{2+}$, $[CuL]^{+}$, $[CuL_2]$, $[CuL_2H_{-1}]^{-}$ and $[CuL_2H_{-2}]^{2-}$), whereas for 2-aminophenol the titration data could be fitted with a somewhat different speciation model ($[CuL]^{+}$, $[CuL_2]$ and $[CuLH_{-1}]$). ($L^{-}$ denotes fully deprotonated form of the ligands.) Herein, ligands coordinate in a bidentate way via (N,O) binding mode.

**Table 14.** Overall stability constants (log*β*), of the Cu(II) complexes of 2AP and 2AE (where $L^{-}$ is the completely deprotonated form of the ligand) determined by pH-potentiometric titrations in $H_2O$, 30%, 60% (*v/v*) DMSO/$H_2O$. {$T$ = 25 °C; $I$ = 0.1 M (KCl)}. This table was adapted from the publication [P2].

| | **medium** | **Cu(II) – 2AP** |
|---|---|---|
| **log*β* [CuL]$^{+}$** | $H_2O$ | 8.18±0.03[a] |
| **log*β* [CuLH$_{-1}$]** | | 0.75±0.06 |
| **log*β* [CuL]$^{+}$** | 30% (*v/v*) DMSO/$H_2O$ | 9.58±0.03 |
| **log*β* [CuL$_2$]** | | 16.30±0.09 |
| **log*β* [CuL]$^{+}$** | 60% (*v/v*) DMSO/$H_2O$ | 12.63±0.03 |
| **log*β* [CuLH$_{-1}$]** | | 1.29±0.07 |
| **log*β* [CuL$_2$]** | | 16.41±0.26 |
| | **medium** | **Cu(II) – 2AE** |
| **log*β* [CuLH]$^{2+}$** | 60% (*v/v*) DMSO/$H_2O$ | 17.03±0.05 |
| **log*β* [CuL]$^{+}$** | | 12.73±0.04 |
| **log*β* [CuL$_2$]** | | 17.99±0.09 |
| **log*β* [CuL$_2$H$_{-1}$]$^{-}$** | | 6.23±0.07 |
| **log*β* [CuL$_2$H$_{-2}$]$^{2-}$** | | –7.38±0.08 |

Overall stability constants were used for computation of concentration distribution curves for both Cu(II)-ligand systems (Figs. 41.a,b) for comparison of the stoichiometry and stability of the species, which formed in various media. It is seen in Fig. 41.a that the complex formation process starts at lower pH, especially at higher DMSO content, whereas the fractions of bis complexes decrease at higher percentage of DMSO.

It is shown in Fig. 41.b that species $[CuLH]^{2+}$ is formed in the acidic pH range, where a coordinated hydroxyl group is present (as -OH group) , and $[CuL]^{+}$ is formed in the pH range 5-10. In particular, inclusion of complex $[CuLH]^{2+}$ in the speciation model yielded a significantly improved agreement between the experimental and computed data. The complexation reaction of Cu(II) was already reported with neutral monodentate ligands, such as aniline and pyridine, where the same type of species (with the coordination of an aromatic $NH_2$ to Cu(II)) was detected [156]. Nevertheless, for 2AP only $[CuL]^{+}$ was found in the acidic region (Fig. 41.b), where both of the aromatic $NH_3^{+}$ and the phenolic OH groups became deprotonated in this species. The bis complex $[CuL_2]$ was found for both ligands in the alkaline pH range. It is noteworthy that precipitation was formed during the titration of the Cu(II) − 2AP system in water at pH > 7, which process hindered the determination of stability constant for the bis complex. In the highly basic pH range, mixed hydroxido species were detected, such as $[CuL_2H_{-1}]^{-}$ and $[CuL_2H_{-2}]^{2-}$ for 2AE, and $[CuLH_{-1}]$ for 2AP.

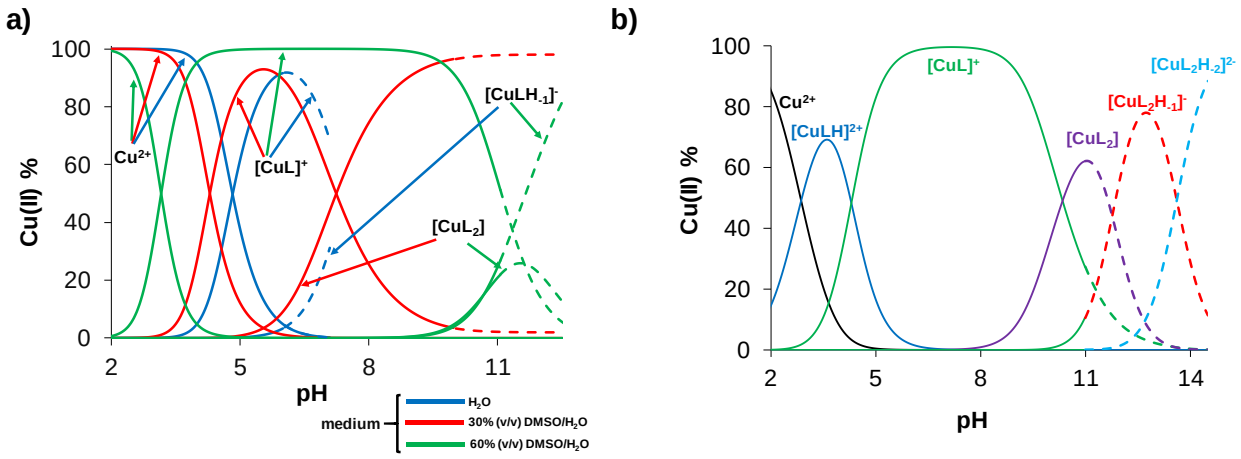


**Figure 41**. Concentration distribution curves for the a) Cu(II)-2AP (1:2) system in the three applied different media and b) Cu(II)-2AE (1:2) system in 60% (*v*/*v*) DMSO/$H_2O$ and. Dashed lines show the pH range where the speciation becomes more uncertain due to the putative hydrolysis of the metal ion. {$c_{2AE}$ = $c_{2AP}$ = 1 mM; $c_{Cu(II)}$ = 0.5 mM; $I$ = 0.10 M (KCl); $T$ = 25.0 °C}. These figures were adapted from publication [P2].

For comparison, Fig. 42 shows the predominance curves calculated for Cu(II)-2AP and Cu(II)-2AE systems at 1:2 metal-to-ligand ratio using equilibrium constants (60% (*v*/*v*) DMSO/$H_2O$)

from Table 14. Based on these calculations, 2AP binds Cu(II) stronger than 2AE in a wide pH range (pH 4 and 10) including the physiological pH.

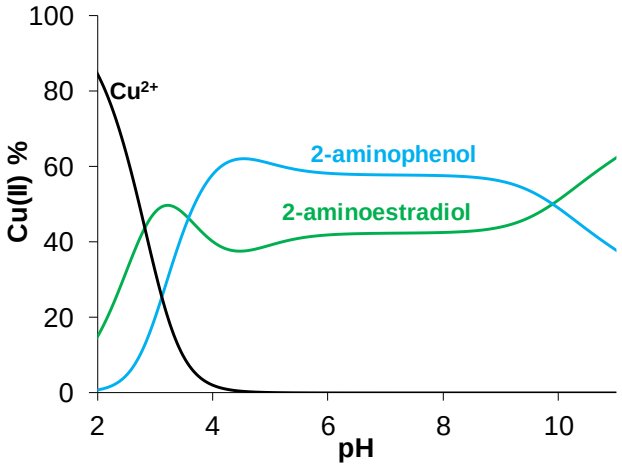


**Figure 42**. Predominance curves for the hypothetic Cu(II)-2-aminophenol (blue line)-2-aminoestradiol (green line) system calculated using the determined overall stability constants. {$c_{2AE}$ = $c_{2AP}$ = 1 mM; $c_{Cu(II)}$ = 0.5 mM; $T$ = 25.0°C; $I$ = 0.1 M (KCl); 60% (*v*/*v*) DMSO/$H_2O$}. This figure was adapted from publication [P2].

In order to prove the proposed binding mode, I successfully isolated the mono complex of 2-aminoestradiol from a mixture of MeOH and buffered aqueous solution (pH ~ 7.4), using 1:1 metal-to-ligand ratio. UV-vis and EPR spectroscopies were applied for the analysis (Fig. S15). The complex formation was confirmed by the appearance of a CT band with $\lambda_{max}$ = 436 nm in the UV-vis spectrum. The EPR spectrum of the isolated complex was recorded in DMSO solution at 77 K. Two kinds of Cu(II) species were found, namely 50% mono and 50% bis complexes. It indicates that in the isolated solid compound the Cu(II)-2AE ratio is ~2:3, which differs from the applied 1:1 ratio. Most probably the unreacted Cu(II) salt and 2AE remained in the solution under the preparation conditions. The anisotropic EPR parameters are collected in Table S14, confirming the suggested (N,O) coordination mode. Synthesis and characterization of Cu(II) complexes of 2-aminophenol were already reported, where the (N,O) binding mode was proved [157].

*5.6.3. Electrochemical studies of 2AP, 2AE in the absence and presence of Cu(II) ions*

The redox properties of 2-aminoestradiol, 2-aminophenol and the influence of the presence of Cu(II) ions on them were investigated at different pH values in 60% (*v*/*v*) DMSO/$H_2O$ mixture by CV. It was already reported that the electrochemical oxidation of aminophenol derivatives usually involves proton transfer to form quinone and also the electrochemical response of aminophenols is strongly dependent on the pH [158]. In order to check the dependence from the pH of the tested compounds, cyclic voltammograms of 2-aminoestradiol and 2-aminophenol were recorded at pH

2, 3, 5, 7.4 and 12 (Figs. 43.a-d). Analysis of these voltammograms revealed a shift to negative potential by increasing the pH.

The electrochemical oxidation of 2-aminophenol was already described in details, where it was found that at more acidic pH values C-N or N-N coupling of 2AP cation radicals results in the formation of cyclic dimer 2-amino-3*H*-phenoxazin-3-one [158]. On the contrary, in the basic pH range N-N coupling results in the formation of azo species 2,2'-dihydroxyazobenzene [158]. It should be noted that only the one-electron oxidation process of 2-aminophenol can be seen at pH 7.4, which is most likely due to the charge neutrality of the molecule [158]. Due to the structural similarity of the tested compounds, analogous mechanism of electrochemical oxidation of 2AE would have been expected.

In the acidic pH range for 2AP (Fig. 43.a), two reversible electron transfer processes are visible and one single anodic peak appears, which shifts to negative potential by increasing pH similarly to 2-aminoestradiol (Fig. 43.c).

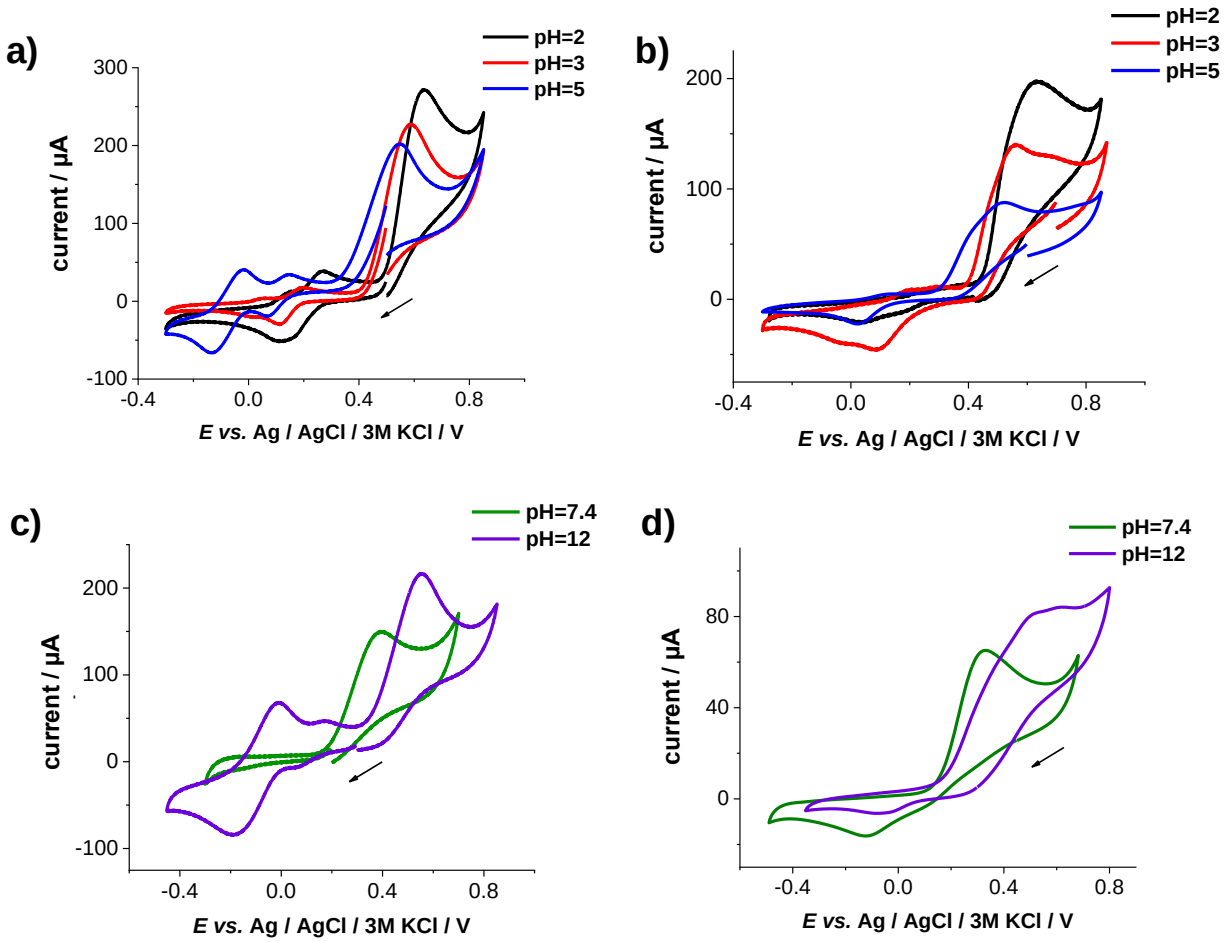


**Figure 43**. Cyclic voltammograms in 60% (*v/v*) DMSO/$H_2O$ at pH 2, 3, 5 for a) 2-aminophenol and b) 2-aminoestradiol; at pH 7.4 and 12 for c) 2-aminoestradiol and d) 2-aminophenol using Pt working electrode. {$T$ = 25.0°C, $I$ = 0.1 M (*n*-$Bu_4NPF_6$), $c_L$ = 1 mM; scan rate = 50 mV/s}. These figures were adapted from the publication [P2].

However, only a single anodic peak was observed for both ligands at pH 7.4, whereas, all another signals disappeared. It can be explained by the formation of an aromatic ammonium cation radical (Figs. 43.b,d). It is worth to mention that different shape and intensity of the peaks were found in all systems at pH 12, where one reversible electron transfer process and one single anodic peak were detected. These processes can be attributed to the formation of azo species.

The impact of the complexation with Cu(II) ions was studied under the same conditions at pH 7.4. The cyclic voltammograms recorded for Cu(II)-2-aminoestradiol and Cu(II)-2-aminophenol systems are presented at Fig. 44. Voltammograms reveal redox processes in both cathodic and anodic regions. The first reduction peaks are at +0.28 V and +0.15 V *vs.* Ag/AgCl/KCl for 2-aminoestradiol and 2-aminophenol, respectively; most probably they belong to the Cu(II) → Cu(I) reduction process. This is followed by the ligand release from the [Cu(I)L] complex of low stability at –0.27 V for 2-aminoestradiol and –0.52 V for 2-aminophenol, respectively. Furthermore, a sharp oxidation peak during the reverse scan at around −0.03 V and –0.13 V for Cu(II)-2AP and Cu(II)-2AE systems, respectively, was observed, which is the typical for the redissolution process.

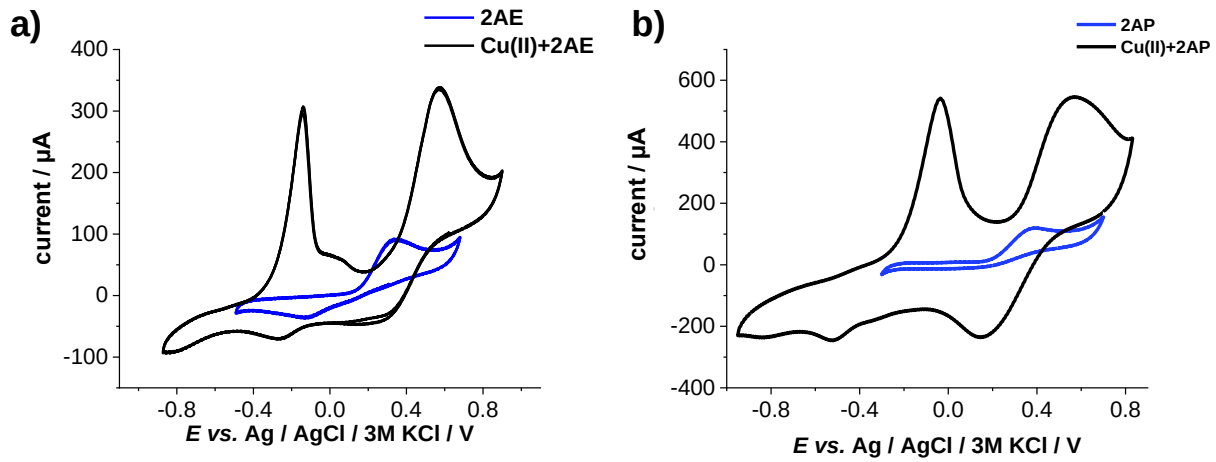


**Figure 44.** Cyclic voltammograms of a) Cu(II)-2-aminoestradiol and b) Cu(II)-2-aminophenol systems at pH 7.4 using Pt working electrode. ($c_L$ = 1 mM, $c_{Cu(II)}$ = 1 mM, $T$ = 25.0°C, $I$ = 0.1 M ($n$-$Bu_4NPF_6$) in 60% (*v*/*v*) DMSO/$H_2O$; scan rate = 50 mV/s). These figures were adapted from publication [P2].

Afterwards, the second oxidation peak under the reverse scan at +0.57 V for 2-aminoestradiol and +0.31 V for 2-aminophenol can be attributed for the regeneration of the Cu(II) complex. In order to check the chemical reversibility of the tested systems, several scans were recorded, which revealed negligible changes in the shape of the corresponding cyclic voltammograms in both the cathodic and anodic regions. Considering these findings, it can be assumed that all tested compounds exhibit redox activity, likely associated to their antioxidant capacities. This aspect has been further studied and will be presented in the next chapter.

*5.6.4 Antioxidant activity of 2AE and 2AP and impact of presence of Cu(II) ions*

It is well-known that aminophenol derivatives exhibit antioxidant activity [101]. Based on this finding, the free radical scavenging activity of 2-aminoestradiol and 2-aminophenol was screened through DPPH assay. The same methodology was employed as described in the previous chapter. Representative UV-vis spectra of 2-aminoestradiol with DPPH are shown in Fig. 45.a. In Fig. 45.b changes of absorbance at the $\lambda_{max}$ of DPPH (517 nm) in time at the different ratios DPPH-to-2AP are compared.

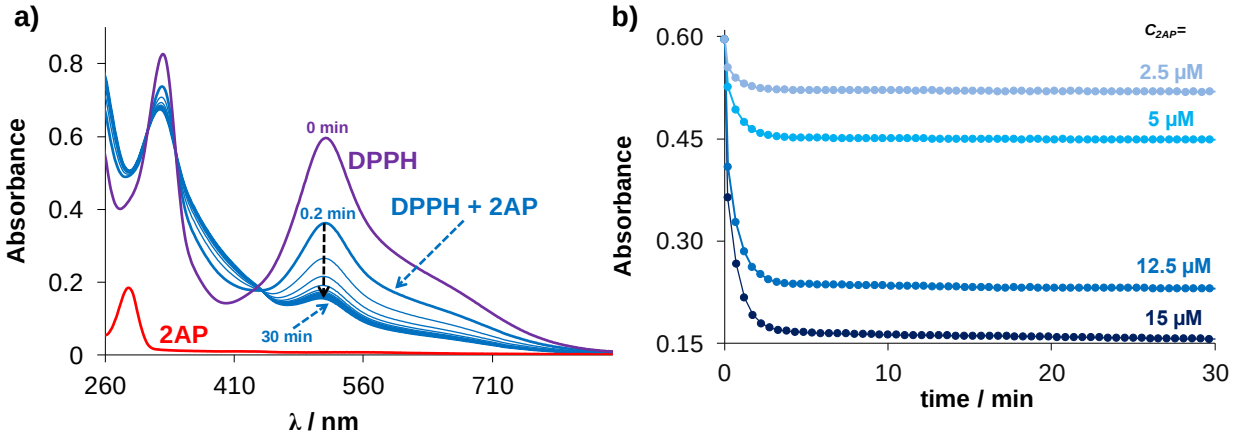


**Figure 45**. a) UV-vis spectra of 2AP ($c$ = 50 µM) (red line), DPPH• ($c$ = 50 µM) (purple line) and the time-dependent spectra of the reaction mixture (DPPH ($c$ = 50 µM), 2AP ($c$ = 15 µM)) (blue lines) in EtOH. ($T$ = 25 °C; $\ell$ = 1 cm). b) Time dependence of absorbance of DPPH• at 517 nm upon reaction with different ratios of 2AP in EtOH. {$c_{DPPH}$ = 50 µM; $c_{2AP}$ = 15; 12.5; 5; 2.5 µM; $T$ = 25°C}. These figures were adapted from publication [P2].

2AP reacted slower with DPPH than 2AE, since the reaction with the latter compound was immediately completed after the reactants were mixed. The free radical scavenging activity was expressed through $IC_{50}$ values (Table 15) which were compared to the reference compound trolox [153]. Slightly lower $IC_{50}$ of 2AP was found in comparison to the trolox, while 2AE displayed a somewhat higher $IC_{50}$ value. Furthermore, the presence of Cu(II) ions significantly increased the antioxidant activity of both tested compounds and also the isolated Cu(II) complex showed similar influence for scavenging effect as in the case of the 'pre-mixed' complex.

**Table 15.** DPPH free radical scavenging activity of 2-aminoestradiol, 2-aminophenol in the absence or in the presence of one equivalent of Cu(II), the isolated Cu(II)-2-aminoestradiol complex and trolox. $IC_{50}$ values; (n.d. = not determined). {$T$ = 25 °C; EtOH, $c_{DPPH}$ = 50 μM; $c_{compound}$ = 2.5 – 100 μM}

| **Sample** | **% of scavenging effect** at DPPH:compound = 1:0.3 ratio | **$IC_{50}$ (μM)** |
|---|---|---|
| **2AE** | 47.8 | 15.8 |
| **2AP** | 77.0 | 9.9 |
| **2AE+1 equiv. Cu(II)**[a] | 95.8 | n.d. |
| **2AP+1 equiv. Cu(II)** | 93.3 | n.d. |
| **$CuCl_2$** | 5.7 | n.d. |
| **trolox** | 63.0 | 12.0[b] |

[a] Scavenging effect at DPPH:compound = 1:0.3 ratio obtained for the isolated Cu(II) – 2AE complex: 93.6%; [b] The obtained data corresponds well to $IC_{50}$ = 16 μM reported in ref [153].

## 6. Conclusions

Nowadays, there is high interest in the development of metal complexes as therapeutic and diagnostic agents. The mechanisms of action always need to be clarified for those metal compounds, which are already in use or entered to clinical trials and not only from the biological points of view but also on the molecular level. For the rational development and optimization process of active pharmaceutical ingredients, the behavior of these metal complexes is important to know in solution, *i.e.* exploring their aqueous solution stability, speciation and redox properties. These characteristics significantly influence their pharmacokinetic properties, as well as their interaction with various endogenous molecules. The main goal of my thesis was the synthesis and characterization of anticancer Cu(II) complexes and the investigation of their solution chemical behavior. Also redox properties, antioxidant activity and interaction with physiological reductants (GSH and AA) were studied for some selected Cu(II) complexes in order to understand better their mechanism of action. Based on these results, the following conclusions were made:

1. Triapine derivatives (VA1-3) were characterized bearing a redox active phenolic moiety at the terminal nitrogen atom and additionally attached morpholine moiety to *N*-pyridyl scaffold (VA4-7). Namely, their proton dissociation processes and lipophilicity were investigated, where p$K_a$ values of pyridinium-$NH^+$ for (VA1-3) set of compounds were in the following order: VA3 > VA2 > VA1. It can be explained by the presence of the electron-donating effect of methyl group in the VA2 ligand and amino group at the pyridine ring in the VA3 ligand, respectively. Whereas, p$K_a$ values were much lower (*ca.* one and half units) for the same group in VA4-7 set in comparison to VA1-3 of triapine analogues due to the electron withdrawing effect of methyl-morpholine group. It was found that introduction of a redox active phenolic moiety at the terminal nitrogen atom is increasing lipophilicity (log$D_{7.4}$ > +2) and the attachment of the positively charged protonated morpholine moiety does not make compounds more hydrophilic. The stability of the complexes in solution was higher than for Cu(II)-triapine complex based on the obtained conditional stability constants. It is worth to mention that the cytotoxic effect was enhanced by the introduction of the redox active phenolic group and by complexation, especially in the case of Cu(II)-VA7; this effect is most probably linked to the coordination of morpholinium group to Cu(II) ions.

2. Exchange of the α-*N*-pyridyl moiety to imidazole and benzimidazole units undoubtedly has effect on lipophilicity and E/Z isomer distribution in aqueous solution. Although E form is dominant for the α-*N*-pyridyl-TSCs, the Z form is predominant for imidazole-TSC derivatives. Moreover, imidazole-TSCs were more hydrophilic than the corresponding α-*N*-pyridyl-TSCs. Interaction of imidazole-TSCs with Cu(II) ions showed the formation of mostly mono complexes in different protonation states ($[CuLH]^{2+}$, $[CuL]^+$ and $[CuLH_{-2}]^-$), in which the

ligand is tridentately coordinated. However, tetrameric species [$Cu_4L_4H_{-4}$] was found predominant in the pH range 5 – 9 (also including the physiological pH). Furthermore, *N*-terminal substitution did not significantly increase the stability of Cu(II) complexes.

3. It was already reported that STSC derivatives have generally lower aqueous solubility than α-*N* heterocyclic TSCs. Whereas, attachment of a positively-charged trimethylammonium group to the aromatic unit definitely increased their aqueous solubility. It should be noted that the trimethylammonium group significantly decreases the p$K_a$ values of the phenolic OH group by more than 1 order of magnitude compared to STSC, due to the electron-withdrawing effect of the attached group. It should be emphasized that *N*-terminal substitution by methyl and ethyl groups does not enhance Cu(II) binding ability, although *N*-terminal phenyl substitution can increase it.

4. The anticancer activity of S(T)SC is increased by conjugation with sterane backbone and complexation with Cu(II) ions. It was found that conjugation by estrone/estradiol moiety increases p$K_a$ values and the studied SCs have higher p$K_a$ values by *ca.* half logarithmic units in comparison to the corresponding TSCs. The determined stability constants indicate significant difference in the Cu(II) binding ability between the tested SCs and TSCs, where the latter ones showed the formation of Cu(II) complexes with high stability in solution. In addition, the stability of the Cu(II) complexes was further increased by *N*-terminal dimethylation.

5. Aminophenols are widely known by their redox properties and versatility of biological activities. Cytotoxic activity of 2-aminophenol was improved by estradiol conjugation, complexation with Cu(II) ions and also that modification could make the compound less sensitive for oxidation. The proton dissociation constants of 2-aminoestradiol were determined in 30 and in 60% (*v/v*) DMSO/$H_2O$ mixtures and extrapolated for the water medium. The obtained p$K_a$ values in three different media confirm the fact that DMSO content has an effect on proton dissociation constants, where p$K_{a1}$ becomes lower and p$K_{a2}$ values are higher by increasing DMSO content. Interaction with Cu(II) ions showed low complex stability for both 2-aminophenol and 2-aminoestradiol based on the determined stability constants.

6. It should be pointed out that a significant difference was found in the reaction rates for Cu(II)-TSCs and Cu(II)-SCs systems with GSH. It can be explained by the formal redox potential of Cu(II)-TSC complexes, which is usually much higher than that of Cu(II)-SCs. Accordingly, the latter one can be reduced faster by GSH. It was observed that the higher the stability of complexes the slower the reduction by GSH and the *N*-terminal substitution by dimethyl groups shows an outstanding affinity towards Cu(II) ions. Moreover, Cu(II) complexes with these substitutes demonstrate a higher anticancer effect and the activity of their Cu(II)

complex even exceeds that of their ligands. Based on this finding, it can be assumed that the *in situ* formed intracellular Cu(II) complexes play a crucial role in the mechanism of action.

7. Antioxidant activity of some selected ligands and their Cu(II) complexes were determined by DPPH assays using spectrophotometry. Based on the obtained data, 2-aminophenol showed the potential to act as antioxidant agent since it was more active than reference compound trolox. However, 2-aminoestradiol and some tested (T)SCs showed a bit lower antioxidant activity compared to it. In the case of aminophenols, the presence of Cu(II) ions could increase the antioxidant activity, although for (T)SCs the opposite effect was observed.

8. For all tested compounds it was found that the anticancer activity was usually enhanced by complexation with Cu(II) ions. In the case of triapine analogues, anticancer effect was increased by attachment of a redox active phenolic moiety at the terminal nitrogen atom. The cytotoxicity of STSC derivatives and 2-aminophenol was improved by sterane-based conjugation. It should be noted that *N*-terminal dimethylation of TSCs significantly enhances anticancer activity of their Cu(II) complexes.

## 7. References


1. G. Colotti, A. Ilari, A. Boffi, V. Morea, *Mini Rev. Med. Chem.* 13 (2013) 211-221.
2. Z. Guo, P. J. Sadler, *Angew. Chem. Int. Ed.* 38 (1999) 1512-1531.
3. U. Ndagi, N. Mhlongo, M. E. Soliman, *Drug Des. Devel. Ther*. 11 (2017) 599-616.
4. E. J. Anthony, E. M. Bolitho, H. E. Bridgewater, O. W. L. Carter, J. M. Donnelly, C. Imberti, E. C. Lant, F. Lermyte, R. J. Needham, M. Palau, P. J. Sadler, H. Shi, F. X. Wang, W. Y. Zhang, Z. Zhang, *Chem. Sci*. 48 (2020) 12888-12917.
5. K. D. Mjos, C. Orvig, *Chem. Rev*. 114 (2014) 4540-4563.
6. C. X. Zhang, S. J. Lippard, *Curr. Opin. Chem. Biol.* 7 (2003) 481-489.
7. R. Oun, Y. E. Moussa, N. J. Wheate, *Dalton Trans.* 47 (2018) 6645-6653.
8. G. Gasser, I. Ott, N. Metzler-Nolte, *J. Med. Chem*. 54 (2011) 3-25.
9. J. Nonnekens, J. H. Hoeijmakers, *EMBO Mol. Med*. 9 (2017) 4-6.
10. Z. E. Gagnon, C. Newkirk, S. Hicks, *J. Environ. Sci. Health A Tox. Hazard. Subst. Environ. Eng.* 41 (2006) 397-414.
11. J. B. Glaister, G. M. Mudd, *Miner. Eng*. 23 (2010) 438-450.
12. N. Vyas, A. Turner, G. Sewell, *Sci. Total Environ*. 493 (2014) 324-329.
13. Y. Roque-Diaz, M. Sanadar, D. Han, M. López-Mesas, M. Valiente, M. Tolazzi, A. Melchior, D. Veclani, *Processes* 9 (2021) 1873.
14. J. Liang, H. Zhong, G. Yang, K. Vellaisamy, D. Ma, C. Leung, *J. Inorg. Biochem*. 177 (2017) 276-286.
15. R. Paprocka, M. Wiese-Szadkowska, S. Janciauskiene, T. Kosmalski, M. Kulik, A. Helmin-Basa, *Coord. Chem. Rev*. 452 (2022) 214307.
16. P. Zhang, P. J. Sadler, *Eur. J. Inorg. Chem*. 12 (2017) 1541-1548.
17. L. Gourdon, K. Cariou, G. Gasser, *Chem. Soc. Rev*. 51 (2022) 1167-1195.
18. N. P. Prajapati, H. D. Patel, *Synth. Commun*. 49 (2019) 2767-2804.
19. J. Karges, R. W. Stokes, S. M. Cohen, *Trends Chem*. 3 (2021) 523-534.
20. R. Baskaran, J. Lee, S. G. Yang, *Biomater. Res*. 22 (2018) 25.
21. P. Chellan, P. J. Sadler, *Chemistry* 26 (2020) 8676-8688.
22. S. M. Valiahdi, P. Heffeter, M. A. Jakupec, R. Marculescu, W. Berger, K. Rappersberger, B. K. Keppler, *Melanoma Res*. 19 (2009) 283-293.
23. R. Wang, H. Chen, W. Yan, M. Zheng, T. Zhang, Y. Zhang, *Eur. J. Med. Chem*. 190 (2020) 112109.
24. FDA Updates Highlighting the Latest Cancer Treatments. *Oncology Times* 43 (2021) 36-37.
25. D. Moianos, G. M. Prifti, M. Makri, G. Zoidis, *Pharmaceuticals* 16 (2023) 901.
26. R. N. Adamek, C. V. Credille, B. L. Dick, S. M. Cohen, *J. Biol. Inorg. Chem*. 23 (2018) 1129-1138.
27. K. M. Jackl, H. Seo, J. Karges, M. Kalaja, S. M. Cohen, *Chem. Sci*. 13 (2022) 2128-2136.
28. A. Y. Chen, R. N. Adamek, B. L. Dick, C. V. Credille, C. N. Morrison, S. M. Cohen, *Chem. Rev*. 119 (2019) 1323-1455.
29. S. Padhyé, G. B. Kauffman, *Coord. Chem. Rev*. 63 (1985) 127-160.
30. S. T. Lobana, R. Sharma, G. Bawa, S. Khanna, *Coord. Chem. Rev.* 253 (2009) 977-1055.
31. J. R. Dilworth, R. Hueting, *Inorg. Chim. Acta* 389 (2012) 3-15.
32. H. Beraldo, D. Gambino, *Mini Rev. Med. Chem*. 4 (2004) 31-39.
33. P. Heffeter, V. F. S. Pape, É. A. Enyedy, B. K. Keppler, G. Szakács, C. R. Kowol, *Antioxid. Redox Signal*. 30 (2019) 1062-1082.
34. E. J. Blanz, F. A. French, *Cancer Res*. 28 (1968) 2419-2422.

35. ClinicalTrials.gov. Available online (accessed on 20 September 2023): https://clinicaltrials.gov/ct2/show/NCT02466971
36. D. S. Kalinowski, P. Quach, D. R. Richardson, *Future Med. Chem*. 6 (2009) 1143-1151.
37. C. A. Kunos, E. Chu, J. H. Beumer, M. Sznol, S. P. Ivy, *Cancer Chemother. Pharmacol*. 79 (2017) 201-207.
38. L. Feun, M. Modiano, K. Lee, J. Mao, A. Marini, N. Savaraj, P. Plezia, B. Almassian, E. Colacino, J. Fischer, S. MacDonald, *Cancer Chemother. Pharmacol.* 50 (2002) 223-229.
39. J. E. Karp, F. J. Giles, I. Gojo, L. Morris, J. Greer, B. Johnson, M. Thein, M. Sznol, J. Low, *Leuk. Res*. 32 (2008) 71-77.
40. R. Trondl, L. S. Flocke, C. R. Kowol, P. Heffeter, U. Jungwirth, G. E. Mair, R. Steinborn, É. A. Enyedy, M. A. Jakupec, W. Berger, B. K. Keppler, *Mol. Pharmacol*. 85 (2014) 451-459.
41. J. Shao, B. Zhou, B. Chu, Y. Yen, *Curr. Cancer Drug Targets.* 6 (2006) 409-431.
42. M. Kolberg, K. R. Strand, P. Graff, K. K. Andersson, *Biochim. Biophys. Acta*. 1699 (2004) 1-34.
43. U. Uhlin, H. Eklund, *Nature* 370 (1994) 533-539.
44. A. Larsson, B. M. Sjöberg, *EMBO J*. 5 (1986) 2037-2040.
45. H. L. Elford, M. Freese, E. Passamani, H. P. Morris, *J. Biol. Chem*. 245 (1970) 5228-5233.
46. R. A. Finch, M. Liu, S. P. Grill, W. C. Rose, R. Loomis, K. M. Vasquez, Y. Cheng, A. C. Sartorelli, *Biochem. Pharmacol.* 59 (2000) 983-991.
47. S. E. Huff, J. M. Winter, C. G. Dealwis, *Biomolecules* 12 (2022) 815.
48. M. J. Duffy, N. C. Synnott, S. O'Grady, J. Crown, *Semin. Cancer Biol.* 79 (2022) 58-67.
49. A. Santoro, B. Vileno, Ò. Palacios, M. D. Peris-Díaz, G. Riegel, C. Gaiddon, A. Krężel, P. Faller, *Metallomics* 11 (2019) 994-1004.
50. A. G. Ritacca, E. Falcone, I. Doumi, B. Vileno, P. Faller, E. Sicilia, *Inorg. Chem*. 62 (2023) 3957-3964.
51. E. Falcone, A. G. Ritacca, S. Hager, H. Schueffl, B. Vileno, E. Y. Khoury, P. Hellwig, C. R. Kowol, P. Heffeter, E. Sicilia, P. Faller, *J. Am. Chem. Soc.* 144 (2022) 14758-14768.
52. X. D. West, A. E. Liberta, S. B. Padhye, R. C. Chikate, P. B. Sonawane, A. S. Kumbhar, R. G. Yerande, *Coord. Chem. Rev*. 123 (1993) 49-71.
53. M. B. Ferrari, S. Capacchi, G. Pelosi, G. Reffo, P. Tarasconi, R. Albertini, S. Pinelli, P. Lunghi, *Inorg. Chim. Acta* 286 (1999) 134-141.
54. Z. Zhang, Y. Gou, J. Wang, K. Yang, J. Qi, Z. Zhou, S. Liang, H. Liang, F. Yang, *Eur. J. Med. Chem.* 121 (2016) 399-409.
55. L. Kennedy, J. K. Sandhu, M.-E. Harper, M. Cuperlovic-Culf, *Biomolecules* 10 (2020) 1429.
56. U. Jungwirth, C. R. Kowol, B. K. Keppler, C. G. Hartinger, W. Berger, P. Heffeter, *Antioxid. Redox Signal.* 15 (2011) 1085-1127.
57. F. Q. Schafer, G. R. Buettner, *Free Radic. Biol. Med*. 30 (2001) 1191-1212.
58. E. Desideri, F. Ciccarone, M. R. Ciriolo, *Nutrients* 11 (2019) 1926.
59. C. R. Kowol, P. Heffeter, W. Miklos, L. Gille, R. Trondl, L. Cappellacci, W. Berger, B. K. Keppler, *J. Biol. Inorg. Chem.* 17 (2012) 409-423.
60. D. B. Lovejoy, P. J. Jansson, U. T. Brunk, J. Wong, P. Ponka, D. R. Richardson, *Cancer Res.* 71 (2011) 5871-5880.
61. S. Hager, V. F. S. Pape, V. Pósa, B. Montsch, L. Uhlik, G. Szakács, S. Tóth, N. Jabronka, B. K. Keppler, C. R. Kowol, É. A. Enyedy, P. Heffeter, *Antioxid. Redox Signal.* 33 (2020) 395–414.
62. S. Kallus, L. Uhlik, S. van Schoonhoven, K. Pelivan, W. Berger, É. A. Enyedy, T. Hofmann, P. Heffeter, C. R. Kowol, B. K. Keppler, *J. Inorg. Biochem.* 190 (2019) 85-97.

63. É. A. Enyedy, N. V. May, V. F. S. Pape, P. Heffeter, G. Szakács, B. K. Keppler, C. R. Kowol, *Dalton Trans.* 49 (2020) 16887-16902.
64. A. Zhitkovich , *Chem. Res. Toxicol.* 33 (2020) 2515-2526.
65. P. Bergsten, G. Amitai, J. Kehrl, K. R. Dhariwal, H. G. Klein, M. Levine, *J. Biol. Chem.* 265 (1990) 2584-2587.
66. N. Travica, K. Ried, A. Sali, I. Hudson, A. Scholey, A. Pipingas, *Front. Aging Neurosci*. 11 (2019) 72.
67. M. Levine, S. J. Padayatty, M. G. Espey, *Adv. Nutr.* 2 (2011) 78-88.
68. M. Levine, *N. Engl. J. Med.* 314 (1986) 892-902.
69. M. J. González, J. R. Miranda-Massari, E. M. Mora, A. Guzmán, N. H. Riordan, H. D. Riordan, J. J. Casciari, J. A. Jackson, A. Román-Franco, *Integr. Cancer Ther*. 4 (2005) 32-44.
70. G. R. Buettner, B. A. Jurkiewicz, *Radiat. Res*. 145 (1996) 532-541.
71. C. Cheignon, F. Collin, P. Faller, C. Hureau, *Dalton Trans.* 45 (2016) 12627-12631.
72. W. Y. Lee, Y. K. Yan, P. P. F. Lee, S. J. Tanb, K. H. Limb, *Metallomics* 4 (2012) 188-196.
73. U. Jungwirth, J. Gojo, T. Tuder, G. Walko, M. Holcmann, T. Schöfl, K. Nowikovsky, N. Wilfinger, S. Schoonhoven, C. R. Kowol, R. Lemmens-Gruber, P. Heffeter, B. K. Keppler, W. Berger, *Mol. Cancer Ther*. 13 (2014) 2436-2449.
74. A.K Renfrew, *Metallomics*, 6 (2014) 1324–1335.
75. V. Pósa, A. Stefanelli, J. H. B. Nunes, S. Hager, M. Mathuber, N. V. May, W. Berger, B. K. Keppler, C. R. Kowol, É. A. Enyedy, P. Heffeter, *Cancers* 14 (2022) 4455.
76. A. Sîrbu, O. Palamarciuc, M. V. Babak, J. M. Lim, K. Ohui, É. A. Enyedy, S. Shova, D. Darvasiová, P. Rapta, W. H. Ang, V. B. Arion, *Dalton Trans*. 46 (2017) 3833-3847.
77. É. A. Enyedy, N. V. Nagy, É. Zsigó, C. R. Kowol, V. B. Arion, B. K. Keppler, T. Kiss, *Eur. J. Inorg. Chem.* 2010 (2010) 1717-1728.
78. É. A. Enyedy, É. Zsigó, N. V. Nagy, C. R. Kowol, A. Roller, B. K. Keppler, T. Kiss, *Eur. J. Inorg. Chem.* 2012 (2012) 4036-4047.
79. O. Dömötör, N. V. May, K. Pelivan, T. Kiss, B. K. Keppler, C. R. Kowol, É. A. Enyedy, *Inorganica Chim. Acta* 472 (2018) 264-275.
80. O. Palamarciuc, M. N. M. Milunović, A. Sîrbu, E. Stratulat, A. Pui, N. Gligorijevic, S. Radulovic, J. Kožíšek, D. Darvasiová, P. Rapta, É. A. Enyedy, G. Novitchi, S. Shovah, V. B. Arion, *New J. Chem*. 43 (2019) 1340-1357.
81. É. A. Enyedy, G. M. Bognár, N. V. Nagy, T. Jakusch, T. Kiss, D. Gambino, *Polyhedron* 67 (2014) 242-252.
82. M. N. M. Milunovic, É. A. Enyedy, N. V. Nagy, T. Kiss, R. Trondl, M. A. Jakupec, B. K. Keppler, R. Krachler, G. Novitchi, V. B. Arion, *Inorg. Chem*. 51 (2012) 9309-9321.
83. M. Born, *Z. Physik.* 1 (1920) 45–48.
84. C. R. Kowol, R. Trondl, V. B. Arion, M. A. Jakupec, I. Lichtscheidl, B. K. Keppler, *Dalton Trans*. 39 (2010) 704-706.
85. P. V. Bernhardt, M. Martínez, C. Rodríguez, M. Vazquez, *Dalton Trans*. 41 (2012) 2122-2130.
86. P. V. Bernhardt, P. C. Sharpe, M. Islam, D. B. Lovejoy, D. S. Kalinowski, D. R. Richardson, *J. Med. Chem*. 52 (2009) 407-415.
87. C. R. Kowol, R. Berger, R. Eichinger, A. Roller, M. A. Jakupec, P. P. Schmidt, V. B. Arion, B. K. Keppler, *J. Med. Chem*. 50 (2007) 1254-1265.
88. F. Bacher, O. Dömötör, A. Chugunova, N. V. Nagy, L. Filipović, S. Radulović, É. A. Enyedy, V. B. Arion, *Dalton Trans*. 44 (2015) 9071-9090.

89. F. Bacher, O. Dömötör, É. A. Enyedy, L. Filipović, S. Radulović, G. S. Smith, V. B. Arion, *Inorganica Chim. Acta*. 455 (2017) 505-513.
90. G. Pelosi, *The Open Crystallograph. J.* 3 (2010) 16–28.
91. R. W. Byrnes, M. Mohan, W. E. Antholine, R.t X. Xu, D. H. Petering, *Biochemistry* 29 (1990) 7046-7053.
92. P. J. Jansson, P. C. Sharpe, P. V. Bernhardt, D. R. Richardson, *J. Med. Chem*. 53 (2010) 5759-5769
93. A. Gulea, D. Poirier, J. Roy, V. Stavila, I. Bulimestru, V. Tapcov, M. Birca, L. Popovschi, *J. Enzyme Inhib. Med. Chem*. 23 (2008) 806-818.
94. M. N. M. Milunović, A. Dobrova, G. Novitchi, N. Gligorijević, S. Radulović, J. Kožišek, P. Rapta, É. A. Enyedy, V. B. Arion, *Eur. J. Inorg. Chem*. 2017 (2017) 4773-4783.
95. F. Bacher, É. A. Enyedy, N. V. Nagy, A. Rockenbauer, G. M. Bognár, R. Trondl, M. S. Novak, E. Klapproth, T. Kiss, V. B. Arion, *Inorg. Chem*. 52 (2013) 8895-8908.
96. F. Bacher, O. Dömötör, M. Kaltenbrunner, M. Mojović, A. Popović-Bijelić, A. Gräslund, A. Ozarowski, L. Filipovic, S. Radulović, É. A. Enyedy, V. B. Arion, *Inorg. Chem*. 53 (2014) 12595-12609.
97. A. Dobrova, S. Platzer, F. Bacher, M. N. M. Milunovic, A. Dobrov, G. Spengler, É. A. Enyedy, G. Novitchi, V. B. Arion, *Dalton Trans*. 45 (2016) 13427-13439.
98. K. Ohui, E. Afanasenko, F. Bacher, R. L. X. Ting, A. Zafar, N. Blanco-Cabra, E. Torrents, O. Dömötör, N. V. May, D. Darvasiova, É. A. Enyedy, A. Popović-Bijelić, J. Reynisson, P. Rapta, M. V. Babak, G. Pastorin, V. B. Arion, *J. Med. Chem.* 62 (2019) 512-530.
99. M. Šimunková, M. Malček, *Acta Chim. Slov.* 13 (2020) 38-48.
100. S. Hager, K. Korbula, B. Bielec, M. Grusch, C. Pirker, M. Schosserer, L. Liendl, M. Lang, J. Grillari, K. Nowikovsky, V. F. S. Pape, T. Mohr, G. Szakács, B. K. Keppler, W. Berger, C. R. Kowol, P. Heffeter, *Cell Death Dis.* 9 (2018) 1052.
101. S. Mitchell, P. Carmichael, R. Waring, *Aminophenols*, John Wiley & Sons, Inc, New York, USA (2003)
102. G. Falcone, O. Giuffrè, S. Sammartano, *J. Mol. Liq*. 159 (2011) 146-151.
103. O. I. Shadyro, V. L. Sorokin, G. A. Ksendzova, O. V. Savinova, S. N. Samovich, E. I. Boreko, *Pharm. Chem. J*. 53 (2019) 646-649.
104. G. A. Ksendzova, V. L. Sorokin, I. P. Edimecheva, O. I. Shadyro, *Free Radic. Res*. 38 (2004) 1183-1190.
105. M. V. Bel'kov, G. A. Ksendzova, P. V. Kuzovkov, G. I. Polozov, I. V. Skornyakov, V. L. Sorokin, G. B. Tolstorozhev, O. I. Shadyro, *J. Appl. Spectrosc*. 74 (2007) 635-641.
106. M. Chinnapattu, K. I. Sathiyanarayanan, P. S. Iyera, *Bioorganic Med. Chem. Lett*. 25 (2015) 952-955.
107. T. Ohba, T. Yamauch, K. Higashiyama, N. Takahashia, *Bioorganic Med. Chem. Lett.* 15 (2007) 847-853.
108. L. Wang, L. Zhao, X. Jia, L. Jiang, Y. Song, Q. Ye, Z. Lyu, *Biomed. Pharmacother*. 109 (2019) 621-628.
109. K. Murakami, M. Yoshino, *Biometals* 35 (2022) 329-334.
110. C. Bunchorntavakul, K. R. Reddy, *Clin. Liver Dis.* 17 (2013) 587-607.
111. E. Yoon, A. Babar, M. Choudhary, M. Kutner, N. Pyrsopoulos, *J. Clin. Transl. Hepatol.* 28 (2016) 131-42.
112. R. Bergman, M. Parkes, *Aliment. Pharmacol. Ther*. 23 (2006) 841-855.
113. S. B Hanauer, D. H. Present, *Rev. Gastroenterol. Disord.* 3 (2003) 81-92.
114. Y. Minato, J. M. Thiede, S. L. Kordus, E. J. McKlveen, B. J. Turman, A. D. Baughn, *Antimicrob. Agents Chemother*. 59 (2015) 5097-5106.

115. H. J. Salavagione, J. Arias, P. Garcés, E. Morallón, C. Barbero, J. L. Vázquez, *J. Electroanal. Chem*. 565 (2004) 375-383.
116. A. P. Mishra, R. K. Mishra, M. D. Pandey, *Russ. J. Inorg. Chem*. 56 (2011) 1757-1764.
117. N. V. Loginova, T. V. Koval'chuk, N. P. Osipovich, G. I. Polozov, V. L. Sorokin, A. A. Chernyavskaya, O. I. Shadyro, *Polyhedron* 27 (2008) 985-991.
118. P. Subbaraj, A. Ramu, N. Raman, J. Dharmaraja, *Spectrochim. Acta A Mol. Biomol. Spectrosc*. 117 (2014) 65-71.
119. M. M. Haque, Md. Kudrat-E-Zahan, L. A. Banu, Md. S. Islam, M. S. Islam, *Bioinorg. Chem. Appl*. 2015 (2015) 923087.
120. F. Tümer, S. A. Güngöra, M. Kösea, F. Koçer, M. Tümer, *J. Mol. Struct*. 1199 (2020) 127059.
121. N. Raman, R. Jeyamurugan, R. U. Rani, T. Baskaran, L. Mitu, *J. Coord. Chem*. 63 (2010) 1629-1644.
122. H. Demirelli, F. Köseoglu, N. Kavak, *J. Solution Chem.* 33 (2004) 1467-1479.
123. F. Kovács, M. K. Gopisetty, D. I. Adamecz, M. Kiricsi, É. A. Enyedy, É. Frank, *RSC Adv*. 11 (2021) 13885-13896.
124. V. Manjula, P. K. Bhattacharya, *J. Inorg. Biochem.* 41 (1991) 63-69.
125. W. M. Haynes (Ed.), *CRC Handbook of Chemistry and Physics* (97th ed.) CRC Press, Boca Raton, USA (2016)
126. F. J. C. Rossotti, H. S. Rossotti, R. J. Whewell, *J. Inorg. Nucl. Chem*. 33 (1971) 2051-2065.
127. H. M. Irving, M. G. Miles, L. D. Pettit, *Anal. Chim. Acta* 38 (1967) 475-488.
128. SCQuery, The IUPAC Stability Constants Database, Academic, Software (Version 5.5), Royal Society of Chemistry, Sourby Old Farm, Timble, Otley, Yorks, 1993-2005.
129. O. Dömötör, M. A. Kiss, G. T. Gál, N. V. May, G. Spengler, M. Nové, A. Čipak Gašparović, É. Frank, É. A. Enyedy, *J. Inorg. Biochem.* 202 (2020) 110883.
130. É. A. Enyedy, E. Farkas, O. Dömötör, M. A. Santos, *J. Inorg. Biochem*. 105 (2011) 444-453.
131. P. Gans, A. Sabatini, A. Vacca, *Talanta.* 43 (1996) 1739-1753.
132. L. Zékány, I. Nagypál, D. L., in: *Computational Methods for the Determination of Stability Constants*, Leggett Plenum Press, New York, USA (1985)
133. F. Xiao, T. Xu, B. Lu, R. Liu, *Food Frontiers*. 1 (2020) 60-69.
134. É. A. Enyedy, D. Hollender, T. Kiss, *J. Pharm. Biomed. Anal*. 54 (2011) 1073-1081.
135. X. Chen, A. Murawski, K. Patel, C. L. Crespi, P. V. Balimane, *Pharm Res*. 7 (2008) 1511-1520.
136. H. Yu, Q. Wang, Y. Sun, M. Shen, H. Li, Y. Duan, *PLoS One* 10 (2015) e0116502.
137. J. R. Lakowicz, (Ed.) Introduction to Fluorescence. In: *Principles of Fluorescence Spectroscopy.* Springer, Boston, USA (2006)
138. A. Rockenbauer, L. Korecz, *Appl. Magn. Reson*. 10 (1996) 29-43.
139. Metrohm, Compact Line Potentiostats: Overview. Available online: https://www.metrohm.com/hu_hu/products/electrochemistry/compact-line.html (accessed on 20 September 2023)
140. J. I. Wirgau, I. Spasojević, H. Boukhalfa, I. Batinić-Haberle, A. L. Crumbliss, *Inorg. Chem.* 41 (2002) 1464-1473.
141. É. A. Enyedy, M. F. Primik, C. R. Kowol, V. B. Arion, T. Kiss, B. K. Keppler, *Dalton Trans*. 40 (2011) 5895-5905.
142. M. F. Zaltariov, M. Hammerstad, H. J. Arabshahi, K. Jovanović, K. W. Richter, M. Cazacu, S. Shova, M. Balan, N. H. Andersen, S. Radulović, J. Reynisson, K. K. Andersson, V. B. Arion, *Inorg Chem*. 56 (2017) 3532-3549.
143. J. Felcman, J. J. R. Fraústo da Silva, *Talanta* 30 (1983) 565-570.

144. T. Gajda, B. Henry, J.-J. Delpuech, *J. Chem. Soc., Dalton Trans*. (1993) 1301-1306.
145. P. G. Daniele, O. Zerbinati, V. Zelano G. Ostacoli, *J. Chem. Soc., Dalton Trans*. (1991) 2711-2715.
146. P. J. Morris, R. B. Martin, *J. Inorg. Nucl. Chem.* 33 (1971) 2913-2918.
147. P. Rapta, J. Kožíšek, M. Breza, M. Gembický, L. Dunsch, *J. Electroanal. Chem*. 566 (2004) 123-129.
148. M. Sala-Rabanal, D. C. Li, G. R. Dake, H. T. Kurata, M. Inyushin, S. N. Skatchkov, C. G. Nichols, *Mol. Pharm*. 10 (2013) 1450-1458.
149. V. Pósa, B. Hajdu, G. Tóth, O. Dömötör, C. R. Kowol, B. K. Keppler, G. Spengler, B. Gyurcsik, É. A. Enyedy, *J. Inorg. Biochem.* 231 (2022) 111786.
150. C. R. Kowol, R. Eichinger, M. A. Jakupec, M. S. Galanski, V. B. Arion, B. K. Keppler, *J. Inorg. Biochem.* 101 (2007) 1946-1957.
151. É. Frank, G. Schneider, *J. Steroid Biochem. Mol. Biol*. 137 (2013) 301-315.
152. C. Borrás, J. Gambini, R. López-Grueso, F. V. Pallardó, J. Viña, *BBA*. 1802 (2010) 205-211.
153. N. K. Utkina, N. D. Pokhilo, *Nat. Prod. Commun*. 7 (2012) 901-904.
154. M. Puiu, D. Oancea, *Chimie*, 1 (2004) 263-268.
155. A. Covington, (Ed.) *Physical chemistry of organic solvent systems.* Springer, Boston, USA (2012)
156. C. C. Chang, C. S. Chung, *Dalton Trans*. 7 (1991) 1685-1689.
157. P. R. Shukla, *J. Inorg. Nucl. Chem*. 29 (1967) 1800-1801.
158. K. Jackowska, J. Bukowska, A. Kudelski, *J. Electroanal. Chem.* 350 (1993) 177-187.

## 8. List of publications, oral presentations and posters

**Scientific publications**

MTMT ID: 10069622

**Papers related to the dissertation:**

**P1. Tatsiana V. Petrasheuskaya**, Ferenc Kovács, Nóra Igaz, Andrea Rónavári, Bálint Hajdu, Laura Bereczki, Nóra V. May, Gabriella Spengler, Béla Gyurcsik, Mónika Kiricsi, Éva Frank, Éva A. Enyedy*

*Estradiol-based salicylaldehyde (thio)semicarbazones and their copper complexes with anticancer, antibacterial and antioxidant activities*

MOLECULES 28 (2023) 54., IF: 4.6, DOI: 10.3390/molecules28010054

Independent citations: 1

**P2. Tatsiana V. Petrasheuskaya**, Ferenc Kovács, Gabriella Spengler, Nóra V. May, Éva Frank, Éva A. Enyedy*

*A comparative study on the complex formation of 2-aminoestradiol and 2-aminophenol with divalent metal ions: solution chemistry and anticancer activity*

JOURNAL OF MOLECULAR STRUCTURE 1261 (2022) 132858., IF: 3.8, DOI: 10.1016/j.molstruc.2022.132858

Independent citations: 1

**P3. Tatsiana V. Petrasheuskaya**, Debora Wernitznig, Márton A. Kiss, Nóra V. May, Dominik Wenisch, Bernhard K. Keppler, Éva Frank, Éva A. Enyedy*

*Estrone-salicylaldehyde N-methylated thiosemicarbazone hybrids and their copper complexes: solution structure, stability and anticancer activity in tumor spheroids*

JOURNAL OF BIOLOGICAL INORGANIC CHEMISTRY 26 (2021) 775-791., IF: 3.862, DOI: 10.1007/s00775-021-01891-7

Independent citations: 2

**P4.** Iuliana Besleaga, Iryna Stepanenko, **Tatsiana V. Petrasheuskaya**, Denisa Darvasiova, Martin Breza, Marta Hammerstad, Małgorzata A. Marć, Alexander Prado-Roller, Gabriella Spengler, Ana Popović-Bijelić, Éva A. Enyedy,* Peter Rapta,* Anatoly Shutalev,* Vladimir B. Arion*

*Triapine analogues and their copper(II) complexes: synthesis, characterization, solution speciation, redox activity, cytotoxicity and mR2 RNR inhibition*

INORGANIC CHEMISTRY 60 (2021) 11297-11319., IF: 5.436, DOI: 10.1021/acs.inorgchem.1c01275

Independent citations: 6

**P5.** Éva A. Enyedy,* **Tatsiana V. Petrasheuskaya**, Márton A. Kiss, Debora Wernitznig, Dominik Wenisch, Bernhard K. Keppler, Gabriella Spengler, Nóra V. May, Éva Frank, Orsolya Dömötör

*Complex formation of an estrone-salicylaldehyde semicarbazone hybrid with copper(II) and gallium(III): solution equilibria and biological activity*

JOURNAL OF INORGANIC BIOCHEMISTRY 220 (2021) 111468., IF: 4.336, DOI: 10.1016/j.jinorgbio.2021.111468

Independent citations: 5

**P6.** Miljan N.M. Milunović,* Oleg Palamarciuc, Angela Sirbu, Sergiu Shova, Dan Dumitrescu, Dana Dvoranová, Peter Rapta, **Tatsiana V. Petrasheuskaya**, Éva A. Enyedy, Gabriella Spengler, Marija Ilic, Harald H. Sitte, Gert Lubec, Vladimir B. Arion*
*Insight into the anticancer activity of copper(II) 5-methylenetrimethylammonium-thiosemicarbazonates and their interaction with organic cation transporters*
BIOMOLECULES 10 (2020) 1213., IF: 4.879, DOI: 10.3390/biom10091213
Independent citations: 7

**P7. Tatsiana V. Petrasheuskaya**, Márton A. Kiss, Orsolya Dömötör, Tamás Holczbauer, Nóra V. May, Gabriella Spengler, Annamária Kincses, Ana Čipak Gašparović, Éva Frank, Éva A. Enyedy*
*Salicylaldehyde thiosemicarbazone copper complexes: impact of hybridization with estrone on cytotoxicity, solution stability and redox activity*
NEW JOURNAL OF CHEMISTRY 44 (2020) 12154-12168., IF: 3.591, DOI: 10.1039/D0NJ01070G
Independent citations: 8

**ΣIF=30.504**

**Oral presentations and posters related to the dissertation:**

1. **Tatsiana V. Petrasheuskaya**, Márton A. Kiss, Ferenc Kovács, Nóra V. May, Gabriella Spengler, Debora Wernitzing, Nóra Igaz, Mónika Kiricsi, Éva Frank, Éva A. Enyedy (lecture)
*Comparative studies of sterane-based thiosemicarbazones and their Cu(II) complexes: synthesis, solution stability, redox properties and biological activity*
MTA Steroid and Terpenoid Chemistry working group meeting, 28.11.2022, Szeged, Hungary

2. **Tatsiana V. Petrasheuskaya**, Gerda T. Gátszegi, Gabriella Spelgler, Peter Rapta, Miljan N. M. Milunovic, Vladimir B. Arion, Éva A. Enyedy (poster)
*Anticancer methylenetrimethylammonium-thiosemicarbazonates and their copper(II) complexes: solution chemistry, redox properties and cytotoxicity*
3rd European NECTAR Conference, 24-26.08.2022, Ljubljana, Slovenia

3. **Tatsiana V. Petrasheuskaya**, Márton A. Kiss, Nóra V. May, Gabriella Spengler, Peter Rapta, Éva Frank, Éva A. Enyedy (poster)
*Comparative solution study on the interactions of Cu(II), Fe(II/III) and Ni(II) with imidazole-derived thiosemicarbazones: impact of methylation, redox and anticancer activity*
16th European Biological Inorganic Chemistry Conference (EuroBIC-16), 17-21.07.2022, Grenoble, France

4. **Tatsiana V. Petrasheuskaya**, Ferenc Kovács, Nóra V. May, Andrea Rónavári, Mónika Kiricsi, Gabriella Spengler, Éva Frank, Éva A. Enyedy (poster)
*Estradiol-based salicylaldehyde (thio)semicarbazones and their copper complexes with anticancer, antibacterial and antioxidant activities*
International Symposium on Metal Complexes (ISMEC 2022), 5-8.06.2022, Valencia, Spain

5. **Tatsiana V. Petrasheuskaya**, Márton A. Kiss, Debora Wernitzing, Dominik Wenisch, Bernard K. Keppler, Nóra V. May, Éva Frank, Éva A. Enyedy (poster)

*Estrone-salicylaldehyde N-methylated-thiosemicarbazone hybrids and their copper complexes: solution study and anticancer activity in tumor spheroids*
International Symposium Thermodynamics of Metal Complexes (ISMEC 2021), 16-18.06.2021, online, Białystok, Poland

6. **Tatsiana V. Petrasheuskaya**, Márton A. Kiss, Orsolya Dömötör, Gabriella Spengler, Debora Wernitzing, Bernard K. Keppler, Nóra V. May, Éva Frank, Éva A. Enyedy (lecture)
*Antitumor thiosemicarbazone-estrone hybrids and their copper complexes*
54th Colloquium on Complex Chemistry and Meeting of the Coordination Chemistry Working Group of the Hungarian Academy of Sciences, 26-27.05.2021, online, Hungary

7. **Tatsiana V. Petrasheuskaya**, Debora Wernitznig, Márton A. Kiss, Nóra V. May, Dominik Wenisch, Bernhard K. Keppler, Éva Frank, Éva A. Enyedy (poster)
*Effects of stepwise terminal $NH_2$-methylation of estrone-salicylaldehyde–thiosemicarbazone and copper coordination, solution speciation, anticancer activity and redox activity*
26th International Symposium on Analytical and Environmental Problems, 23-24.11.2020, online, Szeged, Hungary

8. **Tatsiana V. Petrasheuskaya**, Márton A. Kiss, Orsolya Dömötör, Debora Wernitznig, Dominik Wenisch, Gabriella Spengler, Annamária Kincses, Nóra V. May, Bernhard K. Keppler, Éva Frank, Éva A. Enyedy (lecture)
*Comparative solution study on estrone salicyladehyde (thio)semicarbazones and their copper complexes: impact of hybridization and methylation*
XLIII. Chemistry Days, 27-28.10.2020, Szeged, Hungary

9. **Tatsiana V. Petrasheuskaya**, Márton A. Kiss, Orsolya Dömötör, Gabriella Spengler, Annamária Kincses, Nóra V. May, Éva Frank, Éva A. Enyedy (lecture)
*Synthesis, solution stability and anticancer activity of copper complexes formed with salicylaldehyde thiosemicarbazone-estrone conjugates*
MTA Steroid and Terpenoid Chemistry working group meeting, 22.11.2019, Szeged, Hungary

10. **Tatsiana V. Petrasheuskaya**, Orsolya Dömötör, Gabriella Spengler, Annamária Kincses, Nóra V. May, Márton A. Kiss, Éva Frank, Éva A. Enyedy (oral lecture)
*Antitumor copper complexes of salicylaldehyde thiosemicarbazones: Solution chemistry and biological acitivity*
XLII. Chemistry Days, 28-30.10.2019, Szeged, Hungary

11. **Tatsiana V. Petrasheuskaya**, Orsolya Dömötör, Gabriella Spengler, Annamária Kincses, Márton A. Kiss, Éva Frank, Éva A. Enyedy (poster)
*Copper(II) complexes of salicylaldehyde thiosemicarbazone and its structurally-related analogs: solution stability, redox properties and cytotoxicity*
International Symposium on Metal Complexes (ISMEC 2019), 11-14.06.2019, Hajdúszoboszló/Debrecen, Hungary

12. Dömötör Orsolya, **Tatsiana V. Petrasheuskaya**, Gál G. Tamás, May Nóra V., Nové Márta, Kincses Annamária, Spengler Gabriella, Ana Čipak Gašparović, Kiss Márton A., Frank Éva, Enyedy Éva A. (lecture)
*Cu(II) and Ru(II)(p-cymene) complexes of pyrazolo- and salicyladehyde thiosemicarbazones: synthesis, antitumor activity, stability and structure*

## 9. Acknowledgments

I would like to express my deepest gratitude to my supervisor and head of department, Dr. Éva Anna Enyedy for giving me an opportunity to work in the MTA-SZTE Lendület Functional Metal Complexes Research Group for her continuous help, knowledge, motivation, consistent support and constant guidance that she carried me during my Ph.D. studies.

I am thankful to all members of the Bioinorganic Chemistry Research Group of the University of Szeged for their help and the nice working atmosphere.

I would like to say special thanks to Prof. Vladimir B. Arion (University of Vienna) and to Prof. Peter Rapta (Slovak University of Technology in Bratislava) for accepting me and guiding my work as a guest Ph.D. student at their labs.

I am also grateful to Dr. Nóra V. May (Research Centre for Natural Sciences, Budapest), for her help in the EPR measurements and evaluations of the data.

I sincerely appreciate the contribution of our collaborators without whom my dissertation would not be possible: Dr. Éva Frank, Márton A Kiss, Ferenc Kovács, Dr. Gabriella Spengler, Dr. Nóra Igaz, Dr. Mónika Kiricsi, Dr. Zoltán Kele (University of Szeged); Dr. Tamás Holczbauer, Laura Bereczki (Research Centre for Natural Sciences, Budapest); Dr. Miljan N.M. Milunović, Iuliana Besleaga, Dr. Debora Wernitznig, Dominik Wenisch, Prof. Bernhard K Keppler (University of Vienna).

I am also thankful to the head of the Chemistry Doctoral School, Prof. Ágota Tóth for following the progress of my Ph.D. studies.

Also, I want to say many thanks to Dr. János P. Mészáros for his continuous support, help, inspiration, motivation and for reading my dissertation.

I am grateful for the help and advices of all members of the Department of Molecular and Analytical Chemistry and Dr. Tamás Szabó.

I owe many thanks to my parents, grandparents, my lovely sister and friends for their support, patience, motivation during my study.

I would also like to express gratitude to the treasured colleagues in the Ph.D. room.

Finally, I would like to greatly acknowledge the financial support from the Ernst Mach grant MPC-2021-00073; Scholarship Foundation of the Republic of Austria, Undergraduates, Graduates, Postgraduates ICM-2019-14969; Visegrad Scholarship Program #52010752, #51910905; COST Nectar STSM CA grant 18202 #47209; Mecenatúra 141058.

# 10. Appendix

**Table S1.** *In vitro* cytotoxicity ($IC_{50}$ values in μM) of ligands VA1-3 and complexes Cu(II)-VA1, Cu(II)-VA2 and Cu(II)-VA3 in Colo205, Colo320 and MRC-5 cell lines (72 h exposure). This table was taken from publication [P4].

| $IC_{50}$ (μM) | Colo205 | Colo320 | MRC-5 |
|---|---|---|---|
| **VA1** | > 100 | 6.32 ± 0.49 | > 100 |
| **VA2** | > 100 | > 100 | > 100 |
| **VA3** | 48.2 ± 6.8 | > 100 | > 100 |
| **Cu(II)-VA1** | 2.08 ± 0.12 | 2.21 ± 0.18 | 3.13 ± 0.17 |
| **Cu(II)-VA2** | 0.181 ± 0.039 | 0.159 ± 0.009 | 0.276 ± 0.049 |
| **Cu(II)-VA3** | 26.6 ± 1.6 | 27.6 ± 1.6 | > 100 |
| **$CuCl_2$** | 19.7 ± 0.9 | 20.0 ± 2.3 | 24.5 ± 2.6 |
| **doxorubicin** | 3.28 ± 0.22 | 3.12 ± 0.27 | 5.19 ± 0.21 |

**Table S2.** $IC_{50}$ values after inhibition of cell growth by the imidazole-TSC derivatives and their Cu(II) complexes in human colonic doxorubicin-sensitive (Colo205), multidrug resistant colon adenocarcinoma (Colo320).

| $IC_{50}$ (μM) | Colo205 | Colo320 |
|---|---|---|
| **imidazole-TSC** | 84±9 | 90±6 |
| **Me-imidazole-TSC** | 98±8 | 88±4 |
| **$Me_2$-imidazole-TSC** | 9.98±0.37 | 8.96±0.33 |
| **benzimidazole-TSC** | >100 | >100 |
| **triapine** | 3.28±0.63 | 2.17±0.15 |
| **Cu(II)-imidazole-TSC** | 28.8±1.9 | 58.6±4.2 |
| **Cu(II)-Me-imidazole-TSC** | 38.7±0.8 | 56.3±2.4 |
| **Cu(II)-$Me_2$-imidazole-TSC** | 14.45±1.66 | 28.2±1.2 |
| **Cu(II)- benzimidazole-TSC** | 25.61±0.74 | 15.7±0.7 |
| **Cu(II)-triapine** | 11.4±1.4 | 26.0±0.7 |

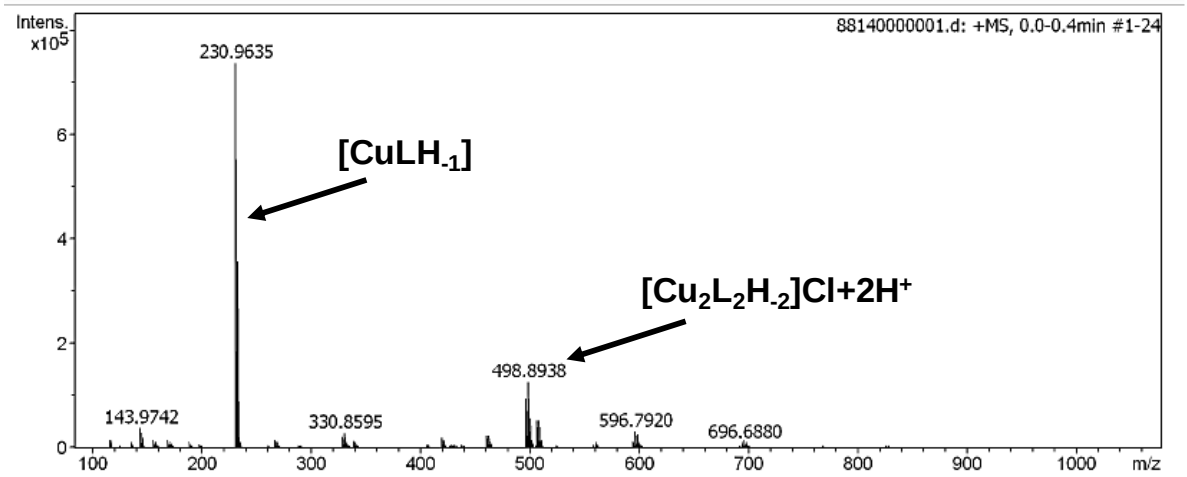


**Figure S1.** ESI-MS spectra of the indicated Cu(II) complexes of the imidazole-TSC. Samples were prepared in MeOH.

**Table S3**. $IC_{50}$ values after inhibition of cell growth by the ligands VA8-11 and their Cu(II) complexes in human colon doxorubicin-sensitive (Colo205), multidrug resistant colon adenocarcinoma (Colo320), neuroblastoma (SH-SY5Y) cell lines and non-cancerous human embryonic lung fibroblast (MRC-5). This table was taken from publication [P6].

| $IC_{50}$ (μM) | Colo205 | Colo320 | SH-SY5Y | MRC-5 |
|---|---|---|---|---|
| **VA8** | >100 | 88.77±5.32 | >100 | >100 |
| **VA9** | >100 | 74.43±3.85 | >100 | >100 |
| **VA10** | >100 | 53.30±2.44 | 49.86±3.97 | >100 |
| **VA11** | >100 | 95.81±1.58 | 31.46±2.66 | >100 |
| **Cu(II)-VA8** | >100 | 65.38±3.71 | 38.15±1.15 | >100 |
| **Cu(II)-VA9** | 53.34±3.31 | 80.64±1.57 | 15.35±1.74 | 51.53±4.67 |
| **Cu(II)-VA10** | 28.59±2.02 | 35.41±1.87 | 8.93±0.50 | 22.6±1.81 |
| **Cu(II)-VA11** | 42.81±4.23 | 65.14±2.93 | 58.64±7.18 | 25.64±2.57 |
| **cisplatin** | 8.14±1.59 | 2.12±0.14 | 0.65±0.08 | 1.73±0.28 |

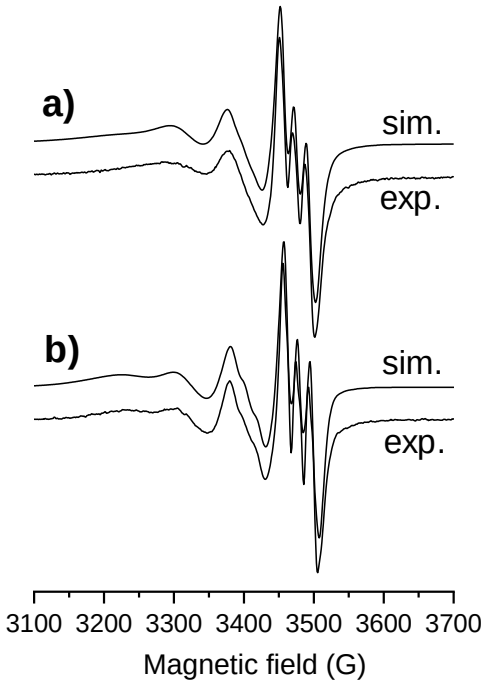


**Figure S2.** Experimental (exp.) and simulated (sim.) isotropic EPR spectrum for complexes Cu(II)-estrone-TSC a) and Cu(II)-thn-TSC b) in DMSO at room temperature. This figure was taken from publication [P7].

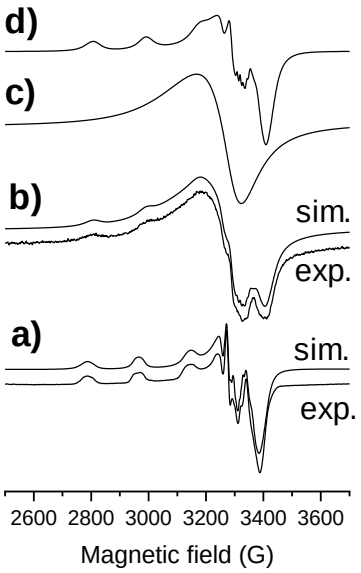


**Figure S3.** Experimental (exp.) and simulated (sim.) anisotropic EPR spectra of complexes of Cu(II)-estrone-TSC a) and Cu(II)-thn-TSC b) in 50% (*v/v*) DMSO/$H_2O$. Calculated component EPR spectra of a dimeric species c) and a monomer species d) taken in 76% and 24%, respectively, in the simulation of spectrum b). The dimeric species was simulated with an isotropic spectrum with $g_o = 2.092$. This figure was taken from publication [P7].

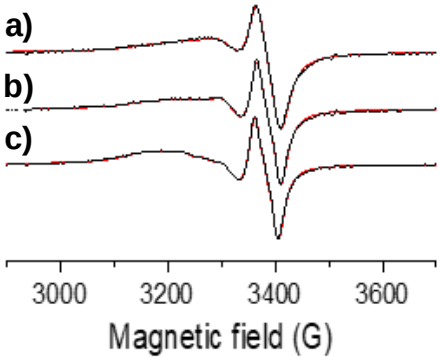


**Figure S4.** Experimental (black) and simulated (red) anisotropic EPR spectra for the a) Cu(II)-estrone-SC (1:1), b) Cu(II)-thn-SC (1:1) and c) Cu(II)-SSC (1:1) systems at room temperature. This figure was taken from publication [P5].

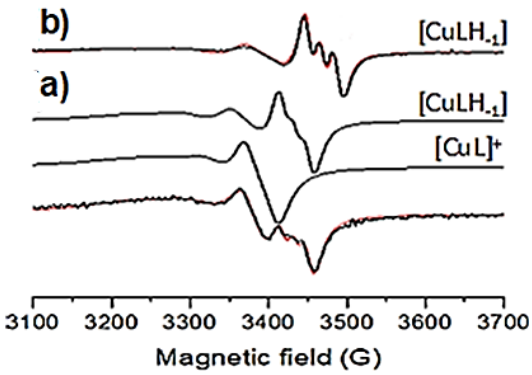


**Figure S5.** Room temperature solution EPR spectra (black) recorded for Cu(II) complexes dissolved in DMSO of a) estradiol-SC, b) estradiol-TSC and simulated (red) spectra together with the obtained component spectra. Spectrum a) were simulated with 50% $[CuL]^+$ and 50% $[CuLH_{-1}]$, b) with 100% $[CuLH_{-1}]$. This figure was adapted from publication [P1].

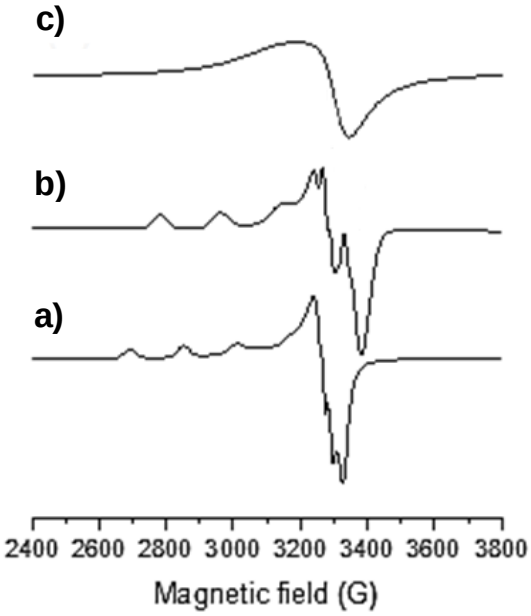


**Figure S6.** Calculated frozen solution EPR spectra of Cu(II) complexes a) estradiol-SC, b) estradiol-TSC and c) an isotropic component originated from oligomerisation process. This figure was adapted from publication [P1].

**Table S4** Isotropic and anisotropic EPR spectroscopic parameters determined for the isolated Cu(II)-estrone-TSC and Cu(II)-thn-TSC complexes in DMSO and for Cu(II)-STSC in 30% (*v/v*) DMSO/$H_2O$. This table was taken from publication [P7]; (n.d. = not determined).

| | **estrone-TSC** | **thn-TSC** | **STSC** |
|---|---|---|---|
| **isotropic parameters** | | | |
| $\mathbf{g_o}$ | 2.0889(3) | 2.0874(1) | 2.0945 |
| $\mathbf{A_o}$ **(G)** | 71.3(1) | 72.8(1) | 73.1 |
| $\mathbf{a_N}$ **(G)** | 18.1(1) | 18.1(1) | 17.7 |
| **anisotropic parameters** | | | |
| $\mathbf{g_x / g_y / g_z}$ | 2.018 / 2.048 / 2.182 | 2.026 / 2.052 / 2.203 | n.d. |
| $\mathbf{A_x / A_y / A_z}$ **(G)** | 36.0 / 23.3 / 180.8 | 30.8 / 17.2 / 174.4 | n.d. |
| $\mathbf{a_{Nx} / a_{Ny} / a_{Nz}}$ **(G)** | 9.5 / 16.4 / 8.5 | 11.6 / 15.6 / 13.0 | n.d. |

**Table S5.** Isotropic and anisotropic EPR parameters[a] determined for the Cu(II) complexes in DMSO. This table was taken from publication [P5].

| **ligand** | **estrone-SC** | **thn-SC** | **SSC** | **SSC**[b] |
|---|---|---|---|---|
| $\boldsymbol{g_o}$ | 2.134 | 2.134 | 2.137 | 2.136 |
| $\boldsymbol{A_o}$ **(G)** | 63.0 | 63.1 | 62.8 | 64.7 |
| $\boldsymbol{a_0^N}$ **(G)** | 14.6 | 14.9 | 14.6 | 14.6 |
| $\boldsymbol{g_x}$ | 2.049 | 2.049 | 2.049 | 2.053 |
| $\boldsymbol{g_y}$ | 2.060 | 2.056 | 2.059 | 2.065 |
| $\boldsymbol{g_z}$ | 2.285 | 2.277 | 2.289 | 2.290 |
| $\boldsymbol{A_x}$ **(G)** | 8.5 | 7.9 | 7.3 | 9.87 |
| $\boldsymbol{A_y}$ **(G)** | 10.6 | 12.2 | 10.6 | 15.1 |
| $\boldsymbol{A_z}$ **(G)** | 164.2 | 166.7 | 163.7 | 161.6 |
| $\boldsymbol{a_x^N}$ **(G)** | 10.2 | 8.7 | 6.5 | n.d. |
| $\boldsymbol{a_y^N}$ **(G)** | 15.8 | 15.5 | 14.7 | 19.9 |
| $\boldsymbol{a_z^N}$ **(G)** | 14.2 | 12.7 | 13.2 | n.d. |
| $\boldsymbol{g_{0,calc.}}$[c] | 2.131 | 2.127 | 2.132 | 2.136 |

[a] The experimental error was ±0.001 for $g$, ± 1 G for $A$ and $a^N$ tensor values. [b] Data for complex $[CuL]^+$ in 30% (*v/v*) DMSO/$H_2O$ taken from ref. [81]. [c] $g_{0,calc.} = (g_x+g_y+g_z)/3$

**Table S6.** Isotropic EPR parameters obtained by the simulation of room temperature EPR spectra recorded in DMSO of Cu(II) complexes formed with estradiol-(T)SCs. This table was adapted from publication [P1].

| **Complexes** | **Components** | $\boldsymbol{g_0}$ | $\boldsymbol{A_0}$ | $\boldsymbol{a_0^N}$ | $\boldsymbol{\alpha}$ **(G)** | $\boldsymbol{\beta}$ **(G)** | $\boldsymbol{\gamma}$ **(G)** | **component ratio** |
|---|---|---|---|---|---|---|---|---|
| **Cu(II) – estradiol-SC** | $[CuLH_{-1}]$ | 2.099 | 56.6 | 15.4 | 36.0 | -20 | 3.7 | 50% |
| | $[CuL]^+$ | 2.118 | 48.0 | 14.3 | 54.0 | -25 | 1.8 | 50% |
| **Cu(II) – estradiol-TSC** | $[CuLH_{-1}]$ | 2.090 | 70.2 | 17.5 | 35.7 | -21.3 | 3 | 100% |

**Table S7.** Crystal data and structure refinement for thn-TSC as [CuL]Cl and thn-SC as [CuL]Cl × $H_2O$, where HL is the fully protonated form. This table was adapted from publications [P7 and P5].

| | **thn-SC as [CuL]Cl × $H_2O$** | **thn-TSC as [CuL]Cl** |
|---|---|---|
| **Color/Shape** | Green/Platelet | Blue/Platelet |
| **Empirical formula** | $C_{12}H_{18}ClCuN_3O_3$, $H_2O$ | $C_{12}H_{14}ClCuN_3OS$ |
| **Moiety formula** | $C_{12}H_{18}ClCuN_3O_4$ | $[Cu(C_{12}H_{14}N_3OS)(Cl)]$ |
| **Formula weight** | 367.28 | 347.31 |
| **Temperature (K)** | 173(2) | 168(2) |
| **Radiation and wavelength λ (Å)** | Mo-$K_\alpha$, 0.71075 | Cu-$K_\alpha$, 1.54187 |
| **Crystal system** | triclinic | orthorhombic |
| **Space group** | *P*-1 | Pbca |
| **Unit cell dimensions** | | |
| **a (Å)** | 6.3832(5) | 12.3620(7) |
| **b (Å)** | 7.8947(6) | 9.1718(5) |
| **c (Å)** | 15.8886(12) | 24.3156(13) |
| **α (°)** | 79.112(6) | 90 |
| **β (°)** | 87.218(6) | 90 |
| **γ (°)** | 70.524(5) | 90 |
| **Volume ($Å^3$)** | 741.19(10) | 2756.9(3) |
| ***Z/Z'*** | 2/1 | 8/1 |
| **Density (calculated) ($Mg/m^3$)** | 1.646 | 1.674 |
| **Absorption coefficient, μ ($mm^{-1}$)** | 1.672 | 5.395 |
| ***F*(000)** | 378 | 1416 |
| **Crystal size (mm)** | 0.50 x 0.30 x 0.05 | 0.30 x 0.15 x 0.05 |
| **Absorption correction** | numerical | numerical |
| **Max. and min. transmission** | 0.785, 0.935 | 0.881059, 0.966635 |
| **θ–range for data collection (°)** | $3.285 \le \theta \le 26.022$ | $3.636 \le \theta \le 68.244$ |
| **Index ranges** | $-7 \le h \le 7; -9 \le k \le 9; -19 \le l \le 19$ | $-14 \le h \le 13; -11 \le k \le 10; -29 \le l$ |
| **Reflections collected** | 16265 | 37286 |
| **Completeness to 2θ** | 0.999 | 0.996 |
| **Independent reflections, ($R_{int}$)** | 2922 (0.0584) | 2513, 0.2143 |
| **Reflections $I>2\sigma(I)$** | 2493 | 1879 |
| **Refinement method** | full-matrix least-squares on $F^2$ | full-matrix least-squares on $F^2$ |
| **Data / restraints / parameters** | 2922 /5 /206 | 2513 /15 /163 |
| **Goodness-of-fit on $F^2$** | 1.052 | 1.262 |
| **Final *R* indices [$I>2\sigma(I)$], $R_1$, $wR_2$** | 0.0370, 0.1006 | 0.1434, 0.2733 |
| **R indices (all data), $R_1$, $wR_2$** | 0.0483, 0.1058 | 0.1806, 0.2908 |
| **Max. and mean shift/esd** | 0.000; 0.000 | 0.000;0.000 |
| **Largest diff. peak and hole ($e \times Å^{-3}$)** | 0.485; -0.408 | 0.942; -0.544 |

**Table S8.** Crystal data and structure refinement for estradiol-SC as $[Cu(HL)Cl_2]$, where HL is full protonated form. This table was adapted from publication [P1].

| | **$[Cu(HL)Cl_2]\times H_2O\times 2CH_3OH$** |
|---|---|
| **Empirical formula** | $C_{22}H_{38}Cl_2CuN_3O_6$ |
| **Formula weight** | 574.99 |
| **Temperature (K)** | 103(2) |
| **Radiation and wavelength** | Mo-$K_\alpha$, $\lambda$ = 0.71073 Å |
| **Crystal system** | orthorhombic |
| **Space group** | $P\ 2_1\ 2_1\ 2_1$ |
| **Unit cell dimensions** | |
| **a (Å)** | 7.2028(3) |
| **b (Å)** | 13.6795(6) |
| **c (Å)** | 26.1919(12) |
| **α (°)** | 90 |
| **β (°)** | 90 |
| **γ (°)** | 90 |
| **Volume** | 2580.7(2) $Å^3$ |
| ***Z*** | 4 |
| **Density (calculated)** | 1.480 $Mg/m^3$ |
| **Absorption coefficient, μ** | 1.095 $mm^{-1}$ |
| ***F*(000)** | 1208 |
| **Crystal color** | brown |
| **Crystal description** | needle |
| **Crystal size** | 0.72 x 0.33 x 0.13 mm |
| **Absorption correction** | numerical |
| **Max. and min. transmission** | 0.8931.000 |
| **θ–range for data collection** | $5.157 \leq \theta \leq 25.347°$ |
| **Index ranges** | $-8 \leq h \leq 8; -16 \leq k \leq 16; -31 \leq l \leq 31$ |
| **Reflections collected** | 71353 |
| **Completeness to 2θ** | 0.988 |
| **Absolute structure parameter** | 0.08(2) |
| **Friedel coverage** | 0.746 |
| **Friedel fraction max.** | 0.996 |
| **Friedel fraction full** | 0.996 |
| **Independent reflections** | 4700 [*R*(int) =0.1398] |
| **Reflections *I*>2σ (*I*)** | 4148 |
| **Refinement method** | full-matrix least-squares on $F^2$ |
| **Data / restraints / parameters** | 4700 /1 /314 |
| **Goodness-of-fit on *F*2** | 1.123 |
| **Final *R* indices [*I*>2σ (*I*)]** | *R*1 =0.0512, *wR*2 =0.0818 |
| **R indices (all data)** | *R*1 =0.0628, *wR*2 =0.0848 |
| **Max. and mean shift/esd** | 0.000;0.000 |
| **Largest diff. peak and hole** | 0.337;-0.351 e×$Å^{-3}$ |

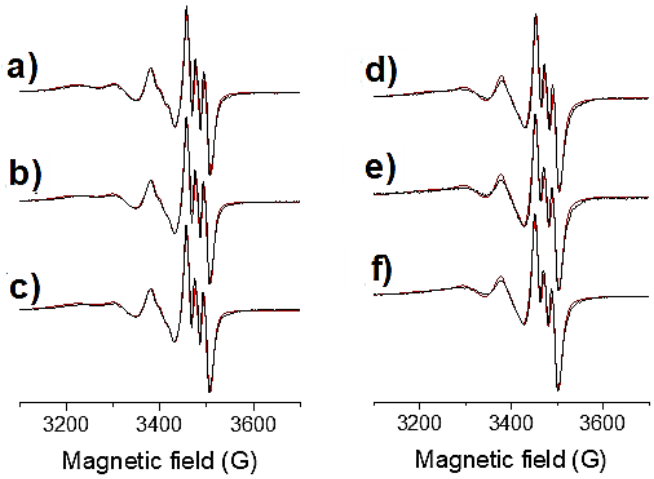


**Figure S7.** Experimental (black) and simulated (red) isotropic EPR spectra for complexes a) Cu(II)-$Me_2$-thn-TSC, b) Cu(II)-Me-thn-TSC, c) Cu(II)-thn-TSC, d) Cu(II)-$Me_2$-estrone-TSC, e) Cu(II)-Me-estrone-TSC, f) Cu(II)-estrone-TSC in DMSO at room temperature. Notably, the abbreviation of the ligands' names stands for the HL forms, thus these complexes are [$CuLH_{-1}$] species. This figure was adapted from publication [P5].

**Table S9** Isotropic EPR spectroscopic parameters[a] determined for the isolated Cu(II)-Me-estrone-TSC, Cu(II)-$Me_2$-estrone-TSC**,** Cu(II)-Me-thn-TSC and Cu(II)-$Me_2$-thn-TSC complexes in DMSO. This table was adapted from publication [P3].

| | $g_0$ | $A_0^{Cu}$ ($\times 10^{-4}$cm$^{-1}$) | $a_0^N$ ($\times 10^{-4}$cm$^{-1}$) |
|---|---|---|---|
| **Me-estrone-TSC** | 2.0887(3) | 69.9(1) | 17.9(1) |
| **$Me_2$-estrone-TSC** | 2.0883(3) | 69.9(1) | 17.9(1) |
| **Me-thn-TSC** | 2.0873(1) | 71.1(1) | 17.7(1) |
| **$Me_2$-thn-TSC** | 2.0869(1) | 71.3(1) | 18.0(1) |

[a] Uncertainties (SD) of the last digits are shown in parentheses.

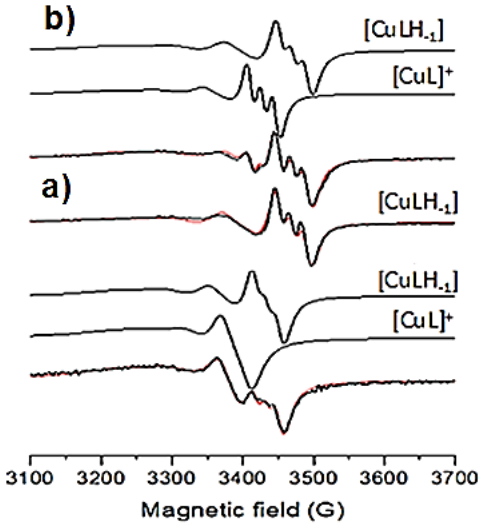


**Figure S8.** Room temperature solution EPR spectra (black) recorded for Cu(II) complexes dissolved in DMSO of a) Me-estradiol-TSC, b) $Me_2$-estradiol-TSC and simulated (red) spectra together with the obtained component spectra. Spectrum a) with 100% [$CuLH_{-1}$] and b) with 18% $[CuL]^+$ 82% [$CuLH_{-1}$]. This figure was adapted from publication [P1].

**Table S10.** Isotropic EPR parameters obtained by the simulation of room temperature EPR spectra recorded in DMSO of Cu(II) complexes formed with estradiol-(T)SCs. This table was adapted from publication [P1].

| Complexes | Components | $g_0$ | $A_0$ | $a_0^N$ | $\alpha$ (G) | $\beta$ (G) | $\gamma$ (G) | component ratio |
|---|---|---|---|---|---|---|---|---|
| **Cu(II)-Me-estradiol-TSC** | $[CuLH_{-1}]$ | 2.088 | 68.7 | 18.0 | 36.9 | -23.9 | 5.4 | 100% |
| **Cu(II)-Me$_2$-estradiol-TSC** | $[CuLH_{-1}]$ | 2.086 | 67.1 | 17.5 | 39.8 | -22.3 | 3.2 | 82% |
| | $[CuL]^+$ | 2.102 | 56.3 | 17.0 | 35.2 | -21.5 | 3.5 | 18% |

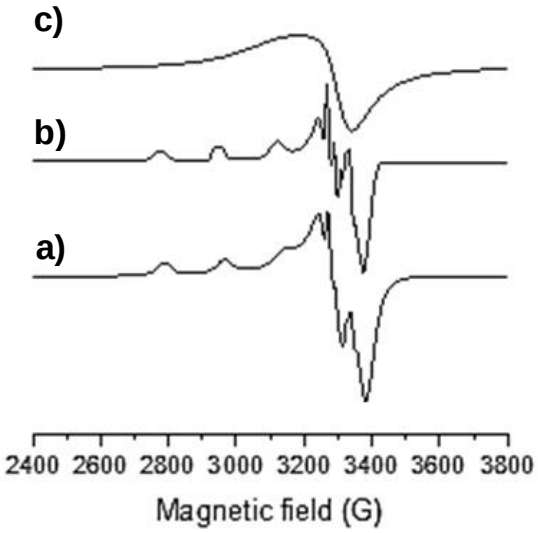


**Figure S9.** Calculated frozen solution EPR spectra of Cu(II) complexes a) Me-estradiol-TSC, b) Me$_2$-estradiol-TSC and c) an isotropic component originated from oligomerisation process. This figure was adapted from publication [P1].

**Table S11.** MIC values determined for the ligands in the absence and presence of one equiv. Cu(II) on various bacteria. This table was adapted from publication [P5].

| MIC (μM) | *S. aureus* | *E. faecalis* | *E. coli* | *K. pneumoniae* |
|---|---|---|---|---|
| | *Gram-positive* | | *Gram-negative* | |
| **estrone-SC** | >100 | >100 | >100 | >100 |
| **thn-SC** | >100 | >100 | >100 | >100 |
| **SSC** | >100 | >100 | >100 | >100 |
| **estrone-TSC** | >100 | >100 | >100 | >100 |
| **thn-TSC** | >100 | >100 | >100 | >100 |
| **STSC** | >100 | >100 | >100 | >100 |
| **estrone-SC + Cu(II)** | >100 | >100 | >100 | >100 |
| **thn-SC + Cu(II)** | >100 | >100 | >100 | >100 |
| **SSC + Cu(II)** | >100 | >100 | >100 | >100 |
| **estrone-TSC + Cu(II)** | 3.125 | 50 | >100 | >100 |
| **thn-TSC + Cu(II)** | 6.25 | 12.5 | 25 | 50 |
| **STSC + Cu(II)** | 6.25 | 50 | 100 | >100 |
| **$CuCl_2$** | >100 | >100 | >100 | >100 |

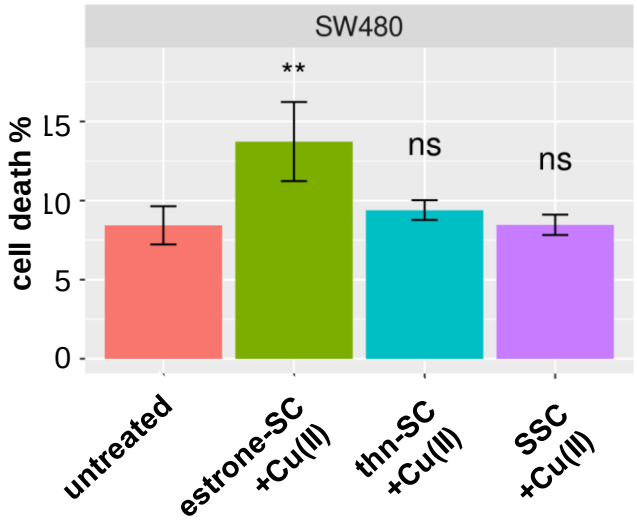


**Figure S10**. Induction of apoptosis in SW480 cells treated for 24 h with the SC ligands premixed with one equiv. Cu(II). Mean + STD (**p≤0.01, ***p≤0.001; Tukey's range test), not significant (ns). This figure was adapted from publication [P3].

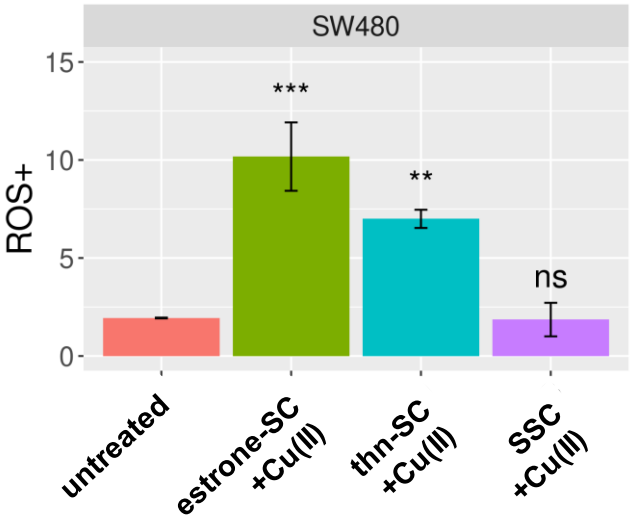


**Figure S11.** Levels of ROS induced in SW480 cells after 24 h of treatment compared to untreated controls detected by flow cytometry. Mean + STD (**p≤0.01, ***p≤0.001; Tukey's range test), not significant (ns). This figure was adapted from publication [P3].

**Table S12.** $IC_{50}$ values (μM) of the complexes and the ligands determined on various cancer cell lines. (24 h incubation time). This table was adapted from publication [P1].

| | **$IC_{50}$ values (μM) on various cell lines** | | | |
|---|---|---|---|---|
| | **MCF-7** | **MCF-7 KCR** | **DU-145** | **A549** |
| **DMSO** | > 20 | > 20 | > 20 | > 20 |
| **Cu** | > 20 | > 20 | > 20 | > 20 |
| **estrone-TSC** | > 20 | > 20 | > 20 | 16.71 |
| **Cu(II)-estrone-TSC** | 4.28 | 12.75 | 11.37 | 4.03 |
| **estradiol-SC** | > 20 | > 20 | > 20 | > 20 |
| **Cu(II)-estradiol-SC** | > 20 | > 20 | > 20 | > 20 |
| **estradiol-TSC** | > 20 | > 20 | > 20 | 20.54 |
| **Cu(II)-estradiol-TSC** | 8.40 | 12.95 | > 20 | 10.03 |
| **Me-estradiol-TSC** | > 20 | > 20 | > 20 | 15.79 |
| **Cu(II)-Me-estradiol-TSC** | 16.74 | > 20 | 15.84 | 3.71 |
| **$Me_2$-estradiol-TSC** | > 20 | > 20 | > 20 | > 20 |
| **Cu(II)-$Me_2$-estradiol-TSC** | 10.05 | > 20 | 7.85 | 3.44 |

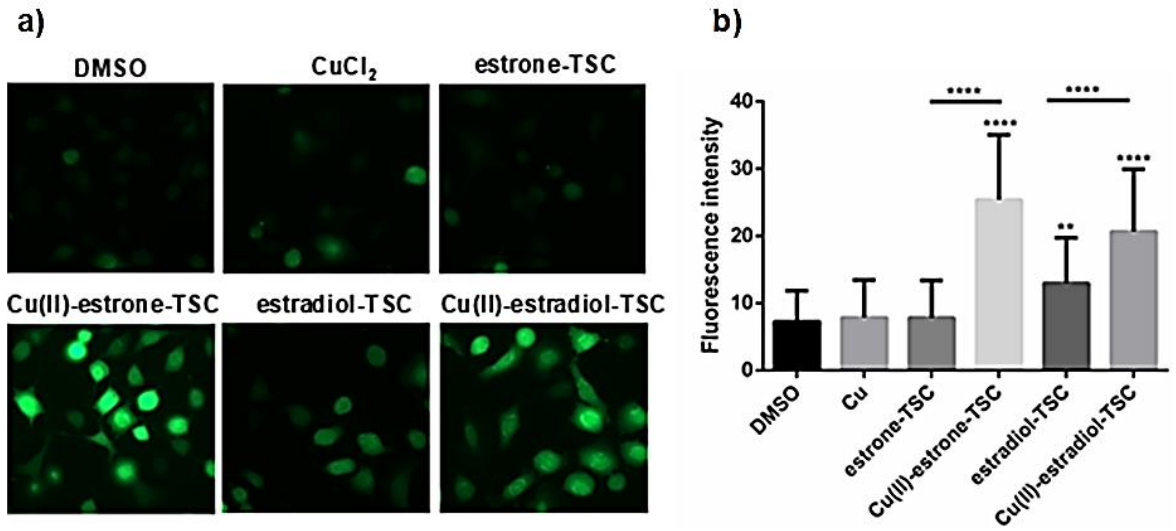


**Figure 12.** a) Representative fluorescence microscopic images show the DCFDA staining to determine ROS levels in A549 cells upon the treatment with estrone-TSC and estradiol-TSC and their Cu(II) complexes (20 μM) in addition to the DMSO blank (90% DMSO-10% PBS buffer) and $CuCl_2$ (20 μM) as indicated in the figure using 6 h incubation time. b) Level of ROS generation measured by $H_2$DCFDA staining on A549 cells. These figures were adapted from publication [P1].

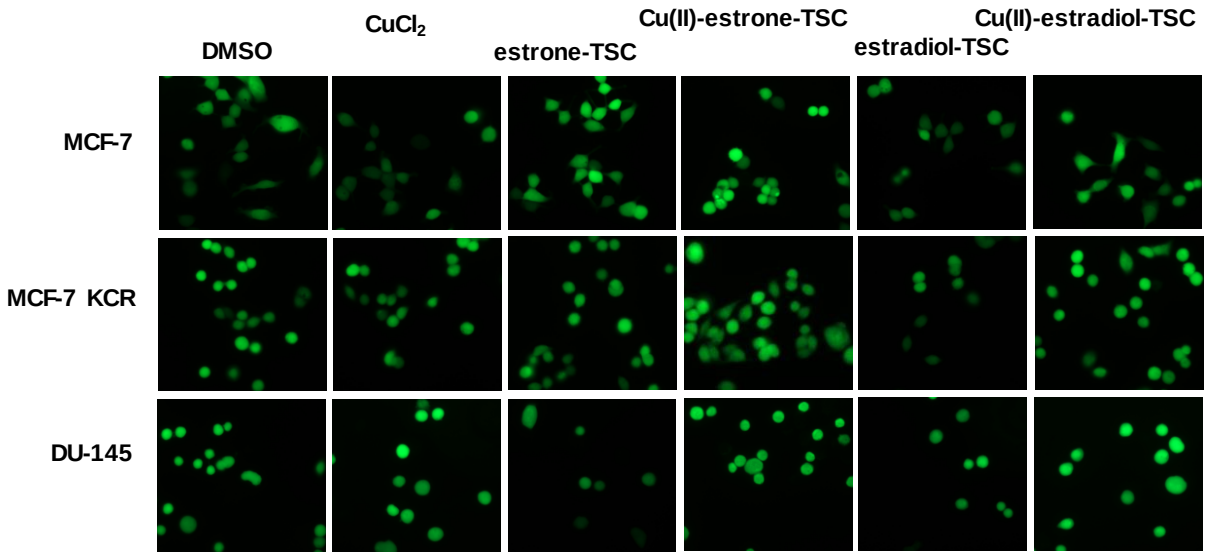


**Figure S13.** Fluorescence microscopic images show the DCFDA staining to determine ROS levels in MCF-7, MCF-7 KCR and DU-154 cells upon the treatment with estrone-TSC and estradiol-TSC and their Cu(II) complexes (20 μM) in addition to the DMSO blank (90% DMSO-10% PBS buffer) and $CuCl_2$ (20 μM) as indicated in the figure using 6 h incubation time. This figure was adapted from publication [P1].

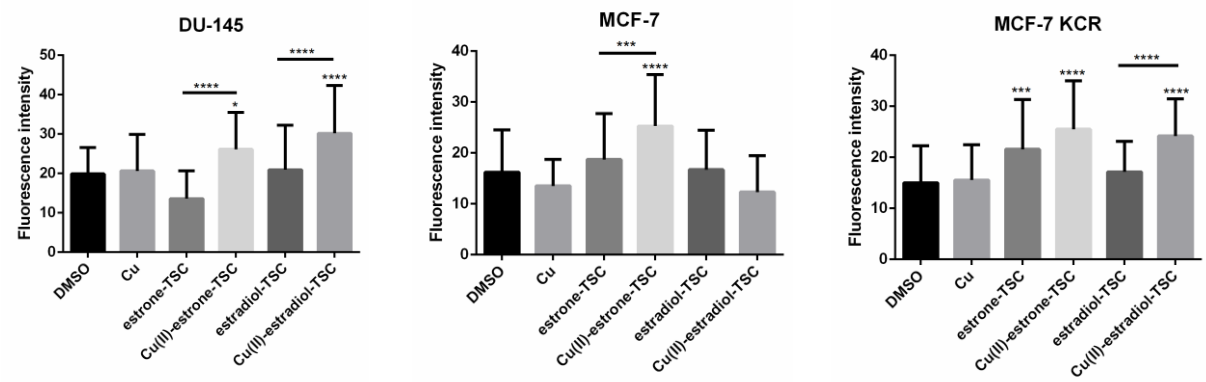


**Figure S14.** Level of ROS generation measured by $H_2$DCFDA staining on MCF-7, MCF-7 KCR and DU-154 cells upon the treatment with estrone-TSC and estradiol-TSC and their Cu(II) complexes (20 μM) in addition to the DMSO blank (90% DMSO-10% PBS buffer) and $CuCl_2$ (20 μM) as indicated in the figure using 6 h incubation time. This figure was adapted from publication [P1].

**Table S13.** *In vitro* cytotoxic effect ($IC_{50}$ values in μM) of 2AE and 2AP without and with one equivalent of Cu(II) ions and for the controls ($CuCl_2$, doxorubicin and cisplatin) in Colo205, Colo320, MCF-7, HeLa and MRC-5 cell lines. (n.d. = not determined). (72 h exposure) This table was adapted from publication [P2].

| $IC_{50}$ / μM | Colo205 | Colo320 | MCF-7 | HeLa | MRC-5 |
|---|---|---|---|---|---|
| **2AE** | 17.3±0.1 | 24±2 | >100 | 29.6±0.6 | >100 |
| **2AP** | >100 | >100 | >100 | >100 | >100 |
| **2AE+Cu(II)** | 39±1 | 28±3 | 51±2 | >100 | 37±4 |
| **2AP+Cu(II)** | 16.1±0.5 | 11±1 | 12.3±0.6 | 7.55±0.01 | 16±2 |
| **$CuCl_2$** | 38±1 | 37±3 | >100 | >100 | 21±1 |
| **doxorubicin** | 0.05±0.01 | 0.19±0.02 | 0.21±0.03 | n.d. | 11±1 |
| **cisplatin** | 23±1 | 1.0±0.03 | 1.4±1.1[b] | 2.3±0.1[b] | 1.1±0.2 |

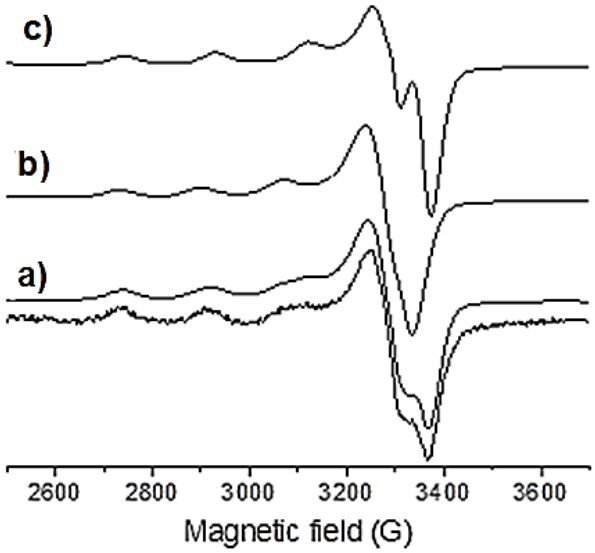


**Figure S15**. a) Frozen solution EPR spectra of the isolated Cu(II)-2-aminoestradiol complex dissolved in DMSO (lower spectrum) together with simulated curve (upper spectrum) which is the superposition of two components: b) the mono complex and c) the bis complex at 50% : 50% ratio. This figure was adapted from publication [P2].

**Table S14**. Anisotropic EPR parameters determined for the isolated product in the Cu(II)-2-aminoestradiol.[a] {DMSO, 77 K} This table was adapted from publication [P2].

| | $g_\perp$ | $g_\parallel$ | $A_\perp$ ($\times10^{-4}$cm$^{-1}$) | $A_\parallel$ ($\times10^{-4}$cm$^{-1}$) | $\omega_\perp$ ($\times10^{-4}$cm$^{-1}$) | $\omega_\parallel$ ($\times10^{-4}$cm$^{-1}$) | $g_{0,calc}$[b] |
|---|---|---|---|---|---|---|---|
| **$[CuL]^+$** | 2.056 | 2.262 | 8 | 173 | 29 | 33 | 2.124 |
| **$[CuL_2]$** | 2.046 | 2.231 | 14 | 192 | 21 | 29 | 2.108 |

[a]The experimental error were ±0.002 for $g_\perp$ and ±0.001 for $g_\parallel$, ± 2 $\times10^{-4}$cm$^{-1}$ for $A_\perp$ and ±1 $\times10^{-4}$cm$^{-1}$ for $A_\parallel$. [b] Isotropic $g_0$ parameters, calculated by the equation $g_{0,calc} = (2g_\perp+g_\parallel)/3$.